

# **Solutions to Blistering: Modification of a Poly(urea-co-urethane) Coating Applied to Concrete Surfaces**

Eleni Papadopoulos (BE. Hons, BSc.)

Thesis submitted to the faculty of Science and Engineering  
of Flinders University  
in fulfilment of the requirements  
for the degree of

**DOCTOR OF PHILOSOPHY**

in

**CHEMISTRY**

Dr Stephen Clarke

Dr Milena Ginic-Markovic



**FLINDERS  
UNIVERSITY**  
ADELAIDE  
AUSTRALIA

December 2008

Adelaide, South Australia

Dedicated to  
my mum, dad, sisters,  
papou and yiayia

# Table of Contents

<b>Summary.....</b>	<b>vi</b>
<b>Declaration.....</b>	<b>viii</b>
<b>Acknowledgements.....</b>	<b>ix</b>
<b>List of Figures.....</b>	<b>x</b>
<b>List of Schemes.....</b>	<b>xvi</b>
<b>List of Tables.....</b>	<b>xvii</b>
<b>Glossary.....</b>	<b>xix</b>
<b>Chapter 1 – Introduction.....</b>	<b>1</b>
1.1 Background .....	2
1.2 Literature Review .....	4
1.2.1 Polyurethane and polyurea reaction chemistry.....	4
1.2.2 Isocyanates .....	8
1.2.3 Polyols.....	10
1.2.4 Emulsion technology.....	11
1.2.5 Kinetics of competing reactions: Presence of Water and the production of Carbon dioxide.....	14
1.2.6 Catalysts .....	17
1.2.7 Theory of Reaction Kinetics.....	19
1.2.7.1 Thermal techniques .....	19
1.2.7.2 Rheological techniques.....	26
1.2.7.3 Spectroscopic techniques.....	29
1.2.8 Fillers.....	31
1.3 Aim and Scope .....	35
1.4 Thesis outline .....	38
1.4.1 Publications .....	40
1.4.2 Conference Presentations .....	40
1.5 References.....	42
<b>Chapter 2–Characterisation Techniques.....</b>	<b>52</b>
2.1 Fourier Transform Infrared (FTIR) .....	53
2.2 Differential Scanning Calorimetry (DSC) .....	54

2.3 Thermogravimetric Analysis (TGA) .....	56
2.4 Dynamic Mechanical Analysis (DMA) .....	56
2.5 Rheology .....	58
2.6 Carbon Dioxide Test Method.....	59
2.6.1 Establishing the test method.....	60
2.7 Error analysis .....	63
2.8 References.....	64

### **Chapter 3- Investigation into the main reactions in the product.....66**

3.1 Part 1: Kinetic study of the Polyurethane reaction between Castor Oil and PMDI 67	
3.1.1 Introduction .....	67
3.1.2 Experimental.....	69
3.1.2.1 Materials and sample preparation .....	69
3.1.2.2 Methods .....	70
3.1.2.2.1 DSC Measurement .....	70
3.1.2.2.2 Rheological Measurement .....	71
3.1.2.2.3 Infrared Spectroscopy.....	71
3.1.2.2.4 Dynamic Mechanical Analysis (DMA).....	72
3.1.3 Results and Discussion.....	73
3.1.3.1 Investigation of the reaction kinetics through DSC .....	73
3.1.3.2 Investigation of the castor oil and PMDI reaction through rheology .....	76
3.1.3.2.1 Kinetic Analysis through the point of gelation .....	76
3.1.3.2.2 Kinetic Analysis from Viscosity data.....	84
3.1.3.2.3 Kinetics of complex viscosity during the initial stages of cure .	86
3.1.3.3 Kinetic studies through FTIR.....	91
3.1.4 Conclusions .....	95
3.2 Part 2: Investigation into the curing kinetics of the Polyurea reaction between Water and Isocyanate .....	96
3.2.1 Introduction .....	96
3.2.2 Materials and Methods.....	96
3.2.2.1 Materials and sample preparation .....	96
3.2.2.2 Methods .....	98
3.2.2.2.1 Blister Simulation Experiment.....	98

3.2.2.2.2	PDSC measurements- Water and PMDI.....	98
3.2.2.2.3	Carbon dioxide Measurements.....	98
3.2.2.2.4	FTIR Analysis .....	98
3.2.3	Results and Discussion.....	100
3.2.3.1	Blister Simulation.....	100
3.2.3.2	Curing Kinetics of the water and isocyanate reaction through PDSC .....	102
3.2.3.3	Volumetric Analysis of Carbon Dioxide Evolution .....	110
3.2.3.4	Cure Kinetics through FTIR .....	115
3.2.4	Conclusions .....	117
3.2.5	References.....	118

**Chapter 4 - Investigation into the reaction kinetics of glycerol and the commercial diisocyanate resin.....121**

4.1	Introduction.....	122
4.2	Materials and Methods .....	124
4.2.1	Materials and sample preparation .....	124
4.2.2	Methods.....	125
4.2.2.1	DSC Measurement .....	125
4.2.2.2	Rheological Measurement .....	126
4.2.2.3	Mid and Near Infrared Spectroscopic Analysis .....	126
4.2.2.4	Dynamic Mechanical Analysis .....	128
4.3	Results and Discussion .....	129
4.3.1	Investigation of reaction kinetics through DSC for the stoichiometric ratio .....	129
4.3.1.1	Applicability of kinetic models.....	132
4.3.1.2	Isoconversional methods .....	138
4.3.1.3	Kinetic differences of the primary and secondary hydroxyls .....	141
4.3.2	Rheological investigation of the stoichiometric ratio of Glycerol to PMDI .....	143
4.3.3	Investigation of the critical ratio of glycerol to PMDI.....	149
4.3.4	Kinetic analysis of the critical ratio using isconversional methods for DSC data.....	152
4.4	Conclusions.....	157
4.5	References.....	158

**Chapter 5- Polyol Emulsion.....161**

5.1 Introduction .....	162
5.2 Experimental .....	165
5.2.1 Materials .....	165
5.2.1.1 Emulsion preparation .....	165
5.2.2 Experimental techniques .....	168
5.2.2.1 Rheological characterisation .....	168
5.2.2.2 Conductivity measurements.....	169
5.2.2.3 Carbon Dioxide measurements .....	169
5.3 Results and Discussion .....	170
5.3.1 Changes in the emulsion structure .....	170
5.3.1.1 Effect on carbon dioxide production.....	173
5.3.2 Variations to the simple emulsion .....	174
5.3.2.1 Emulsion stability.....	175
5.3.2.2 The effect of varying emulsion composition on carbon dioxide evolution and the crosslinking reaction during the reaction with PMDI .....	179
5.3.3 Effect of various emulsion components on the stability of the control emulsion and its subsequent effect on carbon dioxide evolution .....	183
5.3.3.1 Effect of the non-curing components on carbon dioxide evolution .....	185
5.3.4 Addition of a second polyol .....	187
5.3.4.1 Straight addition of glycerol to emulsion .....	188
5.3.4.1.1 Flow properties.....	188
5.3.4.1.2 Carbon dioxide tests .....	189
5.3.4.2 Fractionating the control emulsion with glycerol by removing castor oil .....	191
5.3.4.2.1 Flow properties.....	192
5.3.4.2.2 Carbon dioxide tests .....	193
5.3.4.3 Addition of glycerol to the control polyol emulsion at 4% w/w..	195
5.3.4.3.1 Rheological investigation of the reaction between emulsions and PMDI.....	195
5.3.4.3.2 Carbon dioxide rate analysis .....	197
5.4 Conclusions .....	198
5.5 References.....	200
<b>Chapter 6 - Reactive Aggregate and Combined Solutions.....</b>	<b>202</b>
6.1 Introduction .....	203
6.2 Materials and Methods .....	204

6.2.1	Materials and sample preparation .....	204
6.2.2	Methods .....	206
6.2.2.1	TGA .....	206
6.2.2.2	Carbon dioxide Measurement.....	206
6.2.2.3	DMA .....	206
6.2.2.4	Ageing tests .....	207
6.3	Results and Discussion .....	208
6.3.1	Characterisation of the current industry ratio and improvements.....	208
6.3.2	Ageing of cement .....	210
6.3.2.1	Carbon dioxide environment .....	211
6.3.2.2	Relative humidity environment .....	213
6.3.3	Characterisation of the cured material using DMA for comparison of various proposed solutions .....	215
6.4	Conclusions .....	219
6.5	References.....	220
<b>Chapter 7 – Conclusions and Recommendations.....</b>		<b>221</b>
<b>Appendix A – Material Characterisation.....</b>		<b>228</b>
1	PMDI.....	229
2	Analysis of raw materials .....	232

# Summary

Blistering, during cure, resulting in subsequent coating delamination has been found to occur in a poly (urea-*co*-urethane) cement composite coating used for the protection of new and existing industrial concrete surfaces. Refurbishment of the blistered material, leads to time delays and increased costs.

The reaction kinetics within this product is complex due to one of the reactants being water dispersed. The presence of water causes carbon dioxide evolution during cure through the decomposition of carbamic acid formed from the reaction between water and isocyanate functional groups of the resin. Water also reacts with cement and lime in the reactive aggregate, thus a multitude of reactions occurs, during cure of these complex materials. Due to the complexity of the composite coating, the cure chemistry for the polyurea and polyurethane reactions were investigated individually, with reference to the reactant ratios used by the industry. Although the competing reactions between isocyanate and hydroxyl groups and isocyanate and water molecules has been studied extensively for monomeric systems, carbon dioxide reduction in these systems has resided in the use of catalysts to increase the rate of the preferred reaction. This solution was not economically viable nor was it practical for the industry partners. Solutions were therefore aimed at the reduction or elimination of carbon dioxide in the coating formulation through the addition of a slower reacting polyol. Glycerol was chosen as the slower reacting polyol, because of its ability to reduce the viscosity of the polyol emulsion as well as increase gel times, improving the coating's pot-life and application ability.

The relative rates of cure of the polyurethane/polyurea reactions have not previously been attempted for oligomeric isocyanates with tri-functional polyols, such as castor oil and glycerol dispersed in water. There was a lack of literature describing cure of oligomeric isocyanates and polyol emulsions and the rate of carbon dioxide evolution from these systems. A novel Pressure Differential Scanning Calorimetry (PDSC) technique was used to understand the cure of the polyurea reaction as well as the carbon dioxide evolved from this system and was compared to volumetric tests for this system. The effect of changing the ratios of isocyanate and the reactive components of the polyol emulsion on carbon dioxide evolution was therefore investigated. Understanding how these changes affect the application of the coating

system was also taken into consideration through rheological assessment of the polyol formulation. Hydrated lime or quicklime, added to polyurethane coatings was found to aid in the absorption of carbon dioxide, therefore improvements to the cement aggregate by the addition of hydrated lime or quicklime was also considered. The curing mechanism for the composite coating containing the cement and inert fillers was out of the scope of this thesis.

'I certify that this thesis does not incorporate without acknowledgement any material previously submitted for a degree or diploma in any university; and that to the best of my knowledge and belief it does not contain any material previously published or written by another person except where due reference is made in the text.'

.....

Eleni Papadopoulos

# Acknowledgements

I would like to thank Flinders University, the Australian Research Council (ARC) Linkage grant scheme, Prestige Concreting Additives and Baker Technical Services for funding and sponsoring the industry research project.

Thank you to my supervisors; Stephen Clarke and Milena Ginic-Markovic for their support and encouragement throughout the last few years.

There have also been a multitude of people in these last few years who have brightened my days at Flinders University and who I consider to be good friends. Thank you to people past and present: Durkhanai, Elda, Tony, Tricia, Rachel, Dave C., Paul, Ian, Pamela, Simon, Taryn, Dave V., Andrew, Kim, Dee and Kristina.

I would like to give a special mention to all my friends who have endured having me as their “I can’t...I need to study” friend, over these few years. I have been extremely lucky to have such a great support group, who have given me so much.

I wish to express my most heart-felt gratitude to my family, especially my beautiful mum, Toula Papadopoulos, who has given me all the love and support I have needed to go on this journey. Thank you to my beautiful sisters, Athanasia, Penny and Christina, and to my dad, who although is not here at present, has given me the strength, character and support throughout my life and will be remembered in all my achievements. I would also like to thank the newest additions to my family, Martin, my brother-in-law and finally, Theodore!! My gorgeous little nephew, who has brought me the greatest joy in this past year and has made my journey so much easier.

# List of Figures

Figure 1.1 Blister formation during cure of the poly (urea- <i>co</i> -urethane) floor screed	3
Figure 1.2 Common isocyanates used in polymeric materials <sup>[25]</sup>	9
Figure 1.3 Typical structure of castor oil <sup>[69]</sup>	10
Figure 1.4 Surfactant stabilisation of oil in water droplets through A) solubilisation and B) polymer adsorption <sup>[80]</sup>	11
Figure 1.5 Representation of emulsion stability <sup>[80]</sup>	13
Figure 1.6 Approach to solving blistering in the coating during curing	38
Figure 2.1 Heat flux DSC schematic <sup>[12]</sup>	55
Figure 2.2 $F_d$ represents the applied oscillatory force, while $F_s$ is the clamping force, showing the phase angle $\delta$ produced <sup>[22]</sup>	57
Figure 2.3 Relationship between the complex, storage and loss moduli <sup>[21]</sup>	57
Figure 2.4 CO <sub>2</sub> measurement apparatus	59
Figure 2.5 The amount of CO <sub>2</sub> evolved (from Figure 2.4) from the reaction of the simple polyol emulsion and PMDI.	61
Figure 2.6 Remixing reacting mixture evolved more carbon dioxide that was entrapped in the polymer matrix	61
Figure 2.7 Carbon dioxide evolved by varying the mass of sample in the reaction jar.	62
Figure 3.1 Representation of baseline determined for 12.5 °C min <sup>-1</sup>	70
Figure 3.2 Heat flow profile for castor oil with PMDI at equal stoichiometry	73
Figure 3.3 The advanced integral isoconversional analysis of activation energy with extent of conversion for two different ratios of hydroxyl groups to isocyanate groups.	75
Figure 3.4 $G'$ , $G''$ and $\tan \delta$ versus cure time for the castor oil and PMDI stoichiometric system at 70 °C	77
Figure 3.5 Multiple frequency plot of $\tan \delta$ at 70 °C	79
Figure 3.6 linear relationship of gel time obtained through the maximum in $\tan \delta$ ...	80
Figure 3.7 $G'$ and $G''$ versus cure time for the castor oil and PMDI with an excess of isocyanate at 70 °C.	82
Figure 3.8 Temperature dependence of $G'$ during curing of castor oil and PMDI with excess isocyanate	83

Figure 3.9 Correlation between $G'$ and the time it occurs .....	83
Figure 3.10 Viscosity build up of castor oil and PMDI and the stoichiometric ratio	84
Figure 3.11 Viscosity build up of castor oil and PMDI with excess isocyanate .....	84
Figure 3.12 Viscosity build up follows an exponential function before the gel point for the equal stoichiometric system at A) lower isothermal temperatures and B) higher temperatures .....	86
Figure 3.13 Linearity observed for the natural log of complex viscosity versus time profiles for the castor oil and PMDI system at A) equal stoichiometry and B) excess isocyanate .....	87
Figure 3.14 Rate of viscosity increase shows discontinuity at lower isothermal temperatures for the stoichiometric system .....	88
Figure 3.15 Activation energy obtained for the equal stoichiometric system of Castor oil and PMDI using the apparent kinetic constant established from viscosity profiles .....	90
Figure 3.16 Conversion profile of the isocyanate peak at $\sim 2270\text{ cm}^{-1}$ during polyurethane cure at $60\text{ }^\circ\text{C}$ using FTIR for stoichiometric and excess isocyanate systems .....	91
Figure 3.17 A second order rate model fit for the rate of reaction before and after gelation for the polyurethane system at $60\text{ }^\circ\text{C}$ using FTIR .....	93
Figure 3.18 FTIR spectra of the castor oil and excess isocyanate system at the start of reaction and after 20 min of mixing .....	94
Figure 3.19 Effect of Relative Humidity during curing of Castor oil and PMDI....	100
Figure 3.20 Confirmation of $\text{CO}_2$ present in polyurethane blister formation due to atmospheric moisture .....	101
Figure 3.21 Heat flow profiles of polyurea reaction using PDSC in non-isothermal mode .....	102
Figure 3.22 Activation energy dependence for increasing conversion of the polyurea reaction .....	103
Figure 3.23 Pressure profiles of the polyurea reaction at three heating rates in non-isothermal PDSC mode. ....	105
Figure 3.24 Pressure difference with increasing temperature at various heating rates .....	105
Figure 3.25 Change in the pressure difference with conversion for the polyurea system.....	106

Figure 3.26 Change in the pressure difference profile with temperature, while varying the mole ratio of water to isocyanate.....	107
Figure 3.27 Change in Pressure and heat flow data for increased water content ....	108
Figure 3.28 Isothermally obtained master curve for the polyurea reaction at H <sub>2</sub> O/NCO=1.65 also displaying pressure evolution during cure.....	109
Figure 3.29 Carbon dioxide evolution from the PMDI-water reaction.....	111
Figure 3.30 Rate of CO <sub>2</sub> evolution for the PMDI-water reaction.....	111
Figure 3.31 Rate of CO <sub>2</sub> evolution with respect to water consumption assuming a first order process.....	113
Figure 3.32 First order process for the rate of carbon dioxide evolution.....	114
Figure 3.33 Second order process for the rate of carbon dioxide evolution.....	114
Figure 3.34 Conversion versus time for the consumption of Isocyanate groups at 60 °C for the H <sub>2</sub> O/NCO mole ratio= 1.65.....	115
Figure 3.35 Second order rate equation describes the rate of consumption of isocyanate groups for the polyurea reaction at the mole ratio of H <sub>2</sub> O/NCO=1.65 at 60 °C.....	116
Figure 4.1A) MID-IR of cured sample with residual unreacted isocyanate and B) N-IR of cured polyurethane sample showing residual hydroxyl groups.....	127
Figure 4.2 Heat flow curves (W g <sup>-1</sup> ) as obtained by isothermal DSC runs.....	130
Figure 4.3 Cure rate profiles for non-isothermal DSC.....	131
Figure 4.4 Degree of conversion of polyurethane system vs. time at different curing temperatures fitted to a 2 <sup>nd</sup> order model.....	132
Figure 4.5 Master curve for the polyurethane reaction fitted to an autocatalytic model	134
Figure 4.6 Degree of conversion of polyurethane system vs. time at different curing temperatures fitted to an autocatalytic model.....	134
Figure 4.7 Arrhenius plot for the determination of activation energy through the rate constant found by isothermal calorimetry .....	136
Figure 4.8 Reaction order as determined by non-isothermal DSC using Hernández-Sánchez method. <sup>[44]</sup> .....	137
Figure 4.9 Variation of activation energy with conversion for isothermal DSC cure .....	139
Figure 4.10 Variation of activation energy with conversion for non-isothermal data .....	140

Figure 4.11 A) Gaussian fit of heat flow curve during isothermal cure at 70 °C: 2 peaks fitted pertaining to primary and secondary hydroxyls and B) Rate of cure pertaining to primary and secondary hydroxyls in glycerol. ....	142
Figure 4.12 Viscosity build up of the polyurethane system at various isothermal temperatures at 0.1% strain and inset at 10% strain showing initial viscosity build up .....	143
Figure 4.13 Evolution of $G'$ , $G''$ and $\tan \delta$ at various isothermal cure temperatures at 0.1% strain, 1Hz.....	144
Figure 4.14 Dependence of the gel point on the isothermal curing temperature for the polyurethane system.....	146
Figure 4.15 Extent of reaction for varying mole ratios of OH/NCO .....	149
Figure 4.16 Conversion of isocyanate peak intensity for increasing hydroxyl content .....	150
Figure 4.17 Overlap of the DSC and ATR-FTIR data for the conversion of isocyanate groups with an increasing hydroxyl concentration .....	150
Figure 4.18 Heat of reaction in $\text{kJ mol}^{-1}$ equivalent isocyanate versus %conversion determined by the reduction in intensity of the isocyanate peak using ATR-FTIR.	151
Figure 4.19 Heat flow profiles in A) non-isothermal and B) isothermal mode for the critical mole ratio of OH/NCO. ....	152
Figure 4.20 Non-isothermal dependence of activation energy on conversion for differing mole ratios of OH/NCO .....	154
Figure 4.21 Isothermally determined activation energy dependence on conversion for an excess in hydroxyl mole ratio of OH/NCO=1.5 determined using absolute extents of cure.....	156
Figure 5.1 Steric stabilisation of oil-in-water forming an emulsion <sup>[6]</sup> .....	162
Figure 5.2 Structure of the nonyl-phenol ethoxylate .....	163
Figure 5.3 Differences in viscosity behaviour through changes in the emulsion structure .....	171
Figure 5.4 Conductivity measurements for changes in emulsification procedures .	172
Figure 5.5 Storage modulus behaviour of variations in the emulsification procedure .....	173
Figure 5.6 Effect of emulsion structure on carbon dioxide levels .....	173
Figure 5.7 Viscosity profiles for emulsion series with increasing levels of A: surfactant, B: water and C: castor oil concentrations.....	176

Figure 5.8 Storage modulus profiles for emulsion series with increasing levels of A: surfactant, B: water and C: castor oil concentrations.....	178
Figure 5.9 Carbon dioxide evolution for increasing concentrations of surfactant, water and castor oil concentrations in the simple emulsion .....	180
Figure 5.10 A) Viscosity profiles and B) Storage modulus profiles for variations in the emulsion composition.....	184
Figure 5.11 Levels of carbon dioxide evolution while varying the polyol emulsion to determine the effect of formulation components. ....	186
Figure 5.12 Viscosity profiles for increases in glycerol concentration.....	188
Figure 5.13 Storage modulus and loss modulus changes with 4% w/w glycerol addition .....	189
Figure 5.14 Carbon dioxide evolution for increasing glycerol concentration .....	190
Figure 5.15 Viscosity profiles for increasing fractions of glycerol in the control emulsion.....	192
Figure 5.16 Storage and loss modulus profiles for 4% w/w and 8% w/w fractions of glycerol in the control emulsion .....	193
Figure 5.17 Carbon dioxide evolution for varying weight fractions of glycerol.....	194
Figure 5.18 Comparison of the extent of the crosslinking reaction between polyol emulsions and PMDI.....	197
Figure 5.19 Carbon dioxide evolution with time for the reaction between the polyol emulsion and PMDI and the polyol emulsion with glycerol and PMDI.....	198
Figure 6.1 Comparison of current industry fillers with an increased level of calcium hydroxide .....	208
Figure 6.2 Reduction in carbon dioxide evolution through the addition of calcium hydroxide .....	209
Figure 6.3 Reduction in carbon dioxide evolution through the addition of calcium oxide .....	210
Figure 6.4 TGA results for carbon dioxide exposed Portland cement .....	211
Figure 6.5 Reduction in carbon dioxide levels in the reaction of PMDI with polyol emulsion using carbon dioxide exposed cement at varying time intervals. ....	212
Figure 6.6 Efficacy of Portland cement exposed to a high relative humidity environment over 172 hours .....	213
Figure 6.7 TGA analysis of the hydration reaction over time for Portland cement exposed to a high humidity environment .....	214

Figure 6.8 Correlation of the calcium hydroxide levels present in Portland cement at varying exposure times to a high humidity environment with its ability to reduce carbon dioxide evolution in the coating formulation .....	215
Figure 1.A Typical composition of PMDI <sup>[1]</sup> .....	229
Figure 1.B Typical <sup>1</sup> H-NMR spectrum with peaks representing for A) aromatic and B) alkyl protons <sup>[2]</sup> .....	230
Figure 1.C General structure of PMDI <sup>[4]</sup> .....	230
Figure 2.A IR spectra for A) PMDI obtained by ATR-FTIR compared to B) MDI spectra obtained from SDBS <sup>[2]</sup> .....	233
Figure 2.B IR spectra for A) castor oil obtained by ATR-FTIR compared to B) castor oil spectra obtained from SDBS <sup>[2]</sup> .....	234
Figure 2.C IR spectra for A) glycerol obtained by ATR-FTIR compared to B) glycerol spectra obtained from SDBS <sup>[2]</sup> .....	235
Figure 2.D IR spectra for A) dioctyl phthalate obtained by ATR-FTIR compared to B) dioctylphalate spectra obtained from SDBS <sup>[2]</sup> .....	236

# List of Schemes

Scheme 1.1 Polyurethane reaction.....	4
Scheme 1.2 Reaction between an isocyanate group and hydroxyl group resulting in urethane bond formation.....	4
Scheme 1.3 Reaction between an isocyanate group and water resulting in a highly reactive amine and carbon dioxide .....	5
Scheme 1.4 Reaction between a highly reactive amine and isocyanate group resulting in a urea bond formation.....	5
Scheme 1.5 Urethane bond formation: reaction of polyol with isocyanate.....	5
Scheme 1.6 Urea bond formation: reaction of water with isocyanate.....	6
Scheme 1.7 Carbon dioxide formation resulting from the reaction of a free fatty acid and an isocyanate group.....	7
Scheme 1.8 Formation of carbodiimide <sup>[25]</sup> .....	7
Scheme 1.9 Secondary polyurethane reactions.....	8
Scheme 1.10 Calcium carbonate formation.....	32
Scheme 1.11 Calcium hydroxide formation from calcium oxide.....	32
Scheme 1.12 Hydration of calcium oxide silicates in cement.....	33
Scheme 1.13 Reacting components, PMDI and castor oil.....	69
Scheme 1.14 Reaction between glycerol and PMDI.....	124
Scheme 6.1 Absorption of carbon dioxide by lime in the fillers.....	204

# List of Tables

Table 1-1 Cement/Aggregate Filler for Polyurethanes <sup>[27]</sup> .....	31
Table 1-2 Portland cement molecular composition <sup>[194, 195]</sup> .....	32
Table 1-3 Portland cement Silicate Compositions <sup>[194]</sup> .....	33
Table 3-1 Non-isothermal data for peak temperatures and corresponding conversions obtained for the castor oil- PMDI reaction at equal stoichiometry.....	74
Table 3-2 Gel times (minutes) observed for the stoichiometric system of castor oil and PMDI using uni-frequency and multiple frequency mode .....	78
Table 3-3 Activation Energies determined by various criteria for the stoichiometric system.....	81
Table 3-4 Values for $k_{\eta}$ for equal stoichiometry and excess isocyanate ratios of Castor oil and PMDI .....	89
Table 3-5 Comparison of Activation Energy obtained through various methods .....	91
Table 3-6 Summary of non-isothermal PDSC data for the polyurea reaction.....	103
Table 4-1 Total heat flow and ultimate extents of cure for two time intervals at varying isothermal cure temperatures .....	130
Table 4-2 Peak temperatures for non-isothermal heating rates .....	131
Table 4-3 Autocatalytic model parameters.....	135
Table 4-4 Critical rheological times obtained using the crossover of $G'$ and $G''$ and the frequency independence of $\tan \delta$ .....	147
Table 4-5 Summary of varying activation energies obtained for the complex polyurethane reaction between glycerol and PMDI.....	147
Table 4-6 Reaction data for non-isothermal DSC analysis with an excess in hydroxyl groups.....	153
Table 5-1 Emulsion composition for the change in variable concentrations %w/w	166
Table 5-2 Condition A: Composition of polyol emulsions .....	167
Table 5-3 Condition B: Series of polyol emulsions formed by adding glycerol to control polyol emulsion.....	168
Table 5-4 Condition C: Increasing glycerol composition in control emulsion by removing castor oil.....	168
Table 5-5 Conductivity measurements for emulsion series with increasing levels of surfactant, water and castor oil concentrations .....	179

Table 5-6 Rheological gel times achieved for increasing surfactant, water and castor oil concentrations .....	181
Table 5-7 Storage modulus obtained at the gel times for increasing surfactant, water and castor oil concentrations.....	182
Table 5-8 Conductivity measurements for changes in the control polyol emulsion	187
Table 5-9 Isocyanate to total hydroxyl mole ratio in mixture and reduction in carbon dioxide with increasing glycerol concentration .....	191
Table 5-10 Isocyanate to total hydroxyl mole ratio in mixture and reduction in carbon dioxide with increasing fraction of glycerol showing total replacement of castor oil at 49% w/w .....	195
Table 5-11 Gel times and magnitude of the storage modulus at the gel point .....	196
Table 6-1 Polyol emulsion compositions for coating variations.....	205
Table 6-2 Filler compositions for coating variations .....	205
Table 6-3 Comparison of $T_g$ and storage modulus for various coating compositions .....	216
Table 6-4 Viscosity variations of polyol emulsions and oligomeric isocyanates investigated .....	219
Table 1-A Summary of TGA parameters for raw materials.....	232

# Glossary

## Abbreviations

$A(0)$	Area underneath peak in FTIR spectra at zero time
$A(t)$	Area underneath peak in FTIR spectra at time $t$
$A_p$	Partial area underneath exothermic peak from DSC curves
$A_t$	Total area underneath exothermic peak from DSC curves
ATR	Attenuated Total Reflectance
CO $n$	Castor Oil fraction in emulsion series with total number of emulsions equal to $n$
COD	Coefficient of Distinction
DEG	Diethylene Glycol
DMA	Dynamic Mechanical Analysis
DOF	Degrees of Freedom
DOP	Dioctyl Phthalate
DSC	Differential Scanning Calorimetry
DTGS	Deuterated Triglycine Sulfate
DVLR10	Commercial name for oligomeric diphenylmethane diisocyanate obtained from Bayer Chemicals
$E_a$	Apparent activation energy
$F_n$	Fillers formulation with total number of formulations equal to $n$
FTIR	Fourier Transform Infrared
$G'$	Storage modulus/elastic modulus
$G''$	Loss modulus/viscous modulus
$H_{iso}$	Isothermal heat of reaction from DSC exotherms
HLB	Hydrophilic-Lipophilic Balance
$H_{res}$	Residual heat of reaction from DSC exotherms
$H_{rxn}$	Heat of reaction
$H_T$	Total heat of reaction from DSC exotherms
$k$	reaction rate constant
KBr	potassium bromide
NCO	Isocyanate functional groups

NIR	Near Infrared
NMR	Nuclear magnetic Resonance
OH	Hydroxyl functional groups
P	Pressure
$P_n$	Polyol emulsion formulation with total number of formulations equal to $n$
PDSC	Pressure Differential Scanning Calorimetry
PMDI	oligomeric diphenylmethane diisocyanate
PO	Pine Oil
R	Universal gas constant
RH	Relative Humidity
$S_n$	Surfactant fraction in emulsion series with total number of emulsions equal to $n$
SO	Silicone Oil
$\tan \delta$	$\tan$ of the Loss angle $\delta$
TDI	toluene diisocyanate
TGA	Thermogravimetric Analysis
$t_g$	gel time
$T_g$	Glass transition temperature
$T_p$	Peak temperature obtained in DSC exotherms
VOC	Volatile Organic Compound
$W_n$	Water fraction in emulsion series with total number of emulsions equal to $n$

### **Greek alphabet**

$\alpha$	conversion
$\beta$	heating rate in non-isothermal DSC
$\gamma^*$	complex shear rate
$\Delta$	represents change in a value
$\delta$	loss angle in rheological analysis
$\varepsilon$	extinction coefficient in Beer-lambert's law
$\eta$	viscosity obtained by rheological analysis
$\sigma^*$	complex shear stress

## **Terminology**

**Carbon dioxide evolution.** Evolution of carbon dioxide specifically from the reaction between isocyanate and water in the coating measured through volumetric tests.

**Diffusion control.** Also known as vitrification, used to describe kinetics of cure when the material is cured below the glass transition temperature and there is a change from a chemically controlled system.

**Gel time.** The gel time is the time at which the reaction has reached a constant conversion, when an infinite molecular crosslinked network has formed.

**Pot-life.** The pot-life is considered as the time at which the mixed coating formulation is workable before application and is dependent on the gel time of the reactions.

**%Reduction in CO<sub>2</sub>.** This is a measure of the change in carbon dioxide levels between the control sample and that which is being compared. These values are specifically obtained from the volumetric tests performed.

**Viscosity build-up.** The build up in viscosity represents the molecular weight growth of the polymer during rheological analysis.

**Volumetric analysis.** This term is used for all tests which measures the amount of carbon dioxide evolved from the coating mixture using the apparatus described in Chapter 2.

# **CHAPTER 1**

## **Introduction**

# 1 INTRODUCTION

## 1.1 Background

Concrete floors are by far the most abused surfaces encountered in industry. Although concrete is considered to be tough and durable, most concrete floors cannot withstand continual long-term wear and chemical attack. The porous structure of concrete enables significant chemical attack to occur, through migration of liquids and vapours.<sup>[1]</sup> Mineral acids and organic acids, such as citric acid in fruits, lactic acids in dairy products and organic acids found in wine production, can rapidly attack calcium hydroxide silicates in Portland cement and cause severe damage to the surface.<sup>[2-4]</sup> Other common surface damage is due to forklifts and vehicular traffic.

Industry has routinely sought to apply coatings over concrete surfaces, to improve the appearance of the surface and to protect the concrete floor. Maintenance coating materials currently in use include alkyds, chlorinated rubbers, vinyls, inorganic zincs, epoxies, acrylics and polyurethanes as well as combinations of the aforementioned resins.<sup>[5]</sup> Polyurethanes provide longevity and low maintenance costs with a life expectancy of up to 10-12 years.<sup>[6, 7]</sup> There is a great interest in cement-based polyurethane systems. However, such screeds have not reached their full market potential due to inherent technical, application-related problems such as blistering during cure. Unlike conventional polyurethane coating systems, the highly crosslinked poly(urea-co-urethane) screed discussed within this thesis exhibits exceptional resistance to chemical attack from acids, bases and solvents, whilst retaining the high abrasion resistance properties of polyurethanes, with a life expectancy of 30-35 years. The floor screed under investigation is used in industrial settings on concrete floors to provide a range of protective coatings that are resistant to corrosive chemicals, acids, alkalis and abrasion.

The poly (urea-co-urethane) concrete floor screed system manufactured by Prestige Concreting Additives, and applied by Baker Technical Services, consists of three packaged components – a polyol emulsion, an oligomeric diisocyanate and a blend of inert and cementitious fillers.

The move to solventless polyurethane applications in the coatings industry has been to reduce Volatile Organic Compound (VOC) levels emitted by solvent-borne floor

coatings. Due to the solvent-less composition of the industry coating it places the product as a front-runner for use in industry for specific flooring needs. In addition to minimal VOC emissions, the industry product exhibits little odour release during cure and can be applied at sub-freezing temperatures and in the presence of food preparation/processing.

A major disadvantage for the manufacturers of this coating is the consistency of performance upon application, which is severely compromised by the formation of blisters during cure. A representation of blistering during the first few hours of cure is shown in **Figure 1.1**.

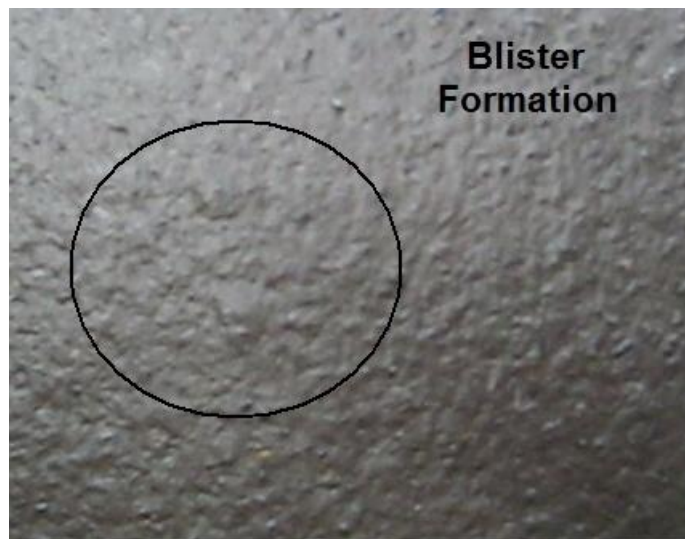


**Figure 1.1** Blister formation during cure of the poly (urea-*co*-urethane) floor screed

This literature survey presents the basics of polyurethane chemistry with particular reference to the crosslinkers used in the industry product. Following this, investigations performed by researchers into the polyurethane reaction kinetics which yield carbon dioxide as either the preferred reaction or as a side reaction will be discussed. Examination of thermoset reaction kinetics and cure profiles and the various methods that have been used in the past to study reaction kinetics is considered. An insight into emulsion technology and stability will be introduced as well as theory surrounding the use of cementitious fillers in polyurethane resins. The review will provide a basis to how the product was systematically investigated for blister formation and how viable solutions to blister formation evolved during the

course of the research.

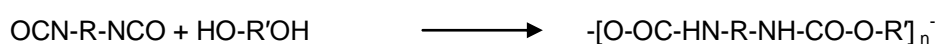
## 1.2 Literature Review

### 1.2.1 Polyurethane and polyurea reaction chemistry

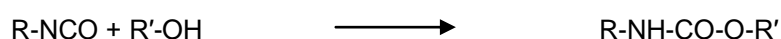
The coating under investigation obtained its properties from the polyurethane and polyurea crosslinks formed during curing. The functionality of the raw materials, in addition to chemical structure, defines the reaction chemistry and cure kinetics of the reacting polyurethane material.<sup>[8-19]</sup>

Urethane and urea polymers are significantly chemically different and exhibit different material properties.<sup>[14, 20-29]</sup> Polyurethane materials containing considerable levels of urea bonds should strictly be considered as poly (urea-*co*-urethane) copolymers, whereby the urea bonds form by the reaction of isocyanate with water. Polyurea, on the other hand, is formed through the reaction of a diamine with an isocyanate crosslinker, or the reaction of water and multifunctional isocyanates.

Polyurethanes are formed by an addition polymerisation reaction between a polyol and an isocyanate (**Scheme 1.1**).<sup>[30, 31]</sup> When an isocyanate functional group reacts with an alcohol, a urethane bond is formed (**Scheme 1.2**). This reaction is relatively slow when uncatalysed<sup>[25]</sup>, although it is highly exothermic.



**Scheme 1.1 Polyurethane reaction**

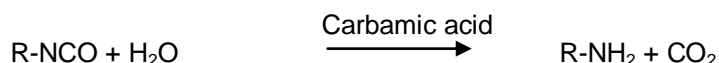


**Scheme 1.2 Reaction between an isocyanate group and hydroxyl group resulting in urethane bond formation**

A poly (urea-*co*-urethane) polymer is formed through the simultaneous reactions of isocyanate with polyol (**Scheme 1.2**) and isocyanate with water (**Scheme 1.3**).<sup>[32-35]</sup>

The isocyanate-water reaction liberates carbon dioxide. This reaction is often utilised to produce polyurethane foam materials, where controlled carbon dioxide evolution from the use of selective catalysts acts as a primary blowing agent.<sup>[13, 14, 36-39]</sup> Carbon dioxide has gained importance as a blowing agent in recent years due to revisions of air quality laws and adoption of the Montreal Protocol, which requires elimination of

carbofluorocarbons (CFCs) from polyurethane foam formulations.<sup>[40, 41]</sup>



**Scheme 1.3** Reaction between an isocyanate group and water resulting in a highly reactive amine and carbon dioxide

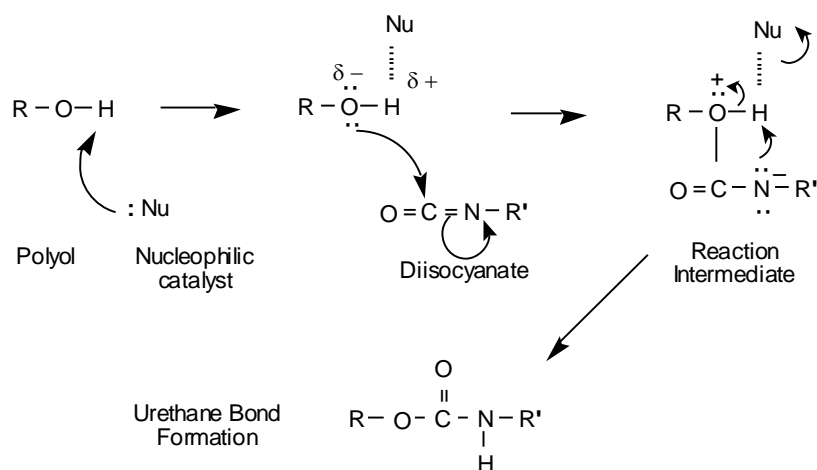
The reaction of an isocyanate group with a primary amine generates a urea bond (**Scheme 1.4**):<sup>[28, 42]</sup>



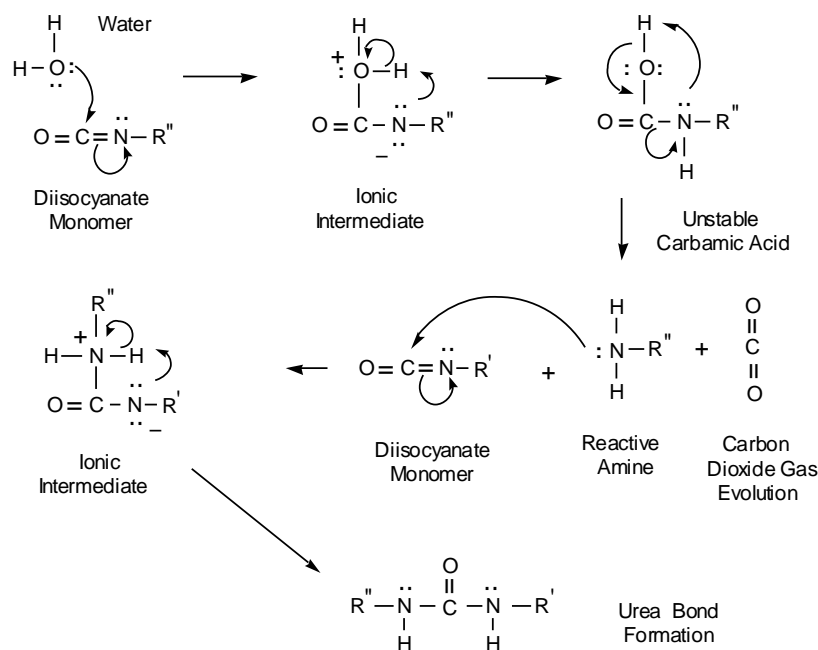
**Scheme 1.4** Reaction between a highly reactive amine and isocyanate group resulting in a urea bond formation

Competing reactions will be apparent if water is present during crosslinking in a polyurethane system. The water-isocyanate reaction yields a carbamic acid intermediate, which undergoes rapid decomposition to form a highly reactive primary amine and carbon dioxide.<sup>[43]</sup> The amine then reacts immediately with isocyanate groups to form urea linkages (**Scheme 1.4**).

**Scheme 1.5** and **Scheme 1.6** detail the reactions that occur during polyurethane crosslinking in the presence of a nucleophilic catalyst and water, respectively.



**Scheme 1.5** Urethane bond formation: reaction of polyol with isocyanate



**Scheme 1.6 Urea bond formation: reaction of water with isocyanate**

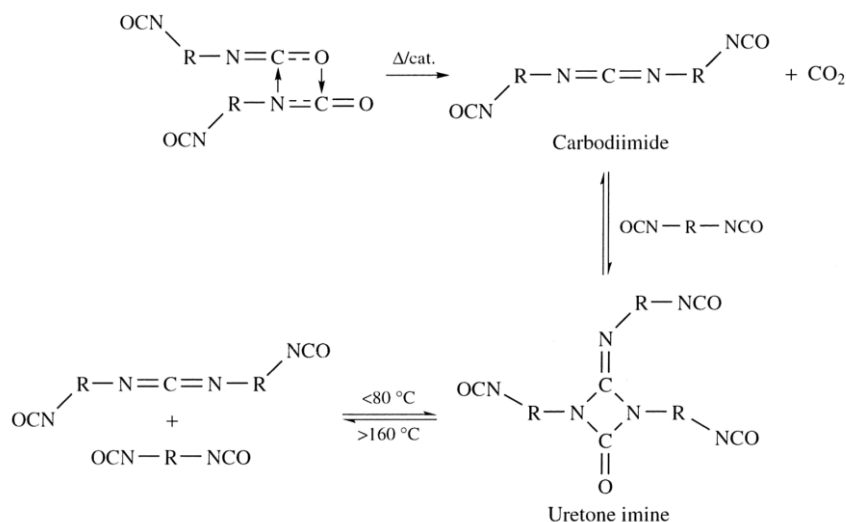
A catalysed polyurethane system is susceptible to blistering when the substrate contains more than 5% humidity,<sup>[23]</sup> which is due to the competition between hydroxyl-polyol groups and water for reaction with isocyanate groups. Carbon dioxide evolution is problematic during cure of polyurethane mixtures containing water. The rate of polyurethane cure will affect the rate of carbon dioxide diffusion from the coating, often resulting in blistering and coating delamination.<sup>[44, 45]</sup> One method of reducing the effect of carbon dioxide evolution in thicker polyurethane coatings is the addition of powdered calcium oxide to absorb the carbon dioxide.<sup>[25, 46-50]</sup>

Other reactions which yield carbon dioxide are isocyanate reactions with carboxylic acids as well as carbodiimide reactions. The reaction of isocyanate with carboxylic acids yields carbon dioxide gas (**Scheme 1.7**).<sup>[13]</sup> Aliphatic isocyanates react readily with fatty acids to give amides, while aromatic isocyanates will react to give anhydrides.<sup>[25]</sup> Anhydrides are only intermediates and may react further with hydroxyl groups or amides present in this system, increasing crosslinking in the product.<sup>[51]</sup> This reaction is important when the polyol contains free fatty acids, such as in the commercial grade castor oil used in the product under investigation.



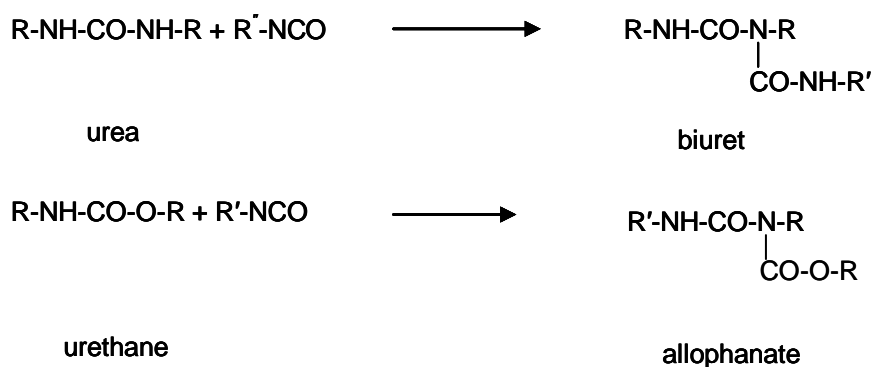
**Scheme 1.7 Carbon dioxide formation resulting from the reaction of a free fatty acid and an isocyanate group.**

In the presence of heat or a catalyst, the reaction of isocyanate with itself yields a carbodiimide and carbon dioxide gas (**Scheme 1.8**).<sup>[25]</sup> The carbodiimide can react further with isocyanate groups to form uretone imines, which decompose back to carbodiimide at temperatures above 160 °C. Carbodiimides may inhibit the hydrolysis of polyurethanes because of their ability to increase the crosslink density of the polymer network at temperatures below 80 °C.<sup>[13, 51]</sup>



**Scheme 1.8 Formation of carbodiimide**<sup>[25]</sup>

Secondary crosslinks of isocyanates form through the hydrogen atoms of the urea and urethane linkages commonly referred to as the biuret and allophanate linkages (**Scheme 1.9**) respectively.<sup>[13]</sup> Allophanate and biuret crosslinks are formed when excess isocyanate is present in the polyurethane/polyurea system, or alternatively when the curing temperature is greater than 120 °C for urethanes, 100 °C for ureas, or for extended periods of time (12-18 hours).<sup>[25]</sup> The presence of secondary reactions is critical to the formation of extensive crosslinking, increasing the hard segments in the polymer network.<sup>[52, 53]</sup>



Scheme 1.9 Secondary polyurethane reactions

### 1.2.2 Isocyanates

There are two main isocyanate classes used in the formation of polyurethanes and polyureas, namely aliphatic and aromatic isocyanates.<sup>[13]</sup> Diphenyl methane diisocyanate (MDI), polymeric MDI and toluene diisocyanate (TDI) are aromatic isocyanates that make up approximately 90% of the total diisocyanate market<sup>[54]</sup>. One major disadvantage of aromatic isocyanates is oxidation from ultraviolet radiation causing yellowing of the cured polyurethane.<sup>[25]</sup> Nevertheless, aromatic isocyanates are widely employed due to their high reactivity and relatively low cost. The high reactivity enables short curing times and low reaction temperatures. Some of the more common isocyanates employed in industry are depicted in **Figure 1.2**.

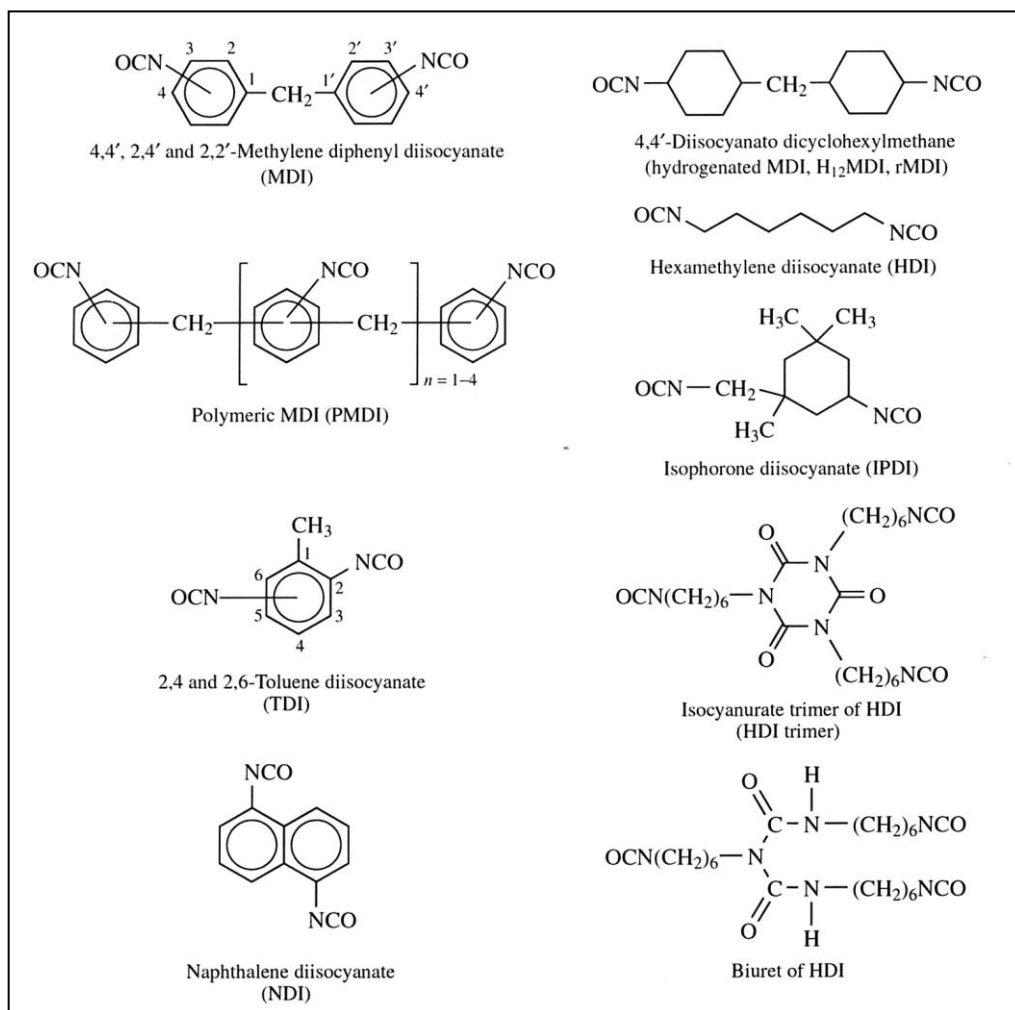


**Figure 1.2 Common isocyanates used in polymeric materials** <sup>[25]</sup>

The isocyanate of interest in this project is 4,4'-methylene diphenyl diisocyanate (PMDI). PMDI is a mixture of varying molecular weight oligoisocyanates and as the number of  $n$  repeat units increases, the viscosity also increases, influencing the physical properties of the resultant material.<sup>[43, 54]</sup> Varying reactivities of the terminal isocyanate groups compared to the internal isocyanate groups could also exist within the PMDI oligomers.<sup>[8, 11]</sup> The terminal/internal isocyanate ratio is reduced as number of repeating units ( $n$ ) is increased. This ratio may have implications for the preference of urethane or urea bond formation in the presence of water, suggesting that molecular weight could play a role in the kinetics of the competing reactions.<sup>[55-57]</sup>

Wang *et al.* <sup>[58]</sup> discussed the difference in reactivity of the isocyanate groups in 2,4'-

TDI, with the isocyanate group in the *para* and *ortho* positions exhibiting different reactivities. The isocyanate group in the *para* position is more reactive than the *ortho* isocyanate group; however, the difference in reactivity decreases because the relative reactivity of the *ortho*-isocyanate group increases with increasing temperature.

### 1.2.3 Polyols

Polyols are the second building block for polyurethane formation, with the hydroxyl functional groups reacting with isocyanate groups to form urethane bonds. Polyols are considered to be chain extenders, with ethylene glycol, glycerine, butanediol, and trimethylolpropane typically used for this purpose.<sup>[25]</sup> Multifunctional polyols include glycerol, trimethylolpropane, pentaerythritol and castor oil.

Castor oil (ricinus oil) is a biodegradable and a renewable product so is largely used in the manufacture of coatings and adhesives.<sup>[8, 59-68]</sup> It is a vegetable product that is highly consistent in its composition, with its structure comprising of a tri-ester of glycerine (**Figure 1.3**).<sup>[69]</sup> Fatty acid content, moisture level, colour and purity are the four main attributes which are used to grade the purity of castor oil. To be useful in polyurethane formation, castor oil must have low free fatty acid content, low water content and high clarity. High free fatty acid content is detrimental, as carboxylic acids can react with isocyanates yielding carbon dioxide gas. Polyurethanes that are made from castor oil are relatively hydrolytically stable. However, as a result of the carbon-carbon double bonds present in the castor oil alkyl chain, oxidation may occur.<sup>[13]</sup>

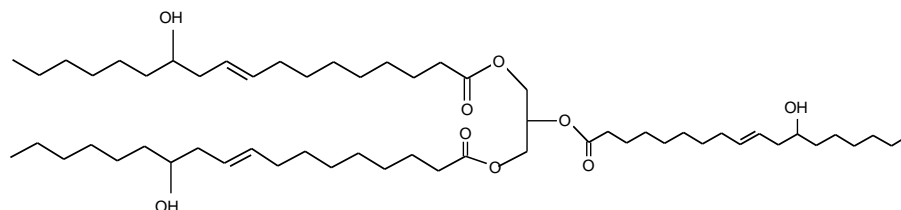


**Figure 1.3** Typical structure of castor oil <sup>[69]</sup>

Glycerol has been used in emulsions and plastics formulations as a plasticizer. It has been shown to reduce particle drop size in emulsion preparations as well as act as a

plasticizer for the formation of thermo-molded plastics. In combination with castor oil, the properties of a thermo-molded plastic were dependent on the ratio of castor oil to glycerol, with higher castor oil to glycerol ratios reducing moisture absorption and improving tensile strength and the Young's modulus.<sup>[70, 71]</sup>

#### 1.2.4 Emulsion technology

The second component of the product under investigation is the polyol emulsion, which is a mixture of castor oil and other components in water, dispersed by a nonyl-phenyl ethoxylated non-ionic surfactant. The polyol emulsion also contains silicone oil for de-aeration properties, pine oil and a phthalate plasticizer. An emulsion is formed when one liquid phase is dispersed in another, with the simplest form of emulsion being either oil in water or a water in oil dispersion.<sup>[72]</sup> Surfactants are regularly used to aid in emulsifying dispersions and can be either ionic (cationic or anionic) or non-ionic in nature (**Figure 1.4**).<sup>[73]</sup> Ionic surfactants enable the formation of micelles through their positive or negative charge causing particle repulsion effects, thus stabilising the dispersion. Non-ionic surfactants are uncharged and stabilise dispersions through steric and polarity effects. Some classes of non-ionic surfactants include alcohol ethoxylates and alkylphenol ethoxylates, whose hydrophilic nature comes from the poly(ethylene oxide) water soluble polymer.<sup>[74-79]</sup>

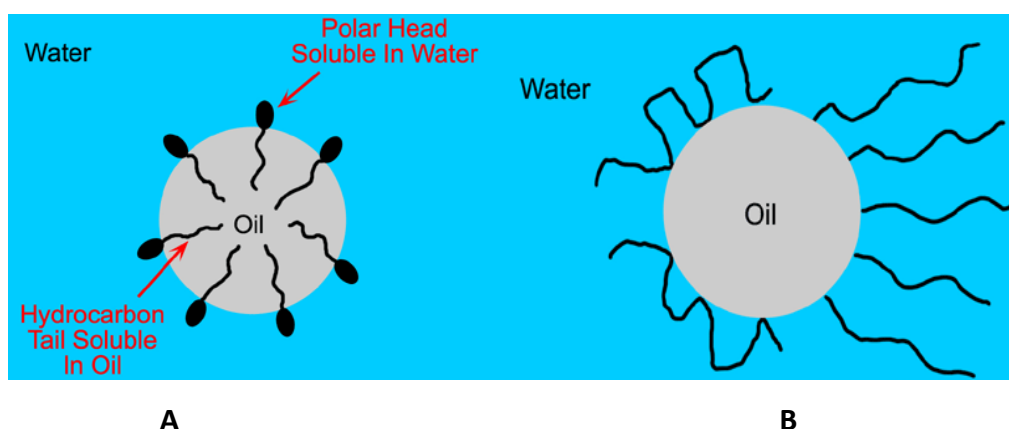


**Figure 1.4 Surfactant stabilisation of oil in water droplets through A) solubilisation and B) polymer adsorption<sup>[80]</sup>**

The appropriate surfactant is required to decrease the interfacial tension between oil and water and stabilise the droplet from coalescing with its neighbouring droplets.<sup>[81]</sup>

<sup>82]</sup> Determination of the most appropriate surfactant system for emulsification is made by considering the Hydrophilic-Lipophilic Balance (HLB).<sup>[72, 83, 84]</sup> HLB is a measure of the hydrophilic component of a surfactant relative to its lipophilic component. Low HLB (3-6) surfactants will normally form a water-in-oil emulsion, while high HLB (8-18) surfactants will tend towards an oil-in-water emulsion. For non-ionic surfactants, where the only hydrophilic group present is that of poly (ethylene oxide), the HLB number may be determined by **Equation (1-1)** where  $E$  represents the weight per cent of oxyethylene:<sup>[83]</sup>

$$HLB = \frac{E}{5} \quad (1-1)$$

Similar systems in the literature have been studied by Otsubo *et al.*<sup>[81]</sup>, Princen<sup>[85]</sup>, and Pal<sup>[82]</sup>. The oil fraction in oil-in-water emulsions is considered as the volume fraction of the dispersed phase which can range from 0-1, with emulsions formulated above a critical volume fraction, considered as high internal phase ratio emulsions.<sup>[82, 86]</sup> Below the critical value, the dispersed droplets are spherical in shape, however past the critical volume fraction; the droplets become deformed by their neighbouring particles existing as polyhedral shapes.<sup>[85]</sup>

Important parameters in the analysis of emulsions are the volume fraction of the dispersed phase, surfactant type, droplet size and ultimately, the stability over time.

The stability of an emulsion is characterised by its resistance to (**Figure 1.5**):<sup>[83, 87-90]</sup>

- creaming or sedimentation (formation of a concentration gradient of droplets within the emulsion without affecting the droplet size or distribution);
- flocculation, where a build up of droplets occurs within the emulsion with no change in droplet size;
- coalescence of flocculated droplets or droplets that have undergone sedimentation or creaming, changing the droplet size and distribution;
- phase separation, and
- Ostwald ripening, where the two phases aren't completely immiscible.

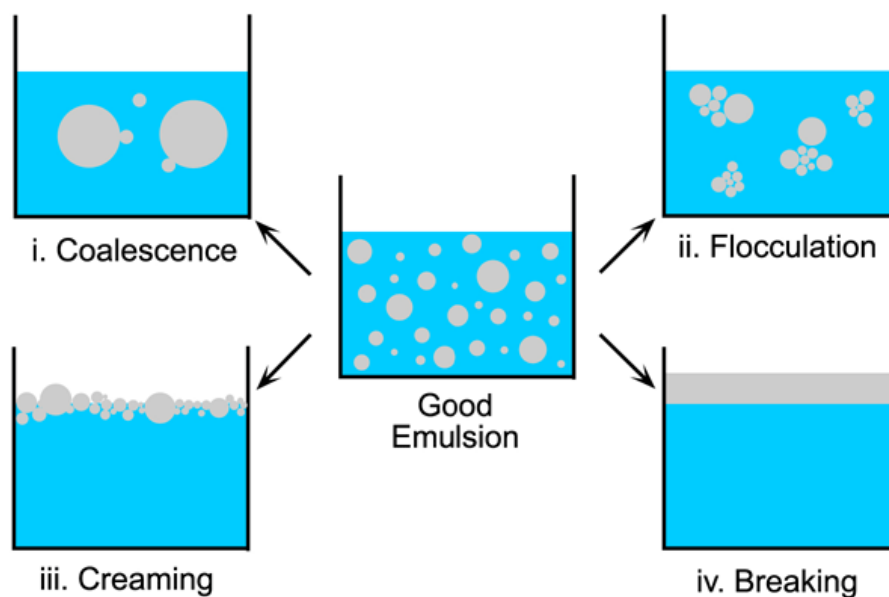


**Figure 1.5 Representation of emulsion stability<sup>[80]</sup>**

Prediction of the stability and degradation of emulsions is therefore extremely important in the determination of emulsion life. Characterisation methods suitable for developing emulsion formulations include; particle size analysis, zeta potential measurements, observation of emulsions for phase separation and creaming over time and emulsion stability. Measurement of emulsion stability is usually performed under centrifugation, whereby the interfacial tension strength is measured. However, rheological measurements such as viscosity behaviour and dynamic viscoelastic behaviour as a function of stress have also been used.<sup>[86, 87, 91, 92]</sup>

### 1.2.5 Kinetics of competing reactions: Presence of Water and the production of Carbon dioxide

The curing kinetics of the competing urethane and urea reactions in polyurethane systems containing water are complicated and have been extensively investigated.<sup>[10, 17, 93-96]</sup> Studies have focussed on various polyurethane systems using several quantitative analysis techniques such as FTIR spectroscopy<sup>[97, 98]</sup>, volumetric<sup>[32]</sup> and rheological techniques<sup>[35, 97, 99]</sup>. The reactions occurring in two-component waterborne polyurethanes are comparable to those in the product under investigation because of the competing urea/urethane chemistry. In the last 10 years, waterborne polyurethane coatings have become a primary focus of many investigations, in response to increased government restrictions on VOC levels.<sup>[100]</sup> The increased use of water-borne coatings has resulted in various kinetic studies, due to unwanted production of carbon dioxide gas being particularly problematic in coating applications.<sup>[10, 100, 101]</sup>

In waterborne systems, the polyol encapsulates the isocyanate after mixing, effectively emulsifying it. This results in an increase in the size observed in the mixed formulation and ensures that the preferred reaction with polyol dominates.<sup>[100, 102-104]</sup> The relative rates of solvent/water evaporation and curing of the polyurethane are important in waterborne systems. Hegedus *et al.*<sup>[30]</sup> suggested a timeline of events. Immediately upon addition and mixing, particle coalescence occurs between polyol and isocyanate, with their subsequent reaction within 2-5 hours, whilst the isocyanate-water reaction occurs at a slower rate and is delayed for more than two hours, as determined by isothermal calorimetry. Particle coalescence occurs 30 minutes after application of the coating to the substrate, as the evaporation of volatiles allows diffusion of polymer molecules across particle boundaries, increasing particle packing and favouring the isocyanate-polyol reaction.

Ihms *et al.*<sup>[10]</sup> and Jacobs *et al.*<sup>[103]</sup> also determined the isocyanate-water reaction is delayed, with the isocyanate-polyol reaction initially possessing a faster reaction rate. Despite this, the isocyanate-water reaction yields a primary amine, which is more reactive than hydroxyl functional groups (on the polyol) as discussed in section 1.2.1, resulting in the urea reactions dominating the crosslinking process.<sup>[33]</sup> In the presence of water, there is a rapid increase in molecular weight and viscosity due to

the reaction with isocyanate, increasing the crosslinking, which subsequently reduces the pot-life of the polyurethane mixture.<sup>[30]</sup>

Carbon dioxide evolution significantly affects film formation and properties upon curing.<sup>[17]</sup> The rate of carbon dioxide evolution and the rate of the polyol-isocyanate reaction can cause reaction bubble formation. Reaction bubbles are more apparent in coatings displaying a greater thickness, although, monitoring the cure conditions and air humidity enables this to be partially controlled.<sup>[100]</sup> The ability of carbon dioxide to diffuse through coatings is explained by the diffusion-controlled mechanism, whereby small molecules act as plasticizers to increase the number of reactions occurring within the polymer network providing greater free volume within the network.<sup>[98]</sup> Similar findings have been determined for different waterborne polyurethane systems, with these studies including the effect of relative humidity, solvent (H<sub>2</sub>O) evaporation and temperature on crosslinking.<sup>[17, 33, 98]</sup> These studies observed that an increase in the relative humidity, increases the amount of water retained by the film. This in turn reduces water evaporation from the film, thus increasing the probability of the water-isocyanate reaction producing more urea and carbon dioxide.<sup>[17, 103]</sup> Urban *et al.*<sup>[17]</sup> monitored the carbon dioxide gas band intensity at 2237-2239 cm<sup>-1</sup> and the isocyanate band intensity at 2275 cm<sup>-1</sup> throughout the reaction of waterborne polyurethane.<sup>[17, 33]</sup> Characteristic vibrational bands of carbon dioxide gas in the 1400-1300 cm<sup>-1</sup> regions verified the assignment of the asymmetric stretch of the carbon dioxide peak at 2339 cm<sup>-1</sup>.<sup>[33]</sup> As the reaction progressed, the isocyanate concentration decreased while the carbon dioxide concentration increased twice as fast as the reduction of isocyanate groups.<sup>[17, 98]</sup> The amount of carbon dioxide produced was attributed to several factors, including the amount of water retained in the film, the relative humidity surrounding the film and the amount of shear stress applied to the system during mixing.<sup>[17]</sup>

Ludwig *et al.*<sup>[98]</sup>, studied the kinetics of an ambient crosslinked acrylic urethane coating using the biuret of hexamethylene diisocyanate (HDI) as the crosslinker. The films were examined for extent of curing at both the film-air interface and the film-steel surface interface using FTIR in Attenuated Total Reflectance (ATR) mode. There was greater curing at the film-steel interface, as the solvent or water concentration was greater at this interface for longer periods of time, providing mobility of the isocyanate groups to react with alcohol groups to form urethane

linkages. The solvent molecules were hindered in movement through the film from the film-steel interface to the film-air interface after the first stage of crosslinking. The evaporation of solvent molecules at the film-air interface increased the viscosity of the film and hindered movement to the top layers. Kaminski *et al.* [33] also studied the effect of water evaporation during film formation. Weight loss of the control sample and polyurethane formulation at low relative humidities (5-10%) was identical for the first eight minutes. After eight minutes, the solvent system continued to evaporate at a high rate whilst the waterborne polyurethane slowed down. It was considered that during the first eight minutes, the evaporation was due to partial vapour pressure, subsequently becoming diffusion controlled [100]. As the relative humidity increased, more water was retained by the film, thus decreasing the isocyanate concentration. The reduction in isocyanate was attributed not only to the direct reaction with water, but also to the ability of water to act as a plasticizer, forming hydrogen bonds with the polar urethane carbonyl groups contained within the network. Water also formed hydrogen bonds with the amide of the urea and the hydroxyl groups of the polyol. These interactions interrupted the polymer network, increasing the free volume of the system and thus allowing the isocyanate groups to gain proximity to the polyol hydroxyl groups. The change in isocyanate concentration with respect to urea and urethane formation was also studied at three different depths by changing the angle of incidence at which infrared radiation enters the ATR crystal. The polyurea content increased in proportion to the increase in the depth of penetration. [100]

Kinetics of the isocyanate-water reaction were also established through volumetric methods, via the direct measurement of carbon dioxide evolution [20, 32]. Borsus *et al.* [20] studied the effect of monofunctional isocyanates (phenyl isocyanate) with water, whilst Ihms *et al.* [32] investigated a difunctional isocyanate (2,4-toluene diisocyanate), as it was representative of an industrial foam. The evolution of carbon dioxide followed first order kinetics with respect to water concentration, with only 72% of the theoretical carbon dioxide evolved over the range of water concentrations tested. This suggested that not all of the water was reacting, or that the reaction intermediate (carbamic acid) was not decomposing.

Temperature also influences the curing reactions in water-borne polyurethane films, with higher temperatures causing the water-isocyanate reaction to dominate over the

polyol-isocyanate reaction.<sup>[35, 100]</sup> The reduced extent of crosslinking between the polyol and isocyanate, causes a reduction in coating elasticity. Decreasing the cure temperature to 5 °C before adding a water dispersed reactant slows the water-isocyanate reaction.<sup>[27]</sup> Investigations employing isothermal calorimetry at 21 °C, suggest the isocyanate-polyol reaction begins almost immediately, whilst the isocyanate-water reaction is delayed for more than two hours at this temperature<sup>[30]</sup>. According to Ludwig *et al.*<sup>[101]</sup>, a reduction in the curing temperature extends the length of time of during which carbon dioxide is produced and increases the rate of carbon dioxide diffusion from the coating. Bittner *et al.*<sup>[100]</sup> postulated that increasing the temperature prior to the start of crosslinking allows the reactants in the aqueous phase to inter-diffuse to a higher extent.

From the above investigations, it is apparent that under ambient conditions the isocyanate-polyol reaction initially possesses a faster rate of reaction, with the isocyanate-water reaction dominating the curing process at later stages or at increased temperatures.

In the product under investigation the polyol-PMDI reaction is highly exothermic, which will increase the rate of the isocyanate-water curing reaction. Thus, investigation of the relative rates of reaction is of primary importance due to the higher functionality of moieties used in this coating system, in addition to the rate of carbon dioxide release, which may affect the polyurethane network formation during cure.

### 1.2.6 Catalysts

Compounds used to promote urethane reactions are generally nucleophilic catalysts such as tertiary amines and the salts of weak acids. Suitable electrophilic catalysts are organometallic compounds.<sup>[13, 25]</sup>

Cement based polyurethane coatings possess an in-built catalytic mechanism when one of the reactant components (either the polyol or isocyanate) is water dispersed. When hydrated, the complex silicates in cement (further detailed in section 1.2.8) form large quantities of hydroxide anions, which act as a nucleophilic catalyst.<sup>[27]</sup>

Catalysts have also been used to promote urea over urethane linkage formation or vice versa. Extensive work has been performed to investigate catalysis of the urea reaction in polyurethane foams.<sup>[10, 20, 32, 37, 105]</sup> However, urea formation is an

unwanted side reaction in some applications, as the carbon dioxide produced causes gassing and foaming, leading to a low gloss and reduced pot life due to a rapid increase in molecular weight and viscosity.<sup>[33]</sup>

The selectivity and catalytic activity of the catalyst used for the isocyanate-polyol reaction or the isocyanate-water reaction is determined by its molecular structure.<sup>[25]</sup>

An example of a tertiary amine catalyst which is selective for the isocyanate-water reaction and has been used in the blowing of foams is, N, N'-dimorpholinodiethyl ether (DMDEE). DMDEE contains five potential hydrogen-bonding sites with a high coordination number for water, allowing water to be in close proximity to the active amine centres. Bis(2-dimethylaminoethyl) ether (BDMAEE) is also highly selective for use in foam formation, but it does not provide as many hydrogen bonding sites as DMDEE. However, BDMAEE allows greater access to the isocyanate-polyol molecules because of less steric hindrance to its nitrogen centre. Tertiary amine catalysts that possess high selectivity for the isocyanate-polyol reaction include triethylene diamine (TEDA), 1,4-diazabicyclo[2.2.2]octane (DABCO) and N,N, N', N'', N''-pentamethyldipropylene triamine. These compounds have fewer sites for chelation of water, are less sterically hindered and are able to bind the larger isocyanate-polyol complex.<sup>[25]</sup>

Organo-tin compounds such as dibutyltin dilaurate (DBTDL), dibutyltin didodecylmercaptide and diisooctyltin diisooctylmercaptoacetate have been used to catalyse isocyanate-polyol reactions. The latter two of these compounds are delayed-action catalysts. Tin mercaptides are usually employed in waterborne systems due to their resistance to hydrolysis. Combinations of tertiary amine and tin catalysts have also been used due to their synergistic action, which conserves the amount of catalyst used.<sup>[25]</sup>

Recently, it has been reported that organo-zirconium catalysts promote preferential selectivity for the isocyanate-polyol reaction for two component waterborne coatings.<sup>[106, 107]</sup> Gas chromatography and titration techniques have been used by Ni *et al.*<sup>[108]</sup> to show that for hexyl isocyanate in the presence of water, only urea formation results with the use of conventional catalysts such as p-toluene sulfonic acid monohydrate (p-TSA), DABCO and DBDL.

In the present project, addition of selective catalysts for the polyurethane reaction is not considered an option. A major disadvantage of using a catalyst is the increased

cost. This alteration to the formulation would not make it an economically viable solution for the industries involved. The large excess of alkali present in the cement fillers in the reaction mix also renders the addition of other catalysts relatively ineffective.

### **1.2.7 Theory of Reaction Kinetics**

In order to better understand the product under investigation, a fundamental understanding of the reaction rates and cure profile is required. Polyurethane thermoset curing utilising monomeric or diisocyanate compounds has been widely investigated [8, 11, 63, 109-114], although little work has been reported using oligomeric isocyanates with trifunctional polyols.<sup>[15, 62, 115]</sup> Characterisation of kinetics through complimentary techniques has become increasingly important in understanding the curing of polyurethane coatings.<sup>[116-118]</sup> Thermoset curing reactions have been extensively studied using three main techniques; Differential Scanning Calorimetry (DSC), rheology and infrared spectroscopy.<sup>[42, 119-121]</sup> The reaction theory for each technique is discussed below.

#### ***1.2.7.1 Thermal techniques***

Thermal methods, such as DSC, are considered to be indirect methods of measuring the reaction rate. Using DSC, the extent of reaction is determined by measuring the change in heat flow. This is a convenient method to use, however it is only suitable for prolonged polyurethane reactions, as the heat evolved during mixing and sample preparation is unable to be monitored.<sup>[122]</sup> DSC has been widely used to study thermoset reactions in both isothermal and non-isothermal modes.<sup>[111, 123-127]</sup> Isothermal analysis is performed by monitoring the heat flow at a constant cure temperature, with the kinetic parameters such as activation energy, reaction order and rate constant obtained through the evaluation of data at several different isothermal temperatures.<sup>[128]</sup> Kinetic analysis by DSC assumes the amount of heat generated from a reaction ( $\Delta H_T$ ) is directly proportional to the degree of cure (or the extent of reaction) and therefore the rate of cure ( $da/dt$ ) can be related to the heat generated by **Equation (1-2)**.<sup>[129]</sup>

$$\frac{d\alpha}{dt} = \frac{1}{\Delta H_T} \frac{dH}{dt} \quad (1-2)$$

where  $dH/dt$  is the differential heat flow during cure.

In isothermal mode, the total heat ( $\Delta H_T$ ) is given by **Equation (1-3)**:

$$\Delta H_T = H_{iso} + H_{res} \quad (1-3)$$

where  $H_{iso}$  is the isothermal heat of reaction and  $H_{res}$  is the residual heat taken from the area under a non-isothermal run performed after the isothermal run.

By using the partial integrals at time equals zero to time equals  $t$ , the conversion can be determined using **Equation (1-4)**:

$$\alpha = \frac{\int_0^t \frac{dH}{dt} dt}{\Delta H_T} \quad (1-4)$$

where  $\alpha$  is the conversion at time  $t$ .

The non-isothermal method for DSC measurement is performed by monitoring the heat of reaction at a constant heating rate. By using the same initial composition and obtaining data at several different heating rates, the kinetic parameters can be evaluated.<sup>[128]</sup> In non-isothermal mode,  $\Delta H_T$  is the total heat per gram of mixture, which is determined by measuring the area underneath the exotherm. The ratio of partial area over total area thus corresponds to a certain degree of conversion, assuming one of the reactants has been completely consumed. Consequently the ratio of partial area over total area under the exotherm is equivalent to the ratio of partial enthalpy over total enthalpy as in **Equation (1-5)**.<sup>[130]</sup>

$$\alpha = \frac{H_{partial}}{\Delta H_T} \quad (1-5)$$

The reaction enthalpy for polyurethane systems has been reported in the literature to range from -69 to -90 kJ mol<sup>-1</sup> equivalent isocyanate.<sup>[115, 122]</sup> Analysis of reaction rates using the rate of heat evolution assumes that there is only one rate-determining step and so the rate is not affected by changes in the reactant concentration.<sup>[118]</sup>

A general approach in determining the conversion function for thermoset reactions, ensuring that the model is truly phenomenological, is achieved by assigning the cure rate to a conversion-dependence function multiplied by the reaction rate constant  $k$ , given by the Arrhenius equation, shown respectively in **Equations (1-6)** and **(1-7)**.

$$\frac{d\alpha}{dt} = kf(\alpha) \quad (1-6)$$

$$k = A_0 \exp\left(\frac{-E_a}{RT}\right) \quad (1-7)$$

Where  $\alpha$  is the conversion and  $k$  is the rate constant.  $A_0$  is the pre-exponential constant,  $E_a$  is the apparent activation energy,  $R$  is the gas constant and  $T$  is the absolute temperature.

It is well known that polyurethane curing reactions follow  $n^{\text{th}}$ -order kinetics where  $n$  is equivalent to two giving a second order cure rate expression shown in **Equation (1-8)**:<sup>[122, 130]</sup>

$$\frac{d\alpha}{dt} = k(1-\alpha)^n \quad (1-8)$$

where  $n$  is the reaction order with the other variables as above.

The simple  $n^{\text{th}}$  order kinetics predicts the maximum reaction rate will occur at  $t = 0$  for an isothermal process.

For non-isothermal kinetic evaluation, the Borchardt-Daniels expression (**Equation (1-9)**)<sup>[131]</sup> has been applied in the calculation of activation energy, frequency factors and reaction order. It requires only a single DSC thermogram, and has been applied to polyurethane systems by Hernandez-Sanchez *et al.*<sup>[130]</sup> through a slight

modification of **Equation (1-9)** to relate the heat flow to the rate of conversion (**Equation (1-10)**).

$$\frac{dH}{dt} = k(A_t - A_p)^n e^{-E/RT} \quad (1-9)$$

Where  $dH/dt$  is the enthalpy change with respect to time,  $k$  is the rate constant at a constant heating rate, and  $A_t$  and  $A_p$  are the total and partial areas under the thermogram.

$$\frac{d\alpha}{dt} = k(1 - \alpha)^n e^{-E/RT} \quad (1-10)$$

Where  $d\alpha/dt$  is the conversion rate and  $\alpha$  is the conversion, derived from a single thermogram.

Hernandez-Sanchez *et al.* <sup>[130]</sup> also applied this equation with some success, using two or three different heating rates in order to determine the activation energy and reaction order by equalising the rate of conversion. They determined that equalising the conversion rates was the only way to evaluate the kinetic parameters in the polyurethane system (2,6-TDI and DEG) while equalising the conversion did not yield any results for that system. However, for a similar system (2,4-TDI/polyol), equalising the conversions and not the conversion rate allowed the kinetic parameters to be evaluated. They observed the difference in reactivity of the isocyanate groups, complexity of the reactions and the heating rate would determine which method was applicable.

Hernandez-Sanchez *et al.* <sup>[132]</sup> developed a more accurate way to determine the reaction order, activation energy and the Arrhenius prefactor from a manipulation of the form of the Arrhenius equation used by Hager *et al.* <sup>[133]</sup> by employing an equalization process of the conversion rate using the simple  $n^{\text{th}}$  order expression. Using the Arrhenius equation in the form shown in **Equation (1-11)** with the application of two heating rates, the reaction order could be calculated and used to determine the activation energy.

$$\frac{\ln \frac{d\alpha}{dt}}{(1-\alpha)^n} = \frac{-E}{RT} + \ln(K_0) \quad (1-11)$$

Where  $d\alpha/dt$  is the conversion rate,  $\alpha$  is the conversion,  $R$  is the universal gas constant,  $T$  is the temperature,  $E$  is the activation energy,  $K_0$  is the Arrhenius prefactor and  $n$  is the reaction order. The data used to calculate the kinetic parameters from this method were manipulated to exclude the beginning and endpoints of the temperature range.<sup>[132]</sup>

If the maximum cure rate for the reaction is found to be at  $t \neq 0$ , then  $n^{th}$  order kinetics do not hold and the reaction is considered to be autocatalytic with two rate constants and two reaction orders as described by Kamal's model<sup>[120]</sup>. Kamal *et al.*<sup>[134-136]</sup> proposed the following empirical kinetic expression (**Equation (1-12)**) for the rate of curing of autocatalytic thermosetting resins.

$$\frac{d\alpha}{dt} = (k_1 + k_2\alpha^m)(1-\alpha)^n \quad (1-12)$$

Where  $k_1$  and  $k_2$  are rate constants that are temperature dependant according to the Arrhenius expressions below, and  $m$  and  $n$  are constants whose sum is equal to the reaction order.

$$k_1 = A_1 \exp\left(\frac{-\Delta E_1}{RT}\right), \quad k_2 = A_2 \exp\left(\frac{-\Delta E_2}{RT}\right) \quad (1-13)$$

$A_1$  and  $A_2$  are pre-exponential factors,  $\Delta E_1$  and  $\Delta E_2$  are activation energies,  $R$  is the gas constant and  $T$  is the absolute temperature.

If the initial cure rate is close to zero then  $k_1$  is assumed to be zero and the rate of cure is described by **Equation (1-14)**:

$$\frac{d\alpha}{dt} = k\alpha^m(1-\alpha)^n \quad (1-14)$$

This form of the autocatalytic model has previously been used to describe polyurethane cure, as the carbamate groups formed have autocatalytic properties.<sup>[68, 137, 138]</sup>

Another approach in determining kinetic profiles is through the use of isoconversional methods (model-free kinetic analysis). Isoconversional methods are useful because a variety of kinetic models yielding different reaction variables such as activation energy, reaction order etc., have been shown to fit the same experimental data.<sup>[139, 140]</sup> During polyurethane polymerisation, several reactions are apparent, because of differing reactivities of functional groups or secondary reactions that occur at higher temperatures or during extended periods of curing.<sup>[25, 52]</sup> Despite the reaction complexity, many authors studying polyurethane reactions assume one reaction model describes the entire cure process.<sup>[8, 56, 67, 112, 138]</sup> The activation energy and other kinetic parameters such as the rate constant and reaction order are assumed to remain constant throughout the entire cure.

Isoconversional methods suggest that if the apparent activation energy changes with conversion then the reaction mechanism is complex and can be used to describe the physical curing process of the reacting system.<sup>[141]</sup> The most popular isoconversional methods used are that of Flynn, Wall and Ozawa.<sup>[131]</sup>

Ozawa developed an expression to evaluate activation energy based on the use of multiple heating rates and is shown in **Equation (1-15)**.<sup>[131]</sup>

$$d \log \phi / d(1/T_p) = -0.4567 E_a / R \quad (1-15)$$

Where  $\phi$  is the heating rate in  $^{\circ}K/min$  and  $T_p$  is the peak temperature of the reaction exotherm.

The Ozawa expression above, contains a factor of 0.4567 determined from mathematical deduction<sup>[131]</sup>. The temperature ( $T_i$ ) is obtained from several thermograms at different heating rates at temperatures with equal conversion. This method works well for single step processes, as the activation energy does not change with conversion, although, can be used as a reasonable approximation for

multi-step processes.<sup>[142]</sup> A major advantage of using this expression, compared to the Borchardt -Daniels expression and the method developed by Hager *et al.*<sup>[133]</sup>, is that the reaction order is not needed to determine the activation energy.

It is also possible to obtain kinetic parameters such as apparent activation energy ( $E_a$ ) from **Equation (1-16)** at a fixed conversion for isothermal data, by using an integral isoconversional method.<sup>[143]</sup> Integrating **Equation (1-6)** for a fixed conversion, such as at the gel point; an expression for time is obtained, as the terms in square brackets are constant and represented by  $A$  (**Equation (1-17)**).<sup>[119, 144]</sup> The activation energy can therefore be determined from the slope of the linear relationship  $\ln t$  vs.  $T^{-1}$ . The dependence of the activation energy on the degree of conversion may also be determined using **Equation (1-17)**.

$$\ln t = \frac{E_a}{RT} + \left[ \ln \left( \int_0^a \frac{d\alpha}{f(\alpha)} \right) - \ln(k_0) \right] \quad (1-16)$$

$$\ln t_{\alpha,i} = A + \frac{E_a}{RT_i} \quad (1-17)$$

Vyazovkin<sup>[145, 146]</sup> states that determination of the kinetic triplet of activation energy, reaction order and rate constant is not required to understand an applied kinetic process and to predict what will occur at varying temperatures and times. Understanding how the activation energy changes with conversion provides information on how the cure progresses.<sup>[141]</sup> The advanced integral isoconversional method developed by Vyazovkin<sup>[145]</sup>, states that at a constant conversion, the reaction rate is only a function of temperature and allows the activation energy to be determined without choosing a reaction model. The kinetic equation used in the advanced integral isoconversional method, **Equation (1-6)**, changes to **Equation (1-18)** when non-isothermal data is used.

$$\frac{d\alpha}{dT} = \frac{A}{\beta} \exp \left( \frac{-E_a}{RT} \right) f(\alpha) \quad (1-18)$$

Where  $\beta = dT/dt$  is the heating rate.

The integral form of the reaction model is represented in **Equation (1-19)**.

$$g(\alpha) = \left(\frac{A}{\beta}\right) \int_0^T \exp\left(\frac{-E_\alpha}{RT}\right) dT = \left(\frac{A}{\beta}\right) I(E_\alpha, T) \quad (1-19)$$

The integral  $I(E_\alpha, T)$  is approximated by a function  $p(x)$ , where  $x = E_\alpha/RT$  and  $p(x)$  is represented by the Senum-Yang approximation (**Equation (1-20)**).<sup>[141, 147]</sup>

$$p(x) = \frac{e^{-x}}{x} \frac{(x^2 + 10x + 18)}{(x^3 + 12x^2 + 36x + 24)} \quad (1-20)$$

In the advanced integral isoconversional method, a set of experiments  $n$  performed at varying heating rates and or temperatures are used to determine the activation energy by minimizing the function in **Equation (1-21)** for constant heating rates.<sup>[141]</sup>

$$\sum_i^n \sum_{j \neq i}^n \frac{[I(E_\alpha, T_{\alpha, i})\beta_j]}{[I(E_\alpha, T_{\alpha, j})\beta_i]} = \min \quad (1-21)$$

In isothermal experiments, the integral is performed over small time intervals where the integral is represented by  $J(E_\alpha, T(t_\alpha))$  and is given in **Equation (1-22)**.<sup>[141]</sup>

$$J(E_\alpha, T_i(t_\alpha)) = \int_{t_{\alpha-\Delta\alpha}}^{t_\alpha} \exp\left(\frac{-E_\alpha}{RT_i(t)}\right) dt \quad (1-22)$$

### 1.2.7.2 Rheological techniques

Rheological techniques have been widely used in conjunction with thermal and spectroscopic methods to elucidate the cure mechanism of reactions.<sup>[35, 56, 99, 110, 129, 148-161]</sup> The rheological investigation of thermosets, identifies critical points of conversion, such as at the gel point and the onset of diffusion control kinetics from chemically controlled kinetics.<sup>[155]</sup> Gelation is a critical component in thermosetting systems as it describes the formation of an infinite molecular network and the commencement of the cross-linking reaction.<sup>[119, 125, 162]</sup> It is important in industrial applications, as the gel time is the point where polymers will no longer flow and also determines the pot-life and processability of the curing system.<sup>[160]</sup> The gel point is a

non-reversible process whereby a constant conversion is achieved.<sup>[163]</sup> This largely depends on the functionality distribution of the monomers and the reactivity of the functional groups.<sup>[16, 113]</sup> Consequently, changing these parameters affects the reaction kinetics and subsequently the pot-life of the polymeric coating.

The most widely accepted criterion to determine the gel point is the frequency independence of  $\tan \delta$ .<sup>[148, 161, 162, 164, 165]</sup> However, it is believed that gelation is a process which stems over a period time and that different criteria can be used to elucidate the gel time, especially when gel particles and fractions appear before the entire sample gels.<sup>[166]</sup> Laza *et al.*<sup>[167-170]</sup> proposed several methods to determine the gel point during isothermal cure, because in some cases, it is not possible to detect gelation by a certain criterion depending on the instrumentation, variables used and curing system studied. Other criteria employed to determine the gel time include:

- The maximum peak in  $\tan \delta$  due to the maximum difference between the elastic and viscous behaviour.<sup>[164]</sup>
- The crossover between  $G'$  and  $G''$ <sup>[119]</sup>
- Tangent line to  $G'$  (where the tangent to  $G'$  at a value of 100 kPa is drawn back to the baseline where  $G'=0$ )<sup>[169]</sup>
- Where the viscosity reaches several determined values (1000, 2000 and 5000 Pa.s)<sup>[171]</sup>
- Frequency dependence of  $G'$  at 1 Hz<sup>[169, 172]</sup>
- Extrapolation of steady state viscosity to infinite viscosity<sup>[127, 173]</sup>

Rheological investigations have also been employed to follow viscosity build up in polyurethane systems.<sup>[16, 113]</sup> Following the build up of viscosity of polyurethane polymerisation further increases our understanding of the curing profile. Viscosity increase in a system is due to an increase in molecular weight from the reaction between functional groups.<sup>[9, 55, 57, 174]</sup> When higher functional moieties ( $\geq 3$ ) are present in the monomers, chain branching will occur, providing a rapid increase in molecular weight.

Piao *et al.*<sup>[35]</sup>, investigated the progress of crosslinking of a waterborne polyurethane through rheological studies. It was reported that when crosslinking occurs, the network structure develops and can thus be broken by the applied shear stress causing shear thinning. Once the structure develops, yielding occurs. The elasticity

( $G'$ ) of the system was found to increase when the reaction between the polyol and polyisocyanate predominated, forming network structures. An increase in isocyanate concentration reduced the viscosity build up of the reacting polyurethane.

Empirical relationships of the viscosity build up in polyurethane systems have previously been applied.<sup>[16, 56, 113, 175-177]</sup> The viscosity of the curing polymer can be described by a first order exponential function shown below (**Equation (1-23)**):

$$\eta_t = \eta_0 e^{kt} \quad (1-23)$$

where  $\eta_0$  is the viscosity at  $t = 0$  and  $k$  is the rate constant for viscosity build up.

The rate of viscosity build up has been shown to follow a first order process for some polyurethane systems and deviates from linearity when the process is diffusion controlled or when there are varying reactivities of functional groups.<sup>[16]</sup>

Diffusion control (vitrification) occurs when the polymer is cured at an isothermal temperature below its glass transition temperature ( $T_g$ ). Similar to gelation, vitrification can be detected through changes in the dynamic mechanical properties, however, vitrification is a gradual thermo-reversible process.<sup>[172]</sup> A common method in determining the vitrification time of a system is through the peak in  $\tan \delta$  at 1 Hz.<sup>[127, 162, 172, 178-180]</sup> Other accepted criteria for the identification of diffusion control, include the point of viscosity divergence, frequency independence of  $G'$  and the appearance of a peak in  $G''$ .<sup>[127, 162]</sup>

### 1.2.7.3 Spectroscopic techniques

FTIR analysis of polyurethane reactions is a direct method of measuring the concentration of a functional group on a reactant and hence the concentration of the reactant. FTIR has been used to monitor several chemical changes simultaneously.<sup>[181-184]</sup> FTIR analysis employs Beer Lambert's Law, which correlates the concentration of a functional group with the band intensity by calculating the molar absorption coefficient (**Equation (1-24)**).

$$A = \varepsilon l c \quad (1-24)$$

Where  $A$  is Absorbance,  $\varepsilon$  is the extinction coefficient,  $l$  is the path length of beam and  $c$  is the concentration.

The conversion can thus be obtained from the spectral peak areas (**Equation 1-25**)<sup>[150]</sup>

$$x(t) = \frac{A(0) - A(t)}{A(0)} \quad (1-25)$$

Where  $x(t)$  is the conversion at time  $t$ ,  $A(0)$  is the area of the initial isocyanate peak in the mixed sample,  $A(t)$  is the area of the isocyanate peak at time  $t$ .

Ritcher and Macosko<sup>[31]</sup>, utilised FTIR as a qualitative analytical tool to study urethane kinetics. They employed an overall  $n^{\text{th}}$  order rate expression (**Equation 1-26**) previously employed by Lipshitz *et al.*<sup>[185]</sup> to define urethane polymerisation. Reported values of  $n$  ranged from 1.5-2, with most investigations assuming a second order reaction.<sup>[31, 130, 185]</sup>

$$r_a = k c^n \quad (1-26)$$

Where  $k = A e^{-E/RT}$

The rate of reaction for polyurethane systems has been shown to follow an Arrhenius rate equation due to the liquid phase present.<sup>[185]</sup> The rate of consumption of isocyanate groups can also be described by **Equation (1-27)**.

$$\frac{d[NCO]}{dt} = -k[NCO]^a[OH]^b \quad (1-27)$$

Where  $k$  is the rate of reaction and given by the Arrhenius equation.

The polyurethane reaction is quite complex and several reactions may occur simultaneously (as detailed in section (1.2.1)).<sup>[122]</sup> Parnell *et al.*<sup>[122]</sup> and Hentschel *et al.*<sup>[186]</sup>, discussed possible urethane dissociation reactions that may occur over 100 °C for some polyurethane systems. The rate of reaction described by the Arrhenius model can thus be considered as an average rate for polyurethane polymerisation reactions and has been applied with success.<sup>[130]</sup>

Urban *et al.*<sup>[45]</sup> employed FTIR in transmission and ATR mode to analyse polyurethane systems, taking into account the effects of water. FTIR showed that as isocyanate groups were consumed, the band at 2270 cm<sup>-1</sup> decreased and as urethane linkages were formed, the bands at 1518 cm<sup>-1</sup> (N-H) and 1145 (C=O) cm<sup>-1</sup> increased in intensity.<sup>[187, 188]</sup> Two requirements are needed to quantitatively measure isocyanate concentration through spectroscopic means; a calibration curve needs to be constructed that relates the band intensity to the concentration of the functional groups and secondly the spectra need to be corrected for optical effects.<sup>[189]</sup>

ATR-FTIR is a good technique to identify the progress of urethane/urea formation, however only the first 1.14 µm depth of the cured coating can be studied and therefore crosslinking times of bulk polyurethane materials may vary.<sup>[17]</sup> NIR-spectroscopy is a non-intrusive real-time method used to determine conversion profiles of the hydroxyl component of polyurethane reactions during reactive injection molding.<sup>[190]</sup>

The use of Raman spectroscopy as an analytical tool for polyurethane reactions, was investigated due to its ease in sample preparation. Raman is a scattering technique and samples of any shape and size can be examined. Isocyanate conversion was analysed according to **Equation (1-27)** by expressing the concentration in terms of conversion and solving the differential equation by the separation of variables technique. Least squares linear regression was then used to apply the Arrhenius kinetic model to the data. Reaction orders and activation energy data obtained through Raman spectroscopy compared well to those achieved by isothermal DSC measurements for the polyurethane reaction.<sup>[122]</sup>

### 1.2.8 Fillers

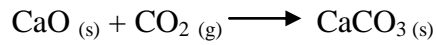
Fillers are often added to polyurethane-based formulations to improve the physical properties of coatings and foams, or to add bulk to the coating and lower the final costs. Typical fillers used in foams and elastic materials include carbon black, hydrated alumina, carbonates, silicates, silica, mineral fillers, glass fibres and cement.<sup>[13]</sup>

Cement is discussed here in more detail due to its application in the project of interest. The third component of cement-based polyurethane coatings consists of the cement plus inert aggregate. The complexity of the reaction kinetics increases when one of the components of the polyurethane formulation is water-dispersed, due to cement hydration (refer to discussion below). The composition of a typical cement plus aggregate mixture is shown in **Table 1-1**.<sup>[27]</sup> Portland cement comprises up to 15% of the cement aggregate, with the remainder being lime and a mixed graded aggregate.

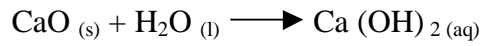
**Table 1-1 Cement/Aggregate Filler for Polyurethanes**<sup>[27]</sup>

<b>Ingredient</b>	<b>Weight %</b>
Mixed graded aggregate	78
Portland Cement	15
Lime	7

The mixed graded aggregate provides the bulk filler that extends the coating volume. Portland cement undergoes reactions when hydrated to increase the cure strength of the coating and to improve the coating's physical properties. Setting of the cement requires the formation of calcium silicate hydrates and calcium carbonate to provide increased strength.<sup>[191, 192]</sup> The lime present in the aggregate helps to control cement hydration. Lime also absorbs a fraction of the carbon dioxide evolved from the reaction between isocyanate and water according to **Scheme 1.10** and **Scheme 1.11**.<sup>[27]</sup>



**Scheme 1.10 Calcium carbonate formation**



**Scheme 1.11 Calcium hydroxide formation from calcium oxide**

The molecular composition of Portland cement is detailed **Table 1-2**<sup>[193]</sup>, while the silicate compositions are presented in **Table 1-3**.<sup>[194]</sup> The most abundant form of calcium oxide in cement is CaO.SiO<sub>2</sub> at 42%, while the amount of free CaO is only 0.9%.

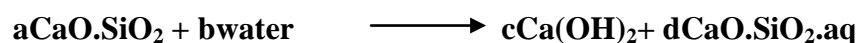
**Table 1-2 Portland cement molecular composition**<sup>[194, 195]</sup>

<b>Composition</b>	<b>%</b>
CaO	64.1
SiO <sub>2</sub>	22.90
Al <sub>2</sub> O <sub>3</sub>	4.5
Fe <sub>2</sub> O <sub>3</sub>	3.11
MgO	0.79
TiO <sub>2</sub>	0.24
Na <sub>2</sub> O	0.54
K <sub>2</sub> O	0.64
SO <sub>3</sub>	2.37
Loss	0.81
	100.00

**Table 1-3 Portland cement Silicate Compositions<sup>[194]</sup>**

<b>Compounds as present in Cement</b>	<b>%</b>
4CaO.Al <sub>2</sub> O <sub>3</sub> .Fe <sub>2</sub> O <sub>3</sub>	9.5
3CaO.Al <sub>2</sub> O <sub>3</sub>	6.7
3CaO.SiO <sub>2</sub>	42
2CaO.SiO <sub>2</sub>	34
Free CaO	0.9
CaSO <sub>4</sub>	4
Loss	2.9

Upon hydration, the main reaction that occurs in Portland cement is shown in **Scheme 1.12**, where calcium hydroxide is formed and the less basic calcium silicate hydrate gel remains.

**Scheme 1.12 Hydration of calcium oxide silicates in cement**

When the solution is saturated with calcium hydroxide, hydration of the calcium oxide silicate continues with the calcium hydroxide formed, deposited as crystals. The remaining hydrated calcium oxide silicate is in equilibrium with the dissolved calcium hydroxide and is stable in contact with the saturated lime solution. Thus, when more water is added, further solubilisation occurs, raising the concentration of calcium hydroxide in solution where it restabilises in its silicate form.<sup>[194]</sup> The amount of calcium hydroxide released from the hydration reaction depends on the water: solid ratio, temperature and the cement particle size distribution.<sup>[196-199]</sup> Studies have also shown that the relative humidity affects the hydration rate during cure.<sup>[193, 200]</sup>

To determine the amount of calcium hydroxide evolved during the hydration process, solvent extraction can be used, however this method yields the total free calcium oxide and hydroxide present in cement. The amount of calcium hydroxide can also be determined by Thermo-Gravimetric Analysis (TGA) through monitoring water

loss at two different temperatures, corresponding to the combination of water associated with silicates and calcium hydroxide, respectively. The quantity of free calcium hydroxide can be determined as the mass loss in the temperature range 460-560 °C and the loss of carbon dioxide from calcium carbonate can be observed in the range 720-920 °C.<sup>[191, 201, 202]</sup> X-ray methods can also be used to determine free calcium hydroxide content, however much lower values are obtained than those from the solvent extraction method.<sup>[194]</sup>

Concrete structures are susceptible to alkali-silica reactions, which occur when alkalis from the mixture or external sources increase the hydroxyl ion content, catalysing the dissolution of silica.<sup>[203, 204]</sup> Once silica is in solution it precipitates, forming alkali-silica gels that are able to hydrate in the presence of water causing swelling. This swelling causes internal pressure in the concrete structure leading to crack formation and propagation, thus reducing the mechanical strength and properties of concrete. To avoid this, non-reactive aggregates, low-alkali cement and lower water: cement ratio are used. The amount of cement is important as it is the reactive aggregate that provides a high alkaline internal environment.<sup>[203]</sup>

### **1.3 Aim and Scope**

A review of the available literature reveals that the blistering and delamination of coating systems due to carbon dioxide evolution in polyurethane coating formulations is very apparent; however, these coating systems comprise of thin films with little work focusing on cement composite polyurethane formulations. Although blending of castor oil and glycerol has been studied for reducing moisture absorption and improving mechanical properties of thermo-moulded plastics, not much work has been published on using this blend in thermoset polyurethane composite coatings, for reduction in carbon dioxide evolution and ultimately unwanted blistering.

Current solutions to reduce carbon dioxide formation in thin film coatings reside in the use of catalysts to ensure that the crosslinking reaction between isocyanate and polyols is the preferred reaction, minimising the water-isocyanate reaction and therefore carbon dioxide production. In the present project, catalysts have not been considered as a solution to the blistering problem due to the economic viability and implementation for the industry partner. The use of multifunctional reactants also makes the use of catalysts less desirable, as the polyurethane reaction proceeds at a fast rate at standard conditions. However, a more attractive and economical route to reduce the carbon dioxide evolution is achieved by the addition of a slower reacting polyol; glycerol, to the product formulation. In addition, using this process requires no additional equipment or processing step for manufacturing, which in turn, means the use of existing resources without new investments.

From a scientific viewpoint, the use of glycerol, which has a very slow reacting secondary hydroxyl, in addition to castor oil (currently used) has a two fold effect on the curing reaction; to increase the crosslinking and minimise the water-isocyanate reaction. Thus, the aim of this work is to improve the composite coating performance through the reduction of carbon dioxide evolution, with one solution being the addition of a second polyol, glycerol.

The cement composite coating investigated in this thesis consists of multifunctional reactants as opposed to many kinetic studies focussing on mono or difunctional reactants. Currently, no systems are present in the literature which completely characterise the reaction of an oligomeric diisocyanate with tri-functional polyols.

For this reason, it was of fundamental and technical importance to study the reactive system of the product under investigation using a combination of thermal, rheological and spectroscopic techniques.

Many thermoset reactions have been extensively investigated through DSC and rheology, determining reaction rates, activation energies and reaction orders. These systems have been analysed through the application of kinetic models, even though a number of differing models can fit the same experimental data. The approximation of a single reaction model may suffer in general applicability because of varying activation energies throughout the cure process. However, for the sake of simplicity and having a general idea of the kinetic data and activation energy, many researchers still use the model based approach.

In contrast, Vyazovkin's isoconversional method (as introduced in section **1.2.7.1**) states that conversion is only a function of temperature, and therefore the reaction mechanism of complex systems can be evaluated without assuming reaction variables. Little work exists in the literature describing complex polyurethane cure using Vyazovkin's advanced integral isoconversional method, thus, it was of fundamental importance to describe the polyurethane reactions using isoconversional methods and to compare this technique to the most commonly used kinetic models for polyurethane systems.

Furthermore, in the coating formulation a significant amount of variables exists which could affect the coating performance. The cure chemistry in the entire formulation is very complex. Reactions exist between the isocyanate and the polyol, isocyanate and the water, as well as the reactions between water in the polyol emulsion and the cement and lime fillers and the reaction of cement and lime with carbon dioxide evolved through the water-isocyanate reaction. A number of variables can affect the reaction rate and curing progression of this coating system, including concentration of components in the polyol emulsion, viscosity effects, particle size distributions of the aggregate and environmental factors affecting reactants and their subsequent curing, such as relative humidity and temperature. Very little is known on the influence of all these variables on the coating performance during application and cure. Thus, the present study was undertaken with the following major goals:

- Identify the cause of blistering.
- Develop a carbon dioxide measurement apparatus to compare formulations.

- Evaluate the reaction kinetics of the multifunctional polyols and water with the commercial diisocyanate resin.
- Characterise systematically the coating composition by changing concentrations of coating components and determining their affect on carbon dioxide evolution, as well as their affect on the stability of the reactants and ease of coating application.
- Determine an economically viable solution for easy implementation by the industry partner

The scope of the project was divided into two overlapping sections of fundamental and applied research in order to solve the blistering problem of the coating as shown in **Figure 1.6**.

Due to the complexity of the composite coating, the cure chemistry for the polyurea and polyurethane reactions were investigated individually with reference to the reactant ratios used by the industry. Although the competing reactions between isocyanate and hydroxyl groups and isocyanate and water molecules has been studied extensively for monomeric systems, the relative rates of cure has not been attempted for oligomeric isocyanates with tri-functional polyols, such as castor oil and glycerol dispersed in water. Thus, there was also a lack of literature describing cure of oligomeric isocyanates and polyol emulsions and the rate of carbon dioxide evolution from these systems. The effect of changing the ratios of isocyanate and the reactive components of the polyol emulsion on carbon dioxide evolution was therefore investigated. Understanding how these changes affect the application of the coating system was also taken into consideration through rheological assessment of the polyol formulation. It is well known that lime added to polyurethane coatings aids in absorption of carbon dioxide, therefore leading to investigations in the improvement of the cement aggregate by the addition of lime was also an option.

The curing mechanism for the composite coating containing the cement and inert fillers, as well as the fundamental aspects of solid-liquid mixing is out of the scope of this thesis; however material properties such as the glass transition temperature and storage modulus were necessary in characterising the final coating properties and the improvements suggested by the work performed.

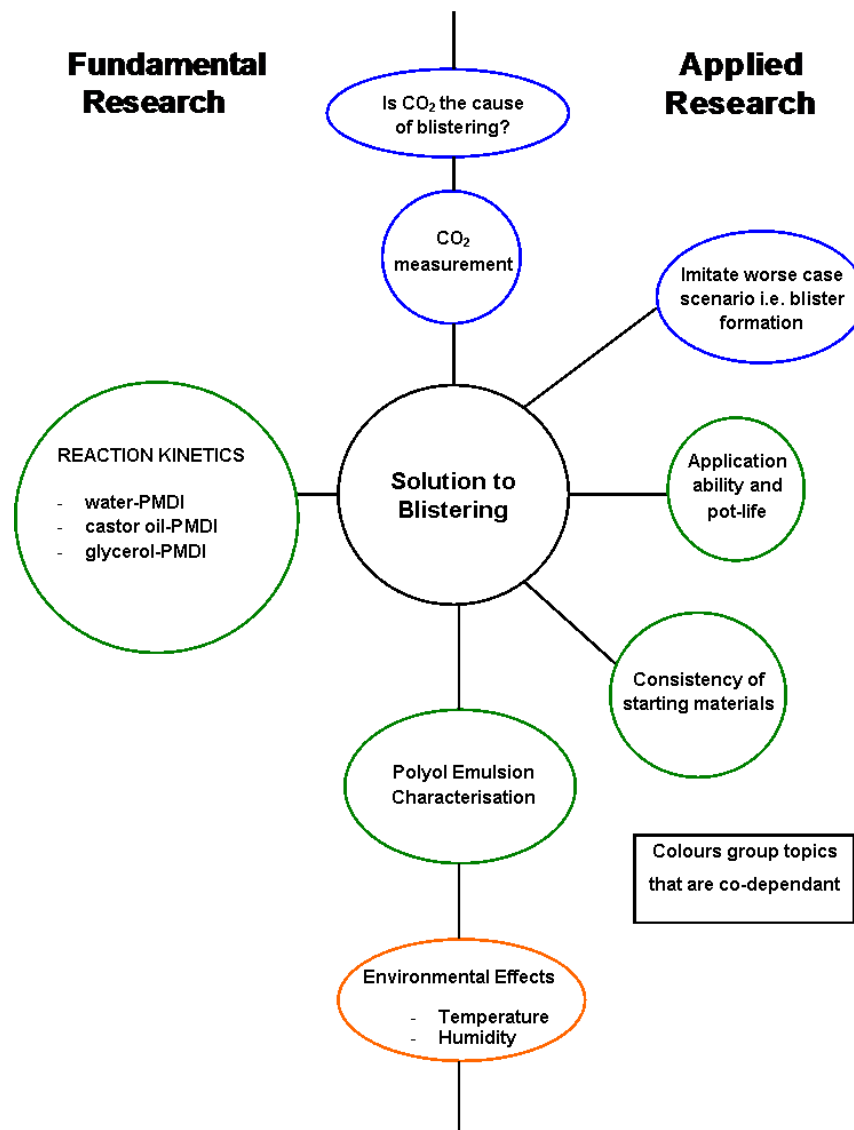


**Figure 1.6 Approach to solving blistering in the coating during curing**

This thesis was produced with the aim of identifying the causes of random blister formation through systematic tests of the coating components and to identify economically viable solutions for the industry partner.

## 1.4 Thesis outline

*Chapter 2* describes the general techniques and methods used in the characterisation of the reaction kinetics and materials used throughout this research. Details pertaining to particular aspects of this work are provided in the relevant chapters.

A review of the literature has shown that very little work has been reported on the reaction between oligomeric isocyanates with trifunctional polyols or water, which are the main two crosslinking reactions within the industry product. The focus of *Chapter 3* is to thus investigate the reaction kinetics and develop an understanding of the curing profile of the polyurethane reaction between castor oil and oligomeric diphenylmethane diisocyanate (PMDI) using isoconversional methods (model-free kinetic analysis) and the kinetics of the polyurea reaction between PMDI and water. The reactions have been studied using complimentary techniques including calorimetry, rheology, infrared spectroscopy and volumetric analysis of carbon dioxide evolution. A novel technique utilising pressure differential scanning calorimetry (PDSC) is employed, to determine the polyurea kinetic profile and to elucidate the mechanism of carbon dioxide evolution.

Glycerol, another trifunctional polyol, has been identified as a solution to the industry problem, as it has the ability to reduce carbon dioxide evolution in the coating, as well as lowering the viscosity of the polyol emulsion to aid application ability. A study of the reaction kinetics between glycerol and PMDI is presented in *Chapter 4*, which is important from a fundamental and technical viewpoint.

The first component of the industry coating package is a water dispersed reactant in the form of a polyol emulsion. The polyol emulsion consists of a castor oil-in-water dispersion, emulsified by a nonyl-ethoxylated surfactant, also containing a plasticizer, fragrant oil and silicone oil used to aid in de-aeration. The polyol emulsion gains its rheological properties as well as its emulsion stability which is detrimental to the shelf-life, from the effective dispersion of the castor oil in water by the non-ionic surfactant. Emulsion stability has been investigated using rheological measurements in *Chapter 5*. The properties of the final coating are also dependant on the reactive components of materials and small variations of the composition can affect the gas expansion rate. Inconsistencies between batches of the polyol emulsion can affect the final outcome of the crosslinking reaction and therefore the final

coating properties, thus, the effect of surfactant, water and castor oil concentration within the polyol emulsion on carbon dioxide evolution is determined. Characterisation of the emulsions has been performed using rheological investigations and volumetric testing of carbon dioxide evolution.

In *Chapter 6*, attempts to characterise the ability of the reactive aggregate (the third component in the coating formulation) to reduce carbon dioxide evolution and methods which improve or inhibit this function have been investigated. The reduction of carbon dioxide evolution through the addition of calcium oxide and calcium hydroxide is detailed, with the subsequent material properties of the optimum compositions tested through Dynamic Mechanical Analysis (DMA). Combinations of the improvements detailed in this chapter and those suggested in Chapter 5 have also been investigated, with the material properties determined through DMA analysis.

Finally, the major conclusions evolved from this work, together with recommendations and future research that could benefit the industry, are summarised in *Chapter 7*.

#### **1.4.1 Publications**

1. Eleni Papadopoulos, Milena Ginic-Markovic and Stephen Clarke, *Reaction kinetics of polyurethane formation using a commercial oligomeric diisocyanate resin studied by calorimetric and rheological methods*, ***Macromol. Chem. Phys.* 2008, 209, 2302–2311.**
2. Westlake, A.; Clarke, D., J.; Markovic, E.; Papadopoulos, E.; Nguyen, K. A.-T.; Constantopoulos, K.; Fisher, M.; Pillar, R.; Mathew, S.; Clarke, S.; McGlashan, S., provisional patent, 2008902610, *Biodiesel additive*, Meat and Livestock Australia Limited, FILED 26-05-2008.

#### **1.4.2 Conference Presentations**

1. E. Papadopoulos, M. Ginic Markovic, S. Clarke and J. Matison, *Highly crosslinked poly (urea-co-urethane) floor coatings*, 27<sup>th</sup> Australasian Polymer

Symposium, Adelaide, Australia, P47, 28 Nov- 2 Dec, **2004**.

2. D. Johns, E. Papadopoulos, S. Clarke and J. Matisons, *Investigation into the properties of a poly (urea-co-urethane) floor coating*, 27<sup>th</sup> Australasian Polymer Symposium, Adelaide, Australia, P49, 28 Nov- 2 Dec, **2004**.
3. E. Papadopoulos, M. Ginic Markovic, S. Clarke and J. Matisons, *Morphology development in a highly crosslinked polyurethane coating*, 3<sup>rd</sup> Australian-Korean Rheology Conference, Cairns, Australia, 17-20 July, **2005**.
4. E. Papadopoulos, M. Ginic Markovic, S. Clarke and J. Matisons, *Investigation of reactions occurring in highly crosslinked poly (urea-co-urethane) coatings*, CONNECT 2005, Sydney, Australia, 139, 3-7 July, **2005**.
5. E. Papadopoulos, M. Ginic Markovic, S. Clarke and J. Matisons, *Activation energy determination for key reactions in a highly crosslinked polyurethane coating*, Pacific Polymer Conference, IX, Maui, Hawaii, 11-14 Dec, **2005**.
6. E. Papadopoulos, M. Ginic Markovic, S. Clarke and J. Matisons, *The reaction kinetics of a highly cross-linked poly (urea-co-urethane) coating for concrete surfaces*, PACIFICHEM 2005, Honolulu, Hawaii, p. 89, 15-20 Dec, **2005**.
7. E. Papadopoulos, M. Ginic Markovic, S. Clarke, *Investigation into the reaction kinetics of glycerol and a commercial diisocyanate resin*, 30<sup>th</sup> Australasian Polymer Symposium, Melbourne, Australia, p. 277, 30 Nov- 4 Dec, **2008**.

## 1.5 References

- [1] P. Oman, "Understanding Vapour Transmission Issues When Coating Concrete", 2004.
- [2] R. E. Beddoe, H. W. Dorner, *Cem. Concr. Res.* **2005**, *35*, 2333.
- [3] A. Almusallam, F. M. Khan, S. U. Dulaijan, O. S. B. Amoudi, *Cem. Concr. Compos.* **2003**, *25*, 473.
- [4] A. Almusallam, F. M. Khan, M. Maslehuddin, *Mater. Struct.* **2002**, *35*, 487.
- [5] C. Izzo, "Overview of Industrial Coating Materials", in *Products Finishing*, **2000**, p. 1215.
- [6] Bayer, "Polyurethane Coatings, Performance, Quality, Safety".
- [7] U.S. 4211680 (1980), Imperial Chemical Industries Limited, London, England, inv. H. J. Shearing;
- [8] S. Ajithkumar, S. S. Kansara, N. K. Patel, *Eur. Polym. J.* **1998**, *34*, 1273.
- [9] S. M. Gasper, D. N. Schissel, L. S. Baker, D. L. Smith, R. E. Youngman, L.-M. Wu, S. M. Sonner, R. R. Hancock, C. L. Hogue, S. R. Givens, *Macromolecules* **2006**, *39*, 2126.
- [10] D. Ihms, J. O. Stoffer, D. Schneider, C. McClain, "The effect of catalysts on kinetics and mechanism of urethane film formation", in *Water-Borne & Higher-Solids Coatings Symposium*, **1983**, 233.
- [11] P. Krol, J. Wojturska, *J. Appl. Polym. Sci.* **2003**, *88*, 327.
- [12] K.-F. Lin, J.-Y. Shyu, *J. Polym. Sci., Part A: Polym. Chem.* **2001**, *39*, 3085.
- [13] G. Oertel, "Polyurethane Handbook", Hanser Publishers, Munich, **1985**.
- [14] G. Woods, "The ICI Polyurethanes Handbook", John Wiley, New York, **1990**.
- [15] Z. S. Petrovic, A. Guo, J. G. Zhang, *J. Polym. Sci., Part A: Polym. Chem.* **2000**, *38*, 4062.
- [16] V. Sekkar, S. Venkatachalam, K. N. Ninan, *Eur. Polym. J.* **2002**, *38*, 169.
- [17] M. W. Urban, C. L. Allison, C. C. Finch, B. A. Tatro, *J. Coat. Technol.* **1999**, *71*, 75.
- [18] S. L. Simon, J. K. Gillham, *J. Appl. Polym. Sci.* **1994**, *51*, 1741.
- [19] C. R. Hegedus, K. A. Kloiber, *J. Coat. Technol.* **1996**, *68*, 39.
- [20] J. M. Borsus, P. Merckaert, R. Jerome, P. Teyssie, *J. Appl. Polym. Sci.* **1982**, *27*, 4029.

- [21] M. Broekaert, "Polyurea Spray Applied Systems for Concrete Protection", Huntsman Polyurethanes.
- [22] M. Broekaert, "Polyurea Spray Coatings: The Technology and Latest Developments", **2003**.
- [23] M. Broekaert, "Polyurea Spray Coatings: The Technology and latest Developments", S.C.a. Inks, Ed., **2004**.
- [24] F. M. B. Coutinho, M. C. Delpech, T. L. Alves, A. A. Ferreira, *Polym. Degrad. Stab.* **2003**, *81*, 19.
- [25] J. Dodge, "Synthetic Methods in Step-Growth Polymers: Polyurethanes and Polyureas Chapter 4", M.E. Rogers and T.E. Long, Eds., John Wiley & Sons, **2003**, p. 197.
- [26] S. W. Guan, "100% Solids Polyurethane and Polyurea Coatings Technology", **2003**.
- [27] G. A. Howarth, *Surf. Coat. Int. Part B: Coating Transactions* **2003**, *86*, 111.
- [28] B. Tamami, H. Yeganeh, G. A. Koohmareh, *Iran. Polym. J.* **2005**, *14*, 785.
- [29] S. K. Yadav, K. C. Khilar, A. K. Suresh, *AIChE J.* **1996**, *42*, 2616.
- [30] C. R. Hegedus, A. G. Gilicinski, R. J. Haney, *J. Coat. Technol.* **1996**, *68*, 51.
- [31] E. B. Ritcher, C. W. Macosko, *Polym. Eng. Sci.* **1978**, *18*, 1012.
- [32] D. Ihms, J. O. Stoffer, D. F. Schneider, C. McClain, *J. Coat. Technol.* **1985**, *57*, 61.
- [33] A. M. Kaminski, M. W. Urban, *J. Coat. Technol.* **1997**, *69*, 113.
- [34] Application: KR, KR. 2004-118159 2005008624 (2005), (S. Korea). invs.: C. Y. Kim, U. M. Lee;
- [35] M. Piao, J. Otaigbe, D. Otts, M. Urban, *Polym. Mater.: Sci. Eng.* **2004**, *90*, 112.
- [36] A. Fuchs, G. A. Prentice, V. Sendjarevic, K. C. Frisch, P. Jackson, C. Mao, "Process Monitoring of Rigid Polyurethane Foams for Automotive Composites", **2004**.
- [37] A. Guo, I. Javni, Z. S. Petrovic, *J. Appl. Polym. Sci.* **2000**, *77*, 467.
- [38] Application: KR, KR. 2004-91215 2006043907 (2006), (Dang-A Hwa Sung Co., Ltd., S. Korea). invs.: S. J. Kim, J. H. Hwang, J. M. Oh;
- [39] S. Peng, P. Jackson, V. Sendjarevic, K. C. Frisch, G. A. Prentice, A. Fuchs, *J. Appl. Polym. Sci.* **2000**, *77*, 374.
- [40] P. M. Morrisette, *Nat. Resour. J.* **1989**, *29*, 793.

- [41] D. W. Dedeaux, E. L. Rister, R. L. Zimmerman, F. C. Kohoutek, "TEXACAT Catalysts in Water-Blown Rigid Foam", in *34th Annual Polyurethane Technical/Marketing Conference*, **1992**, 341.
- [42] T. J. Hsu, L. J. Lee, *Polym. Eng. Sci.* **1988**, 28, 955.
- [43] I. P. o. C. S. (IPCS), "Concise International Chemical Assessment Document No. 27, Diphenylmethane diisocyanate (MDI)", **2001**.
- [44] M. S. McGovern, "New Polymers set in a Flash", in *Aberdeen's Concrete Repair Digest*, **1996**, p. 7/140.
- [45] M. Urban, W. Ludwig, *J. Coat. Technol.* **1996**, 68, 93.
- [46] Application: RU RU. 98-122574 2151160 (2000), (Obshchestvo S Ogranichennoi Otvetstvennost'yu Nauchno-Proizvodstvennaya Firma \"Ehlastomer\", Russia). invs.: V. P. Medvedev, A. M. Ogrel, V. V. Luk'yanichev;
- [47] Application: JP, JP. 2002-265423 2003160632 (2003), (Sanyo Chemical Industries, Ltd., Japan). invs.: K. Miura, J. Ryugo;
- [48] Application: US, US. 96-6325735604266 (1997), (Ecomat, Inc., USA). inv. J. N. Mushovic;
- [49] Application: JP, JP. 2004-6417 2005200490 (2005), (Auto Chemical Industry Co., Ltd., Japan). invs.: H. Saito, Y. Yaguchi;
- [50] Application: JP, JP. 91-132405 04298593 (1992), (Sumitomo Durez Co., Ltd., Japan; Sumitomo Bakelite Co., Ltd.). invs.: K. Takahashi, S. Tayama, W. Ujigawa;
- [51] W. Posthumus, A. J. Derksen, J. A. M. Van den Goorbergh, L. C. J. Hesselmans, *Prog. Org. Coat.* **2007**, 58, 231.
- [52] T. Ando, *Nippon Kagaku Kaishi* **1993**, 10, 1201.
- [53] G. Anzuino, A. Pirro, O. Rossi, L. Polo Friz, *J. Polym. Sci.: Polym. Chem.* **1975**, 13, 1657.
- [54] "MDI and TDI: Health and the Environment. A source Book and Practical Guide", 12.
- [55] M. D. Hartley, H. J. Williams, *Polym. Eng. Sci.* **1981**, 21, 135.
- [56] D. S. Kim, C. W. Macosko, *Korea Polym. J.* **1996**, 4, 54.
- [57] R. R. Koch, *Journal of Paint Technology* **1970**, 42, 243.
- [58] Z. Wang, P. Gao, *Surf. Coat. Int. Part B: Coating Transactions* **2001**, 84, 21.
- [59] R. A. C. Altafim, C. R. Murakami, S. Claro Neto, L. C. R. Araujo, G. O. Chierice, *Mater. Res.* **2003**, 6, 187.

- [60] R. A. C. Altafim, J. F. Resende da Silva, D. P. Gonzaga, C. Ribeiro, J. Godoy, H. C. Basso, B. Bueno, C. Calil Junior, J. C. Sartori, R. A. P. Altafim, A. Silveira, *Mater. Res.* **2006**, *9*, 77.
- [61] F. M. Dias, F. A. R. Lahr, *Mater. Res.* **2004**, *7*, 413.
- [62] Z. S. Petrovic, D. Fajnik, *J. Appl. Polym. Sci.* **1984**, *29*, 1031.
- [63] J. M. E. Rodrigues, M. R. Pereira, A. G. de Souza, M. L. Carvalho, A. A. Dantas Neto, T. N. C. Dantas, J. L. C. Fonseca, *Thermochim. Acta* **2005**, *427*, 31.
- [64] C. S. Sanmathi, S. Prasannakumar, B. S. Sherigara, *J. Appl. Polym. Sci.* **2004**, *94*, 1029.
- [65] K. Somani, S. Kansara, R. Parmar, N. Patel, *Int. J. Polym. Mater.* **2004**, *53*, 283.
- [66] B. Suthar, D. Klempner, K. C. Frisch, Z. S. Petrovic, Z. Jelcic, *J. Appl. Polym. Sci.* **1994**, *53*, 1083.
- [67] H. Yeganeh, M. R. Mehdizadeh, *Eur. Polym. J.* **2004**, *40*, 1233.
- [68] H. Yeganeh, M. A. Shamekhi, *J. Appl. Polym. Sci.* **2006**, *99*, 1222.
- [69] M. C. CHEM, "Castor oil", in ISIS Draw, C. Oil, Ed., [www.groshea.com](http://www.groshea.com).
- [70] Y. Song, Q. Zheng, *Bioresour. Technol.* **2008**, *99*, 7665.
- [71] G. Yilmaz, R. O. J. Jongboom, J. J. G. Van Soest, H. Feil, *Carbohydr. Polym.* **1999**, *38*, 33.
- [72] P. F. Macedo Janus, L. Fernandes Leonardo, R. Formiga Fabio, F. Reis Michael, N. Junior Toshiyuki, A. L. Soares Luiz, E. S. T. Egito, *AAPS Pharm. Sci. Tech.* **2006**, *7*, E21.
- [73] P. Walstra, "Formation of Emulsions", in *Encyclopedia of Emulsion Technology: Basic Theory*, P. Becher, Ed., Marcel Dekker INC, **1983**, p. 1/.
- [74] T. C. G. Kibbey, K. F. Hayes, *J. Contam. Hydrol.* **2000**, *41*, 1.
- [75] D.-B. Ljubica, D. Petar, V. Sovilj, "Structure Building in O/W Emulsions in Shear Induced By Surfactant-nongelling Polymer Interactions", in *3rd International Symposium on Food Rheology and Structure*, 529.
- [76] J. Mougel, O. Alvarez, C. Baravian, F. Caton, P. Marchal, M.-J. Stebe, L. Choplin, *Rheol. Acta* **2006**, *45*, 555.
- [77] O. Ozer, E. Baloglu, G. Ertan, V. Muguet, Y. Yazan, *Int. J. Cosm. Sci.* **2000**, *22*, 459.
- [78] W. Warisnoicharoen, A. B. Lansley, M. J. Lawrence, *Int. J. Pharm.* **2000**, *198*, 7.

- [79] W. Warisnoicharoen, A. B. Lansley, M. J. Lawrence, *Pharm. Sci.* [online computer file] **2000**, 2.
- [80] R. Grove, "Notes On Making Cola ", **2005**, p. 2008.
- [81] Y. Otsubo, R. K. Prud'homme, *Rheol. Acta* **1994**, 33, 29.
- [82] R. Pal, *Colloid and Polymer Science* **1999**, 277, 583.
- [83] T. Tadros, B. Vincent, "Emulsion Stability", in *Encyclopedia of Emulsion Technology: Basic Theory*, P. Becher, Ed., Marcel Dekker INC, **1983**.
- [84] K. Shinoda, K. H., "Phase Properties of Emulsions: PIT and HLB", in *Encyclopedia of Emulsion Technology: Basic Theory*, P. Becher, Ed., Marcel Dekker INC., **1983**.
- [85] H. M. Princen, *J. Colloid Interface Sci.* **1985**, 105, 150.
- [86] A. Ponton, P. Clement, J. L. Grossiord, *J. Rheol.* **2001**, 45, 521.
- [87] J. Jiao, J. Burgess Diane, *AAPS Pharm. Sci.* **2003**, 5, E7.
- [88] N. A. Mishchuk, A. Sanfeld, A. Steinchen, *Adv. Colloid Interface Sci.* **2004**, 112, 129.
- [89] I. Roland, G. Piel, L. Delattre, B. Evrard, *Int. J. Pharm.* **2003**, 263, 85.
- [90] R. J. Kauten, J. E. Maneval, M. J. McCarthy, *J. Food Sci.* **1991**, 56, 799.
- [91] K. H. Kim, J. M. S. Renkema, T. Van Vliet, *Food Hydrocolloids* **2001**, 15, 295.
- [92] P. Sherman, "Rheological Properties of Emulsions", in *Encyclopedia of Emulsion Technology: Basic Theory*, P. Becher, Ed., Marcel Dekker INC., **1983**.
- [93] P. Chaffanjon, J. R. A. Grisgby, J. E. L. Rister, R. L. Zimmerman, *J. Cell. Plast.* **2003**, 39, 187.
- [94] J. O. Stoffer, D. Ihms, C. McClain, D. Schneider, "Solution Kinetics of the Water-Toluene Diisocyanate Reaction", in *Water-Borne and Higher-Solids Coatings 14th Symposium*, **1987**, p. 14/428.
- [95] J. M. Borsus, R. Jerome, P. Teyssie, *J. Appl. Polym. Sci.* **1981**, 26, 3027.
- [96] S. D. Seneker, T. A. Potter, *J. Coat. Technol.* **1991**, 63, 19.
- [97] S. Benali, J. Bouchet, G. Lachenal, *J. Near Infrared Spectrosc.* **2004**, 12, 5.
- [98] B. W. Ludwig, M. W. Urban, *J. Coat. Technol.* **1996**, 68, 93.
- [99] H. Bui, M. Dvorchak, M. Hudson, J. Hunter, "The Rheology of Mixing in Two-Component Waterborne Polyurethane Coatings", in *Waterborne, High Solids and Powder Coatings Symposium*, New Orleans, LA, **1997**, 515.
- [100] A. Bittner, P. Ziegler, "Water-Borne Two-Pack Polyurethane Coatings for

Industrial Applications", in *New Technologies for Coatings and Inks 3rd Congress*, Nurnberg, Germany, **1995**.

[101] B. W. Ludwig, M. W. Urban, *J. Coat. Technol.* **1994**, 66, 59.

[102] M. Bock, J. Petzoldt, *Water-Borne & Higher-Solids and Powder Coatings Symposium* **1995**, 502.

[103] P. B. Jacobs, P. C. Yu, *J. Coat. Technol.* **1993**, 65, 45.

[104] W. Kubitza, *J. Oil and Colour Chemists' Assoc.* **1992**, 75, 340.

[105] S. Wong, K. C. Frisch, *Polym. Mater.: Sci. Eng.* **1984**, 50, 480.

[106] Z. A. He, W. J. Blank, M. E. Picci-King, E. Picci, *J. Coat. Technol.* **2002**, 74, 31.

[107] W. J. Blank, Z. A. He, E. T. Hessel, *Prog. Org. Coat.* **1999**, 35, 19.

[108] H. Ni, H. A. Nash, J. G. Worden, M. D. Soucek, *J. Polym. Sci.: Part A: Polym. Chem.* **2002**, 40, 1677.

[109] F. Dimier, N. Sbirrazzuoli, B. Vergnes, M. Vincent, *Polym. Eng. Sci.* **2004**, 44, 518.

[110] S. Florez, M. E. Munoz, A. Santamaria, *J. Rheol.* **2005**, 49, 313.

[111] J. T. Haponiuk, M. Strankowski, T. Lazarewicz, *J. Therm. Anal. Calorim.* **2003**, 74, 609.

[112] D. S. Kim, J.-T. Kim, W. B. Woo, *J. Appl. Polym. Sci.* **2005**, 96, 1641.

[113] A. H. Navarchian, F. Picchioni, L. P. B. M. Janssen, *Polym. Eng. Sci.* **2005**, 45, 279.

[114] V. Sekkar, K. Narayanaswamy, K. J. Scariah, P. R. Nair, K. S. Sastri, H. G. Ang, *J. Appl. Polym. Sci.* **2006**, 101, 2986.

[115] J. Chappel, P. Argust, *Thermochimi. Acta* **1996**, 289, 303.

[116] T. Provder, C. M. Neag, G. Carlson, C. Kuo, R. M. Holsworth, *Anal. Calorim.* **1984**, 5, 377.

[117] L. Troger, N. Hilbrandt, M. Epple, *Journal de Physique IV* **1997**, 7, 323.

[118] M. Ginic-Markovic, N. R. Choudhury, J. G. Matisons, D. R. G. Williams, *J. Therm. Anal. Calorim.* **2000**, 59, 409.

[119] C.-Y. M. Tung, P. J. Dynes, *J. Appl. Polym. Sci.* **1982**, 27, 569.

[120] J. M. Kenny, *J. Appl. Polym. Sci.* **1994**, 51, 761.

[121] S. Du, Z.-S. Guo, B. Zhang, Z. Wu, *Polym. Int.* **2004**, 53, 1343.

[122] S. Parnell, K. Min, M. Cakmak, *Polymer* **2003**, 44, 5137.

- [123] M. L. Costa, L. C. Pardini, M. C. Rezende, *Mater. Res.* **2005**, 8, 65.
- [124] R. Pal, *J. Rheol.* **1997**, 41, 141.
- [125] R. B. Prime, C. Michalski, C. M. Neag, *Thermochim. Acta* **2005**, 429, 213.
- [126] C. C. Su, E. M. Woo, Y. P. Huang, *Polym. Eng. Sci.* **2004**, 45, 1.
- [127] H. Yu, S. G. Mhaisalkar, E. H. Wong, *Macromol. Rapid Commun.* **2005**, 26, 1483.
- [128] P. Hugo, S. Wagner, T. Gnewikow, *Thermochim. Acta* **1993**, 225, 143.
- [129] C. D. Han, K.-W. Lem, *J. Appl. Polym. Sci.* **1983**, 28, 3155.
- [130] F. Hernandez-Sanchez, H. Vazquez-Torres, *J. Polym. Sci.: Part A: Polym. Chem.* **1990**, 28, 1579.
- [131] E. A. Turi, "Thermal Characterization of Polymeric Materials", Academic Press, New York, **1997**, p. 1174.
- [132] F. Hernandez-Sanchez, R. Vera-Graziano, *J. Appl. Polym. Sci.* **1992**, 46, 571.
- [133] S. L. Hager, T. B. MacRury, R. M. Gerkin, F. E. Critchfield, *ACS Polymer Preprints* **1980**, 21.
- [134] M. R. Kamal, *Polym. Eng. Sci.* **1974**, 14, 231.
- [135] M. R. Kamal, S. Sourour, *Polym. Eng. Sci.* **1973**, 13, 59.
- [136] M. R. Kamal, S. Sourour, M. Ryan, "Integrated Thermo-Rheological Analysis of the Cure of Thermosets", in 31st Annual Technical Conference: ANTEC International, Quebec, Canada, **1973**, 187.
- [137] P. Krol, B. Atamanczuk, J. Pielichowski, *J. Appl. Polym. Sci.* **1992**, 46, 2139.
- [138] H. Yeganeh, M. A. Shamekhi, *Polym. Int.* **2005**, 54, 754.
- [139] X. Ramis, J. M. Salla, *J. Polym. Sci., Part B: Polym. Phys.* **1997**, 35, 371.
- [140] S. Vyazovkin, *Thermochim. Acta* **2000**, 355, 155.
- [141] S. Vyazovkin, *J. Therm. Anal.* **1997**, 49, 1493.
- [142] S. Vyazovkin, *Int. J. Chem. Kinet.* **1996**, 28, 95.
- [143] F. B. Arlas, L. Rueda, P. M. Stefani, K. Caba, I. Mondragon, A. Eceiza, *Thermochim. Acta* **2007**, 459, 94.
- [144] A. Cadenato, J. M. Salla, X. Ramis, J. M. Morancho, L. M. Marroyo, J. L. Martin, *J. Therm. Anal.* **1997**, 49, 269.
- [145] S. Vyazovkin, *J. Comput. Chem.* **2000**, 22, 178.
- [146] S. Vyazovkin, *Proceedings of the NATAS Annual Conference on Thermal Analysis and Applications* **2003**.

- [147] S. Vyazovkin, *J. Therm. Anal. Calorim.* **2006**, 83, 45.
- [148] J. J. Cai, R. Salovey, *Polym. Eng. Sci.* **2001**, 41, 1853.
- [149] B.-S. Chiou, R. J. English, S. A. Khan, *Macromolecules* **1996**, 29, 5368.
- [150] B.-S. Chiou, S. A. Khan, *IS&T's Annual Conference* **1997**, 50th, 570.
- [151] B.-S. Chiou, S. R. Raghavan, S. A. Khan, *Macromolecules* **2001**, 34, 4526.
- [152] W. D. Cook, K. Dean, J. S. Forsythe, *Materials Forum* **2001**, 25, 30.
- [153] A. J. Franck, "Understanding Rheology of Thermosets", *TA instruments*.
- [154] A. J. Franck, W. Kunze, "Synergy of the combined application of thermal analysis and rheology in monitoring and characterizing changing processes in materials", *TA instruments Germany*, **2006**.
- [155] P. J. Halley, M. E. Mackay, *Polym. Eng. Sci.* **1996**, 36, 593.
- [156] S. Han, K. K. Wang, C. A. Hieber, C. Cohen, *J. Rheol.* **1997**, 41, 177.
- [157] H. Kim, K. Char, *Korea-Aust. Rheol. J.* **2000**, 12, 77.
- [158] G. Liang, K. Chandrashekhara, *J. Appl. Polym. Sci.* **2006**, 102, 3168.
- [159] Y. Otsubo, T. Amari, K. Watanabe, T. Nakamichi, *J. Rheol.* **1987**, 31, 251.
- [160] A. B. Spoelstra, *Polym. Eng. Sci.* **1996**, 36, 2153.
- [161] H. H. Winter, F. Chambon, *J. Rheol.* **1986**, 30, 367.
- [162] H. Teil, S. A. Page, V. Michaud, J. A. E. Manson, *J. Appl. Polym. Sci.* **2004**, 93, 1774.
- [163] A. Yousefi, P. G. Lafleur, *Polym. Compos.* **1997**, 18, 157.
- [164] A. Y. Malkin, S. G. Kulichikhin, *Adv. Polym. Sci.* **1991**, 101, 217.
- [165] R. J. Varley, *Macromol. Mater. Eng.* **2007**, 292, 46.
- [166] A. Y. Malkin, I. Y. Gorbunova, M. L. Kerber, *Polym. Eng. Sci.* **2005**, 45, 95.
- [167] D. Lahlali, M. Naffakh, M. Dumon, *Polym. Eng. Sci.* **2005**, 45, 1581.
- [168] J. M. Laza, C. A. Julian, E. Larrauri, M. Rodriguez, L. M. Leon, *Polymer* **1998**, 40, 35.
- [169] J. M. Laza, J. L. Vilas, F. Mijangos, M. Rodriguez, L. M. Leon, *J. Appl. Polym. Sci.* **2005**, 98, 818.
- [170] J. M. Laza, J. L. Vilas, M. Rodriguez, M. T. Garay, F. Mijangos, L. M. Leon, *J. Appl. Polym. Sci.* **2002**, 83, 57.
- [171] J. S. Martin, J. M. Laza, M. L. Morras, M. Rodriguez, L. M. Leon, *Polymer* **2000**, 41, 4203.
- [172] J. Lange, N. Altmann, C. T. Kelly, P. J. Halley, *Polymer* **2000**, 41, 5949.

- [173] K. Dean, W. D. Cook, P. Burchill, M. Zipper, *Polymer* **2001**, 42, 3589.
- [174] C. M. Nunez, B.-S. Chiou, A. L. Andrady, S. A. Khan, *Macromolecules* **2000**, 33, 1720.
- [175] V. Sekkar, K. A. Devi, K. N. Ninan, *J. Appl. Polym. Sci.* **2001**, 79, 1869.
- [176] V. Sekkar, V. N. Krishnamurthy, S. R. Jain, *J. Appl. Polym. Sci.* **1997**, 66, 1795.
- [177] S. D. Lipshitz, C. W. Macosko, *Polym. Eng. Sci.* **1976**, 16, 803.
- [178] M. Doyle, P.-O. hagstrand, J. A. E. Manson, *Polym. Eng. Sci.* **2003**, 43, 297.
- [179] C. Texier, M. Taha, A. Maazouz, J. P. Pascault, *Polym. Eng. Sci.* **1997**, 37, 1238.
- [180] F. Prochazka, T. Nicolai, D. Durand, *Macromolecules* **1996**, 29, 2260.
- [181] I. Alig, W. Jenninger, J. E. K. Schawe, *Thermochim. Acta* **1999**, 330, 167.
- [182] J. Dupuy, S. Benali, A. Maazouz, G. Lachenal, D. Bertrand, *Macromol. Symp.* **2002**, 184, 249.
- [183] M. W. Urban, "Vibrational Spectroscopy of Molecules and Macromolecules on Surfaces", **1993**.
- [184] M. W. Urban, "ATR Spectroscopy of Polymers", *ACS*, **1996**.
- [185] S. D. Lipshitz, C. W. Macosko, *J. Appl. Polym. Sci.* **1977**, 21, 2029.
- [186] T. Hentschel, H. Munstedt, *Polymer* **2001**, 42, 3195.
- [187] M. W. Urban, *Prog. Org. Coat.* **2000**, 40, 195.
- [188] M. W. Urban, C. L. Allison, *J. Coat. Technol.* **1999**, 71, 73.
- [189] A. M. Kaminski, M. W. Urban, *J. Coat. Technol.* **1997**, 69, 55.
- [190] S. Benali, D. Bertrand, J. Dupuy, G. Lachenal, A. Maazouz, *The Institute of Measurement and Control* **2007**, 29, 417.
- [191] D. Hermawan, T. Hata, S. Kawai, W. Nagadomi, Y. Kuroki, *J. Wood Sci.* **2002**, 48, 179.
- [192] J. Zelic, D. Rusic, R. Krstulovic, *J. Therm. Anal. Calorim.* **2002**, 67, 613.
- [193] R. G. Patel, D. C. Killoh, L. J. Parrott, W. A. Gutteridge, *Mater. Struct.* **1988**, 21, 192.
- [194] F. M. Lea, "The Chemistry of Cement and Concrete", Third edition, Edward Arnold Ltd, **1970**.
- [195] I. Papayianni, T. Valliasis, *Cem. Concr. Compos.* **2005**, 27, 249.
- [196] D. P. Bentz, E. J. Garboczi, C.-J. Haecker, O. M. Jensen, *Cem. Concr. Res.*

**1999**, 29, 1663.

[197] D. P. Bentz, O. M. Jensen, K. K. Hansen, J. F. Olesen, H. Stang, C.-J. Haecker, *J. Am. Ceram. Soc.* **2001**, 84, 129.

[198] J. J. Thomas, H. M. Jennings, *J. Am. Ceram. Soc.* **2002**, 85, 2293.

[199] D. P. Bentz, *Cem. Concr. Res.* **2006**, 36, 238.

[200] K. A. Snyder, D. P. Bentz, *Cem. Concr. Res.* **2004**, 34, 2045.

[201] J. Zelic, R. Krstulovic, E. Tkalcec, P. Krolo, *Cem. Concr. Res.* **2000**, 30, 145.

[202] I. Pane, W. Hansen, *Cem. Concr. Res.* **2005**, 35, 1155.

[203] C. L. Collins, J. H. Ideker, K. E. Kurtis, *J. Microscopy* **2004**, 213, 149.

[204] Z. Wu, T. R. Naik, "Use of Clean-Coal Ash for Managing ASR", in *ACI International Spring 2004 Centennial Convention*, Washington, D.C., **2004**, 12.

[205] S. A. Baser, D. V. Khakhar, *J. Cell. Plast.* **1993**, 29, 197.

[206] C. Ligoure, M. Cloitrea, C. Le Chateliera, F. Montia, L. Leibler, *Polymer* **2005**, 46, 6402.

# **CHAPTER 2**

## **Characterisation Techniques**

## 2 CHARACTERISATION TECHNIQUES

This chapter describes the techniques used for the investigation into the poly (urea-co-urethane) cement composite coating. Specific methods pertaining to the particular aspects of the work are described in the relevant chapters. Unless specified elsewhere, the details discussed for each technique are applicable throughout the thesis.

### 2.1 Fourier Transform Infrared (FTIR)

Infrared spectroscopy is an analytical technique which examines the interaction between a material and electromagnetic radiation in either the near (13000-4000  $\text{cm}^{-1}$ ), mid (4000-400  $\text{cm}^{-1}$ ) or far (400-40  $\text{cm}^{-1}$ ) infrared regions where molecular vibrational and rotational bands are observed.<sup>[1-3]</sup>

Chemical functional groups absorb infrared radiation of characteristic frequencies so that infrared analysis can be used to detect the presence of different chemical moieties present in the sample. FTIR analysis of polyurethane reactions is a direct method of measuring the concentration of a reactant and has been used to monitor several chemical changes simultaneously.<sup>[4-7]</sup> Quantitative FTIR analysis employs Beer Lambert's Law, which correlates the concentration with the band intensity by calculating the molar absorption coefficient (**Equation (2-1)**)<sup>[8]</sup>.

$$A = \varepsilon l c \quad (2-1)$$

Where  $A$  is Absorbance,  $\varepsilon$  is the extinction coefficient,  $l$  is the path length of beam and  $c$  is the concentration.

Many different configurations exist for the analysis of changes in functional groups as reactions progress and for final film properties. The configurations have been chosen based on their availability, surface sensitivity, non-specific sample geometry requirements and the ability to rapidly acquire sample spectra without the need for lengthy preparation such as KBr grinding or gas purging.

The cure kinetics was obtained using a Nicolet 8700 spectrophotometer fitted with a

transmission cell. Transmission experiments were performed using disposable pressed KBr discs to which a thin coating of the mixed sample was applied. Spectra were taken intermittently to determine the curing profile with a maximum of 2 scans per time interval over the wave number range of 400-4000  $\text{cm}^{-1}$  using a DTGS detector, aperture of 100 and resolution of 4  $\text{cm}^{-1}$ .

Attenuated Total Reflectance (ATR) has been used extensively for the qualitative analysis of films and coatings.<sup>[6, 7, 9, 10]</sup> This technique requires the sample to be placed in intimate contact with the ATR crystal. ATR spectra were obtained using a 'Smart Orbit' ATR accessory containing a diamond crystal internal reflection element. The maximum penetration of infrared radiation into the sample was 1  $\mu\text{m}$  and the average number of scans used to obtain an infrared spectrum was 32 at a resolution of 4  $\text{cm}^{-1}$ . Both mid and near-infrared were used in this configuration using a DTGS detector. Data analysis was carried out using the Omnic 7.1 software to subtract the background from the sample spectra and to analyse the subsequent IR spectra.

## 2.2 Differential Scanning Calorimetry (DSC)

Heat flux DSC is a thermal analysis technique that measures the amount of energy absorbed or released by a sample as it is heated, cooled or held at a constant temperature. It is commonly used to analyse material characteristics such as melting, crystallisation, glass transition, curing and chemical reactions.<sup>[11]</sup>

A schematic of the heat flux DSC cell is shown in **Figure 2.1**. Heat transfer to and from the sample and reference pans occurs through a constantan disc. The temperature difference between the sample and reference pans is measured through the use of thermocouples and is converted to heat flow data which may then be plotted as a function of time or temperature. Differences in heat flow compared to the reference pan, correspond to either endothermic (absorption of heat) or exothermic (release of heat) processes that provide information about physical and chemical changes. A purge gas maintains a uniform and stable thermal environment which assures a better baseline and increased signal-to-noise ratio.

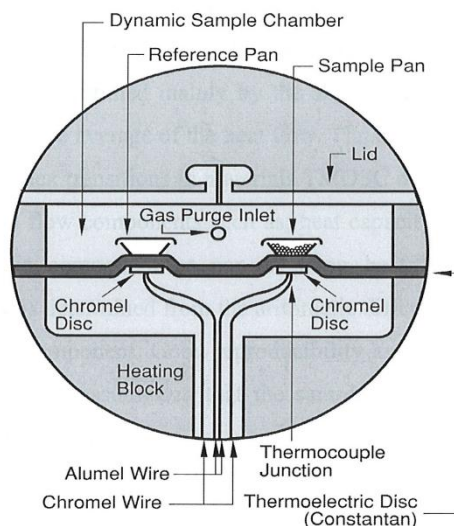


**Figure 2.1 Heat flux DSC schematic<sup>[12]</sup>**

A TA Instruments 2920 DSC equipped with liquid nitrogen cooling accessory (LNCA) unit under a continuous nitrogen purge (50 ml/min) was used for the measurement of reaction conversion for the polymerisation of polyol with isocyanate in isothermal and non-isothermal DSC modes as detailed in Chapter 1.<sup>[13-19]</sup> Specific heating programs are detailed in the relevant chapters.

A limitation of the standard DSC cell is that it cannot be used to analyse reactions which evolve gasses or if the reactants are highly volatile. Pressure Differential Scanning Calorimetry (PDSC) can overcome this problem, eliminating sample evaporation.<sup>[20]</sup> The high pressure cell was used for all reactions involving water under constant volume conditions, with an oxygen gauge pressure of 3792 kPa (550 psig) to minimise evaporation of water. Specific heating programs and sample weights are detailed in the relevant chapters. The instrument cell constant and temperature for both standard and pressure DSC were calibrated using a sample of pure indium. Analysis was carried out using Universal Analysis 2000 v3.3B software (TA Instruments).

## 2.3 Thermogravimetric Analysis (TGA)

Thermogravimetric analysis is based upon the accurate measurement of changes in the mass of a sample as a function of time or temperature when undergoing a specific heating program.<sup>[11]</sup> The sample is placed on a tared platinum crucible or aluminium pan and onto an analytical balance enclosed by a furnace. The enclosed furnace is purged with the desired gas and flow rate. A trace of the mass or the mass change with temperature or time is obtained.

The materials used in this study were characterised by thermogravimetric analysis performed using a TGA 2950 instrument as supplied by TA Instruments. The conventional mode of heating from room temperature to 600 °C in aluminium pans or to 900 °C using platinum crucibles at a heating rate of 10 °C min<sup>-1</sup> under a nitrogen atmosphere with a constant flow rate of 50 ml min<sup>-1</sup> was employed. Temperature calibrations were performed using the Curie temperatures of nickel and alumel standard reference materials (TA instruments). Analysis was carried out using Universal Analysis 2000 v3.3B software from TA instruments.

## 2.4 Dynamic Mechanical Analysis (DMA)

DMA characterises the viscoelastic properties of materials as a function of both frequency of applied oscillatory stress/strain and temperature. DMA supplies an oscillatory force causing a sinusoidal stress to be applied to the sample which then generates a sinusoidal strain (**Figure 2.2**). Measuring the amplitude of deformation at the peak of the sine wave and the phase lag between the stress and strain sine waves, a variety of fundamental material parameters can be determined.<sup>[21, 22]</sup>

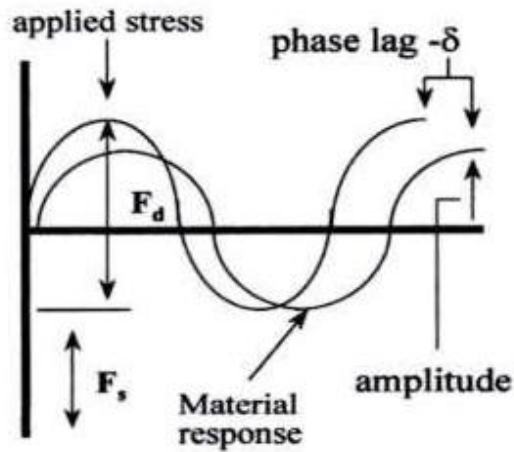


Figure 2.2  $F_d$  represents the applied oscillatory force, while  $F_s$  is the clamping force, showing the phase angle  $\delta$  produced<sup>[22]</sup>

These include the storage modulus  $G'$  also called the real or elastic modulus which represents the energy stored within the sample, the loss modulus  $G''$  (imaginary or viscous modulus) which represents the energy dissipated, the complex modulus ( $G^*$ ) and the damping factor ( $\tan \delta$ ). The complex modulus is defined by **Equation (2-2)**.<sup>[21]</sup>

$$G^* = G' + iG'' = \frac{\sigma^*}{\gamma^*} \quad (2-2)$$

The relationship between the complex, storage, loss modulus and phase angle is depicted vectorially in **Figure 2.3**.

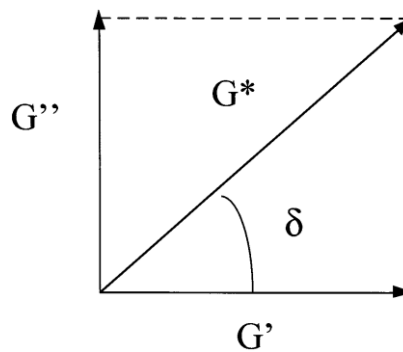


Figure 2.3 Relationship between the complex, storage and loss moduli<sup>[21]</sup>

DMA measurements were performed using a TA Instruments DMAQ800 in single cantilever bending deformation mode. A frequency of 1 Hz and a peak displacement of 20  $\mu\text{m}$  were selected to measure the glass transition temperature  $T_g$ , which was taken as the temperature at which the loss factor  $\tan \delta$  reached a maximum. The temperature was scanned from -70  $^{\circ}\text{C}$  to 140  $^{\circ}\text{C}$  and ramped at a rate of 2  $^{\circ}\text{C min}^{-1}$  [23]

## 2.5 Rheology

An AR-2000 controlled stress and direct strain control rheometer from TA Instruments, (US) was used to study the curing behaviour of the polyols with oligomeric diphenylmethane diisocyanate (PMDI) as well as to characterise the emulsion stability. [24-33]

6 cm  $2^{\circ}$  and 2 cm  $2^{\circ}$  cone and plate configurations were used for all measurements. Calibrations were performed for the instrumental inertia and geometry prior to each experiment. The instrument performance was regularly calibrated with an oil standard.

A torque induction motor applies a sinusoidal or linear stress to the sample through the upper plate of the geometry with the sample deformation monitored by the deflection of the upper plate using an optical encoder. Analysis of the applied stress and resultant strain enables the calculation of various rheological parameters. In dynamic or oscillatory measurements, the angular frequency becomes analogous to the rate of shear in usual rheological measurement. [34, 35] The complex viscosity **Equation (2-3)** contains an elastic component in addition to a term similar to the ordinary steady state viscosity.

$$\eta^* = \eta' - i \eta'' \quad (2-3)$$

The dynamic viscosity  $\eta'$  is related to the steady state viscosity and represents the rate of energy dissipation. The elastic viscosity  $\eta''$  measures the stored energy and is related to the storage modulus through **Equation (2-4)**.

$$G' = \omega \eta'' \quad (2-4)$$

## 2.6 Carbon Dioxide Test Method

Measurement of the relative amount of carbon dioxide evolved from the reaction between water in the polyol emulsion and isocyanate from the PMDI was performed through volumetric water-displacement. The test method measures the volume of carbon dioxide gas in millilitres, released from the reacting mixture through the displacement of water from an inverted glass cylinder as set up in **Figure 2.4**.



**Figure 2.4** CO<sub>2</sub> measurement apparatus

The apparatus consists of a 5 L pyrex beaker filled to a specified level with 250 ml glass jars used as the reaction vessels. Airtight screw cap lids seal the glass jars which have silicon tubing (of equal length) inserted for gas transfer. The other end of the silicon tube is inserted into the water-filled inverted 250 ml measuring cylinders. The reacting mixture is firstly mixed in a glass jar using an overhead drill mixer at 650 rpm for 3 min. It is then transferred to clean jars, measuring the weight of sample placed in each jar. The jars are then screwed into position as soon as possible. The mixtures are left for a period of at least 24 hrs to measure the total volume of carbon dioxide released. Minimal carbon dioxide dissolves in the water, as was

initially established by allowing the evolved carbon dioxide gas to remain in the measuring cylinder for up to a period of 4-5 days displaying a constant reading from 24 hours after the polyol emulsion and PMDI reaction was initiated.

### **2.6.1 Establishing the test method**

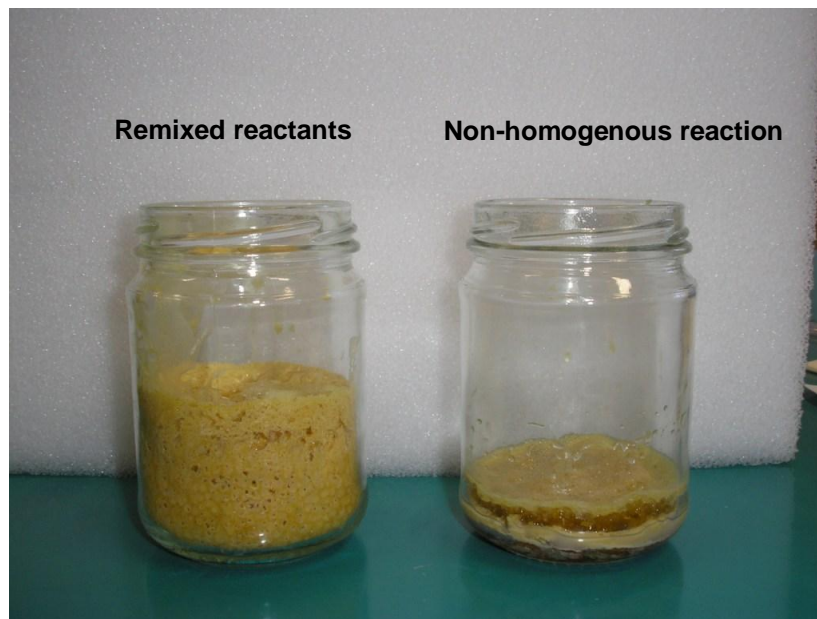
Initially, a simple control polyol emulsion was made in order to minimise variables while testing the emulsion. The simple emulsion consisted of castor oil, the surfactant and water at the industry ratio. Dioctyl phthalate (DOP), Pine oil (PO) and silicone oil (SO) were omitted from the formulation.

When reacting the simple emulsion with the industry ratio of PMDI (NCO/OH=1.7), it was found that the polyol mixed well with the PMDI and formed a light brown creamy mixture. As the mixture started to react however, separation of the polyol layer with the PMDI occurred. This reacting mixture formed an interface where the reaction progressed further, with the PMDI separating to the bottom of the jar. Although this mixture separated, however, repeated tests gave equivalent levels of evolved CO<sub>2</sub> ( $4.13 \pm 0.04$  ml/g of mixture) (**Figure 2.5**). Therefore, it is believed the curing mechanism and kinetics at the interface is the same even when the reaction mixture is not homogeneous. Although separation of the mixture gave consistent results in carbon dioxide gas evolution, the total volume of gas was not measurable from the reaction, due to the non-homogeneity. To overcome this problem, modification of the system was investigated that would prevent separation and maintain homogeneity of the mix during the course of the reaction. An attempt to keep the reacting mixture homogeneous was made by remixing the already reacting components. When the reacting mixture started to separate, it was remixed for a further minute and then left to react. Remixing caused the sample to foam up, because the carbon dioxide evolved was entrapped in the reacting mixture. This comparison is shown in **Figure 2.6**.



a) 144 ml      b) 146 ml

**Figure 2.5**      The amount of CO<sub>2</sub> evolved (from Figure 2.4) from the reaction of the simple polyol emulsion and PMDI.



a)

b)

**Figure 2.6** Remixing reacting mixture evolved more carbon dioxide that was entrapped in the polymer matrix

The remixing procedure, although partly successful at maintaining homogeneity, did not provide consistent results. In some instances a homogeneous mix was obtained

upon remixing, then on other occasions separation would be observed. Not all of the reactants remained in contact with each other after the initiation of the reaction, causing variable results.

A third procedure was trialled, which successfully overcame these issues. The reacting mixture was kept homogeneous by using talc as a fine powder to maintain even dispersion of the reactants. This allowed the true extent of reaction to be evaluated. It was found when talc was mixed with the reactants, at a level of talc to liquid ratio of 0.18, the product mixture evolved an average level of  $6.6 \pm 0.5$  ml  $\text{CO}_2/\text{g}$  mixture compared with approximately 4 ml  $\text{CO}_2/\text{g}$  mixture of the separating reactant mixture.

A calibration curve was constructed to determine the effect of sample mass on evolution of carbon dioxide gas from the reacting mixture. This was required to evaluate surface area and depth effects. It was found, that a linear relationship existed between the amount of reacting material and carbon dioxide gas released from the reacting mixture for quantities less than 15 grams of mixture (**Figure 2.7**).

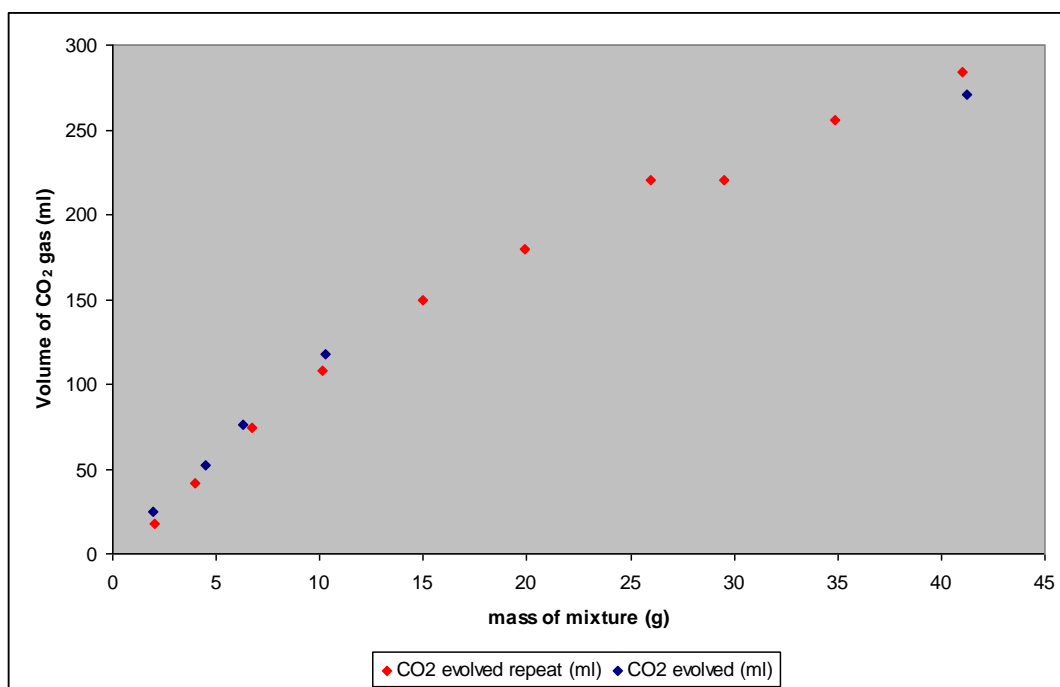


**Figure 2.7** Carbon dioxide evolved by varying the mass of sample in the reaction jar

All carbon dioxide tests in this thesis were performed within this region.

## 2.7 Error analysis

Errors are reported as the standard error of the mean and determined according to **Equation (2-5)**:

$$\sigma_E = \frac{SD}{\sqrt{N}} \quad (2-5)$$

The standard deviation (SD) was determined for multiple runs and divided by the square root of the number of experiments to obtain the standard error.

Error propagation was performed according to **Equations (2-6)** and **(2-7)** wherever necessary.

Adding or Subtracting ( $g = y \pm t$ )

$$\sigma_{Eg} = \sqrt{(\sigma_y)^2 + (\sigma_t)^2} \quad (2-6)$$

Multiplying or subtracting ( $g = y \cdot t$  or  $g = y/t$ )

$$\sigma_{Eg} = g \cdot \sqrt{\left(\frac{\sigma_y}{y}\right)^2 + \left(\frac{\sigma_t}{t}\right)^2} \quad (2-7)$$

All errors reported in chapters 3-6 are under 10% relative error, unless otherwise stated in the relevant chapters and are calculated by **Equation (2-8)**.

$$\%RE = \frac{\sigma_{Eg}}{g} \times 100 \quad (2-8)$$

## 2.8 References

- [1] P. Crews, J. Rodriguez, M. Jaspars, "Organic Structure Analysis", Oxford University Press, New York, **1998**.
- [2] P. Coleman, "Practical Sampling Techniques for Infrared Analysis", *CRC Press*, **1993**.
- [3] P. R. Griffiths, J. A. de Haseth, "Fourier Transform Infrared Spectroscopy", *John Wiley and Sonsa*, New York, **1986**.
- [4] I. Alig, W. Jenninger, J. E. K. Schawe, *Thermochim. Acta* **1999**, 330, 167.
- [5] J. Dupuy, S. Benali, A. Maazouz, G. Lachenal, D. Bertrand, *Macromol. Sympos.* **2002**, 184, 249.
- [6] M. W. Urban, "Vibrational Spectroscopy of Molecules and Macromolecules on Surfaces", **1993**.
- [7] M. W. Urban, "ATR Spectroscopy of Polymers", *ACS*, **1996**.
- [8] B.-S. Chiou, S. A. Khan, *IS&T's Annual Conference* **1997**, 50th, 570.
- [9] M. Urban, W. Ludwig, *J. Coat. Technol.* **1996**, 68, 93.
- [10] M. W. Urban, C. L. Allison, C. C. Finch, B. A. Tatro, *J. Coat. Technol.* **1999**, 71, 75.
- [11] P. K. Gallagher, "Thermoanalytical Instrumentation, Techniques and Methodology", in *Thermal Characterization of Polymeric Materials*, 2nd edition, E.A. Turi, Ed., **1997**.
- [12] G. Hohne, W. Hemminger, H.-J. Flammersheim, "Differential Scanning Calorimetry", Springer, Berlin, **1996**.
- [13] A. Atarsia, R. Boukhili, *Polym. Eng. Sci.* **2000**, 40, 607.
- [14] I. Brnardic, M. Ivankovic, H. Ivankovic, H. J. Mencer, *J. Appl. Polym. Sci.* **2006**, 100, 1765.
- [15] M. L. Costa, L. C. Pardini, M. C. Rezende, *Mater. Res.* **2005**, 8, 65.
- [16] F. Hernandez-Sanchez, R. Vera-Graziano, *J. Appl. Polym. Sci.* **1992**, 46, 571.
- [17] J. M. Kenny, A. Trivisano, *Polym. Eng. Sci.* **1991**, 31, 1426.
- [18] A. Y. Malkin, I. Y. Gorbunova, M. L. Kerber, *Polym. Eng. Sci.* **2005**, 45, 95.
- [19] R. B. Prime, C. Michalski, C. M. Neag, *Thermochim. Acta* **2005**, 429, 213.
- [20] S. Shamis, **2003**.
- [21] D. S. Jones, *Int. J. Pharm.* **1999**, 179, 167.
- [22] K. P. Menard, "Dynamic Mechanical Analysis Basics: Part 4 Applications to

Thermosets and Curing", Perkin Elmer3.

[23] W. D. Cook, F. Chen, S. K. Ooi, C. Moorhoff, R. Knott, *Polym. Int.* **2006**, *55*, 1027.

[24] W. D. Cook, K. Dean, J. S. Forsythe, *Materials Forum* **2001**, *25*, 30.

[25] D. Harran, A. C. Senhaji, G. Marin, "Rheological Study of the Gelation in a Thermosetting Resin", in *Xth International Congress on Rheology*, Sydney, **1988**, p. 1/389.

[26] J. Jiao, J. Burgess Diane, *AAPS Pharm. Sci.* **2003**, *5*, E7.

[27] H. Kim, K. Char, *Korea-Australia Rheol. J.* **2000**, *12*, 77.

[28] K.-W. Lem, C. D. Han, *J. Appl. Polym. Sci.* **1983**, *28*, 3185.

[29] G. Liang, K. Chandrashekhara, *J. Appl. Polym. Sci.* **2006**, *102*, 3168.

[30] M. Piao, J. Otaigbe, D. Otts, M. Urban, *Polym. Mater. Sci. Eng.* **2004**, *90*, 112.

[31] A. Yousefi, P. G. Lafleur, *Polym. Compos.* **1997**, *18*, 157.

[32] A. Ponton, P. Clement, J. L. Grossiord, *J. Rheol.* **2001**, *45*, 521.

[33] P. Sherman, "Rheological Properties of Emulsions", in *Encyclopedia of Emulsion Technology: Basic Theory*, P. Becher, Ed., Marcel Dekker INC., **1983**.

[34] L. E. Nielsen, "Polymer Rheology", *New York*, **1977**.

[35] C. W. Macosko, R. G. Larson, "Rheology: Principles, Measurements, and Applications", *Wiley-VCH*, New York, **1994**.

# CHAPTER 3

## Investigation into the main reactions in the product

Part 1: A kinetic study of Polyurethane formation

Part 2: A kinetic study of Polyurea formation

Results from Part 1 of this chapter have been published in *Macromol. Chem. Phys.* **2008**, *209*, 2302–2311

## **3 INVESTIGATION INTO THE MAIN REACTIONS IN THE PRODUCT**

### **3.1 Part 1: Kinetic study of the Polyurethane reaction between Castor Oil and PMDI**

#### **3.1.1 Introduction**

Oligomeric diphenylmethane diisocyanate (PMDI) is widely used as a curing resin for coatings and adhesives.<sup>[1-5]</sup> The urethane network formed through the crosslinking reaction of PMDI and the polyol provides a continuous matrix which adds to the structural integrity of the coating. Fast setting times encountered during application of this product when reacted with castor oil is problematic. Reaction rate, kinetics of cure and state of cure are therefore key aspects of understanding and controlling the coating performance. Although polyurethane thermoset cure through the use of monomeric or diisocyanate compounds has been widely investigated<sup>[6, 7]</sup>, very little work has been reported, using oligomeric isocyanates with trifunctional polyols.<sup>[8]</sup> The focus of Part 1 in this chapter is to investigate the reaction kinetics and develop an understanding of the curing profile of the polyurethane reaction between castor oil and PMDI. The curing reaction has been studied using complimentary techniques including calorimetry, rheology and infrared spectroscopy. The use of isoconversional methods (model-free kinetic analysis) to establish cure kinetics are preferred to model fitting methods, as a variety of kinetic models yielding different reaction variables such as activation energy, reaction order etc., have been shown to fit the same experimental data.<sup>[9]</sup> Isoconversional analysis has previously been used to describe the crosslinking reaction for a limited number of complex polyurethane systems.<sup>[10, 11]</sup>

Model fitting methods assume one activation energy to describe the entire cure process, even if the reaction mechanism has multiple steps. Isoconversional methods can provide information on the cure profile by determining the conversion dependence of the apparent activation energy.<sup>[12]</sup> The advanced integral isoconversional method as developed by Vyazovkin<sup>[13]</sup> will be employed to develop the cure profile. The kinetic equations used in the integral isoconversional method

are presented in Chapter 1 (**section 1.2.7.1**).

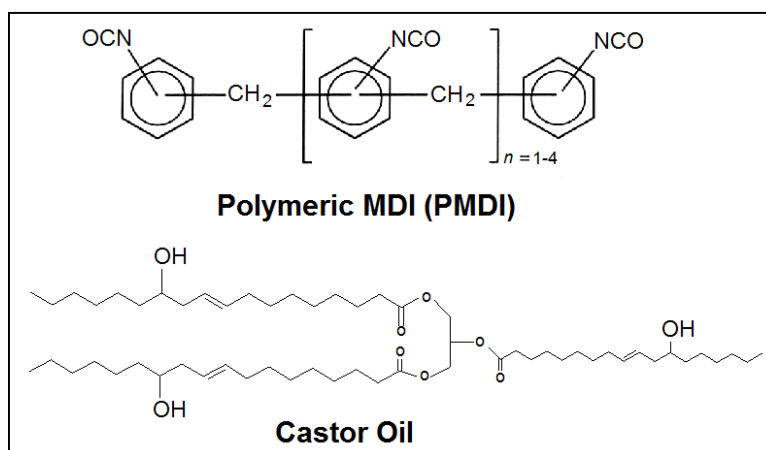
Rheological techniques ascertain further information about the curing reaction and have also been employed to follow the curing system. The reacting polyurethane undergoes chain extension and subsequent branching due to the higher functional moieties present in the reacting components.<sup>[14]</sup> Monitoring the viscosity build up during the pre-gel stages, which is a consequence of the increase in molecular weight and an indication on the magnitude of chain extension and chain branching, provides information on the reaction rate and cure profile.<sup>[15-17]</sup> Understanding the variables that influence viscosity build up in the pre-gel stage, therefore allows for greater control of the pot-life and the workability time of this coating resin. Another important cure property of a material, measurable through rheological investigations is gelation. Gelation is a critical component in thermosetting systems because it describes the formation of an infinite molecular network and hence the start of the crosslinking reaction.<sup>[14, 18]</sup> Investigation of gel times will help elucidate the reaction kinetics of the polyurethane reaction, providing further information on the workability time of the coating.

### 3.1.2 Experimental

#### 3.1.2.1 Materials and sample preparation

Oligomeric diphenylmethane diisocyanate (PMDI) with a functionality of 2.7 and viscosity of 200-250 mPa.s was used as received from Dow Plastics (PAPI 20). Refer to Appendix A for characterisation. Castor oil was obtained from ACE Chemical Company with a hydroxyl value of 160 and free fatty acid content less than 1 %, which was used as received. Both the PMDI and castor oil were cooled in an ice bucket in closed containers before mixing at a temperature of  $0\text{ }^{\circ}\text{C} \pm 3\text{ }^{\circ}\text{C}$ , to slow the reaction between the components.

A stoichiometric ratio NCO/OH of 1:1 was used to provide a model system. The kinetic behaviour of this system was also compared to the product ratio of excess isocyanate, NCO/OH= 1.7:1. The materials were mixed at standard conditions using an overhead drill mixer with a 5 cm diameter fan blade. A mixing time of 1 minute was used to ensure minimum heat loss to the atmosphere. The reacting components can be seen in **Scheme1.13**.



Scheme 3.1 Reacting components, PMDI and castor oil

### 3.1.2.2 Methods

#### 3.1.2.2.1 DSC Measurement

Kinetic studies were carried out using a DSC 2920 (TA instruments). Samples were sealed in hermetic aluminium pans with an average sample weight of  $5 \pm 0.5$  mg. The DSC was pre-cooled to  $-30$  °C. The sample was prepared and placed in an ice bath to minimise heat loss from the reacting system. The sample was placed at  $-20$  °C and was run in non-isothermal mode from  $-20$  °C to  $170$  °C at various heating rates of 5, 7.5, 10, 12.5, 15 and  $20$  °C  $\text{min}^{-1}$ . **Figure 3.1** displays a typical thermogram obtained at  $12.5$  °C  $\text{min}^{-1}$ .

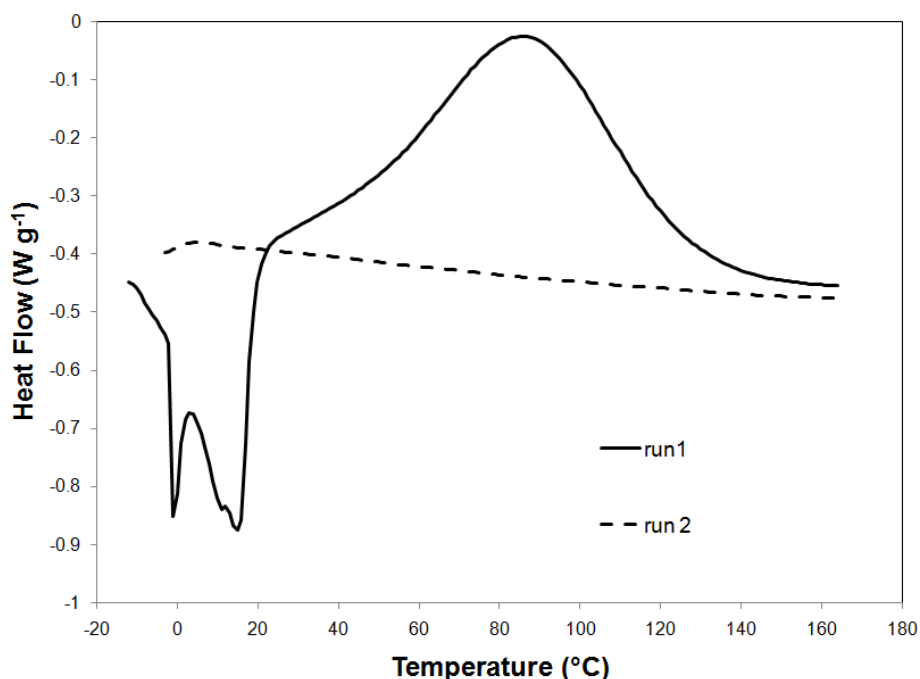


**Figure 3.1** Representation of baseline determined for  $12.5$  °C  $\text{min}^{-1}$

It is noticed that two initial endothermic peaks are obtained which represent the melting points of frozen castor oil and PMDI. A second and third non-isothermal heating run was then performed from  $-10$  °C to  $170$  °C at a heating rate of  $10$  °C  $\text{min}^{-1}$  and showed no further exothermic event, furthermore the third non-isothermal run overlapped the second, suggesting the second non-isothermal run was suitable for use as a baseline to calculate the heat of reaction.<sup>[19]</sup> In between the non-isothermal steps, the sample was quenched in an ice bath as the DSC cooled down to  $-10$  °C

using liquid nitrogen feed. The cell constant calibration was performed using an indium (99.99% pure) standard. Nitrogen at a flow rate of 50 ml min<sup>-1</sup> was used as the purge gas. Model-free kinetic software was unavailable for isoconversional analysis.

#### 3.1.2.2.2 *Rheological Measurement*

An AR-2000 controlled stress and direct strain control rheometer from TA Instruments, (US) was used to study the curing behaviour of castor oil and PMDI reaction.

A 2 cm 2° cone and plate configuration was used to achieve a thin gap allowing a large surface-to volume ratio for isothermal curing. All dynamic measurements in oscillatory mode were performed using a multi frequency technique ranging from 0.6 Hz to 1.2 Hz with four data points and a strain of 10 %. Isothermal measurements were performed within the interval of 30 °C to 100 °C.

#### 3.1.2.2.3 *Infrared Spectroscopy*

The cure kinetics was obtained using a Nicolet 8700 spectrophotometer fitted with a transmission cell. Transmission experiments were performed using disposable pressed KBr discs to which a thin coating of the mixed sample was applied. After the sample was placed on the KBr disc and into a brass holder, transmission spectra were obtained at an isothermal temperature of 60 °C over a 40 minute period. Samples were kept at the isothermal temperature using a temperature-controlled furnace. An isothermal temperature of 60 °C was chosen to give a direct comparison between analytical techniques during isothermal cure as temperatures outside this range were not sensitive due to equipment limitations. Spectra were taken intermittently to determine the curing profile with a maximum of 2 scans per time interval at a resolution of 4 cm<sup>-1</sup>. Backgrounds of KBr discs were collected before each sample. The area underneath the isocyanate peak at 2270 cm<sup>-1</sup><sup>[20]</sup> was used to calculate the conversion through **Equation (1-25)**.<sup>[21]</sup> Where direct comparison of spectra was required, normalisation to the CH<sub>2</sub> stretching vibration at 2928 cm<sup>-1</sup> was performed.<sup>[22]</sup>

#### 3.1.2.2.4 *Dynamic Mechanical Analysis (DMA)*

DMA measurements were performed using a TA Instruments DMAQ800 in single cantilever bending deformation mode. The samples were cured isothermally at 70 °C for 24 hours followed by post-curing at 180 °C for 3 hours. A frequency of 1 Hz and a peak displacement of 20 μm were selected. The temperature was scanned from -70 °C to 140 °C and ramped at a rate of 2 °C min<sup>-1</sup>. The glass transition temperature  $T_g$ , was taken as the temperature at which the loss factor  $\tan \delta$  reached a maximum. Liquid nitrogen was used to achieve the sub-ambient temperature for glass transition measurement.

### 3.1.3 Results and Discussion

#### 3.1.3.1 Investigation of the reaction kinetics through DSC

The non-isothermal heat flow profiles shown in **Figure 3.2** exhibit a shift in the peak temperature, with higher peak temperatures observed with an increase in the heating rate.

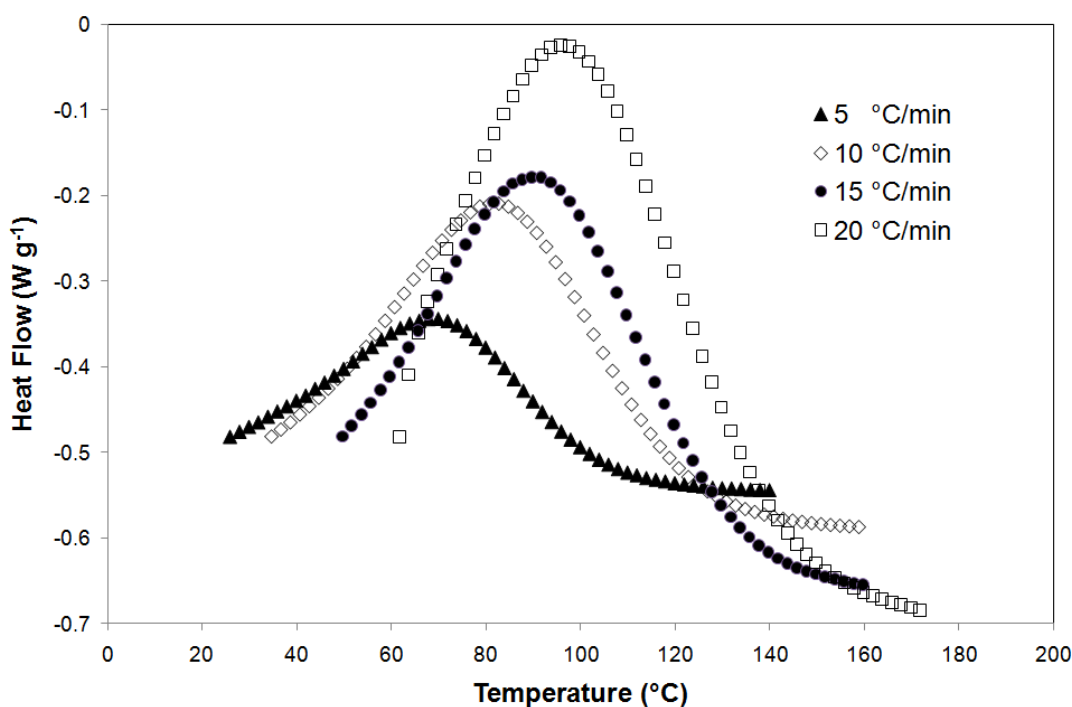


**Figure 3.2** Heat flow profile for castor oil with PMDI at equal stoichiometry

This behaviour is a direct consequence of the kinetics of the reaction. As the heating rate increases there is a higher amount of unreacted groups present at higher temperatures. This occurs regardless of the reaction order and has been observed in other polymeric systems.<sup>[23]</sup> A summary of the peak temperatures and corresponding conversion (**Equation (1-5)**) at the peak temperature at various heating rates is given in **Table 3-1**.

The non-isothermal heat of reaction was found to be approximately the same for all heating rates giving an average value of  $24.9 \pm 1.3 \text{ kJ mol}^{-1}$  equivalent isocyanate. This is very much smaller than polyurethane systems in the literature<sup>[8]</sup>. Two reasons for this are; oligomeric isocyanates have previously not been investigated for their reaction with castor oil and this mixture has an extremely fast rate of reaction upon mixing, resulting in heat loss before placed in the DSC cell, even with preventative

measures in place to minimise this heat loss (refer to experimental section).

Peak temperatures and conversions at the peak temperature obtained for the system with excess isocyanate are within the same range as that observed for the stoichiometric system and subsequently are not shown. The exothermic heat of reaction determined for the system with excess isocyanate was found to be  $11 \pm 0.6$  kJ mol<sup>-1</sup> equivalent isocyanate. This is under half of that seen for the equal stoichiometric mixtures of castor oil and oligomeric isocyanate.

**Table 3-1 Non-isothermal data for peak temperatures and corresponding conversions obtained for the castor oil- PMDI reaction at equal stoichiometry**

Heating rate (°C min <sup>-1</sup> )	Peak Temperature (°C)	Conversion at Peak (%)
5	69.68 ± 0.36	56.3 ± 0.42
7.5	77.48 ± 0.15	51.0 ± 4.24
10	82.82 ± 0.07	53.5 ± 2.12
12.5	86.69 ± 0.30	55.2 ± 0.45
15	91.02 ± 0.22	48.5 ± 2.12
20	97.75 ± 0.51	45.5 ± 3.53

The conversion at the peak temperature is approximately the same at all heating rates, although a slight reduction is observed with an increase in heating rate, with the exception of 7.5 and 10 °C min<sup>-1</sup>.

The kinetic profile was investigated using model-free kinetics developed by Vyazovkin *et al.* [12, 24, 25] and is displayed in **Figure 3.3**. The advanced integral isoconversional method together with the Senum-Yang approximation [12] was used to determine the dependence of the activation energy on conversion.

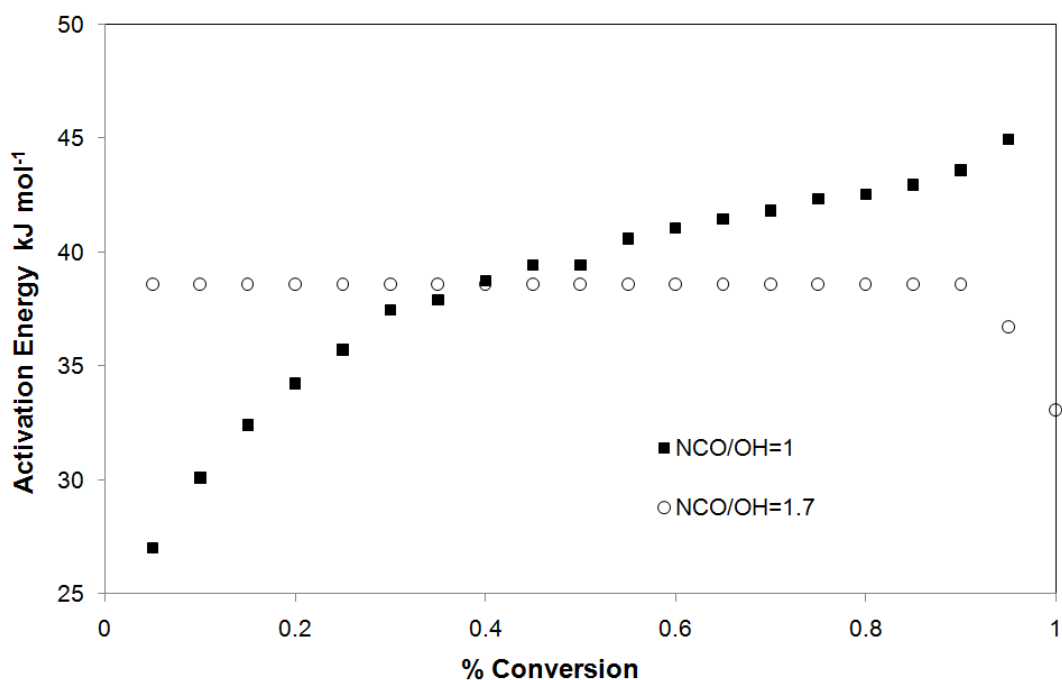


**Figure 3.3** The advanced integral isoconversional analysis of activation energy with extent of conversion for two different ratios of hydroxyl groups to isocyanate groups.

The activation energy increases with the extent of conversion from 27 to 44.9 kJ mol<sup>-1</sup> for a stoichiometric ratio of hydroxyl groups to isocyanate groups. This suggests a multi-step mechanism. According to Vyazovkin<sup>[26]</sup>, processes that exhibit an increasing activation energy with an increase in the extent of conversion are a result of competing reactions, although some independent and consecutive reactions may also exhibit this profile. The mechanism for castor oil reacting with non-oligomeric diisocyanates has been investigated previously<sup>[27, 28]</sup>, and found to be of a second-order kinetic reaction. However, when asymmetric diisocyanates have been used, two different reaction rates were observed relating to the different positions of the isocyanate group.<sup>[27, 29]</sup> Ajithkumar *et al.*<sup>[29]</sup> reported two distinct rates of reaction when applying a second order model to the reaction between TDI and castor oil. They attributed this to the 4-position isocyanate group being more reactive than the 2-position due to steric hindrance.

It is expected that the increasing activation energy with conversion is due to the difference in reactivity of the terminal isocyanate groups to the internal isocyanate groups of the varying weight oligomers in PMDI. This will be discussed further in the rheological analysis performed (**section 3.1.3.2**).

The reaction using an excess in isocyanate groups shows a constant activation energy of  $38.6 \text{ kJ mol}^{-1}$ , with a slight decline observed at higher conversions. This system showed no evidence of competing reaction rates for the differing positions of the isocyanate group. The system with an excess of isocyanate groups is likely to have the hydroxyl groups completely consumed by the faster reacting isocyanate group before the slower reacting isocyanate group had a chance to react. The apparent activation energies obtained for the castor oil and PMDI reaction was in good agreement with similar systems reported in the literature.<sup>[8, 27, 29]</sup>

### ***3.1.3.2 Investigation of the castor oil and PMDI reaction through rheology***

#### *3.1.3.2.1 Kinetic Analysis through the point of gelation*

Isothermal curing of a thermosetting resin is usually characterized by gelation and vitrification.<sup>[30]</sup> Knowing the gel time is important in industrial applications to ensure enough time is available for application after mixing. The incipient formation of a continuous network of polymer chains describes the start of gelation. This occurs at a fixed extent of conversion if the mechanism of reaction is not a function of temperature. Monitoring the rheological properties of thermosetting resins such as viscosity, the loss tangent ( $\tan \delta$ ), loss modulus ( $G''$ ) and storage modulus ( $G'$ ); the gel time ( $t_g$ ) and cure profile can be elucidated.

Criteria that have previously been used to determine the gel point are:

1. The crossover of  $G'$  and  $G''$  where  $\tan \delta$  is 1 for stoichiometric systems<sup>[31]</sup>
2. The maximum peak in  $\tan \delta$  (based on where there is a maximum difference between elastic and viscous behaviour)<sup>[30]</sup>
3. Frequency independence of  $\tan \delta$ <sup>[32]</sup>
4. Frequency dependence of  $G'$  at 1 Hz<sup>[30, 33]</sup>

Criteria 3 and 4 have been reported elsewhere in determining the vitrification point of crosslinking systems<sup>[33]</sup>. The criterion 4 which uses the frequency dependence of  $G'$  however, in determining vitrification, is only correct if gelation has already occurred in the system. This criterion can only be used to obtain gel time if it occurs before the system vitrifies.

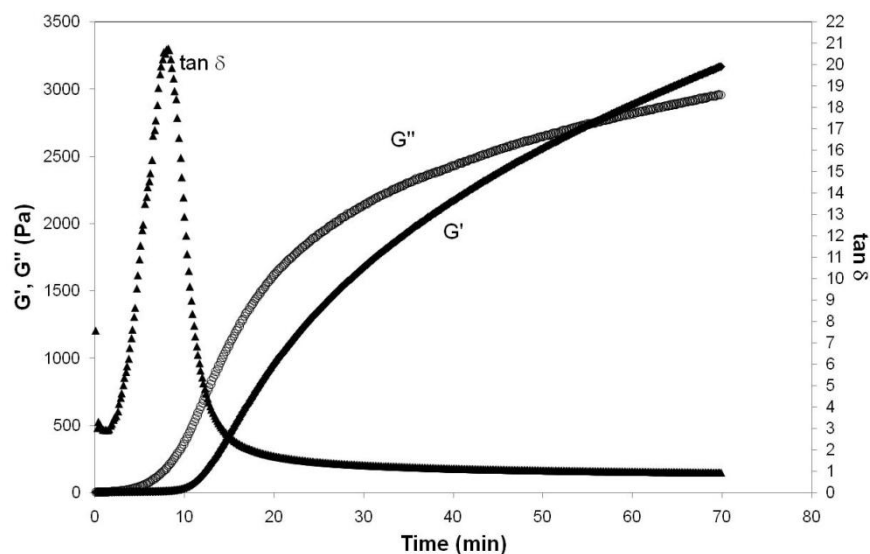


**Figure 3.4**  $G'$ ,  $G''$  and  $\tan \delta$  versus cure time for the castor oil and PMDI stoichiometric system at 70 °C

The cure was investigated using isothermal oscillatory analysis for mole ratios of NCO/OH equal to 1 and 1.7. A typical experiment for the stoichiometric system is shown in **Figure 3.4** where a maximum is seen in  $\tan \delta$  before the crossover of  $G'$  and  $G''$ . The cross-over of  $G'$  and  $G''$  was found for 70 °C, 80 °C and 90 °C out of the temperature range chosen (30 to 90 °C at 1 Hz and 10% strain) due to the length of time the samples were left to react. A strain of 10% was used and was within the viscoelastic region of the strain sweep, which allowed for the early pre-gel curing stages of the product to be determined. As the network formed however, a 10% strain may have been too large for the newly formed structure not to be disturbed, thus not obtaining as high a viscosity build up or storage modulus as one would otherwise have expected. Instrumental limitations disallowed a change in % strain while curing progressed, in order to obtain a full spectrum of the cure profile without compromising the structure.<sup>[34]</sup> The gel times established from the cross-over of  $G'$  and  $G''$  in uni-frequency mode at 1 Hz are displayed in **Table 3-2**.

**Table 3-2 Gel times (minutes) observed for the stoichiometric system of castor oil and PMDI using uni-frequency and multiple frequency mode**

<b>Temperature (°C)</b>	<b><math>G' = G''</math></b>	<b><math>\tan \delta_{(\max)}</math> 1 Hz</b>	<b><math>\tan \delta_{(\max)}</math> multifrequency</b>	<b><math>G'</math> frequency dependence</b>
<b>Criterion</b>	<b>1</b>	<b>2</b>	<b>2, 3</b>	<b>4</b>
20	-	95.9	-	-
30	-	62.5	-	-
40	-	40.3	-	-
50	-	26.4	-	-
60	-	16.3	18.1	18
70	55.6	8.2	12.3	10
80	47.7	5.6	7.1	8
90	26.8	3.6	5.2	6
100	-	-	1.3	2.7

Isothermal time sweeps were also performed at multiple frequencies allowing the determination of the gel time according to criteria 2 and 4. Multifrequency mode increased the time taken for this cross over to occur and the reactions were terminated before the intersection of  $G'$  and  $G''$ . In multifrequency mode, the time in which  $\tan \delta$  reached its maximum was independent of the frequency, as shown in **Figure 3.5**.

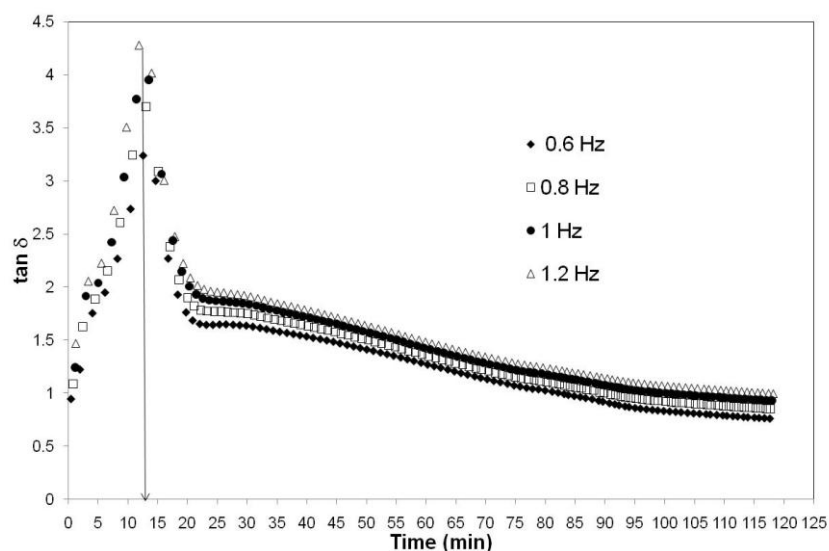


**Figure 3.5 Multiple frequency plot of  $\tan \delta$  at 70 °C**

Winter and Chambon<sup>[32]</sup> have shown that  $G'$  and  $G''$  follow a power law behaviour as a function of frequency close to the gel point. The true gel point therefore occurs when  $\tan \delta$  intersects at the same time for all frequencies.<sup>[32, 35]</sup> As  $\tan \delta$  reaches a maximum value before the crossover of  $G'$  and  $G''$ , the incipient gelation is regarded to occur at this point, as all frequencies exhibit the maximum peak in  $\tan \delta$  at the same time. Close gel times were obtained using the maximum in  $\tan \delta$  from uni-frequency (1 Hz) (criterion 2) and multiple frequency modes (0.6 Hz to 1.2 Hz) (criterion 3) as shown in **Table 3-2**.

The multifrequency data showed very similar gelation times when analysed according to frequency independence of  $\tan \delta$  (criterion 3) and the frequency dependence of  $G'$  (criterion 4). This is also displayed in **Table 3-2**. The values of gel time obtained using the cross-over of  $G'$  and  $G''$  are much higher than that observed using the other criteria. This is explained by the fact that gelation of a thermosetting resin is not instantaneous and occurs over a period of time.<sup>[30]</sup> It is evident that depending on which criterion was chosen to determine the gel point, different values are obtained. The gel point in general, decreases with an increase in isothermal cure temperature, which suggests at higher temperatures, the molecular mobility increases in the initial stages of cure, allowing crosslinking to occur at a faster rate.

The degree of conversion at the gel point is considered constant for thermosetting

systems <sup>[18, 36, 37]</sup> allowing for a direct relationship between the gel time ( $t_{gel}$ ) and the apparent curing constant  $K_c$ , given in **Equation (3-1)**: <sup>[18, 38]</sup>

$$t_{gel} = A' \times \left( \frac{1}{K_c} \right) \quad (3-1)$$

The curing process is described by an overall activation energy  $E_a$  where the temperature dependence of the gel time follows the Arrhenius law<sup>[17]</sup> and can be obtained from **Equation (3-2)**.

$$\ln(t_{gel}) = A'' + \frac{E_a}{RT} \quad (3-2)$$

The activation energy can thus be found from the slope of  $\ln(t_{gel})$  versus  $1/T$  ( $K^{-1}$ ) shown through a linear relationship in **Figure 3.6** (for a maximum in  $\tan \delta$  at 1 Hz).

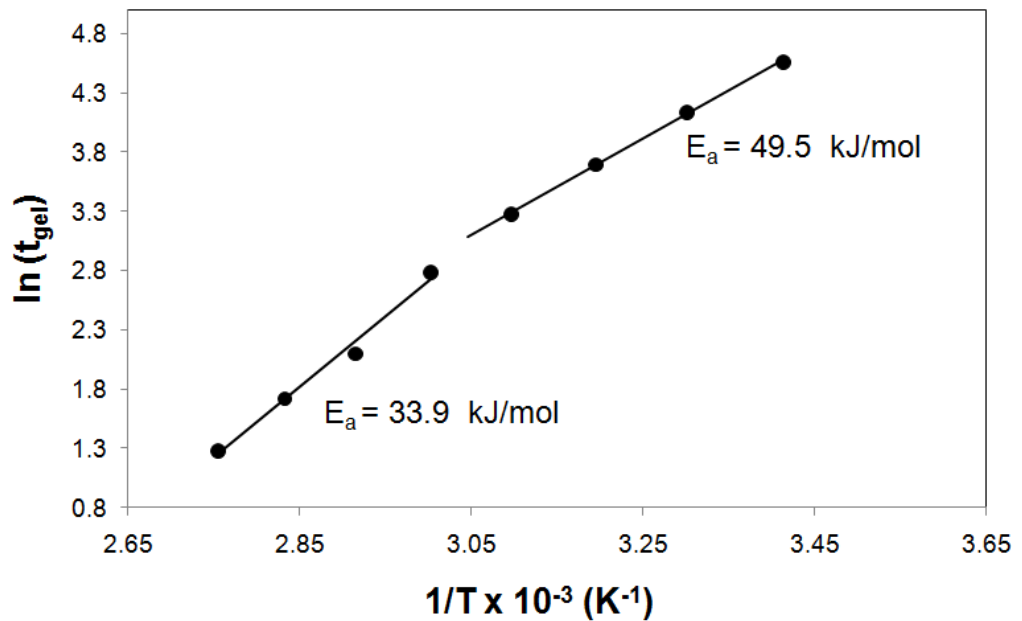


**Figure 3.6** linear relationship of gel time obtained through the maximum in  $\tan \delta$

It is noticed however, that two slopes exist in **Figure 3.6** indicating that the activation energy changes with temperature and therefore, with the extent of

conversion as observed in DSC analysis.

The activation energy determined at  $T \leq 50$  °C was found to be  $33.9 \pm 0.7$  kJ · mol<sup>-1</sup> while at  $T \geq 60$  °C was  $49.5 \pm 4.0$  kJ · mol<sup>-1</sup>. Thus the activation energy range through isothermal rheological analysis at the gel time, corresponds very closely to the range detected using non-isothermal DSC isoconversional analysis (**Figure 3.3**).

The activation energy (**Table 3-3**) was determined for all criteria, using the gel times shown in **Table 3-2**. All criteria give values relatively close to one another, which also corresponded well with those, determined using the isoconversional methods for DSC data (**Figure 3.3**).

**Table 3-3 Activation Energies determined by various criteria for the stoichiometric system**

<b>Criteria</b>	<b>Activation Energy (kJ mol<sup>-1</sup>)</b>	<b>R<sup>2</sup></b>
1. $G' = G''$	$37.6 \pm 13.3^*$	0.89
2. $(\tan \delta)_{\max}$ @ 1 Hz (average)	$42.3 \pm 1.8$	0.99
3. $(\tan \delta)_{\max}$ multi frequency	$43.4 \pm 2.8$	0.99
4. $G'$ frequency dependence	$44.3 \pm 6.2$	0.95

\*%RE<40%

An excess of isocyanate, as is present in the industrial product was also investigated to develop a better fundamental understanding about specific application properties and limitations of the current ratio used by the industry partner. The typical curing profile for a system with excess isocyanate is shown in **Figure 3.7**.

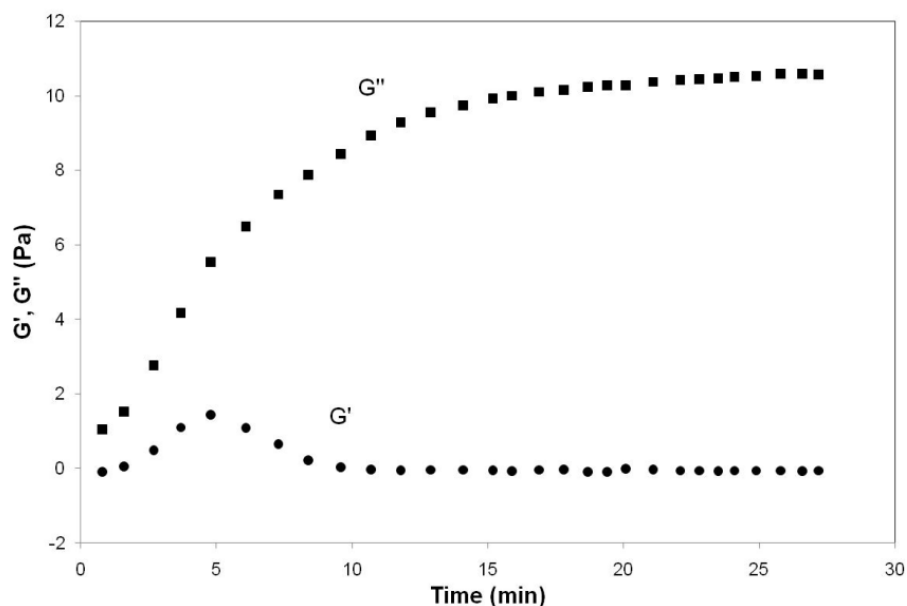


**Figure 3.7**  $G'$  and  $G''$  versus cure time for the castor oil and PMDI with an excess of isocyanate at 70 °C

The elastic modulus  $G'$ , represents the build up of network formation in the system, and shows a very different curing behaviour to the system having an equal stoichiometric ratio of isocyanate to hydroxyl groups.  $G'$  can be seen to increase to a maximum value and then rapidly decline in magnitude until it reaches its initial value. At the same time, the loss modulus  $G''$ , which describes the flow behaviour of the system, tends to increase in magnitude past the maximum  $G'$  value, until the flow behaviour of the system starts to plateau. The viscous behaviour is much larger in magnitude than the elastic component over the entire cure profile. As the viscous behaviour predominates the curing, the  $\tan \delta$  profiles do not show any distinct maxima and are highly scattered. **Figure 3.8** shows the behaviour of the elastic modulus  $G'$  with an increase in isothermal cure temperature.

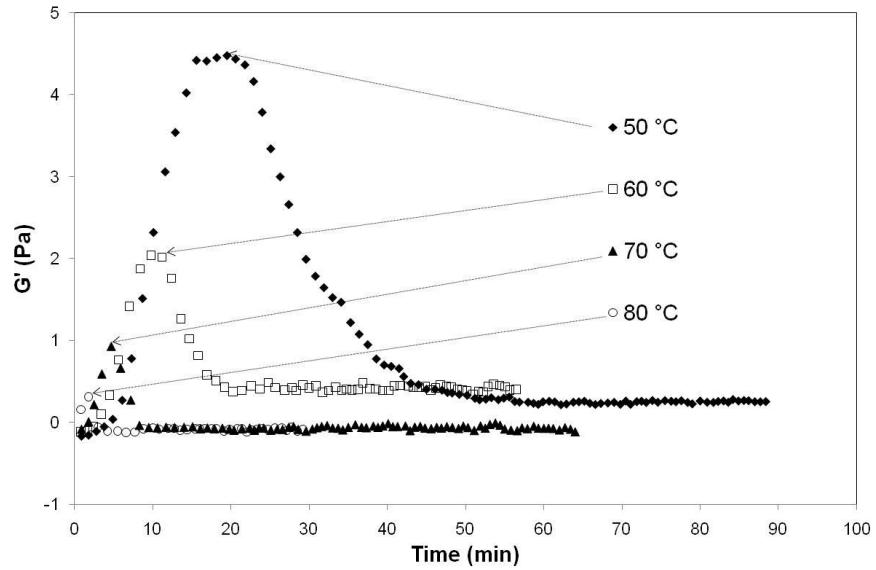


**Figure 3.8** Temperature dependence of  $G'$  during curing of castor oil and PMDI with excess isocyanate

A correlation between the cure time and the isothermal temperature is observed. The ability for a network structure to form in this system rapidly reduces with an increase in isothermal curing temperature. The magnitude of  $G'$  at 80 °C is extremely small and a directly proportional relationship was found to exist between the time and the maximum value obtained for  $G'$  (**Figure 3.9**).

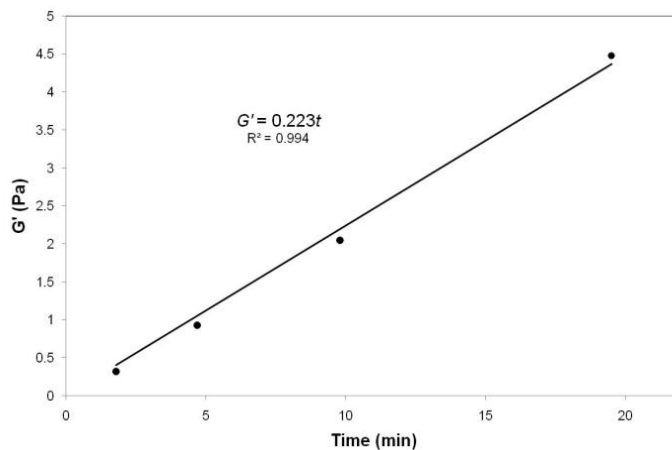


**Figure 3.9** Correlation between  $G'$  and the time it occurs

The time observed at the maxima of  $G'$  can be explained by the limiting number of functional groups of the castor oil being completely consumed (explained further in relation to **Figure 3.11**).

### 3.1.3.2.2 Kinetic Analysis from Viscosity data

Viscosity data was obtained using oscillatory dynamic analysis by following the complex viscosity  $\eta^*$  of the curing system.

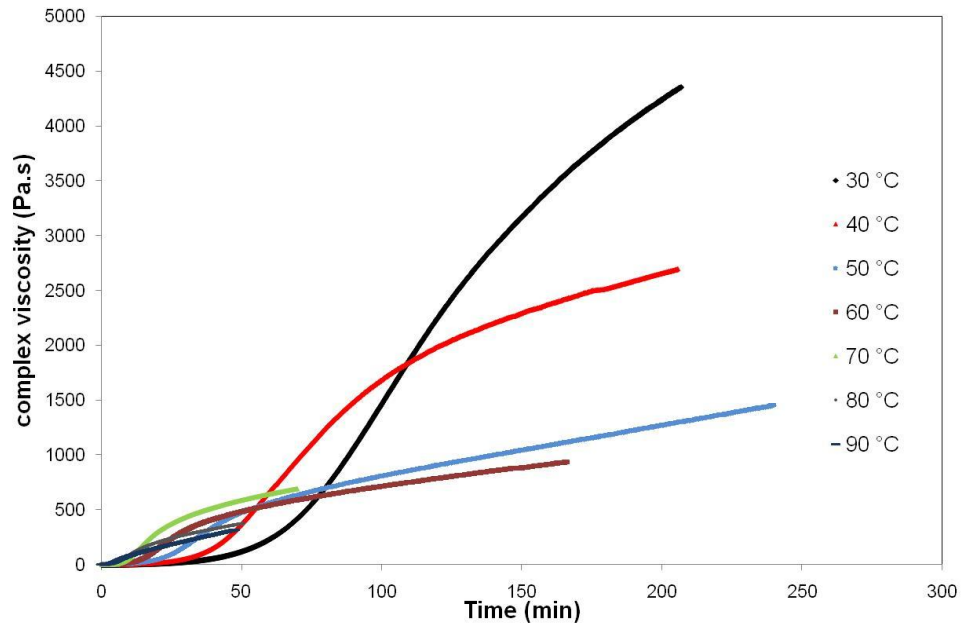


Figure 3.10 Viscosity build up of castor oil and PMDI and the stoichiometric ratio

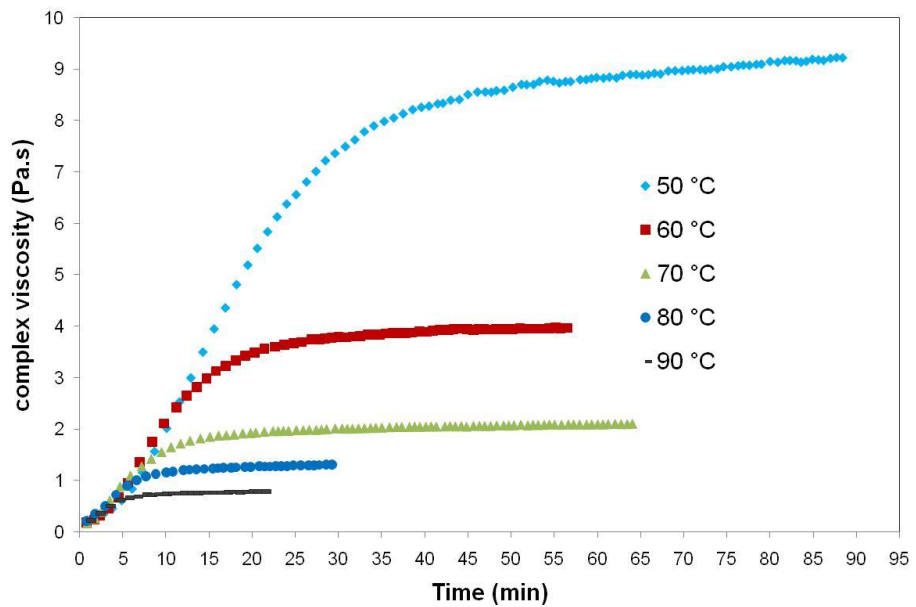


Figure 3.11 Viscosity build up of castor oil and PMDI with excess isocyanate

It was observed that the rate of initial viscosity build up increased with an increase in isothermal cure temperature for the stoichiometric system (Figure 3.10). This was

not seen for the system with excess isocyanate (**Figure 3.11**). It is also evident that as the isothermal cure temperature was reduced, the viscosity build up was much greater for the stoichiometric system.

The complex viscosity curves shown in **Figure 3.11**, exhibit a plateau beyond the time of the  $G'$  maxima (**Figure 3.7**), suggesting full cure has been reached for this system. This, results in the formation of a polyurethane adduct, with hydroxyl termination, that prevents further crosslinking. The resultant material is a hydroxyl terminated viscous liquid. The plateau region is the viscous liquid behaviour of this polyol/isocyanate adduct, which is observed to decrease with increasing temperature. After the end of viscosity build up due to the complete consumption of hydroxyl groups and formation of the polymer adduct, the plateau can be seen to increase slightly over the course of the experimental time. This slight increase in viscosity is most likely due to the reaction of excess isocyanate groups with moisture in the air.

The viscosity build up in the stoichiometric system is influenced by the functionality distribution of the base polymer as well as the relative reactivity of functional groups involved in the curing process.<sup>[17]</sup> The slow onset of diffusion control at isothermal temperatures below the glass transition temperature for the stoichiometric system, explains the higher viscosity achieved in the later stages of cure.<sup>[33]</sup> The glass transition temperature found for the stoichiometric system is  $T_g = 57.68 \pm 0.99^\circ\text{C}$ , suggesting the onset of vitrification at 30 °C and 40 °C is responsible for the continuing increase in viscosity build up at lower isothermal temperatures.

### 3.1.3.2.3 Kinetics of complex viscosity during the initial stages of cure

The time dependency of polyurethane viscosity during the initial cure stages can be expressed through an exponential function represented in **Equation (3-3)**:<sup>[30, 39]</sup>

$$\eta(t) = \eta_0 e^{k_\eta t} \quad (3-3)$$

where  $\eta_0$  is the viscosity at  $t = 0$  and  $k_\eta$  is the rate constant for the viscosity increase.

It is assumed that before the gel time (taken as the maximum in  $\tan \delta$ ), the viscosity build up follows a first order process and adheres well to the exponential function for the stoichiometric system at higher temperatures (**Figure 3.12**).<sup>[17, 30, 40]</sup> The exponential function was also observed to fit the data well for the excess isocyanate system up to the point where all the hydroxyl groups were consumed.

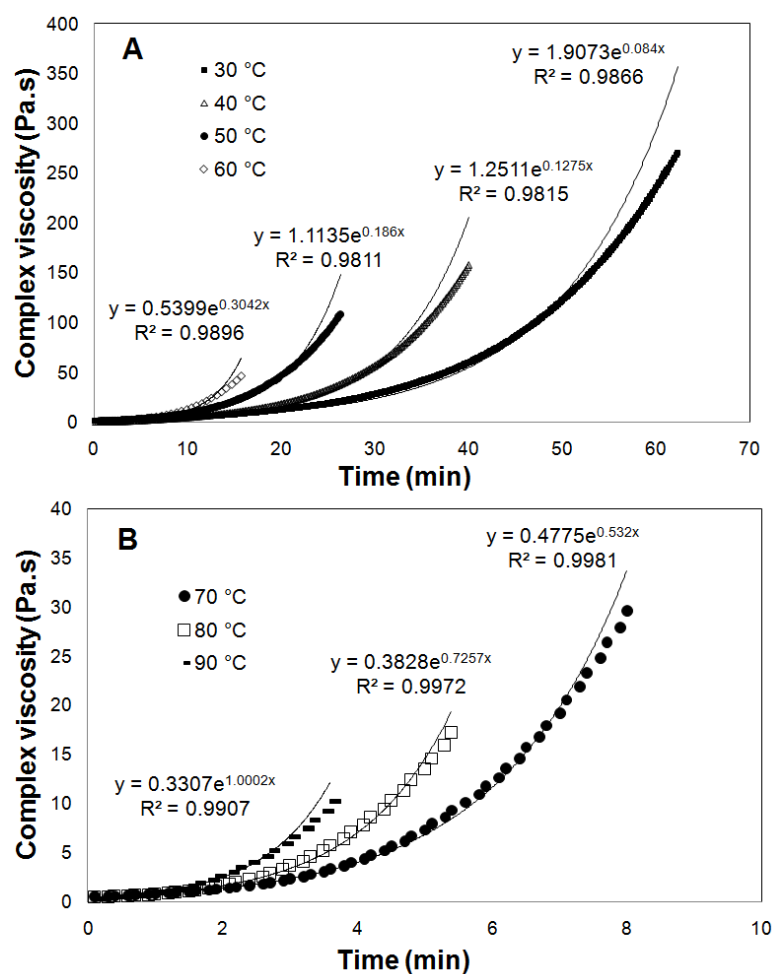


**Figure 3.12** Viscosity build up follows an exponential function before the gel point for the equal stoichiometric system at A) lower isothermal temperatures and B) higher temperatures

Taking the logarithm of **Equation (3-3)** and plotting  $\ln \eta$  against  $t$  should yield a straight line with the slope equal to the rate of viscosity increase  $k_\eta$ .<sup>[40, 41]</sup> **Figure 3.13** displays the rate of viscosity increase in the polyurethane system for the stoichiometric (A) and excess isocyanate ratios (B), showing that linearity exists.

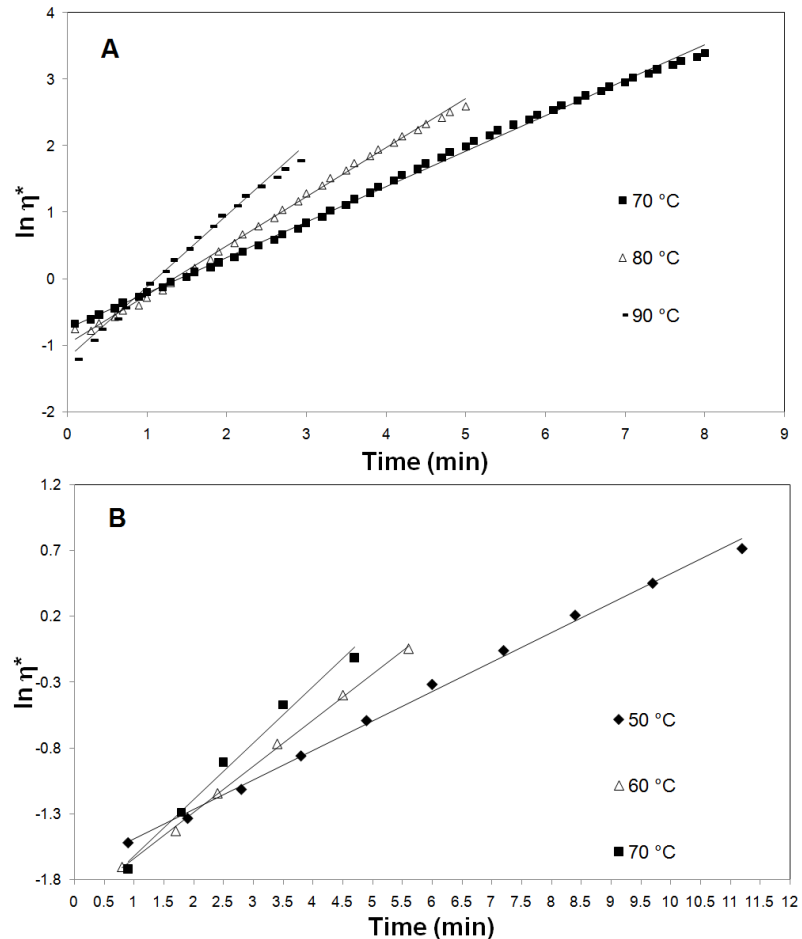


**Figure 3.13** Linearity observed for the natural log of complex viscosity versus time profiles for the castor oil and PMDI system at A) equal stoichiometry and B) excess isocyanate

The rate of viscosity increase for the lower temperatures of the stoichiometric ratio is shown in **Figure 3.14** and displays a discontinuity in the rate at early stages of viscosity build up.

The discontinuity can arise from the difference in the chemical reactivity of functional groups as suggested by Sekkar *et al.*<sup>[17]</sup>, with the more reactive isocyanate group dominating the viscosity build up in the first stage of curing.

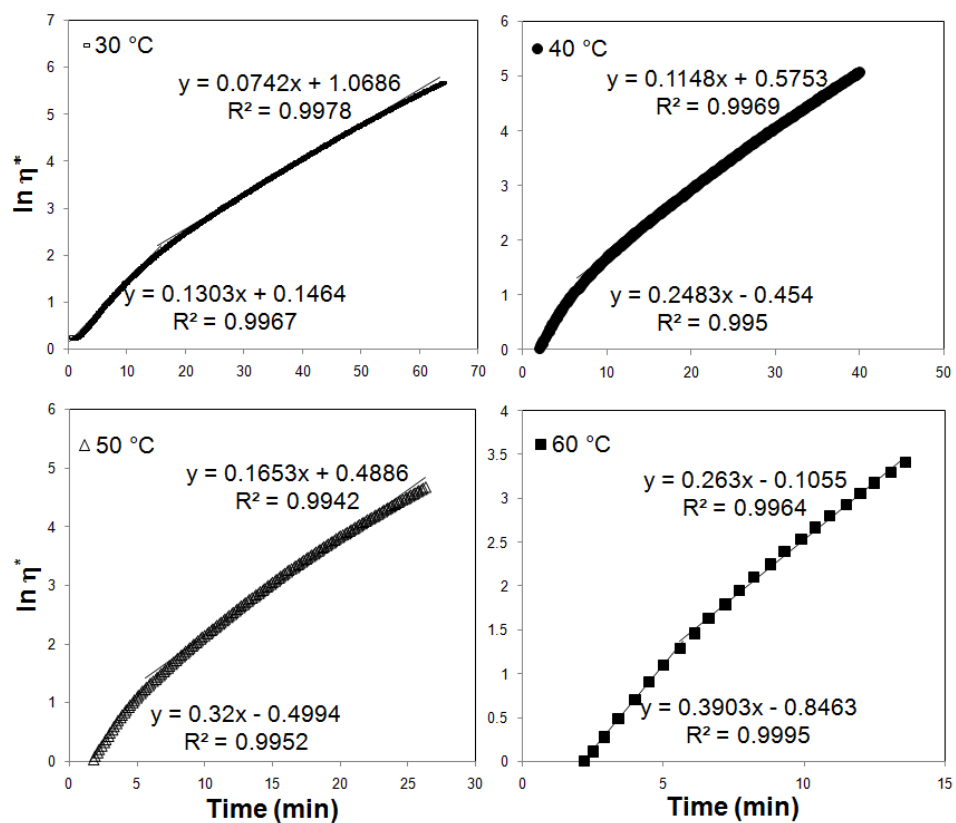


**Figure 3.14** Rate of viscosity increase shows discontinuity at lower isothermal temperatures for the stoichiometric system

As reported earlier, the difference in reactivity of terminal ( $k_{NCO1}$ ) and internal isocyanate ( $k_{NCO2}$ ) groups of the oligomers present in PMDI also cause the system to behave as two simultaneous competitive reactions as shown by the increase in activation energy with conversion in DSC analysis (**Figure 3.3**). This is further substantiated by the rheological data; as the isothermal curing temperature is increased, the discontinuity is minimised and only one reaction rate is observed. In other words, the difference in the rate constants of the functional groups narrows with the increase in curing temperature. It has previously been shown in the reaction between TDI and castor oil, that at temperatures greater than 125 °C, the reactivity of the 2-position isocyanate was increased, showing no difference in reactivity of the two groups.<sup>[29]</sup> This may also be the reason why the exponential function fits the higher temperatures better (**Figure 3.12**).

The apparent kinetic constants are shown in **Table 3-4**. The value of the viscosity rate constant  $k_{\eta}$ , increases as the curing temperature is increased for the stoichiometric system and follows the same trend for the first three temperatures

studied in the system with excess isocyanate. Some dispersion in the values was observed for temperatures above 70 °C.

**Table 3-4 Values for  $k_\eta$  for equal stoichiometry and excess isocyanate ratios of Castor oil and PMDI**

T (°C)	NCO/OH=1		NCO/OH=1.7
	$k_{NCO1}$ (min <sup>-1</sup> )	$k_{NCO2}$ (min <sup>-1</sup> )	$k_\eta$ (min <sup>-1</sup> )
30	0.130	0.074	-
40	0.248	0.114	-
50	0.32	0.166	0.255
60	0.390	0.263	0.308
70	0.532		0.429
80	0.737		0.345
90	1.075		0.304

It is noticed that the rate of reaction is faster for the stoichiometric system in the initial stages of cure.

The apparent activation energy for viscosity build up was determined using the Arrhenius relationship (**Equation (3-4)**), by plotting  $\ln k_\eta$  versus the inverse temperature (for isothermal curing temperatures from 60 °C to 90 °C). The linear relationship is shown in **Figure 3.15** for the stoichiometric system.

$$\ln k_\eta = \ln k_{\eta_\infty} - \frac{E_a}{RT} \quad (3-4)$$

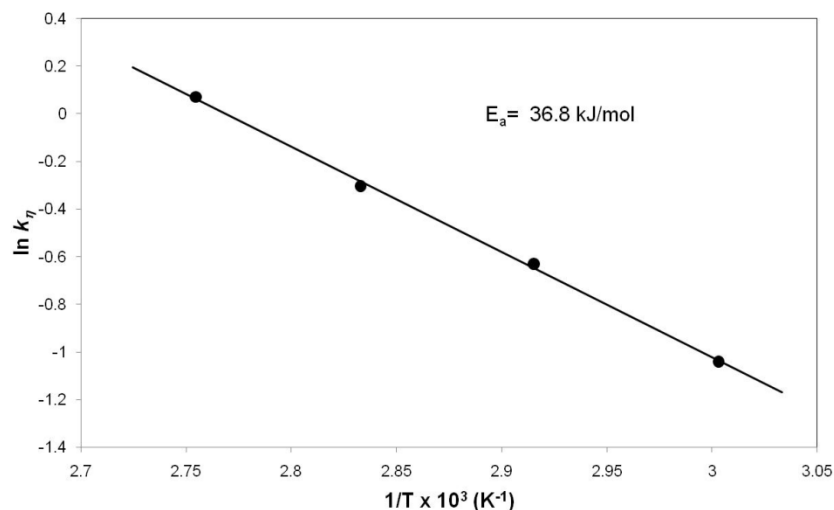


**Figure 3.15** Activation energy obtained for the equal stoichiometric system of Castor oil and PMDI using the apparent kinetic constant established from viscosity profiles

The apparent activation energy of the viscosity rate constant was found to be  $36.8 \pm 0.96 \text{ kJ mol}^{-1}$  ( $R^2 = 0.998$ ) for the stoichiometric system before gelation and  $23.9 \pm 4.2 \text{ kJ mol}^{-1}$  ( $R^2 = 0.97$ ) for the system with an excess of isocyanate groups. The stoichiometric ratio exhibited a lower activation energy (**Table 3-5**) compared to that determined by all other gel point criteria (**Table 3-3**), except for the crossover of  $G'$  and  $G''$ , which gave equivalent values within experimental error.

A summary of activation energies obtained through the various analytical methods is presented in **Table 3-5**. It is evident that good agreement is achieved between DSC and rheological techniques in measuring the activation energy of the stoichiometric system.

**Table 3-5 Comparison of Activation Energy obtained through various methods**

Technique	Method	$E_a$ kJ mol <sup>-1</sup>	
		NCO/OH= 1	NCO/OH=1.7
DSC	Advanced Integral	27-45	38.6
Gel Time	(tan $\delta$ ) <sub>max</sub>	43.43 $\pm$ 2.8	
Viscosity build up	$k_\eta$ (min <sup>-1</sup> )	36.8 $\pm$ 0.96	23.9 $\pm$ 4.2*

\*%RE<20

### 3.1.3.3 Kinetic studies through FTIR

Fourier transform infrared spectroscopy (FTIR) was used as a complimentary technique for comparison of the curing profile for both stoichiometric and excess isocyanate systems. The conversion profiles for these reactions are shown in **Figure 3.16**. The conversion profile of the reaction mixture was determined at 60 °C by following the reduction of the isocyanate peak at 2270 cm<sup>-1</sup> obtained using **Equation (1-25)**.<sup>[42]</sup>

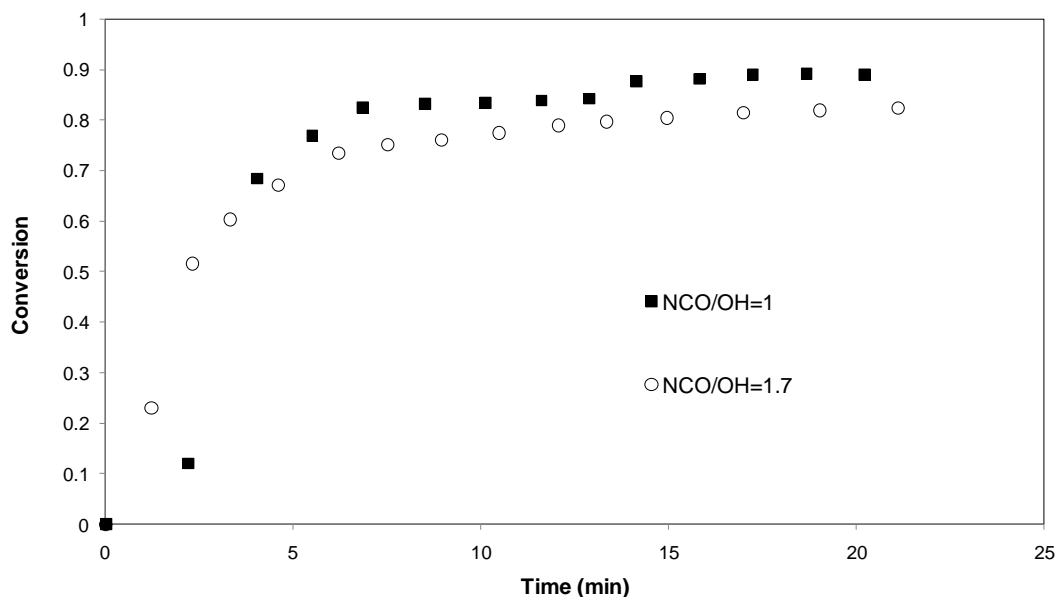


**Figure 3.16 Conversion profile of the isocyanate peak at ~2270 cm<sup>-1</sup> during polyurethane cure at 60 °C using FTIR for stoichiometric and excess isocyanate systems**

High conversions were reached for both systems at 60 °C with the maximum for the stoichiometric system reaching 90% conversion while that of the excess isocyanate system reaching 80% conversion after 20 minutes. The reaction is therefore largely controlled by chemical kinetics. Polyurethanes have been shown to follow second

order kinetics represented by **Equation (3-5)**.<sup>[14, 43, 44]</sup>

$$\frac{d\alpha}{dt} = k(1-\alpha)^2 \quad (3-5)$$

Integrating **Equation (3-5)** from the beginning of the reaction ( $t = 0$  min,  $\alpha = 0$ ) to time  $t$  and conversion  $\alpha$ , gives:

$$\frac{1}{1-\alpha} = kt + 1 \quad (3-6)$$

A plot of  $1/(1-\alpha)$  as a function of time would result in a straight line with the slope equal to the rate constant. It can be seen in **Figure 3.17**, the reaction follows a second order model before and after a critical time for the system with excess isocyanate.<sup>[45, 46]</sup> At this point ( $t \sim 6$  min) the conversion is 75%, which corresponds to all hydroxyl groups being consumed, suggesting the end of reaction and formation of the isocyanate polymer adduct. After this point, there is a slower increase in conversion which is due to the reaction of the excess isocyanate with moisture in the air giving a larger conversion. This is evident in **Figure 3.18** by the presence of the urea carbonyl stretching band at  $1701-1718 \text{ cm}^{-1}$  as well as the presence of the water hydroxyl stretching band at  $3500 \text{ cm}^{-1}$ . Urethane amide stretching and bending bands at  $3348 \text{ cm}^{-1}$  and  $1590 \text{ cm}^{-1}$  respectively, can also be clearly seen.<sup>[22]</sup>

The stoichiometric system slightly differs, in that two stages of functional group consumption are noticed. It is obvious that the second order rate equation does not describe the cure process for oligomeric isocyanate with castor oil well. At the end of each stage of isocyanate consumption, the conversions achieved are 82% and 89% respectively. The second rate increase of the stoichiometric system is explained by the catalysis of the reaction between hydroxyl groups and the slower reacting isocyanate groups present in the oligomeric MDI by the carbamate groups formed in the initial stages of reaction (**Figure 3.17**), or due to reactions with moisture in the air.<sup>[29, 44, 47]</sup> This correlates well to DSC results where the activation energy increases with conversion which was explained by the presence of isocyanate groups with differing reactivities within the molecule.

The stoichiometric system has a faster initial rate of reaction than the excess isocyanate system, due to the ability for more interactions of functional groups, also shown in rheological measurements (Table 3-4).

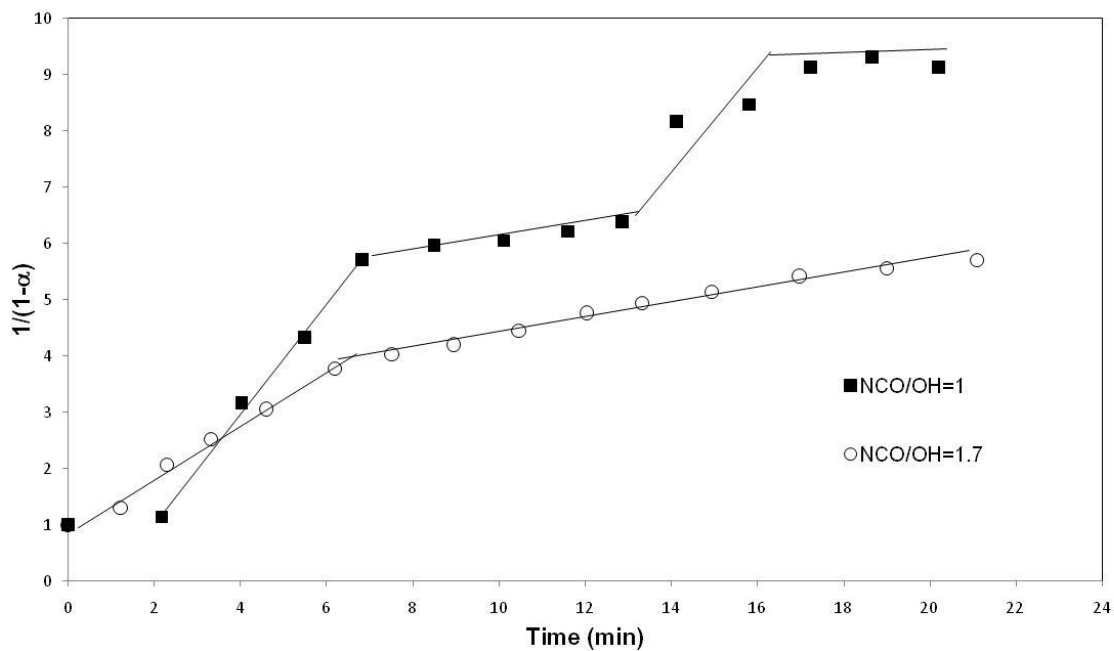
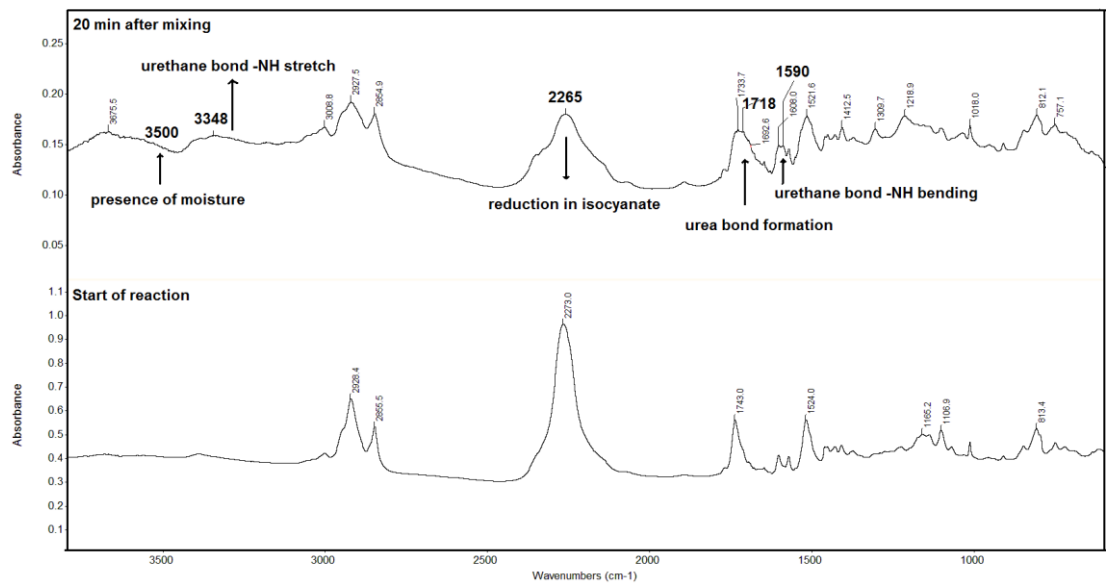


Figure 3.17 A second order rate model fit for the rate of reaction before and after gelation for the polyurethane system at 60 °C using FTIR



**Figure 3.18 FTIR spectra of the castor oil and excess isocyanate system at the start of reaction and after 20 min of mixing**

### 3.1.4 Conclusions

The kinetics of cure for the polyurethane reaction between castor oil and oligomeric isocyanate was monitored using different techniques and showed that activation energies were in good agreement with each other.

DSC results as analysed through isoconversional methods showed a competitive reaction scheme for the stoichiometric system, suggesting the presence of isocyanate groups with different reactivities present in the PMDI oligomers. An increase in the rate of reaction during isothermal FTIR also confirmed this.

Greater conversions were achieved at lower isothermal temperatures for the stoichiometric system in rheological measurements due to curing below the glass transition temperature leading to vitrification.

A low viscosity build up was evident for the excess isocyanate system due to the complete consumption of the hydroxyl groups. A polyurethane adduct was formed exhibiting a reduction in viscosity with increasing temperature once all hydroxyls were consumed.

The viscosity growth in the resin was described by an exponential equation before the point of gelation for the stoichiometric system and the rate of viscosity increase was described by a viscometric rate constant  $k_{\eta}$  in the initial stages of cure. FTIR results showed the reaction was highly kinetically controlled and that higher than expected conversions were achieved for the excess isocyanate system due to the reaction of isocyanate groups with moisture in the air.

## **3.2 Part 2: Investigation into the curing kinetics of the Polyurea reaction between Water and Isocyanate**

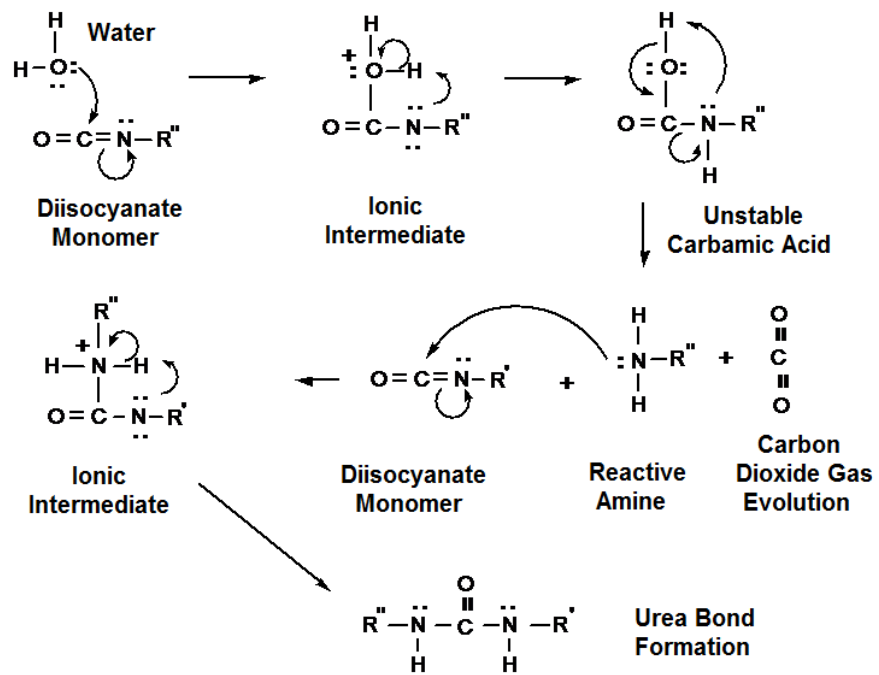
### **3.2.1 Introduction**

The presence of water in a polyol emulsion reacts with the oligomeric diisocyanate, which yields urea bonds and the subsequent release of carbon dioxide. The formation of urea linkages increases crosslinking in coatings, while the side reaction resulting in carbon dioxide has been attributed to blister formation and coating delamination during cure.<sup>[42]</sup> The co-curing kinetics of the urethane and urea reactions in polyurethane systems containing water is complicated and has been investigated by many authors.<sup>[48-53]</sup> To date, the only studies performed with the oligomeric diisocyanate resin as used in this product, have been for adhesion studies of wood products leading to a more complicated process due to the presence of the hydroxyl groups in the wood.<sup>[54]</sup> A number of quantitative techniques have previously been used to measure carbon dioxide evolution, including volumetric analysis and spectroscopic analysis.<sup>[7, 22]</sup> In this research, the polyurea reaction was investigated using a combination of thermal, spectroscopic and volumetric techniques. A novel technique utilising pressure differential scanning calorimetry (PDSC) was employed to determine the polyurea kinetic profile and to elucidate the mechanism of carbon dioxide evolution.

### **3.2.2 Materials and Methods**

#### ***3.2.2.1 Materials and sample preparation***

The water used in these reactions was laboratory grade Reverse Osmosis water. The materials (PMDI and water), were mixed at standard conditions using an overhead drill mixer with a 5 cm diameter fan blade at 450 rpm. Components were well mixed while minimising the introduction of air to the mixture. The general reaction scheme of water and isocyanate is given in Chapter 1: Scheme 1.6; however, is also included in this section for reference as **Scheme 3.2**.



Scheme 3.2 General reaction scheme for water and PMDI

### 3.2.2.2 Methods

#### 3.2.2.2.1 Blister Simulation Experiment

A stoichiometric ratio of PMDI and Castor oil were used to test blister formation in the laboratory at standard temperature and pressure. The materials were mixed for 3 minutes at standard conditions using an overhead drill mixer with a 5 cm diameter fan blade at 450 rpm. One glass jar was left open to the conditions in the room while the other was closed with a screw cap lid. A TESTO digital psychrometer was used to measure the relative humidity during mixing and over the course of 7 days of curing.

#### 3.2.2.2.2 PDSC measurements- Water and PMDI

Kinetic studies were performed using a TA PDSC (pressure DSC) cell attachment, in order to suppress the evaporation of water seen in normal DSC mode. Samples were placed in open aluminium pans with a sample size of  $20 \pm 1.5$  mg. A cell pressure of 550 psi or  $3795 \pm 3$  kPa at a starting temperature of  $30 \pm 5$  °C was employed in the chamber. This was found to be the best pressure to measure the system for all non-isothermal and isothermal reactions. The heating rates chosen for non-isothermal mode were 5, 10 and 20 °C min<sup>-1</sup>. Averages of three sample runs were performed for each heating rate.

Isothermal experiments were performed for systems where the ratios of isocyanate to water at 65 °C were varied at 550 psi. Non-isothermal measurements were also performed for various ratios at 10 °C min<sup>-1</sup>.

#### 3.2.2.2.3 Carbon dioxide Measurements

The method and apparatus used, is reported in chapter 2 section 2.6.

#### 3.2.2.2.4 FTIR Analysis

The cure kinetics was obtained using a Nicolet 8700 spectrophotometer fitted with a transmission cell. Transmission experiments were performed using pressed KBr discs as a disposable medium for applying a thin coating of the mixed sample. The sample was placed on the KBr disc and into a brass holder, allowing transmission spectra to be collected at an isothermal temperature of 60 °C over a 120 minute period. Samples were maintained at the isothermal temperature using a temperature-

controlled furnace. An isothermal temperature of 60 °C was chosen to give a direct comparison between analytical techniques during isothermal cure as it was found that temperatures outside this range were not sensitive due to equipment limitations. Spectra were taken intermittently to determine the curing profile with a maximum of two scans per transmission run at a resolution of 4 cm<sup>-1</sup>. Backgrounds of KBr discs were collected before each series.

The transmission spectrum for the carbon dioxide gas obtained from the blister simulation experiment was performed using a gas cylinder cell which was purged with nitrogen gas prior to placement of the syringed carbon dioxide. The glass jar, with the simulated blister, as well as the syringe that was used to remove carbon dioxide gas from the blister, was also purged with nitrogen gas, before removal of carbon dioxide from the blister.

### 3.2.3 Results and Discussion

#### 3.2.3.1 Blister Simulation

Blister formation was simulated in the laboratory by curing castor oil with PMDI in the presence of room humidity. The samples were mixed at a relative humidity of 43%. One sample was left to cure at room conditions over 7 days, while a control sample was isolated from changes in the relative humidity of the room. The relative humidity in the room decreased to 28% on day 2 without any noticeable blister formation. On day 4 the relative humidity increased to 47% after which it remained at the increased level with dome formation appearing on day 5.

**Figure 3.19** displays the effect of curing at varying relative humidities (B) compared to a constant relative humidity (A). Curing at room conditions showed a distinct dome after 5 days compared to the control sample.

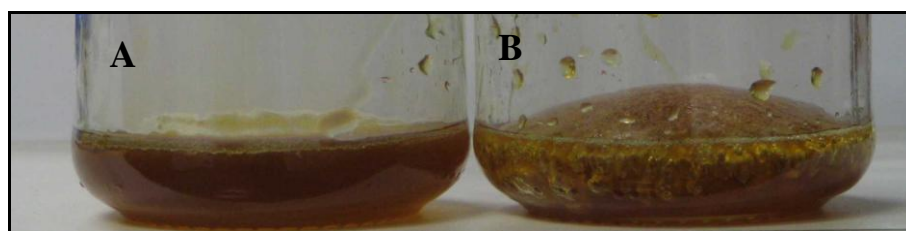


**Figure 3.19** Effect of Relative Humidity during curing of Castor oil and PMDI

The gas entrapped by the dome was captured in a transmission gas cell and tested through FTIR shown in **Figure 3.20**. A definitive transmittance peak of carbon dioxide at  $2300\text{-}2390\text{ cm}^{-1}$  as well as the characteristic overtones of carbon dioxide at  $3600\text{-}3800\text{ cm}^{-1}$  are observed.<sup>[22]</sup> FTIR results thus confirm that blister formation is due to carbon dioxide gas formed from the water-isocyanate reaction. Furthermore, the increased hardness noticed in sample B compared to the gel-like structure of sample A, are due to the urea crosslinks formed in the water-isocyanate reaction.

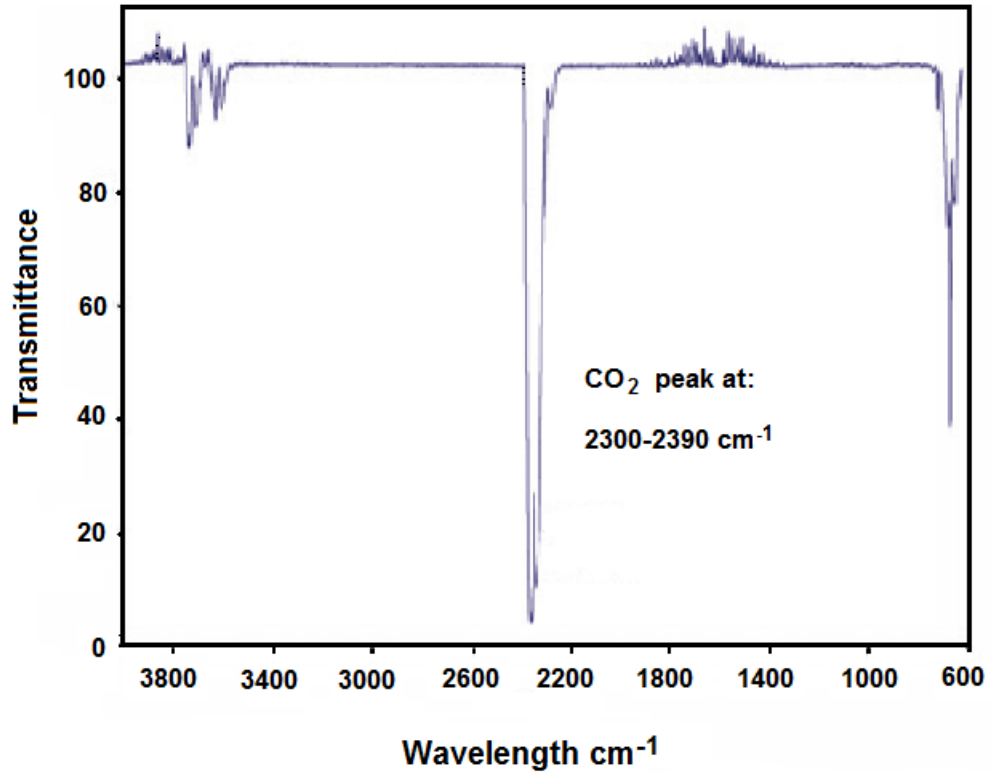


**Figure 3.20 Confirmation of CO<sub>2</sub> present in polyurethane blister formation due to atmospheric moisture**

It is evident that the castor oil and PMDI reaction is susceptible to atmospheric moisture. The water isocyanate reaction kinetics are therefore of prime importance in establishing the cure profile and will be investigated in the following sections.

### 3.2.3.2 Curing Kinetics of the water and isocyanate reaction through PDSC

The cure profile of the water and PMDI reaction was performed using PDSC in non-isothermal mode with a ratio of water to isocyanate of 1.65:1 consistent with the ratio present in the product under investigation. The heat profiles are shown in **Figure 3.21**, which show an increase in peak reaction temperature with an increase in heating rate. Peak temperatures and conversions at the peak, as well as the respective heat of reactions are given in **Table 3-6**. At  $10\text{ }^{\circ}\text{C min}^{-1}$  the heat of reaction is approximately  $38 \pm 0.28\text{ kJ mol}^{-1}$  equivalent isocyanate, which is greater than the polyurethane reaction between castor oil and oligomeric isocyanate reaction studied in Part 1 (**Table 3-1** cf.  $24.9 \pm 1.3\text{ kJ mol}^{-1}$ ).

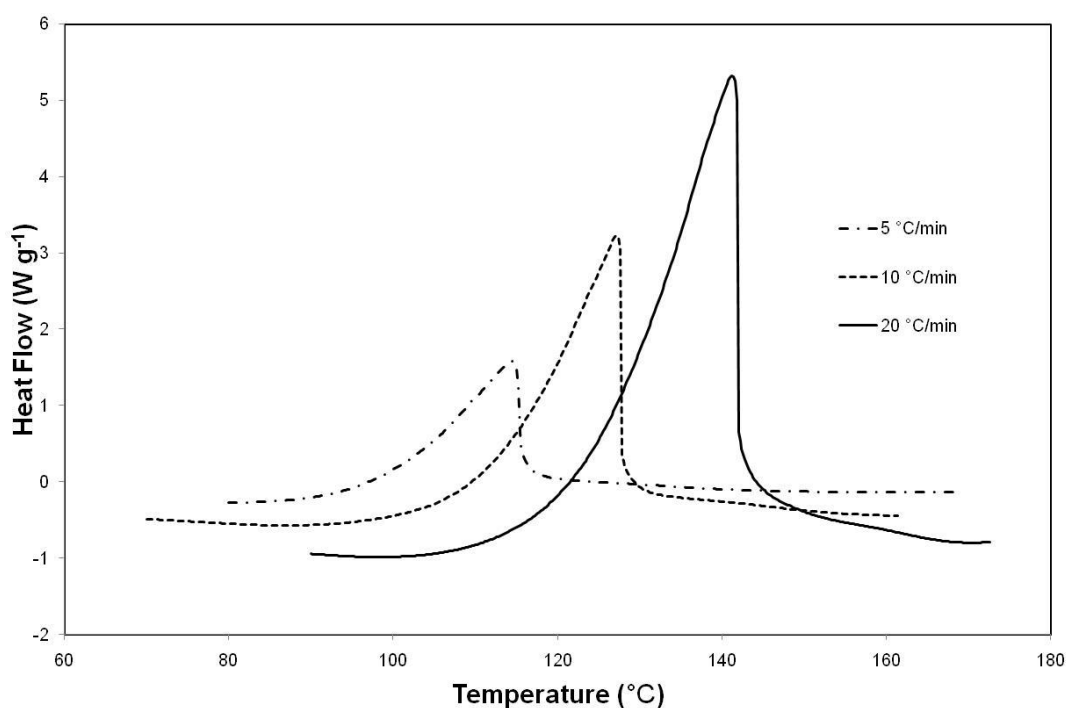


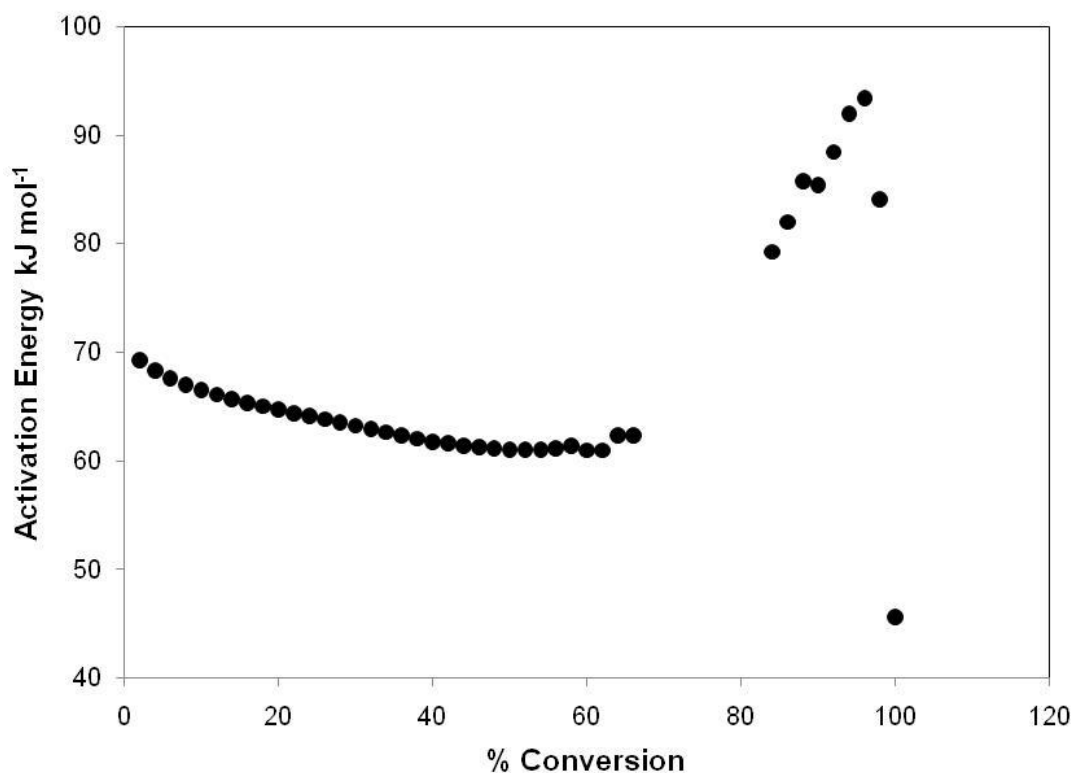
**Figure 3.21** Heat flow profiles of polyurea reaction using PDSC in non-isothermal mode

It is also evident that the peak reaction temperatures for the polyurea system are higher than those for the polyurethane reaction studied in Part 1 (**Table 3-1**), suggesting the polyurea reaction is delayed, although when initiated, achieves a greater exothermic heat of reaction.

**Table 3-6 Summary of non-isothermal PDSC data for the polyurea reaction**

Heating rate (°C min <sup>-1</sup> )	Heat of Reaction (J g <sup>-1</sup> )	T (°C) at Peak	Conversion at peak	T (°C) at CO <sub>2</sub> release	Conversion at CO <sub>2</sub> release
5	282.8 ± 2.5	114.5 ± 0.09	0.61	113.6	0.55
10	248.6 ± 1.9	128.5 ± 1.13	0.86	125.4	0.52
20	238.2 ± 5.8	141.4 ± 0.92	0.51	141.2	0.50

The kinetic profile was investigated using model-free kinetics developed by Vyazovkin *et al.* [12, 24, 25] and is displayed in **Figure 3.22**. The advanced integral isoconversional method together with the Senum-Yang approximation [12] was used to determine the dependence of the activation energy on conversion.

**Figure 3.22 Activation energy dependence for increasing conversion of the polyurea reaction**

Very high activation energies are achieved for the polyurea reaction (~70 kJ mol<sup>-1</sup>) compared to the polyurethane reaction (~ 38-45 kJ mol<sup>-1</sup>) (**Figure 3.3**). This

confirms the polyurea reaction requires more energy to start the polymerisation reaction compared to the polyurethane reaction studied in Part 1. There are two distinct parts to the kinetic scheme, as observed in **Figure 3.22**, suggesting a multicomponent reaction. This is evident due to the complex mechanistic reactions that occur, which are represented in **Scheme 3.2**. The activation energy profile (**Figure 3.22**) shows a slight decline from  $70 \text{ kJ mol}^{-1}$  to  $60 \text{ kJ mol}^{-1}$  up to a conversion of 60%, after which a rapid increase in activation energy is observed. Initially, the reaction between water and oligomeric isocyanate yields a highly unstable carbamic acid intermediate which readily decomposes to carbon dioxide and a highly reactive amine. The amine further reacts with isocyanate groups to form urea crosslinks. The decline in activation energy suggests that as the reaction proceeds, catalysis occurs by either the reactants or intermediates formed, or the heat evolved during this reaction. As the decline in activation energy is not greatly pronounced, it is thought that the large exothermic event initially catalyses this system. At 60% conversion, a rapid increase in activation energy (from  $60 \text{ kJ mol}^{-1}$  to  $95 \text{ kJ mol}^{-1}$ ) is observed, which suggests competitive reactions occur where the reactive amine, produced in-situ, is competing with water for isocyanate groups.<sup>[26]</sup> It is this competing reaction of in-situ formed amines with isocyanate functional groups that forms polyurea crosslinks.

The pressure profiles of the polyurea reaction at the industry ratio of water:PMDI, determined by the instrumentation, are shown in **Figure 3.23**. A change in the pressure profiles is representative of a gaseous expansion.<sup>[55]</sup> In **Figure 3.23**, an increase in pressure is noticed with an increase in temperature, as expected, with a definitive event occurring at each heating rate, causing a rapid increase in pressure for a certain temperature, which is specific to the heating rate. The pressure profiles exhibit a change in pressure due to a combination of events. These include; the increasing temperature due to the heating rate, an increase in temperature due to the exothermic reaction, as well as an increase in pressure in the system due to carbon dioxide evolution. To determine the pressure increase in the system due to the reaction (exothermic heat + carbon dioxide evolution), the difference in pressure over the temperature range measured was elucidated. This required the subtraction of the pressure profile due to the heating rate component. **Figure 3.24** depicts the pressure difference, with increasing temperature for all heating rates.

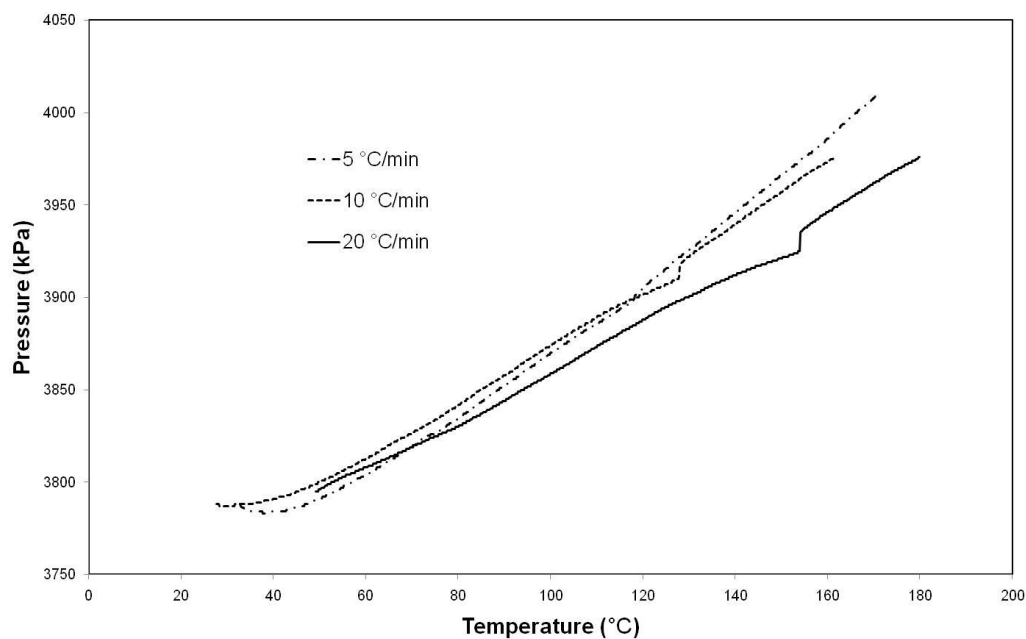


**Figure 3.23** Pressure profiles of the polyurea reaction at three heating rates in non-isothermal PDSC mode.

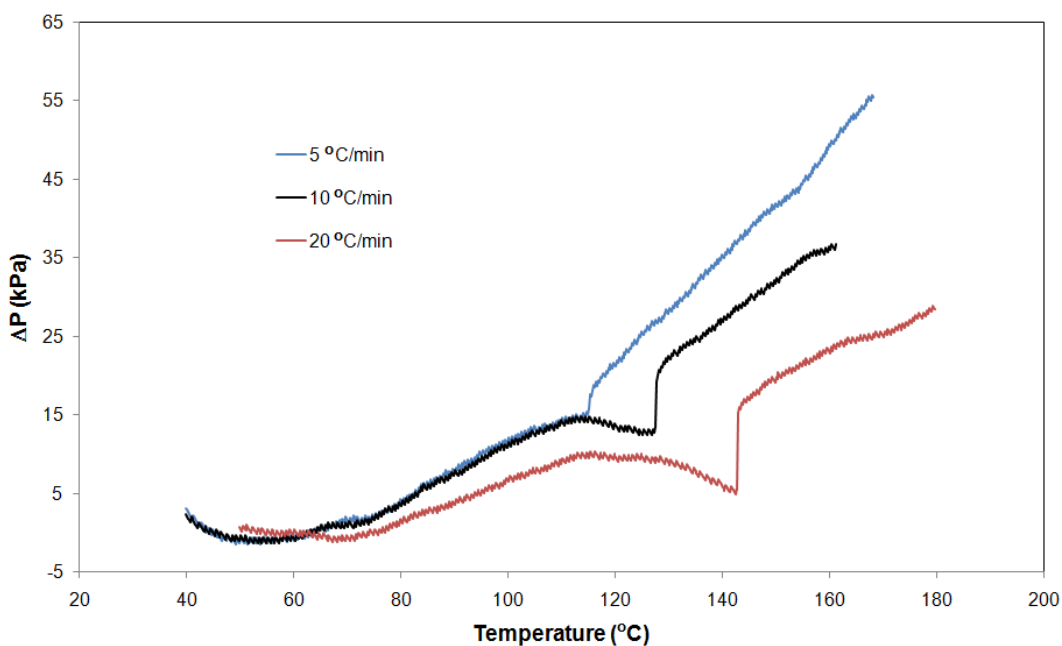


**Figure 3.24** Pressure difference with increasing temperature at various heating rates

Referring to **Figure 3.24**, an initial pressure increase and subsequent decrease is noticed, with the reduction being more pronounced at higher heating rates. The profile then comes to a point (a specific temperature, for each heating rate) where the pressure profile sharply increases. At this temperature (shown as  $T$  °C of  $\text{CO}_2$  release

in **Table 3-6**), the conversion increases by 20%, although, no exothermic heat is evolved at this point, according to **Figure 3.21**. This implies one step of the reaction scheme (**Scheme 3.2**) undergoes an increase in reaction rate. Initially, the water and isocyanate reaction is slow; however, as the reaction heat in the system builds up due to the polyurea reaction, the water and isocyanate reaction is catalysed by the heat produced, increasing the rate of the reaction, releasing a greater amount of carbon dioxide at this point. The temperatures and corresponding conversion at this point are given in **Table 3-6**. The conversion at the time of carbon dioxide evolution is approximately 50% within experimental error for all heating rates.

In **Figure 3.24**, an increase in the pressure difference, from the point where carbon dioxide is released to the end of the reaction, is observed with a decrease in heating rate. This conforms well to the heat flow data generated, where a greater heat of reaction was evident at lower heating rates. The heat flow is representative of the extent of reaction and subsequently the amount of carbon dioxide evolved causing the pressure increase. Quantitative analysis of carbon dioxide evolution could not be performed as the volume of the pressure cell and the component of pressure due to the exothermic heat were not measurable. The pressure component due to the exothermic heat of reaction is required, because the pressure difference calculated equates to the pressure change due to the exothermic heat plus that of carbon dioxide evolution.

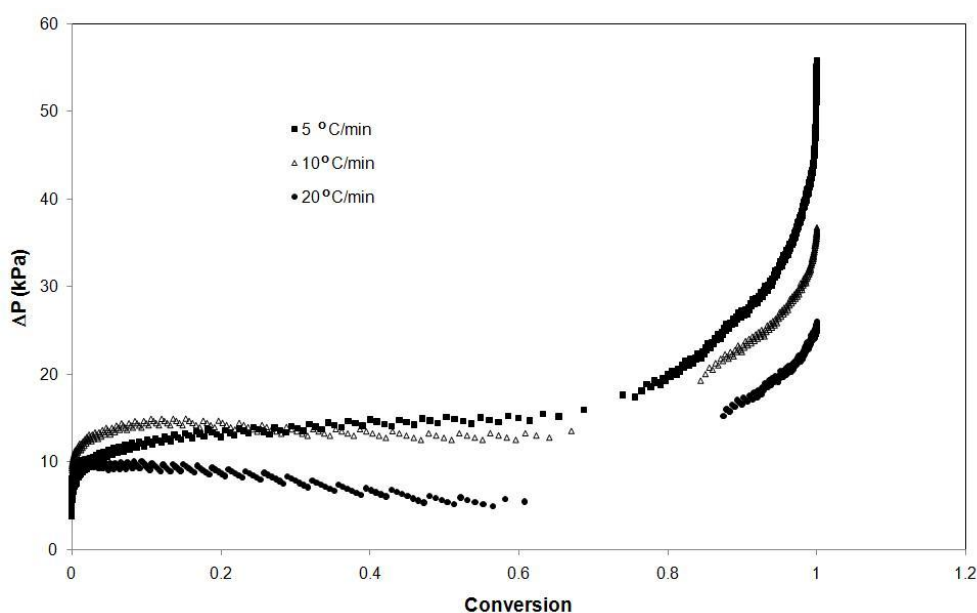


**Figure 3.25** Change in the pressure difference with conversion for the polyurea system

In addition, a rapid change in the pressure difference is observed in **Figure 3.25** when 60% to 70% conversion is reached. Earlier, it was observed that at approximately 50% conversion for all heating rates, a rapid change in conversion occurred. Thus, an increase in the pressure due to carbon dioxide evolution and/or the exothermic heat produced from the reaction, does not occur directly at the point where there is a large change in the pressure difference (as depicted in **Figure 3.24**), but occurs gradually from 60% conversion. At 60% conversion, there is also an increase in the activation energy of the system (**Figure 3.22**), suggesting that a more energy intensive reaction step is occurring at this point.

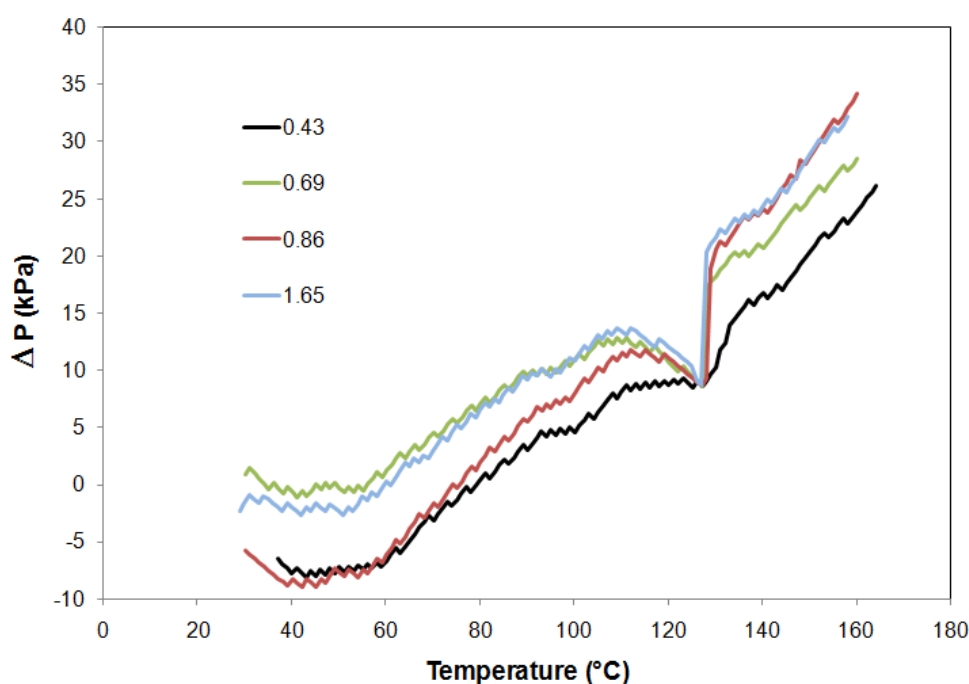


**Figure 3.26** Change in the pressure difference profile with temperature, while varying the mole ratio of water to isocyanate

Varying ratios of water to isocyanate were investigated to determine the effect of changes in water concentration on the reaction profile and its implications on the product (**Figure 3.26**). Increasing the mole ratio of water to isocyanate resulted in an increase in the pressure difference up to the ratio of water/isocyanate = 0.86, after which a plateau was reached (**Figure 3.27**). The change in the pressure difference therefore corresponds to the carbon dioxide evolution where one mole of carbon dioxide is released for every mole of water to isocyanate reacted.

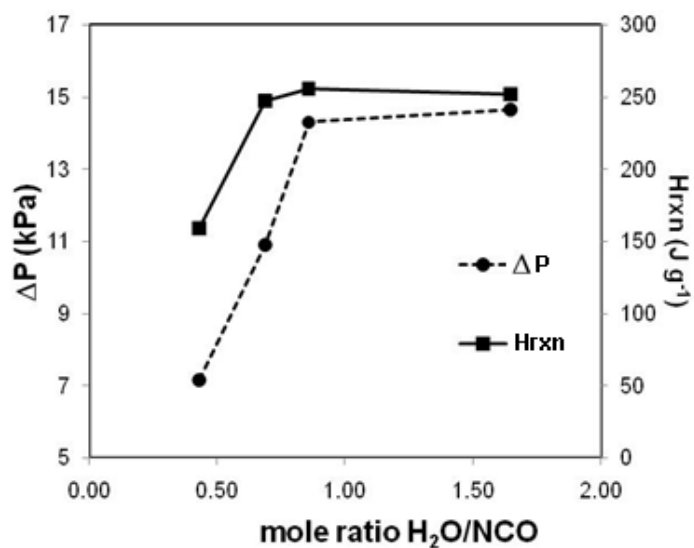


**Figure 3.27** Change in Pressure and heat flow data for increased water content

The heat of reaction followed the same profile as the pressure change, with increasing water content. Although, a slight increase was evident past the ratio 1:1, due to a second isocyanate group reacting to form the urea bond, releasing heat (**Scheme 3.2**).

Isothermal studies were also performed with the product ratio ( $H_2O/NCO=1.65$ ) investigated at a temperature of 65 °C. The isothermal temperature was chosen to allow integration of the exotherm from a constant baseline. Isothermal reaction kinetics could not be elucidated using a range of temperatures, because the only temperature giving a clear baseline without extending the reaction time was at 65 °C. The isothermal run provides similar results to that obtained for non-isothermal studies above and is presented in **Figure 3.28** which displays the master curve for the polyurea reaction at the product ratio. The pressure change with conversion is also shown. It can be seen that in isothermal mode, the maximum rate of reaction occurs at approximately 66% conversion. A shoulder is observed in the master curve at approximately 78-80% conversion after which the reaction subsides. Changes in the pressure profile with conversion correspond to the changes in the rate of reaction. At 70% conversion there is a change in the pressure profile after which it increased to a maximum value at approximately 85% conversion. This suggests that the maximum amount of carbon dioxide evolution occurs at approximately 90% conversion after

the maximum rate of reaction (heat flow) is reached. This corresponds well to non-isothermal data confirming that the heat of reaction accelerates the water-isocyanate reaction, and produced an increase in reaction rate and the pressure profile at 80% conversion. The conversion at which this occurs is slightly higher than that obtained for non-isothermal analysis; however, the pressure versus conversion profiles (**Figure 3.25**) show that the pressure increased over a range in conversion after the sudden increase in pressure change at 50% conversion.

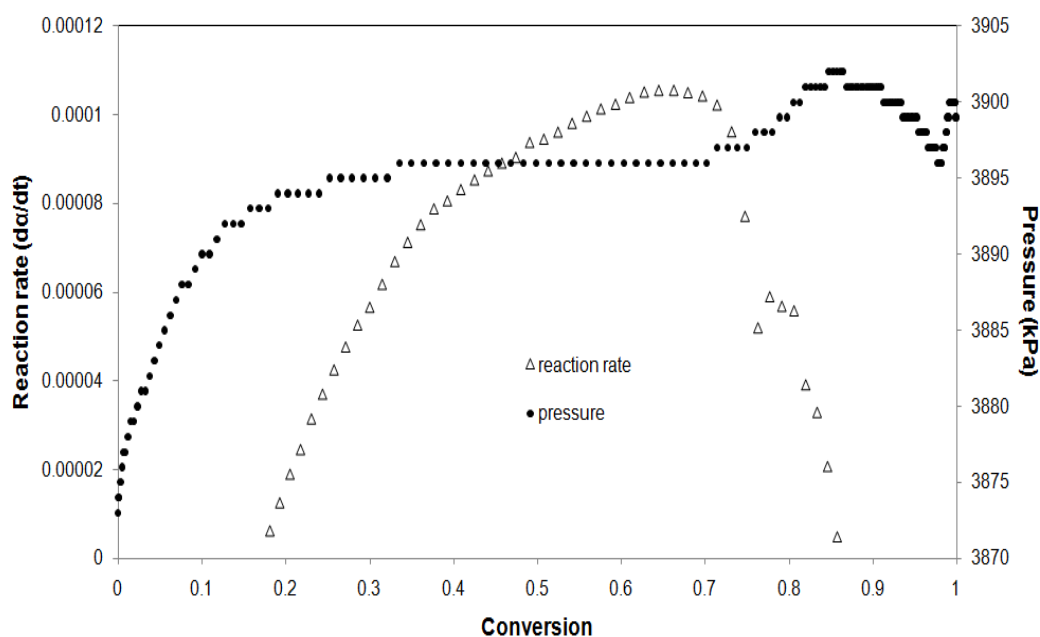


**Figure 3.28** Isothermally obtained master curve for the polyurea reaction at  $H_2O/NCO=1.65$  also displaying pressure evolution during cure

The effect of varying the water concentration on the reaction kinetics of the system was also investigated using isothermal PDSC; however, highly variable results of the heat flow were obtained for other ratios of water to isocyanate. Although the mixture of water and isocyanate was initially well mixed, it existed as a dispersion of the two components. Over the length of time required for the isothermal reaction, the mixture separated which resulted in the variations observed.

### ***3.2.3.3 Volumetric Analysis of Carbon Dioxide Evolution***

The polyurea reaction at varying ratios of water to isocyanate was investigated using the volumetric technique for carbon dioxide evolution. Samples were left to cure for a maximum of 80 hours to detect changes in carbon dioxide levels over time. **Figure 3.29** shows the progression of the isocyanate- water reaction at increasing mole ratios of water to isocyanate. The mole ratio of water to isocyanate in the industry formulation is 1.65. No significant change in carbon dioxide evolution was observed with an increasing concentration of water. In all ratios tested, a limiting isocyanate mole ratio was present. The average volume of carbon dioxide produced after 67 hours was approximately  $18.06 \pm 0.26$  ml/gram of PMDI or  $2.23 \pm 0.032$  L mol<sup>-1</sup> of isocyanate. The theoretical volume of carbon dioxide production, assuming half of the isocyanate is consumed by water and half is consumed by the highly reactive amine is 12.23 litres of carbon dioxide per mole of isocyanate at standard temperature and pressure. Thus, a definitive discrepancy is apparent, indicating that either not all the isocyanate reacted, the carbamic acid intermediate did not completely decompose, or alternatively some of carbon dioxide was trapped inside the cured material.

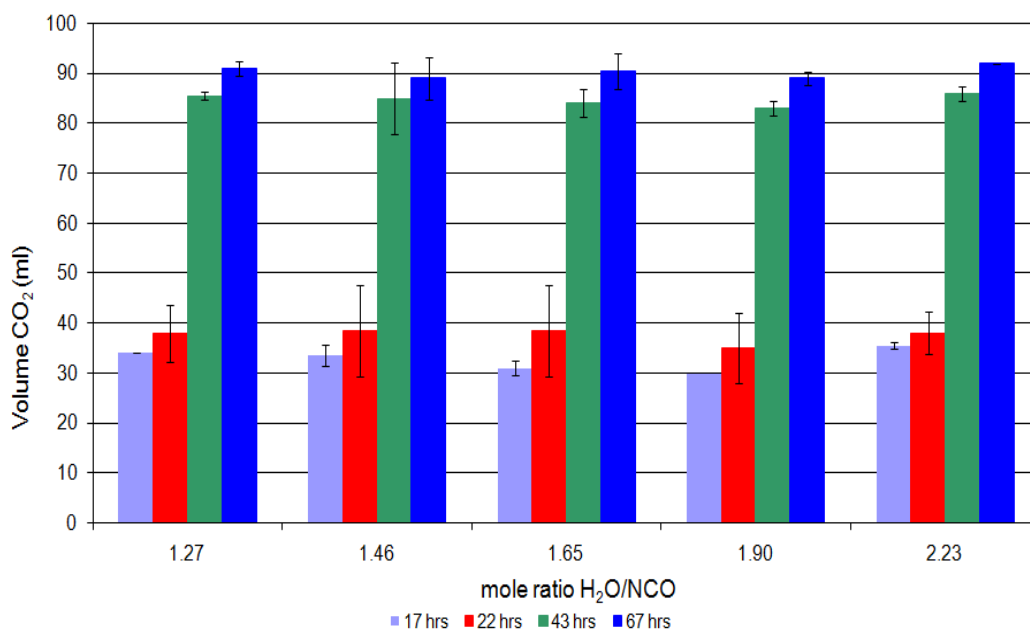


**Figure 3.29 Carbon dioxide evolution from the PMDI-water reaction**

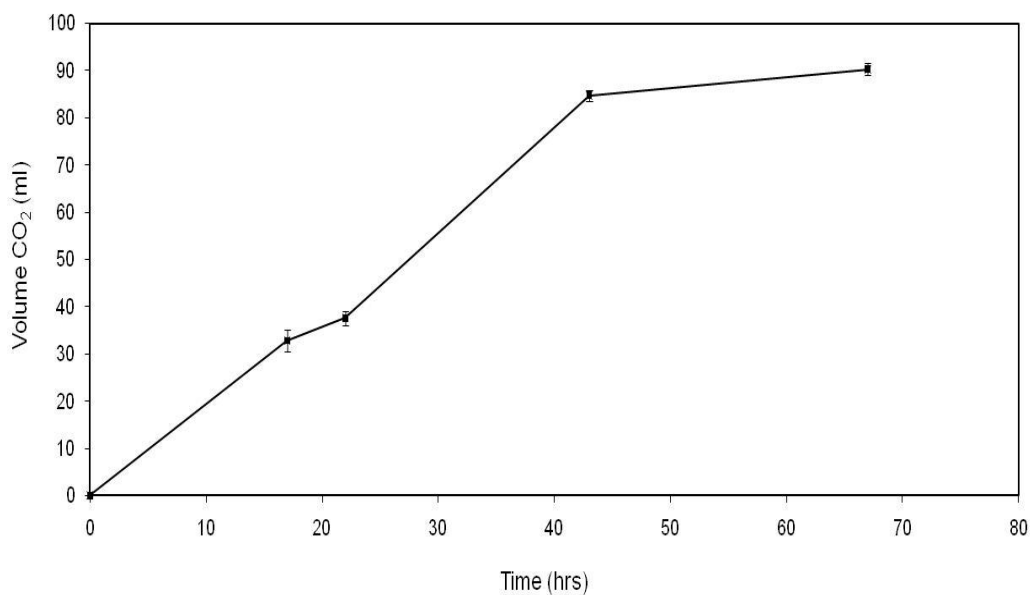


**Figure 3.30 Rate of CO<sub>2</sub> evolution for the PMDI-water reaction**

The profile of carbon dioxide evolution for the industry ratio is displayed in **Figure 3.30** for a period of 70 hours. A linear relationship exists for carbon dioxide evolution with time up to a period of 40 hrs, after which a plateau is reached. Using the linear relationship up to a period of 40 hours we can determine if the evolution of carbon dioxide is a first order process with respect to water consumption. <sup>[7]</sup>

If a relationship exists between the loss of water and the carbon dioxide evolved, **Equation (3-7)** should hold.

$$V_{CO_2 @t} = V_{CO_2TOT} \left( 1 - \left[ \frac{C_{H_2O@t}}{C_{H_2O@t=0}} \right] \right) \quad (3-7)$$

The rate of water consumption can be described by:

$$\frac{dC_{H_2O}}{dt} = -kC_{H_2O} \quad (3-8)$$

Integration of **Equation (3-8)** and substitution into **Equation (3-7)** yields:

$$\ln \left( \frac{V_{CO_2TOT}}{V_{CO_2TOT} - V_{CO_2@t}} \right) = kt \quad (3-9)$$

Where  $k$  is the rate constant and can be determined from the slope of **Equation (3-9)** when the term on the *L.H.S.* is plotted against time ( $t$ ).

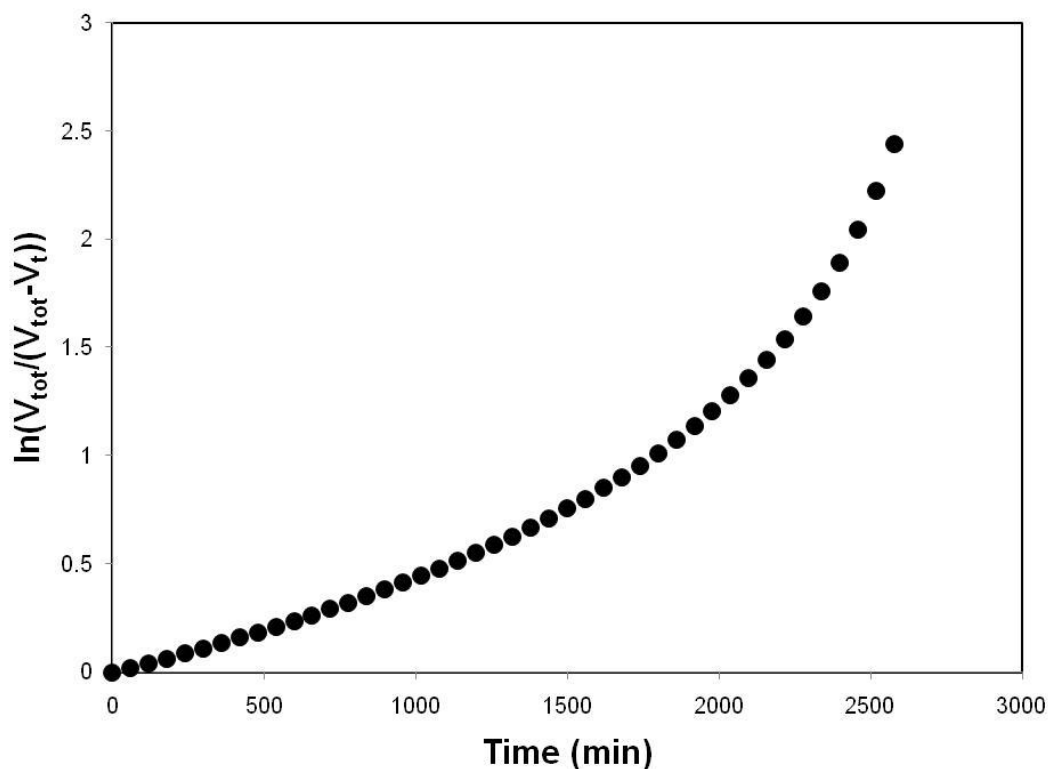


**Figure 3.31** Rate of CO<sub>2</sub> evolution with respect to water consumption assuming a first order process

As can be seen from **Figure 3.31**, a linear relationship is observed up to 660 min (11 hours) of the reaction, signifying the evolution of carbon dioxide is a first order process with respect to water consumption at the start of the reaction. The value for the rate of carbon dioxide evolution is  $k = 4 \times 10^{-4} \pm 4.4 \times 10^{-6} \text{ min}^{-1}$ .

The rate of evolution of carbon dioxide with respect to the total amount of carbon dioxide evolved over the first 40 hours (2500 minutes) was also investigated. **Figure 3.32** displays the application of a first order rate of reaction and it is evident that non-linearity exists. However, when a second order rate equation was applied to the data, the rate of evolution of carbon dioxide observed in **Figure 3.33** was linear up to a period of 900 minutes (15 hours) giving a rate of  $4.74 \times 10^{-4} \pm 1.2 \times 10^{-5} \text{ min}^{-1}$ . Thus, the rate of carbon dioxide evolution with respect to the consumption of water and with respect to the carbon dioxide evolved is within experimental error.

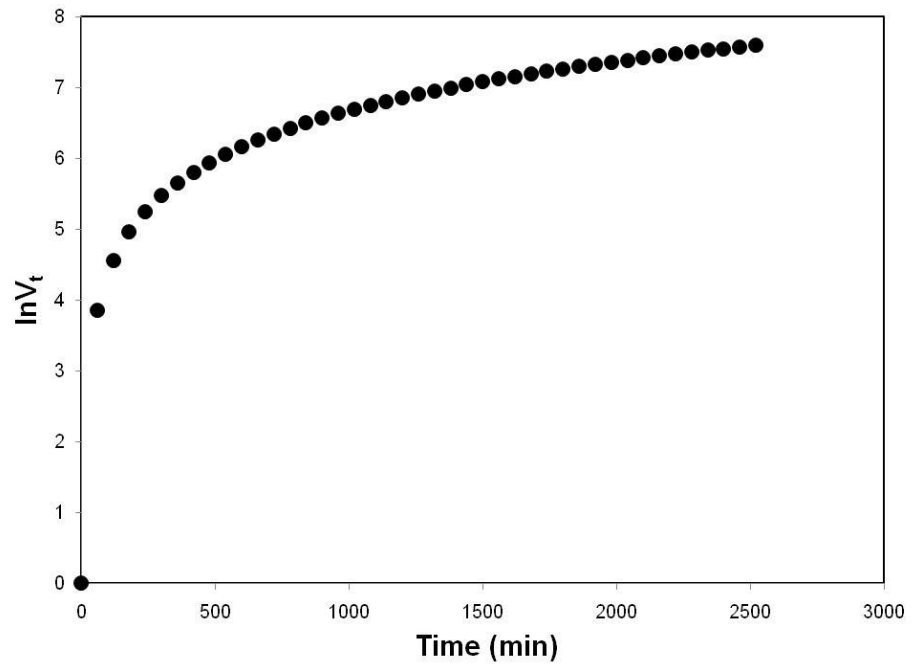


Figure 3.32 First order process for the rate of carbon dioxide evolution

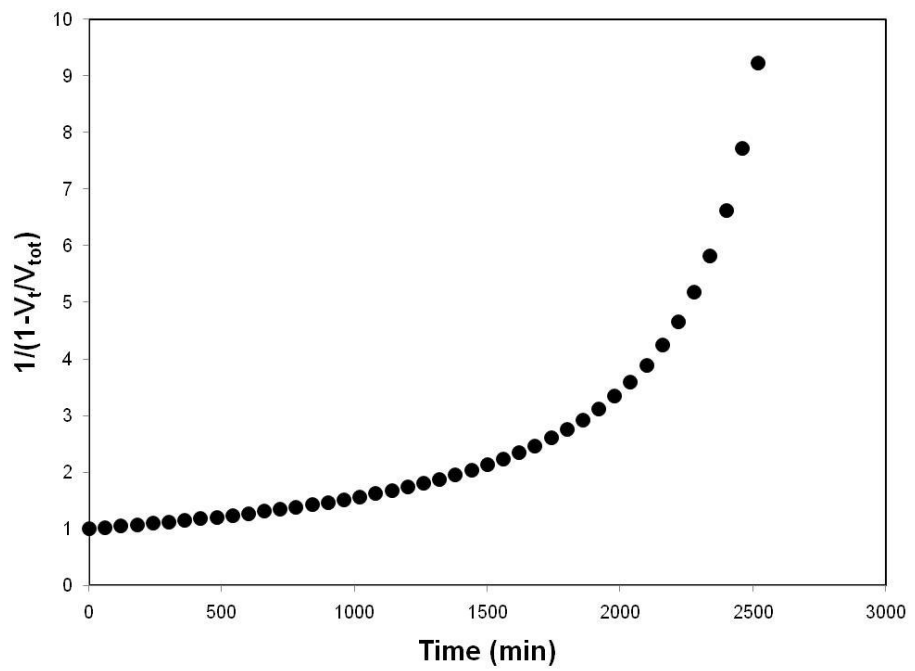
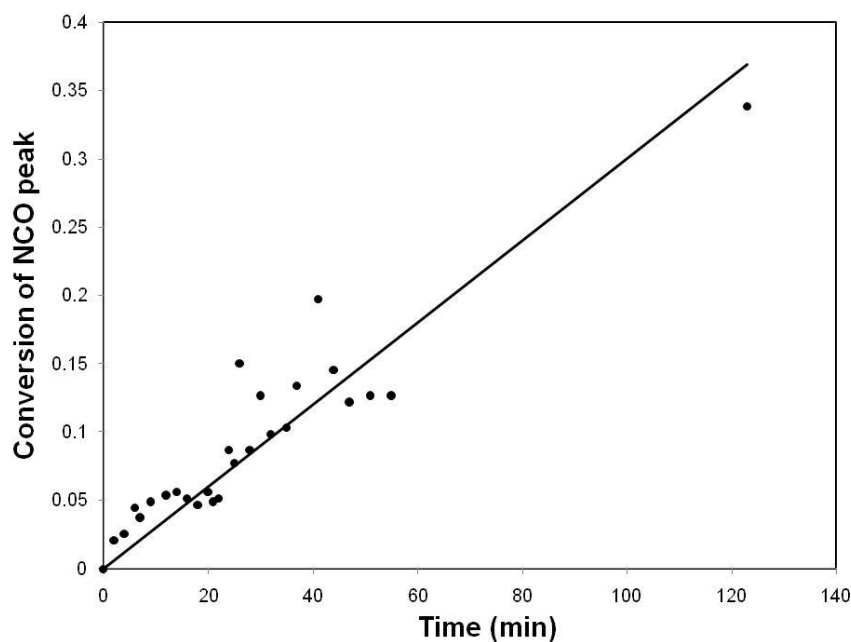


Figure 3.33 Second order process for the rate of carbon dioxide evolution

### 3.2.3.4 Cure Kinetics through FTIR

The conversion of isocyanate groups was followed using transmission mode and calculated using Beer's law for a mole ratio of water to isocyanate = 1.65 [56]. The results shown in **Figure 3.34** were variable over the period the reaction was analysed, which was attributed to the experimental method as well as the production of carbon dioxide as the reaction progressed. The film thickness on the KBr discs may have changed in between measurements due to the vertical sampling technique used and carbon dioxide evolution. The total conversion (using **Equation (1-25)**) reached after 120 min at 60 °C was 34%, indicating the reaction between water and isocyanate is extremely slow. Applying a linear relationship to the conversion data (**Figure 3.34**) allowed more points to be analysed using the line of best fit. Using the line of best fit, the a 2<sup>nd</sup> order model was applied to the conversion data and shown in **Figure 3.35**. A good fit to the second order rate equation for the rate of conversion of isocyanate groups was observed for a period of 120 minutes, fitting the data even more closely below 60 minutes (**Figure 3.35-insert**). The rate of conversion of isocyanate groups was found to be  $k_{\text{NCO}} = 4.5 \times 10^{-3} \pm 1.5 \times 10^{-4} \text{ min}^{-1}$  which is one order of magnitude higher than the rates determined for carbon dioxide evolution using the volumetric technique.



**Figure 3.34** Conversion versus time for the consumption of Isocyanate groups at 60 °C for the H<sub>2</sub>O/NCO mole ratio= 1.65

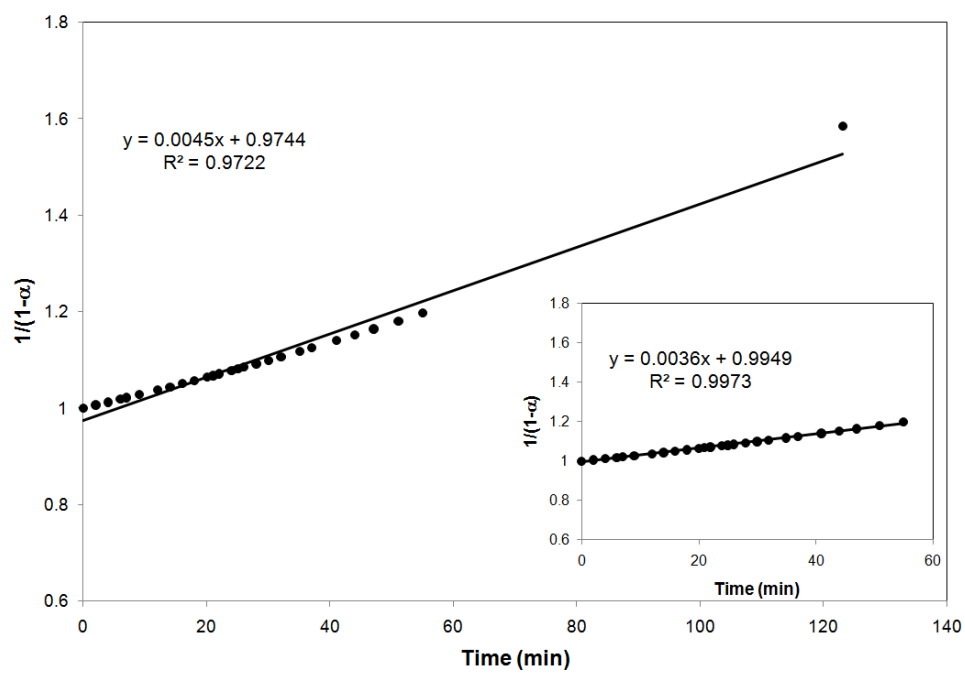


**Figure 3.35** Second order rate equation describes the rate of consumption of isocyanate groups for the polyurea reaction at the mole ratio of  $\text{H}_2\text{O}/\text{NCO}=1.65$  at  $60^\circ\text{C}$ .

### 3.2.4 Conclusions

Pressure differential scanning calorimetry (PDSC) was employed to determine the reaction kinetics of the polyurea reaction where the heat of reaction was found to be higher than that achieved for the polyurethane reaction (38 kJ mol<sup>-1</sup> equiv. NCO *cf.* 25 kJ mol<sup>-1</sup> equiv. NCO). Higher peak temperatures and activation energies (70 kJ mol<sup>-1</sup> *cf.* 38-45 kJ mol<sup>-1</sup>) were also achieved, suggesting the polyurea reaction requires a greater amount of energy to activate, although once activated is more exothermic than the polyurethane reaction. A 20% jump in conversion was achieved at approximately 60% conversion, evidenced both in non-isothermal and isothermal mode.

The evolution of carbon dioxide could be detected using PDSC through the pressure increase during cure. It is unsure whether there is a gradual release in carbon dioxide, or if a larger amount of carbon dioxide is released causing the large pressure increase after 60% conversion due to the acceleration of the water and isocyanate reaction.

Volumetric analysis demonstrated that no change in carbon dioxide evolution was evident with increasing water to isocyanate mole ratios. The rate of carbon dioxide evolution followed a second order rate equation and was found to be first order with respect to water consumption in the initial stages of cure, with both rates of equal magnitude. FTIR studies also showed a second order rate of conversion of isocyanate groups.

In summary:

The rate of the water and isocyanate reaction is:

- 1<sup>st</sup> order with respect to water consumption using volumetric carbon dioxide analysis, therefore: Rate  $\propto$  [H<sub>2</sub>O]
- 2<sup>nd</sup> order with respect to isocyanate consumption using FTIR analysis, therefore: Rate  $\propto$  [NCO]<sup>2</sup>
- 2<sup>nd</sup> order with respect to carbon dioxide evolution using volumetric carbon dioxide analysis, therefore; Rate  $\propto$  [CO<sub>2</sub>]<sup>2</sup>

Thus the overall rate of the water-isocyanate reaction is  $\propto$  [H<sub>2</sub>O][NCO]<sup>2</sup>.

### 3.2.5 References

- [1] E. Van Anglen, *AFE Facilities Engineering* 1997, September/October, 29.
- [2] B. W. Ludwig, M. W. Urban, *J. Coat. Technol.* **1996**, 68, 93.
- [3] A. Bittner, P. Ziegler, "Water-Borne Two-Pack Polyurethane Coatings for Industrial Applications", in *New Technologies for Coatings and Inks 3rd Congress*, Nurnberg, Germany, **1995**.
- [4] C. Simon, B. George, A. Pizzi, *J. Appl. Polym. Sci.* **2002**, 86, 3681.
- [5] F. M. Dias, F. A. R. Lahr, *Mater. Res.* **2004**, 7, 413.
- [6] D. P. Harper, "The evaluation of 4-4' Diphenylmethane Diisocyanate cure in a saturated steam environment", in *Department of Civil and Environmental Engineering*, Washington State University, Washington, **1998**.
- [7] D. Ihms, J. O. Stoffer, D. F. Schneider, C. McClain, *J. Coat. Technol.* **1985**, 57, 61.
- [8] J. Chappel, P. Argust, *Thermochim. Acta* **1996**, 289, 303.
- [9] S. Vyazovkin, *Thermochim. Acta* **2000**, 355, 155.
- [10] F. Dimier, N. Sbirrazzuoli, B. Vergnes, M. Vincent, *Polym. Eng. Sci.* **2004**, 44, 518.
- [11] F. B. Arlas, L. Rueda, P. M. Stefani, K. Caba, I. Mondragon, A. Eceiza, *Thermochim. Acta* **2007**, 459, 94.
- [12] S. Vyazovkin, *J. Therm. Anal.* **1997**, 49, 1493.
- [13] S. Vyazovkin, *J. Comput. Chem.* **2000**, 22, 178.
- [14] R. B. Prime, C. Michalski, C. M. Neag, *Thermochim. Acta* **2005**, 429, 213.
- [15] S. M. Gasper, D. N. Schissel, L. S. Baker, D. L. Smith, R. E. Youngman, L.-M. Wu, S. M. Sonner, R. R. Hancock, C. L. Hogue, S. R. Givens, *Macromolecules* **2006**, 39, 2126.
- [16] C. M. Nunez, B.-S. Chiou, A. L. Andrady, S. A. Khan, *Macromolecules* **2000**, 33, 1720.
- [17] V. Sekkar, K. A. Devi, K. N. Ninan, *J. Appl. Polym. Sci.* **2001**, 79, 1869.
- [18] H. Teil, S. A. Page, V. Michaud, J. A. E. Manson, *J. Appl. Polym. Sci.* **2004**, 93, 1774.
- [19] F. Hernandez-Sanchez, H. Vazquez-Torres, *J. Polym. Sci. Part A: Polym. Chem.* **1990**, 28, 1579.
- [20] T. J. Hsu, L. J. Lee, *Polym. Eng. Sci.* **1988**, 28, 955.

- [21] B.-S. Chiou, S. A. Khan, *IS&T's Annual Conference* **1997**, 50th, 570.
- [22] A. M. Kaminski, M. W. Urban, *J. Coat. Technol.* **1997**, 69, 113.
- [23] V. L. Zvetkov, *Polymer* **2001**, 43, 1069.
- [24] S. Vyazovkin, *Proceedings of the NATAS Annual Conference on Thermal Analysis and Applications* **2003**, 31st, 026/1.
- [25] S. Vyazovkin, *J. Therm. Anal. Calorim.* **2006**, 83, 45.
- [26] S. Vyazovkin, *Int. J. Chem. Kinet.* **1996**, 28, 95.
- [27] J. M. E. Rodrigues, M. R. Pereira, A. G. de Souza, M. L. Carvalho, A. A. Dantas Neto, T. N. C. Dantas, J. L. C. Fonseca, *Thermochim. Acta* **2005**, 427, 31.
- [28] H. Yeganeh, M. A. Shamekhi, *J. Appl. Polym. Sci.* **2006**, 99, 1222.
- [29] S. Ajithkumar, S. S. Kansara, N. K. Patel, *Eur. Polym. J.* **1998**, 34, 1273.
- [30] J. M. Laza, J. L. Vilas, F. Mijangos, M. Rodriguez, L. M. Leon, *J. Appl. Polym. Sci.* **2005**, 98, 818.
- [31] P. J. Halley, M. E. Mackay, *Polym. Eng. Sci.* **1996**, 36, 593.
- [32] H. H. Winter, F. Chambon, *J. Rheol.* **1986**, 30, 367.
- [33] J. Lange, N. Altmann, C. T. Kelly, P. J. Halley, *Polymer* **2000**, 41, 5949.
- [34] R. J. Varley, *Macromol. Mater. Eng.* **2007**, 292, 46.
- [35] B.-S. Chiou, S. R. Raghavan, S. A. Khan, *Macromolecules* **2001**, 34, 4526.
- [36] C.-Y. M. Tung, P. J. Dynes, *J. Appl. Polym. Sci.* **1982**, 27, 569.
- [37] H. Yu, S. G. Mhaisalkar, E. H. Wong, *Macromol. Rapid Commun.* **2005**, 26, 1483.
- [38] J. M. Laza, J. L. Vilas, M. Rodriguez, M. T. Garay, F. Mijangos, L. M. Leon, *J. Appl. Polym. Sci.* **2002**, 83, 57.
- [39] A. Y. Malkin, I. Y. Gorbunova, M. L. Kerber, *Polym. Eng. Sci.* **2005**, 45, 95.
- [40] A. H. Navarchian, F. Picchioni, L. P. B. M. Janssen, *Polym. Eng. Sci.* **2005**, 45, 279.
- [41] V. Sekkar, K. Narayanaswamy, K. J. Scariah, S. Bandyopadhyay, P. R. Nair, K. S. Sastri, MACRO 2004, *International Conference on Polymers for Advanced Technologies*, Thiruvananthapuram, India, Dec. 15-17, **2004**, OP 93/1.
- [42] M. Urban, W. Ludwig, *J. Coat. Technol.* **1996**, 68, 93.
- [43] F. Hernandez-Sanchez, R. Vera-Graziano, *J. Appl. Polym. Sci.* **1992**, 46, 571.
- [44] H. Yeganeh, M. A. Shamekhi, *Polym. Int.* **2005**, 54, 754.
- [45] B.-S. Chiou, S. A. Khan, *Macromolecules* **1997**, 30, 7322.

- [46] N. Markovic, N. K. Dutta, D. R. G. Williams, J. Matisons, *Silicon Chem.* **2005**, 2, 223.
- [47] H. Yeganeh, M. R. Mehdizadeh, *Eur. Polym. J.* **2004**, 40, 1233.
- [48] M. W. Urban, C. L. Allison, C. C. Finch, B. A. Tatro, *J. Coat. Technol.* **1999**, 71, 75.
- [49] P. Chaffanjon, J. R. A. Grisgby, J. E. L. Rister, R. L. Zimmerman, *J. Cell. Plast.* **2003**, 39, 187.
- [50] D. Ihms, J. O. Stoffer, D. Schneider, C. McClain, "The effect of catalysts on kinetics and mechanism of urethane film formation", in *Water-Borne & Higher-Solids Coatings Symposium*, **1983**, 233.
- [51] J. O. Stoffer, D. Ihms, C. McClain, D. Schneider, "Solution Kinetics of the Water-Toluene Diisocyanate Reaction", in *Water-Borne and Higher-Solids Coatings 14th Symposium*, **1987**, p. 14/428.
- [52] J. M. Borsus, R. Jerome, P. Teyssie, *J. Appl. Polym. Sci.* **1981**, 26, 3027.
- [53] S. D. Seneker, T. A. Potter, *J. Coat. Technol.* **1991**, 63, 19.
- [54] R. A. C. Altafim, J. F. Resende da Silva, D. P. Gonzaga, C. Ribeiro, J. Godoy, H. C. Basso, B. Bueno, C. Calil Junior, J. C. Sartori, R. A. P. Altafim, A. Silveira, *Mater. Res.* **2006**, 9, 77.
- [55] B. Hentschel, V. Schliephake, *Thermochim. Acta* **1993**, 225, 239.
- [56] W. D. Cook, K. Dean, J. S. Forsythe, *Materials Forum* **2001**, 25, 30.

# **CHAPTER 4**

**Investigation into the reaction kinetics of  
glycerol and the commercial diisocyanate resin**

## 4 INVESTIGATION INTO THE REACTION KINETICS OF GLYCEROL AND THE COMMERCIAL DIISOCYANATE RESIN

### 4.1 Introduction

The urethane network formed through the crosslinking reaction of oligomeric diphenylmethyl diisocyanate (PMDI) and the polyol, provides a continuous matrix that adds to the structural integrity of the coating. However, problems arise during the curing reaction; water present in the polyol emulsion can cause random blistering to occur as a result of carbon dioxide evolution within the product from competing reactions between isocyanate and water.<sup>[1-4]</sup> Furthermore, an important factor in the application of this coating resin is workability time, which is dependent on the time of gelation. Beyond the gel point the polymer does not flow due to the development of a continuous covalent network which is dependent on the curing reactions occurring in the product.<sup>[5, 6]</sup>

The research in this chapter is a fundamental study into the reaction kinetics between the polyol, glycerol and the commercial diisocyanate resin (PMDI). A requirement within the project framework is not to only reduce the amount of carbon dioxide evolved by the product but to also reduce the viscosity of the application mixture to improve product workability. This was achieved through the addition of glycerol as a second polyol (see Chapter 5 for full details), hence the need for a fundamental study into the kinetics of the glycerol-PMDI reaction.

Reaction rate, kinetics of cure and state of cure are key aspects of understanding and controlling the coating performance. Thermoset cure has been investigated extensively for epoxies and polyester polymers,<sup>[7-9]</sup> and although many authors have investigated polyurethane thermoset cure through the use of idealised monomer units containing diisocyanate functional groups<sup>[10-18]</sup>, very little work has been performed on the use of oligomeric isocyanates with trifunctional polyol.<sup>[19-21]</sup>

Several different reactions can occur during polyurethane polymerisation, due to: a) inconsistent reactivities of functional groups b) secondary reactions taking place at higher temperatures and c) extended periods of cure.<sup>[22, 23]</sup> Mechanistically, the reaction system is therefore extremely complex. Despite this reaction complexity, many researchers assume only one reaction model describes the entire curing process

[10, 14, 24-26]. Differential scanning calorimetry (DSC) has been widely used for studying thermoset reactions in both isothermal and non-isothermal modes,<sup>[27-29]</sup> however, there have been minimal investigations using isoconversional DSC analysis to study complex polyurethane cure. DSC was employed to establish the kinetic parameters using isoconversional methods and using general kinetic models for comparison. In addition, comprehensive rheological investigations were performed to further understand the cure profile of the stoichiometric ratio. The reacting polyurethane undergoes chain extension and subsequent branching due to the higher functional moieties present in the reacting components.<sup>[28]</sup> Viscosity build up of the system, is a consequence of the increase in molecular weight and, provides information on the reaction rate and cure profile.<sup>[30, 31]</sup> Two important transitions which are measurable through rheological investigations are gelation and vitrification. When the material is cured above its glass transition temperature it will undergo gelation at a critical conversion, which is determined as the time where the polymer can no longer flow. Gelation is a critical component in thermosetting systems as it describes the formation of an infinite molecular network.<sup>[28, 32]</sup> If the material is cured below its glass transition temperature, two transitions are noticed in rheological measurements; gelation and vitrification. Vitrification is a gradual process in which the curing kinetics changes from chemically controlled to diffusion controlled.<sup>[32]</sup>

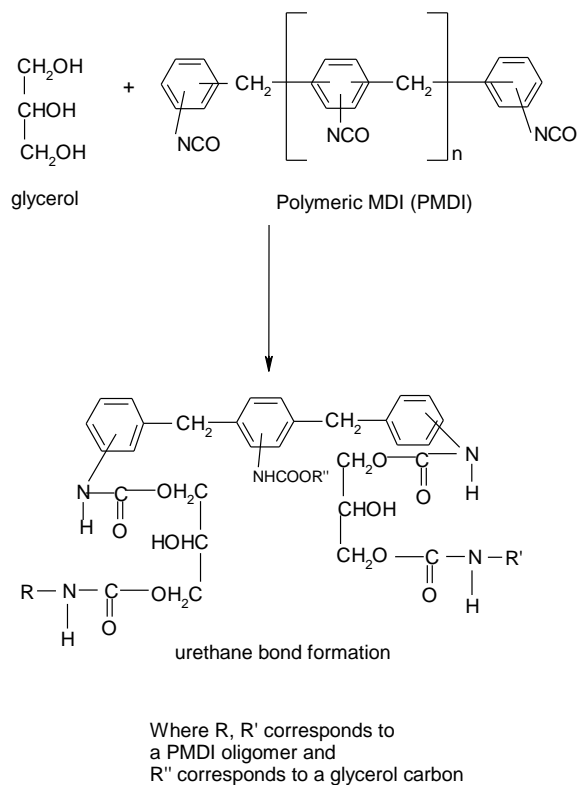
The optimum curing ratio between glycerol and PMDI was also examined through non-isothermal DSC and the kinetics of cure for the optimum ratio elucidated through isoconversional analysis and compared with the stoichiometric ratio.

## 4.2 Materials and Methods

### 4.2.1 Materials and sample preparation

PMDI as described in Chapter 3, as well as glycerol 99.9% pure was obtained from Sigma Aldrich and was used as received (Appendix A).

A stoichiometric ratio of NCO to OH was used to describe a model system. The materials were mixed at standard conditions using an overhead drill mixer with a 5 cm diameter fan blade. The general reaction for isocyanate and polyol can be seen in **Scheme1.14**.



**Scheme 4.1** Reaction between glycerol and PMDI

## 4.2.2 Methods

### 4.2.2.1 DSC Measurement

Kinetic studies were performed using a DSC 2920 (TA instruments). Samples were sealed in hermetic aluminium pans with an average sample weight of  $5 \pm 0.5$  mg. Cell constant calibration was performed using an indium (99.99% pure) standard. Nitrogen at a flow rate of  $50 \text{ ml min}^{-1}$  was used for the purge gas.

The isothermal method employed, required the DSC cell to be pre-heated to the appropriate isothermal temperature before quickly placing the sample in the cell at one of the following isothermal temperatures of;  $70 \text{ }^\circ\text{C}$ ,  $80 \text{ }^\circ\text{C}$ ,  $90 \text{ }^\circ\text{C}$  and  $100 \text{ }^\circ\text{C}$ . Thermal equilibrium was achieved within one minute of sample insertion. The isothermal curing reaction exhibiting an exothermic peak was considered complete when the signal levelled back to the baseline. The total area under the exotherm was used to obtain the isothermal heat of reaction;  $Q_T$ . Following the completion of this reaction, samples were quickly quenched to room temperature using a water bath and were reheated using a temperature rate of  $10 \text{ }^\circ\text{C min}^{-1}$  to determine the residual heat of reaction ( $Q_{res}$ ). A second non-isothermal ramping run was then performed at  $10 \text{ }^\circ\text{C min}^{-1}$  from  $-10 \text{ }^\circ\text{C}$  to  $180 \text{ }^\circ\text{C}$  to ensure no further reactivity in the system. Absolute extents of cure were determined by choosing the maximum heat of reaction ( $Q_{rxn}$ ) of the sample as the sum of the isothermal heat ( $Q_T$ ) and the residual heat of reaction ( $Q_{res}$ ) determined at  $70 \text{ }^\circ\text{C}$ .<sup>[11]</sup> The maximum heat of reaction achieved using this method was  $54 \pm 2 \text{ kJ mol}^{-1}$  equivalent isocyanate for the mole ratio of OH/NCO=1 and  $74 \pm 4 \text{ kJ mol}^{-1}$  equivalent isocyanate for the mole ratio of OH/NCO=1.5. Generally, polyurethane reactions have a reaction enthalpy between  $-80$  and  $-90 \text{ kJ mol}^{-1}$  equivalent isocyanate<sup>[19, 33, 34]</sup>, with Chappel *et al.*<sup>[19]</sup> reporting a lower value of  $-69 \text{ kJ mol}^{-1}$  equivalent isocyanate. It is important to note that the relative extents of cure were determined through integration of the DSC peaks of the isothermal curves up to a time of 30 min at each temperature.

Non-isothermal cure was determined as fractional areas of DSC peaks with the total heat release in each non-isothermal experiment assigned to  $\alpha=1$  for heating ramps of  $5$ ,  $10$  and  $20 \text{ }^\circ\text{C min}^{-1}$ . Samples were ramped between  $-10 \text{ }^\circ\text{C}$  to  $250 \text{ }^\circ\text{C}$ , depending on the heating rate used. A second non-isothermal run was performed under the same conditions and showed no further exothermic reaction.<sup>[35]</sup>

#### ***4.2.2.2 Rheological Measurement***

An AR-2000 controlled stress and direct strain control rheometer from TA Instruments, (US) was used to study the cure profile of the coating system through gelation and viscosity build up. A 2 cm 2° cone and plate configuration was used to achieve a thin gap allowing a large surface-to volume ratio for isothermal curing. Dynamic measurements in oscillatory mode were performed at a frequency of 1 Hz or using a multi frequency technique ranging from 1 Hz to 10 Hz with a strain of 0.1%, 10 % or 100% (initial tests were performed to ensure the response was in the viscoelastic region). A limitation of the equipment was the inability to change strains during the evolution of the network structure.<sup>[36]</sup> In order to detect the initial network formation, a higher strain (10%) was required and performed in multifrequency mode. To obtain information on the network formation as it evolved, without breaking the network structure, a much smaller strain is required. Therefore to achieve this, the experiment was repeated using a smaller strain of 0.1% at 1 Hz. A strain of 100% was also used in multifrequency mode to detect the gel time when  $\tan \delta$  becomes frequency independent.<sup>[32]</sup> A conditioning step, with pre-shearing, was used to ensure the same deformation history for all samples tested. This procedure removed the potential for unaccounted anomalies resulting from thermal and deformational history. Isothermal measurements were performed at 70 °C, 80 °C, 90 °C and 100 °C.

#### ***4.2.2.3 Mid and Near Infrared Spectroscopic Analysis***

A Nicolet FTIR Nexus 8700 spectrophotometer, fitted with a diamond ATR (attenuated total reflectance), was used to quantitatively determine residual isocyanate and hydroxyl groups in the cured sample. The maximum penetration of infrared radiation into the sample using this technique is 1  $\mu\text{m}$  and the average number of scans used, to obtain an infrared spectrum, was 32 at a resolution of 4  $\text{cm}^{-1}$ . A background spectrum of air was collected which was then subtracted from the collected IR spectrum for each sample was collected.

**Figure 4.1A** shows a typical IR spectrum of cured polyurethane, after DSC analysis. The DSC analysis consisted of an isothermal run followed by two non-isothermal runs to ensure full reaction has occurred. FTIR analysis was used to measure the isocyanate peak at a wavelength of  $2270\text{ cm}^{-1}$ . Residual hydroxy groups were measured at  $7000\text{ cm}^{-1}$  using near infrared-ATR of a sample cured isothermally at  $70\text{ }^{\circ}\text{C}$  for 24 hrs following subsequent heating for 3 hrs at  $180\text{ }^{\circ}\text{C}$  (**Figure 4.1B**).<sup>[37-39]</sup>

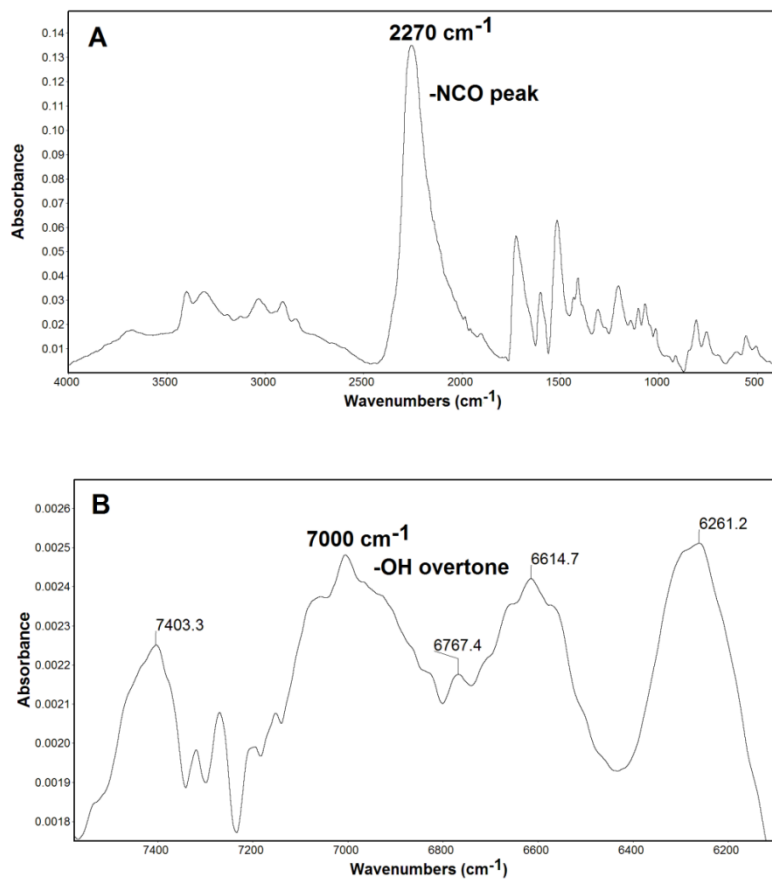


**Figure 4.1A) MID-IR of cured sample with residual unreacted isocyanate and B) N-IR of cured polyurethane sample showing residual hydroxyl groups**

#### ***4.2.2.4 Dynamic Mechanical Analysis***

DMA measurements were performed using a TA Instruments DMAQ800 in single cantilever bending deformation mode. The samples were cured isothermally at 70 °C for 24 hours followed by post-curing at 180 °C for 3 hours. DMA tests were carried out at a frequency of 1 Hz, amplitude of 20 μm, in the temperature range of -100 °C to 180 °C with heating ramp of 2 °C min<sup>-1</sup>.

The glass transition temperature  $T_g$ , was taken as the temperature at which the loss factor  $\tan \delta$  reached a maximum. Liquid nitrogen was used to achieve the sub-ambient temperatures. The ultimate glass transition temperature ( $T_g$ ) of the cured material, determined by DMA, from an average of 3 samples, was  $104 \pm 3$  °C.

## 4.3 Results and Discussion

### 4.3.1 Investigation of reaction kinetics through DSC for the stoichiometric ratio

The polyurethane system was cured at isothermal temperatures below its ultimate glass transition temperature allowing gelation and vitrification to occur during the course of reaction, resulting in incomplete cure. **Figure 4.2** shows the heat flow profiles for the system cured isothermally at four different temperatures. From **Figure 4.2** the increase in cure time at lower isothermal temperatures is evident. Isothermal experiments at 90 °C and 100 °C levelled off to baseline after 30 minutes of reaction time. It is important to note that the isothermal heat of reaction ( $Q_T$ ) after 30 minutes, increased with an increase in isothermal cure temperature (**Table 4-1**).

In contrast, the isothermal heat of reaction decreased with an increase in isothermal cure temperature when the isothermal signal was allowed to level off to baseline for 70 °C (120 min) and 80 °C (60 min) (**Table 4-1**), indicating the complexity of the curing reaction and the change in reaction conditions. Unreacted isocyanate and hydroxyl groups (**Figure 4.1A** and **Figure 4.1B** respectively) were detected after the DSC samples underwent isothermal curing followed by two non-isothermal scans. As stated above, the polyurethane samples were isothermally cured below the  $T_g$  (104 °C), resulting in vitrification of the system, hence the presence of free unreacted isocyanate and hydroxyl groups. This phenomenon is caused by diffusion limitation of the reactive groups embedded in the polymer matrix upon cross-linking. Thus, the polyurethane system undergoes incomplete cure, reaching what is known as the ultimate extent of cure. [35, 40] The conversion ( $\alpha$ ) at time  $t$ , is calculated from **Equation (4-1)** and shown in **Table 4-1** for 30 minute and 120 minute time intervals.

$$\alpha = \frac{\int_0^t \frac{dQ}{dt} dt}{Q_{rxn}} \quad (4-1)$$

where  $\alpha$  is the conversion at time  $t$ .

From **Table 4-1** it is evident that the conversion trend at different curing temperatures changes with curing time, indicating the complexity of curing reaction kinetics. The increase in conversion with temperature (except 100°C) is indicative of the chemically driven reaction kinetics. At 100°C, the isothermal temperature reaches the glass transition temperature resulting in vitrification, which retards the chemical reaction. More importantly, greater conversions are achieved at longer cure times for isothermal temperatures at 70 °C and 80 °C, indicating inconsistent reactivities of functional groups. The presence of a secondary hydroxyl group in glycerol, if provided sufficient time to react is likely to increase the conversion at lower temperatures.

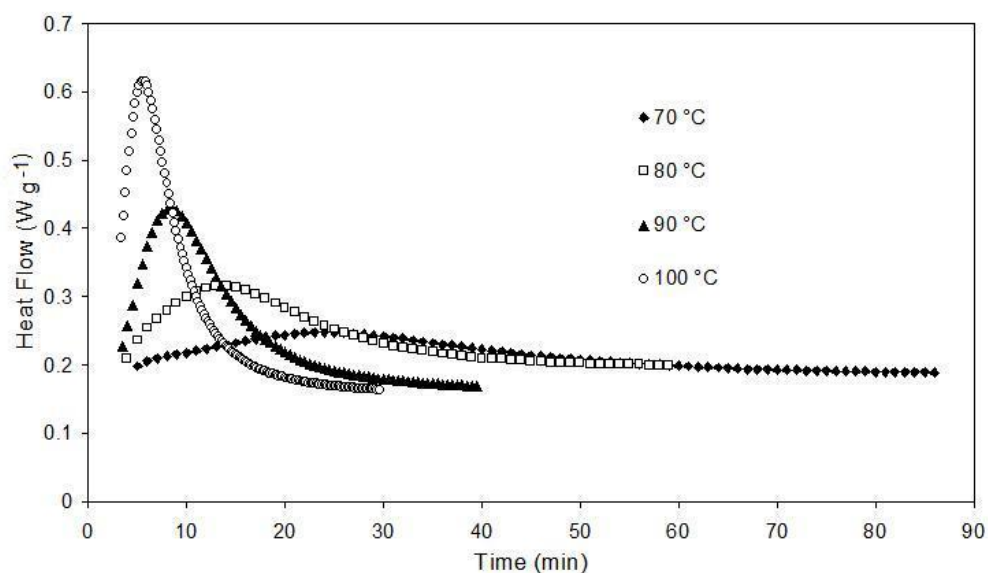


**Figure 4.2** Heat flow curves ( $\text{W g}^{-1}$ ) as obtained by isothermal DSC runs

**Table 4-1** Total heat flow and ultimate extents of cure for two time intervals at varying isothermal cure temperatures

Isothermal temperature ( $^{\circ}\text{C}$ )	$Q_T \text{ J g}^{-1}$ 30 min	$Q_T \text{ J g}^{-1}$ 120 min	% Conversion at 30 min	% Conversion ( at baseline)
70	$48.4 \pm 3.4$	$252.6 \pm 12.62$	$13.8 \pm 1.1$	$72.2 \pm 4.3$
80	$104.7 \pm 4.1$	$155.5 \pm 7.3$	$29.9 \pm 1.5$	$44.5 \pm 2.6$
90	$128.9 \pm 1.1$	$133.2 \pm 2.7$	$36.8 \pm 1.3$	$38.1 \pm 1.5$
100	$73.4 \pm 1.6$	$73.4 \pm 1.6$	$21.0 \pm 0.8$	$21.0 \pm 0.8$

As a comparative study the non-isothermal method for DSC measurement was obtained by monitoring the heat of reaction at a constant heating rate. The cure rate versus conversion profiles are shown in **Figure 4.3**. It is noticed that the maximum cure rate occurs at approximately 40% conversion and a second shoulder is formed with an increase in heating rate at approximately 80% conversion. This will be discussed further in **section 4.3.1.3**. Temperatures obtained at the peak are displayed in **Table 4-2**.

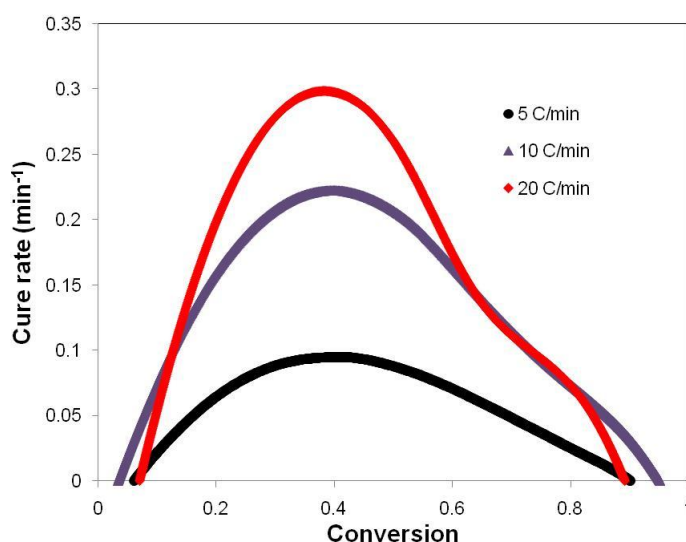


**Figure 4.3** Cure rate profiles for non-isothermal DSC

**Table 4-2** Peak temperatures for non-isothermal heating rates

Heating Rate $^{\circ}\text{C min}^{-1}$	$H_{\text{rxn}} \text{ J g}^{-1}$	$T_{\text{peak}} (^{\circ}\text{C})$	% Conversion @ $T_{\text{peak}}$
5	$226.4 \pm 2.5$	$111.16 \pm 0.21$	$41.21 \pm 1.11$
10	$256.7 \pm 1.2$	$124.34 \pm 0.04$	$40.77 \pm 2.15$
20	$245.7 \pm 2.3$	$140.86 \pm 0.23$	$38.53 \pm 0.01$

#### 4.3.1.1 Applicability of kinetic models

Many authors have reported that polyurethane cure follows a second order reaction.<sup>[28, 41-44]</sup> The degree of conversion versus time profile for the polyurethane system at different isothermal temperatures was thus fitted to the second order model and is presented in **Figure 4.4**.

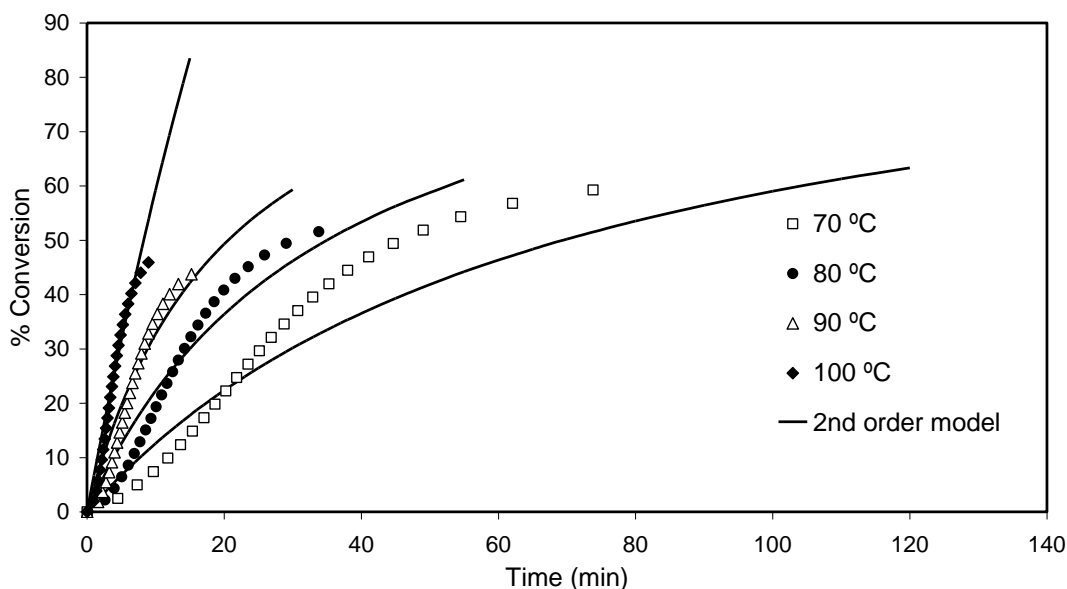


**Figure 4.4** Degree of conversion of polyurethane system vs. time at different curing temperatures fitted to a 2<sup>nd</sup> order model

At lower temperatures, the second order model over estimates the conversion early in the reaction (up to 20-30% cure) and underestimates the conversion later in the reaction. The second order relationship describes higher temperatures much more accurately, although it does predict higher conversions at the end of reaction. The reaction rate constant ( $k$ ) was determined as the slope of the line when substituting the experimental data into the second order rate model (**Equation (1-7)**  $n=2$ ). The beginning and endpoints of the data were omitted from the calculation. The rate constant was found to increase for an increase in cure temperature and can thus be described by the Arrhenius equation (**Equation (1-6)**). Taking the logarithm of the Arrhenius equation and plotting  $\ln k$  vs.  $1/T$  ( $K^{-1}$ ), the activation energy was determined to be  $96 \pm 11 \text{ kJ mol}^{-1}$  ( $R^2=0.97$ ). This is much higher than that observed for similar systems within the literature.<sup>[15, 26, 28, 45]</sup> However, as discussed above, if the reaction has its highest rate of cure at  $t \neq 0$  during an isothermal cure process and

the maximum peak occurs at 30-40% of the total conversion in the cure rate versus conversion plot, then the reaction is said to be autocatalytic.<sup>[7, 27, 29, 46-48]</sup> The maximum cure rate at each isothermal temperature was observed at approximately 20-30% conversion (**Figure 4.5**), which is indicative of an autocatalytic process. Carbamate groups formed during polyurethane cure have autocatalytic properties, thus **Equation (1-13)** was used for the analysis of isothermal DSC data.<sup>[15, 26, 45, 49]</sup>

The degree of conversion of the polyurethane reaction at four isothermal temperatures fitted to an autocatalytic model is presented in **Figure 4.6**. The model fits the conversion profiles well for all temperatures except 70 °C, and slightly higher conversions are predicted at 80 °C and 90 °C. This is caused by the diffusion limitation of the reactive groups that are embedded in the polymer matrix upon cross-linking.<sup>[35]</sup> Furthermore, the degree of conversion versus time for polyurethane cure fitted to an autocatalytic model (**Figure 4.6**) shows a better fit than the second order model (**Figure 4.4**). It can also be seen from **Figure 4.5** that the reaction becomes diffusion controlled towards the end of cure, as lower conversions are observed compared to the kinetic model. This is more evident for higher temperatures where the secondary hydroxyl has less time to react due to the isothermal cure temperature approaching the glass transition temperature. The entire cure process includes both the fast primary hydroxyl reactions as well as the slower reactions of the secondary hydroxyl group present in glycerol.<sup>[19]</sup> The presence of the secondary hydroxyl group allows for higher conversions to be achieved if cured at lower temperatures and for longer times.

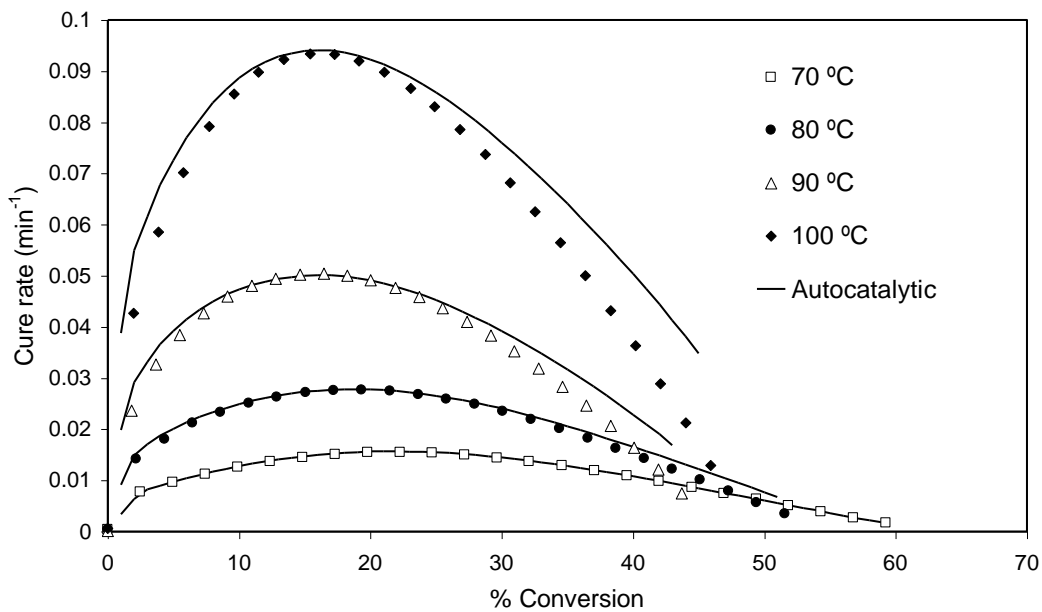


Figure 4.5 Master curve for the polyurethane reaction fitted to an autocatalytic model

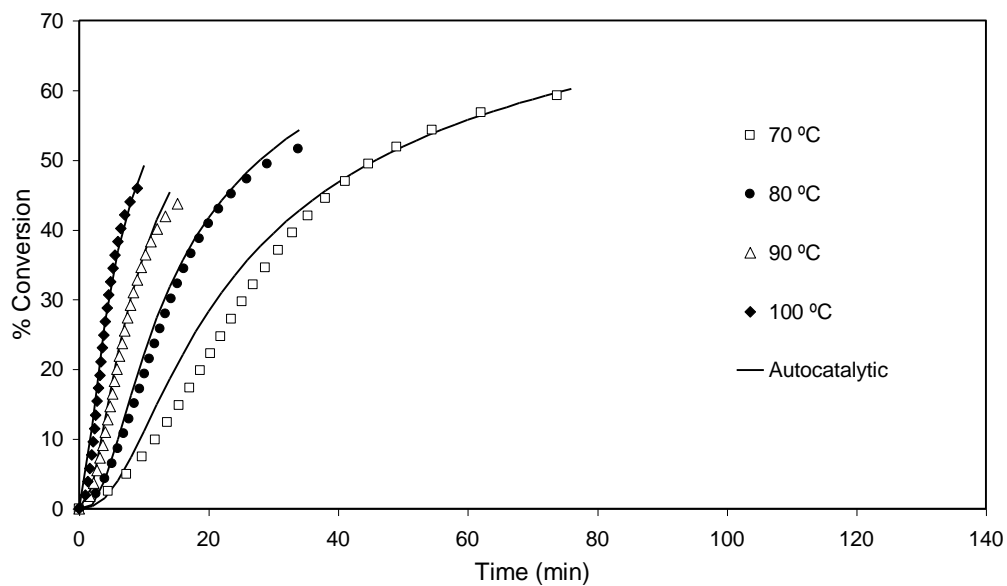
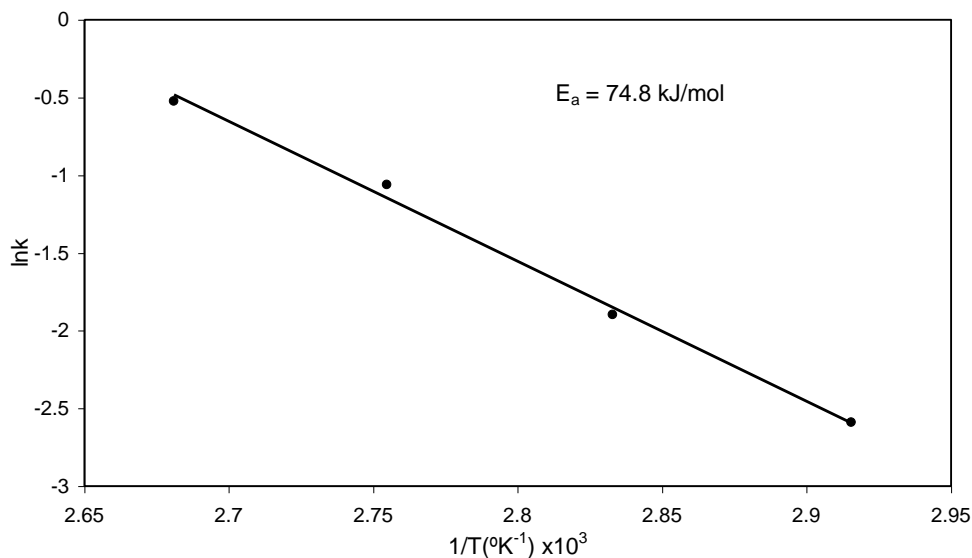


Figure 4.6 Degree of conversion of polyurethane system vs. time at different curing temperatures fitted to an autocatalytic model

**Table 4-3** Autocatalytic model parameters

<b>Isothermal</b>			
<b>Temperature (°C)</b>	<b><math>k(T)</math></b>	<b><math>m</math></b>	<b><math>n</math></b>
70	0.0749	0.542	3.21
80	0.15	0.551	3.81
90	0.346	0.61	4.76
100	0.591	0.592	4.48
Average		0.57	4.07

A summary of the autocatalytic model parameters (obtained from TA kinetic software) for each temperature is given in **Table 4-3**. The total order ( $m+n$ ) of the reaction was found to be an average of 4.6. This is relatively high for polyurethane reactions and shows that both  $m$  and  $n$  are fractional values with  $m \sim 0.57$  and  $n \sim 4.07$ . The varying rates of reactivity of the primary and secondary hydroxyls of the glycerol and the isocyanate may be the reason for such a high reaction order providing further evidence of an extremely complex reaction mechanism. <sup>[15, 33]</sup> Thus, the entire cure reaction is only reasonably described by the autocatalytic model chosen. The relationship between the cure rate constant and cure temperature is shown in **Figure 4.7**.



**Figure 4.7** Arrhenius plot for the determination of activation energy through the rate constant found by isothermal calorimetry

It can be seen that Arrhenius equation (**Equation (1-6)**) is obeyed, giving an activation energy of approximately  $74.8 \pm 3.6 \text{ kJ mol}^{-1}$  ( $R^2 = 0.99$ ). This value is lower than that achieved using a second order model ( $96 \pm 11 \text{ kJ mol}^{-1}$   $R^2 = 0.97$ ), although still higher than observed literature values.

Non-isothermal kinetic analysis of the polyurethane system was also determined by applying an  $n^{\text{th}}$  order model as suggested by Hernández-Sánchez *et al.* [44] In order to determine the reaction order, activation energy and the Arrhenius prefactor, they applied an equalisation process using two heating rates based on the modified form of the Arrhenius equation and  $n^{\text{th}}$  order model (**Equation (4-2)**). Using two heating rates, equations (4-3) and (4-4) are formed and the division of **Equation (4-3)** by **Equation (4-4)** gives the base **Equation (4-5)** from which the reaction order, activation energy or Arrhenius pre-factor can be calculated from various equalisation processes. Applying an equalization process for the temperature ( $T_1 = T_2$ ) at two heating rates, and taking the logarithm of the equation, the reaction order was calculated using **Equation (4-6)**. [50]

$$\frac{d\alpha}{dt} = K(1 - \alpha)^n e^{\frac{-E}{RT}} \quad (4-2)$$

$$\frac{d\alpha_1}{dt} = K(1 - \alpha_1)^n e^{\frac{-E_a}{RT_1}} \quad (4-3)$$

$$\frac{d\alpha_2}{dt} = K(1 - \alpha_2)^n e^{\frac{-E_a}{RT_2}} \quad (4-4)$$

$$\frac{d\alpha_1/dt}{d\alpha_2/dt} = \left(\frac{1-\alpha_1}{1-\alpha_2}\right)^n \exp\left[\frac{-E_a}{R}\left(\frac{1}{T_1} - \frac{1}{T_2}\right)\right] \quad (4-5)$$

$$\ln\left(\frac{\frac{d\alpha}{dt}_1}{\frac{d\alpha}{dt}_2}\right) = n \ln\left(\frac{1-\alpha_1}{1-\alpha_2}\right) \quad (4-6)$$

Where  $\alpha$  is the conversion,  $d\alpha/dt$  is the conversion rate,  $R$  is the universal gas constant,  $T_i$  is the temperature,  $E_a$  is the apparent activation energy,  $n$  is the reaction order and  $K$  is the Arrhenius pre-factor.

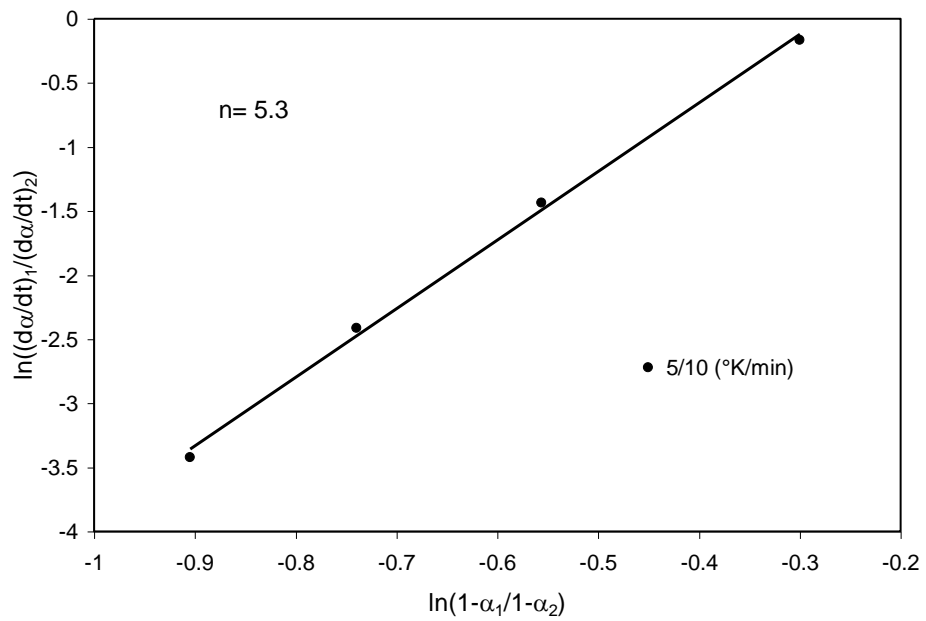


**Figure 4.8** Reaction order as determined by non-isothermal DSC using Hernández-Sánchez method.<sup>[44]</sup>

The reaction order was determined as the slope of  $\ln ((1-\alpha_1)/(1-\alpha_2))$  versus  $\ln ((d\alpha/dt)_1/(d\alpha/dt)_2)$  for a combination of heating rates; 5 and 10 °K min<sup>-1</sup>, 5 and 20 °K min<sup>-1</sup>, and 10 and 20 °K min<sup>-1</sup>. An average reaction order of ~ 5.3 was obtained and a representation is shown in **Figure 4.8**. This reaction order is in good agreement with that obtained through isothermal DSC methods, where an autocatalytic model was chosen with two reaction orders ( $m + n$ ) their sum being ~ 4.64.

The activation energy can be obtained by the equalisation of the conversion rates ( $d\alpha_1/dt=d\alpha_2/dt$ ) at two heating rates, and taking the logarithm of the equation as shown in **Equation (4-7)**.

$$\ln \frac{1-\alpha_1}{1-\alpha_2} = -\frac{E_a}{nR} \left( \frac{1}{T_2} - \frac{1}{T_1} \right) \quad (4-7)$$

Plotting the left hand side versus the inverse temperature difference, shown on the right hand side in brackets, gives a straight line whose slope can be used to calculate the activation energy. The activation energy calculated using this method was found to be  $90 \pm 5$  kJ mol<sup>-1</sup>. This value is slightly higher than the autocatalytic model, however agrees well with that obtained using the n<sup>th</sup> order isothermal kinetic model.

The reaction orders ascertained using autocatalytic and n<sup>th</sup> order models were in good agreement, even though the activation energies obtained were higher for the n<sup>th</sup> order model. This supports the discussions of Vyazovkin <sup>[51]</sup> and represents a good case for using isoconversional methods with systems whose reactions occur predominately in liquid and solid phases, as the activation energy is most likely to change with conversion and medium temperature.

#### **4.3.1.2 Isoconversional methods**

Vyazovkin<sup>[51-53]</sup> suggests that although one is able to determine the pre-exponential factor and the reaction model, these are not necessary to predict the outcome of a process, especially for complex systems. Vyazovkin <sup>[51-53]</sup> discusses the application of isoconversional methods to detect multi step mechanisms by plotting the apparent activation energy versus the conversion. If there is more than one process occurring, the activation energy varies with the extent of conversion. Isoconversional analysis

has previously been used to describe the crosslinking reaction for limited number polyurethane systems, despite their complexity.<sup>[11, 54]</sup> In general, absolute extents of cure are used when evaluating the cure profile, however for reactions undergoing incomplete cure, this yields an error in the activation energy at higher conversions.<sup>[35]</sup> Thus the relative extents of cure along with **Equation (1-16)** were used to determine the change in activation energy with conversion shown in **Figure 4.9** (data at 100 °C was omitted from the calculation as a substantial amount of heat may have been undetected in the early stages as the reaction is very fast).

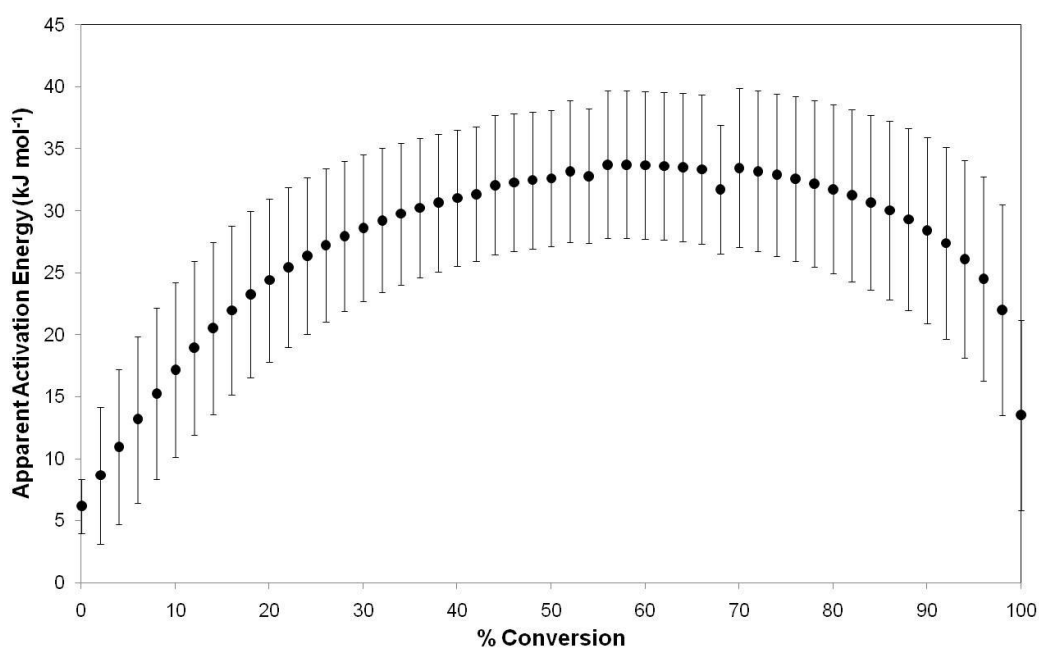


**Figure 4.9** Variation of activation energy with conversion for isothermal DSC cure

It can be seen that the activation energy ( $E_a$ ) increases up to a critical conversion (approximately 60%) after which a decrease occurs. This suggests a diffusion controlled process is apparent in the later stages of the reaction.<sup>[55]</sup> A similar convex shaped activation energy profile was obtained for a polyurethane process using model free kinetics and was attributed to autocatalytic cure in the initial stages, followed by diffusion control.<sup>[54]</sup> The activation energy increases from 5 kJ mol<sup>-1</sup> to 33.7 kJ mol<sup>-1</sup>, which is ~ 30% lower than reported values in the literature for polyurethane systems and is much lower than that obtained using both n<sup>th</sup>-order and autocatalytic models in the previous section.<sup>[33, 44, 56]</sup>

As a comparative study, non-isothermal DSC kinetics was analysed using isoconversional methods (**Figure 4.3**). The non-isothermal method for DSC

measurement is obtained by monitoring the heat of reaction at a constant heating rate. Using the same initial composition and obtaining data at several different heating rates, the kinetic parameters can be evaluated. Ozawa's expression as shown in **Equation (1-14)** was used to calculate the activation energy.  $T_p$  is the peak temperature obtained from an average of five thermograms at three different heating rates (*i.e.* at equal conversion) (**Table 4-2**). Plotting the left side numerator versus denominator at various heating rates, a straight line was obtained with a slope of  $(E_a/R)$  giving an activation energy of  $58.6 \pm 2.6 \text{ kJ mol}^{-1}$   $R^2 = 0.99$ . This activation energy is higher than the isothermal isoconversional method.

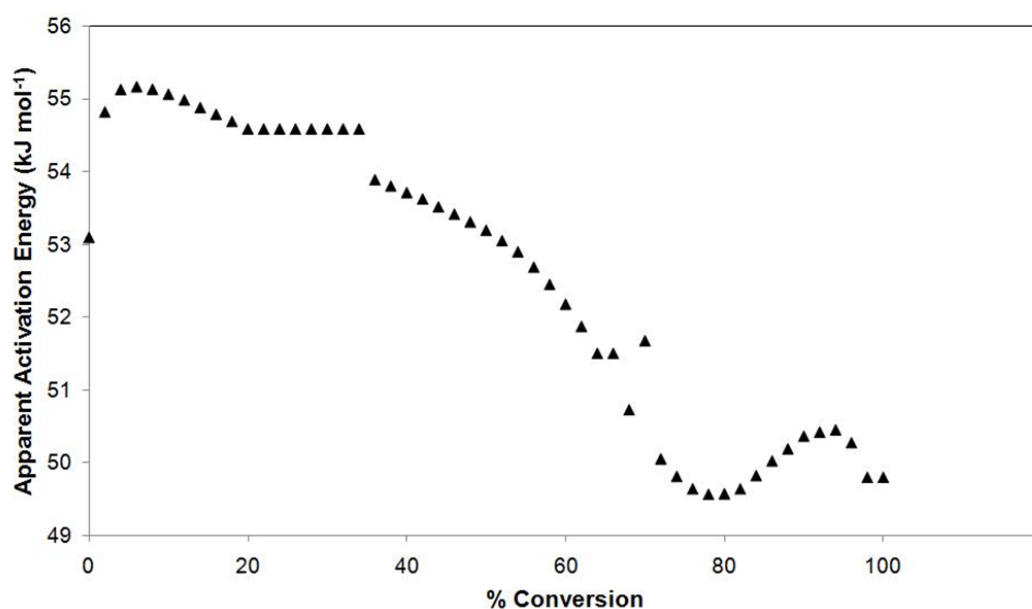


**Figure 4.10** Variation of activation energy with conversion for non-isothermal data

The variation of the activation energy with conversion determined through **Equation (1-20)**, is displayed in **Figure 4.10** and a steady decrease in activation energy with conversion is observed with a small increase in the later stages of conversion. This small increase towards the later stages of cure has previously been explained by the formation and reaction of allophanate, which is known to occur in polyurethane systems at temperatures above  $140 \text{ }^\circ\text{C}$ .<sup>[11, 23]</sup> The profile of the non-isothermal method has a narrower range of activation energy from  $49.5 \text{ kJ mol}^{-1}$  to  $55 \text{ kJ mol}^{-1}$  and is practically constant when compared to the isothermal plot, thus very minimal diffusion control is apparent (**Figure 4.9**). These activation energies are similar to the

values reported in the literature.<sup>[33, 44]</sup> As the isothermal method and non-isothermal method differ in their chemically driven and diffusion controlled kinetics, with isothermal cure representing incomplete cure, the non-isothermal method is a more reliable representation of the activation energy for the overall reaction.

#### ***4.3.1.3 Kinetic differences of the primary and secondary hydroxyls***

Differing reactivity of the primary and secondary hydroxyl groups in glycerol is evident from non-isothermal and isothermal DSC data. The cure rate versus conversion profile in **Figure 4.3** displays a second shoulder at approximately 80% conversion, apparent due to the slower reacting secondary hydroxyl group. In isothermal DSC experiments, lower isothermal cure temperatures lead to an increase in curing time and conversion. The presence of the secondary hydroxyl group in glycerol, if given sufficient time to react is likely to increase the conversion at lower temperatures while increasing vitrification times.

The entire cure process therefore includes both fast primary hydroxyl reactions as well as the slower reactions of the secondary hydroxyl group.<sup>[19]</sup> Using curve fitting software (*Origin 7.5*) and fitting two peaks to the isothermal heat flow versus time curves for 70 °C (120 min) 80 °C (60 min), 90 °C (40 min) and 100 °C (16 min) the conversion due to the primary and secondary hydroxyls can be differentiated. An example is shown for an isothermal run performed at 70 °C in **Figure 4.11 A**.

The experimental data fitted well to a Gaussian model, with a reduced chi-squared of  $7.74 \times 10^{-6}$ , COD of 98 and correlation of 0.99. (Iterations performed= 200 with a 0.95 confidence interval and a tolerance of 0.05. DOF= 52 and number of points = 58.) The conversion of the primary hydroxyl group was calculated from the area under the 1<sup>st</sup> peak fitted to the heat flow curves, while the conversion of the secondary hydroxyl group was calculated from the area of the second peak fitted to the heat flow curves. The secondary hydroxyl group conversion for the isothermal temperature of 100 °C was omitted from the data-set presented, because the reaction ceased too early for reliable determination of the second peak area. Plotting the conversion versus time at each temperature for both peaks separately and determining the slope of the line, the relative reaction rates of the primary and secondary hydroxyls can be elucidated and shown in **Figure 4.11 B**.

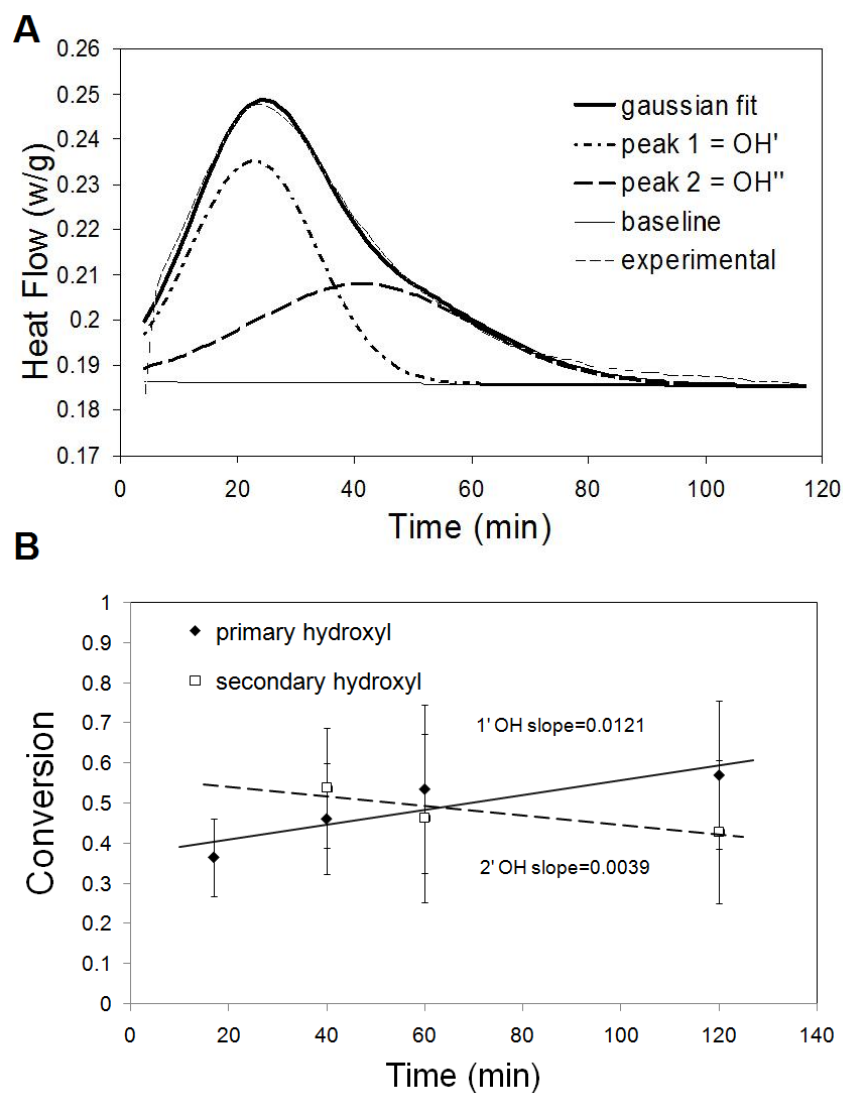


**Figure 4.11 A) Gaussian fit of heat flow curve during isothermal cure at 70 °C: 2 peaks fitted pertaining to primary and secondary hydroxyls and B) Rate of cure pertaining to primary and secondary hydroxyls in glycerol.**

From the slope of the straight lines, the primary hydroxyl is found to react three times faster than the secondary hydroxyl in glycerol, which has also been reported by Chappel *et al.*<sup>[19]</sup>, using an alternative method.

### 4.3.2 Rheological investigation of the stoichiometric ratio of Glycerol to PMDI

Rheological behaviour of network formation was monitored for the duration of cure for the polyurethane system. During isothermal cure, viscosity changes are detected due to an increase in molecular weight. The viscosity increases with time (**Figure 4.12**) due to urethane bond formation; however, many stages were noticed indicating this is a very complex reaction system.

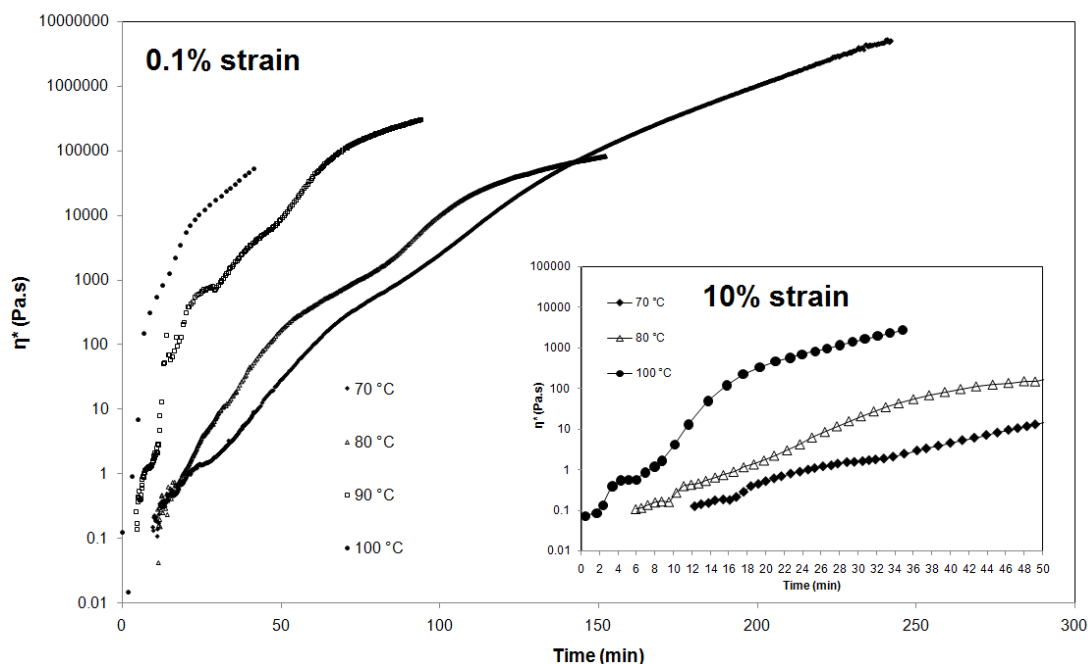


**Figure 4.12** Viscosity build up of the polyurethane system at various isothermal temperatures at 0.1% strain and inset at 10% strain showing initial viscosity build up

The inset in **Figure 4.12** represents the initial stages of viscosity build-up (90 °C data omitted for clarity-profile is clear in the main Figure). From the Figure insert, it is expected that the reaction mixture remains homogeneous with the more reactive functional groups combining until the point in time where the viscosity slightly decreases and proceeds to further increase with time producing a small peak. This reduction in viscosity is caused by heterogeneous curing, because the reaction product is insoluble in the reacting matrix.<sup>[57]</sup> The small peak observed is more pronounced at higher temperatures, while at 70 °C it extends over a longer period of time. It is suggested that formation of microgel particles and the start of gelation occur at this point, after which a rapid increase in the rate was observed, transitioning

to two main stages of viscosity build up. The two stages seen in **Figure 4.12** are assigned to the difference in reactivity of the primary and secondary hydroxyl groups in the glycerol as was established using DSC data. Furthermore, at each of these two stages of viscosity build up, a change in the rate is noticed, which could be apparent due to the difference in reactivity of the terminal isocyanate groups to the internal isocyanate groups of the varying weight oligomers in PMDI.<sup>[58]</sup> The evolution of the elastic modulus,  $G'$ , loss modulus,  $G''$  and  $\tan \delta$  for each temperature is shown in **Figure 4.13**. The behaviour of  $\tan \delta$  depends on the cure temperature and can be related to the two main stages of viscosity build up and the sudden increase in  $G'$  and  $G''$ .

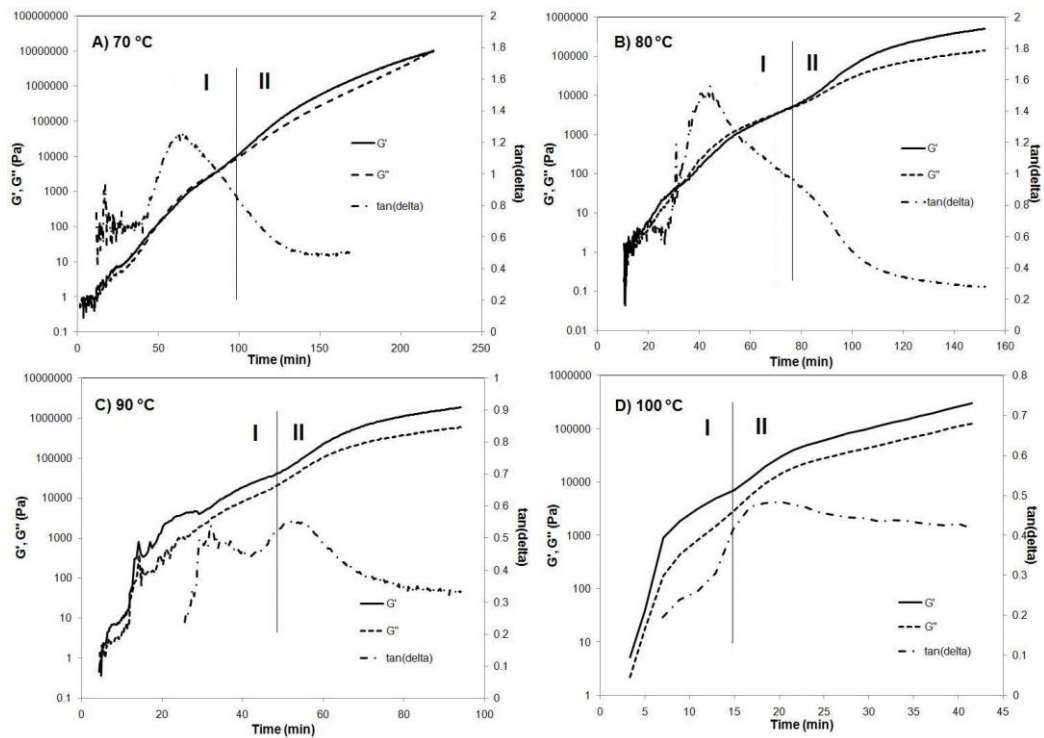


**Figure 4.13** Evolution of  $G'$ ,  $G''$  and  $\tan \delta$  at various isothermal cure temperatures at 0.1% strain, 1Hz

With the cure temperature below the ultimate glass transition temperature, two  $\tan \delta$  peaks were observed and were found to be in direct relation to the slope changes observed in viscosity. The  $\tan \delta$  peak is broad and spans over a longer period of time at 70 °C; forming a shoulder at 80 °C, while at 90 °C, two distinct peaks were observed. This variation in  $\tan \delta$  with increasing temperature, where a more distinct

second peak is observed at 90 °C, confirmed that primary and secondary hydroxyls respond differently to temperature. This same influence of temperature was also seen in isothermal DSC scans. At 100 °C, the isothermal temperature matched the glass transition temperature resulting in a lower viscosity build-up in the later stage of cure. In contrast, at temperatures below the glass transition temperature, there is an onset of diffusion control resulting in an increase of the magnitude of viscosity build-up,  $G'$  and  $G''$ .

The initial cure behaviour was monitored at 10% strain because the evolution of  $G'$ ,  $G''$  and  $\tan \delta$  at 0.1% strain was highly scattered. Initially, the loss modulus starts growing while the storage modulus is below the sensitivity of the equipment. After the crossover of  $G'$  and  $G''$  determined at 10% strain and shown in **Table 4-4**, the behaviour is followed using 0.1% strain, as shown in **Figure 4.12**. The variation of  $G'$  and  $G''$  depends on the isothermal temperature used. At 70 °C and 80 °C the same profile is observed for  $G'$  and  $G''$ , whereby the storage modulus rises above the loss modulus until a point where the loss modulus grows faster than the storage modulus and coincides with the peak in  $\tan \delta$ . Once past the maximum  $\tan \delta$ , the storage modulus continues to grow and increases at a rate which is faster than the loss modulus pertaining to a more elastic system. This growth of the storage modulus occurs from the reactions between the primary hydroxyl and less reactive isocyanate groups as discussed earlier. The storage modulus undergoes a second rate rise which, as discussed above, occurs through reactions of the secondary hydroxyl groups. It can be seen in **Figure 4.13A** at 70 °C, the storage and loss modulus start to come together towards the end of the profile. At this point, the system no longer flows and represents the gel point. Gel times were established using the multifrequency technique where  $\tan \delta$  becomes independent of frequency and are given in **Table 4-4**. The dependence of gel time on isothermal cure temperature is depicted in **Figure 4.14**. The point where  $\tan \delta$  intersects for all frequencies is highlighted by a circle. As the cure temperature gets closer to the glass transition temperature of the system, the gel time is harder to detect by the crossover of the  $\tan \delta$  curves, as the onset of diffusion control and gelation occur at the same time, giving rise to very complex rheological behaviour.<sup>[59]</sup>

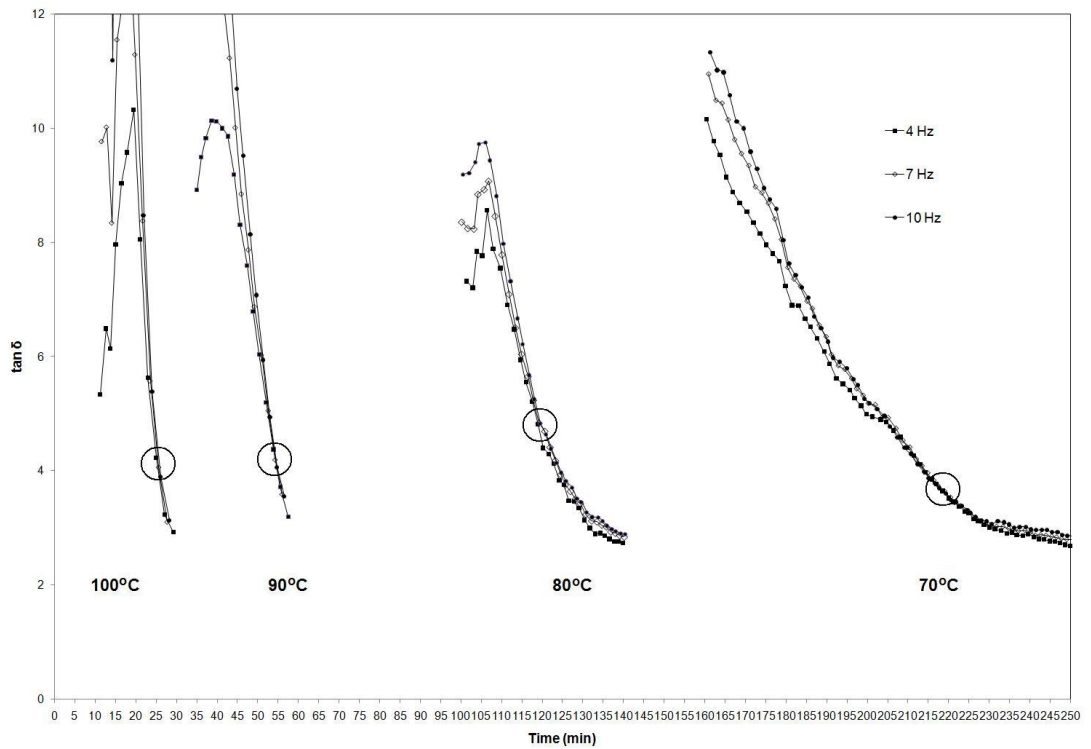


**Figure 4.14** Dependence of the gel point on the isothermal curing temperature for the polyurethane system

The degree of conversion at the gel point can be considered as a constant for thermosetting systems<sup>[32, 60, 61]</sup> allowing for a direct relationship between the gel time ( $t_{gel}$ ) and the apparent curing constant  $K_c$ :<sup>[32, 62]</sup>

$$t_{gel} = A' \times \left( \frac{1}{K_c} \right) \quad (4-8)$$

The curing process can be described by an overall activation energy  $E_a$  where the temperature dependence of the gel time follows the Arrhenius law ( $K_c(T) = A'' \exp(-E_a/RT)$ ), and can be obtained by plotting:

$$\ln(t_{gel}) = A''' + \frac{E_a}{RT} \quad (4-9)$$

The overall activation energy attained at the gel point (an isoconversional method) is

$77.4 \pm 4.4 \text{ kJ mol}^{-1}$ . This value is much higher than the activation energy range obtained using isoconversional DSC analysis; however is in very good agreement with the activation energy obtained using the autocatalytic model.

The crossover of the storage modulus and loss modulus is also used to characterise gelation for stoichiometric systems or systems with excess hardener.<sup>[59, 63]</sup> In this case, it is suggested that the crossover represents the initial cure phase of the reacting system with the formation of microgel particles, just before phase separation occurs. Using the times where  $G'=G''$  (**Table 4-4**), the apparent activation energy at early stages of the reaction is  $51.3 \pm 5.2 \text{ kJ mol}^{-1}$  and is closer to that obtained using isoconversional, non-isothermal DSC kinetics.

**Table 4-4 Critical rheological times obtained using the crossover of  $G'$  and  $G''$  and the frequency independence of  $\tan \delta$**

<b>Isothermal temperature</b> (°C)	<b><math>G'=G''</math></b> <b>(min)</b>	<b><math>\tan \delta</math> frequency independence</b> <b>(min)</b>
70	11.9	218
80	8.4	119
90	5.1	54
100	2.8	25

A summary of the various activation energies obtained using isothermal/non-isothermal modes and model and isoconversional methods are given in **Table 4-5**.

**Table 4-5 Summary of varying activation energies obtained for the complex polyurethane reaction between glycerol and PMDI**

<b>Method</b>	<b>Isothermal</b>	<b>Non-isothermal</b>
Isoconversional-Vyazovkin's	5-35	50-55
Isoconversional-Ozawa's	na	$58.6 \pm 2.6$
Isoconversional-Rheology	$77.4 \pm 4.4$	na
$n^{\text{th}}$ order model	$96 \pm 11$	$90 \pm 5$
Autocatalytic model	$74.8 \pm 3.6$	na

A comparison between isoconversional and model implementation to determine the activation energy of the complex polyurethane reaction showed that much higher activation energies were achieved by using kinetic models in both isothermal and non-isothermal modes, with the exception of rheological data which agreed well with the autocatalytic model.

A comparison between the kinetic models showed higher activation energies using the  $n^{\text{th}}$  order model, however the reaction orders obtained using both models were in good agreement.

Isothermal isoconversional analysis gave much lower activation energies than non-isothermal isoconversional data, which could be attributed to the data used for isothermal analysis consisting of only the first 40 minutes of the reaction, whereas non-isothermal DSC isoconversional analysis represented the entire cure profile of the reaction. Activation energy data obtained using isoconversional non-isothermal DSC was much closer to the values obtained in the literature for similar systems. [15, 26, 28, 45] Thus it is concluded that the most reliable methods for obtaining activation energy from DSC data is the use of non-isothermal isoconversional methods for the polyurethane reaction. The advantage of using the isoconversional method is the ability to follow the activation energy with conversion which gives rise to information about the complexity of cure, especially when there are multiple reaction mechanisms present. [52]

Given the complexity of the system studied, investigation of the optimum ratio of glycerol to PMDI was investigated, in order to achieve maximum cure. In the following section, varying mole ratios were investigated to determine the critical ratio of glycerol to PMDI, achieving maximum cure.

### 4.3.3 Investigation of the critical ratio of glycerol to PMDI

Varied mole ratios of glycerol to PMDI were analysed using non-isothermal DSC, in order to determine the optimum mole ratio of OH/NCO to achieve the maximum conversion at a heating rate of  $10\text{ }^{\circ}\text{C min}^{-1}$ . The magnitude of the heat of reaction, as well as the peak reaction temperature at each mole ratio of OH/NCO groups investigated is displayed in **Figure 4.15**.

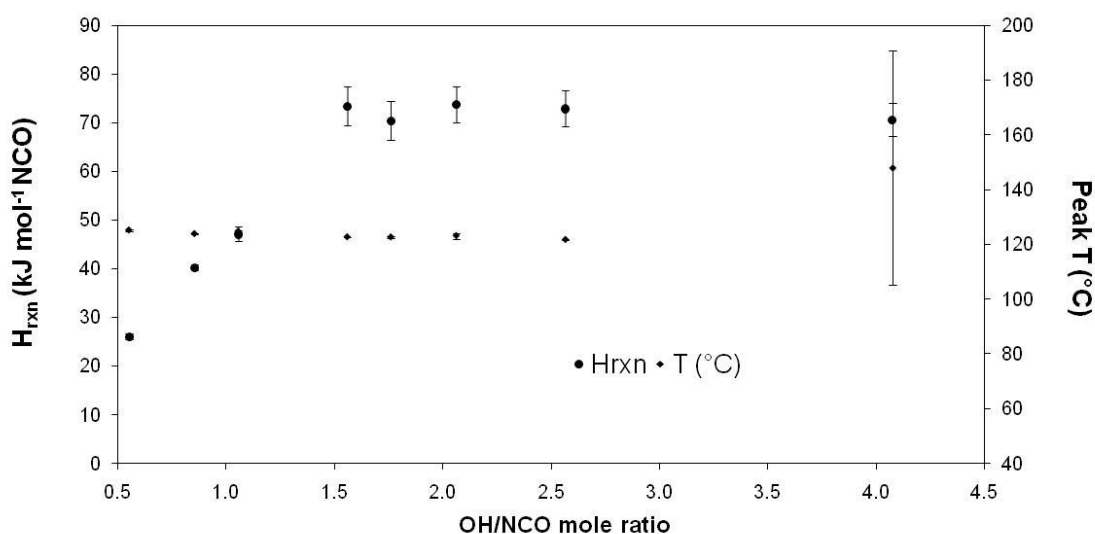


**Figure 4.15** Extent of reaction for varying mole ratios of OH/NCO

It is noticed from **Figure 4.15**, that a critical ratio of OH/NCO = 1.5 was reached, after which the heat of reaction remained constant. It was also noticed that the peak reaction temperature was practically constant for all ratios. Conversion at the peak temperature for all ratios was found to be approximately 40%. ATR-FTIR analysis of the DSC cured samples was performed for each mole ratio and the conversions displayed in **Figure 4.16**. The isocyanate peak at  $2235\text{ cm}^{-1}$  was normalised to an internal standard at  $2911\text{ cm}^{-1}$  representing the stretching vibrations of  $\text{CH}_2$  groups.<sup>[64]</sup> It was noticed that at the critical ratio of OH/NCO, the conversion as determined by the reduction in the isocyanate peak intensity also increased up to a ratio of OH/NCO=1.5 at approximately 90%, after which 100% conversion of isocyanate groups became evident. Thus, an excess hydroxyl mole ratio is required for complete conversion of isocyanate groups in this system. This is also evidenced

in **Figure 4.17**, where DSC and ATR-FTIR data were in good agreement, following the same profile with an increase in hydroxyl content. An excess of hydroxyl groups might be required to overcome the slower reaction of the secondary hydroxyl group. Reaction of the secondary hydroxyl group is limited once the reaction becomes diffusion controlled as previously established.

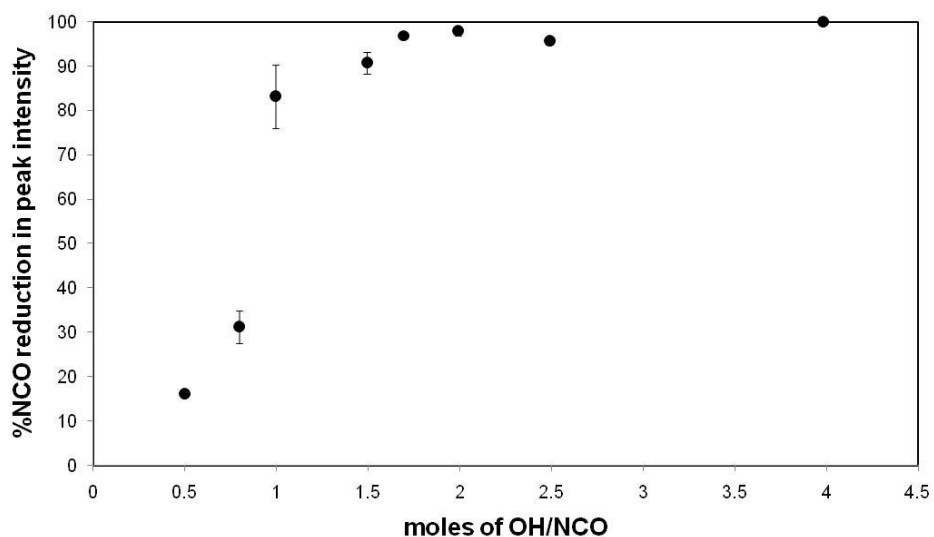


**Figure 4.16** Conversion of isocyanate peak intensity for increasing hydroxyl content

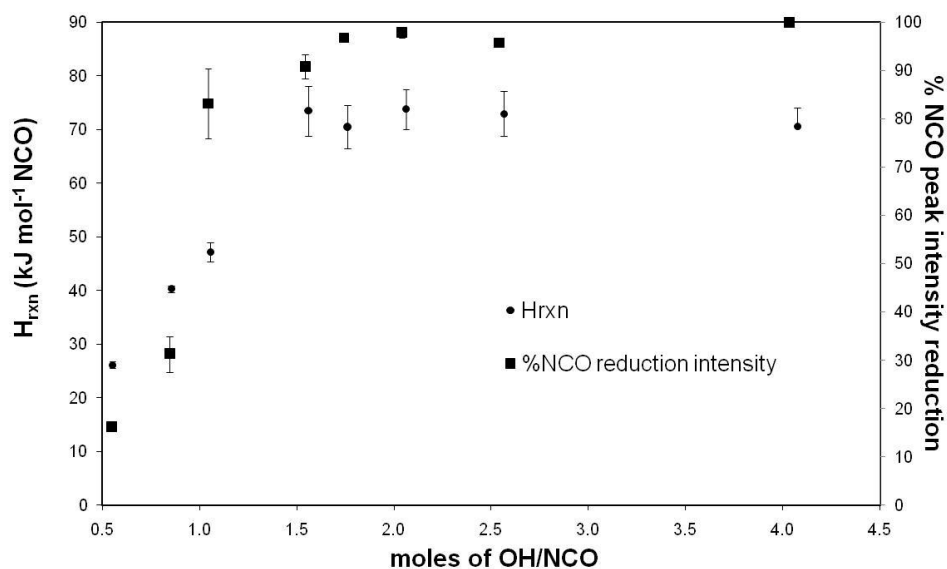


**Figure 4.17** Overlap of the DSC and ATR-FTIR data for the conversion of isocyanate groups with an increasing hydroxyl concentration

To determine the existence of a relationship between the heat of reaction through DSC and % isocyanate peak reduction through ATR-FTIR, the data were plotted against each other and shown in **Figure 4.18**.

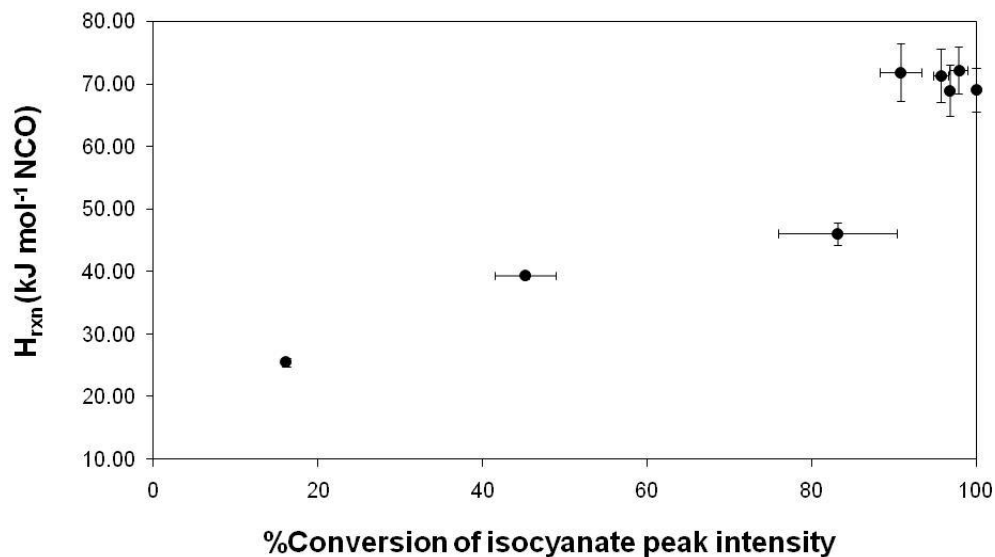


**Figure 4.18 Heat of reaction in  $\text{kJ mol}^{-1}$  equivalent isocyanate versus %conversion determined by the reduction in intensity of the isocyanate peak using ATR-FTIR**

No direct correlation (**Figure 4.18**) existed between the heat of reaction as determined by DSC analysis and the conversion of isocyanate as determined by ATR-FTIR for increasing OH/NCO over the entire range investigated. However, a correlation between the methods did exist for the ratios above and below the critical ratio of OH/NCO =1.5.

The critical ratio will be investigated further using model-free kinetics in the next section.

#### 4.3.4 Kinetic analysis of the critical ratio using isconversional methods for DSC data

The critical mole ratio of  $\text{OH/NCO} = 1.5$  was investigated further through isothermal and non-isothermal calorimetry. Heat flow profiles are shown in **Figure 4.19**.

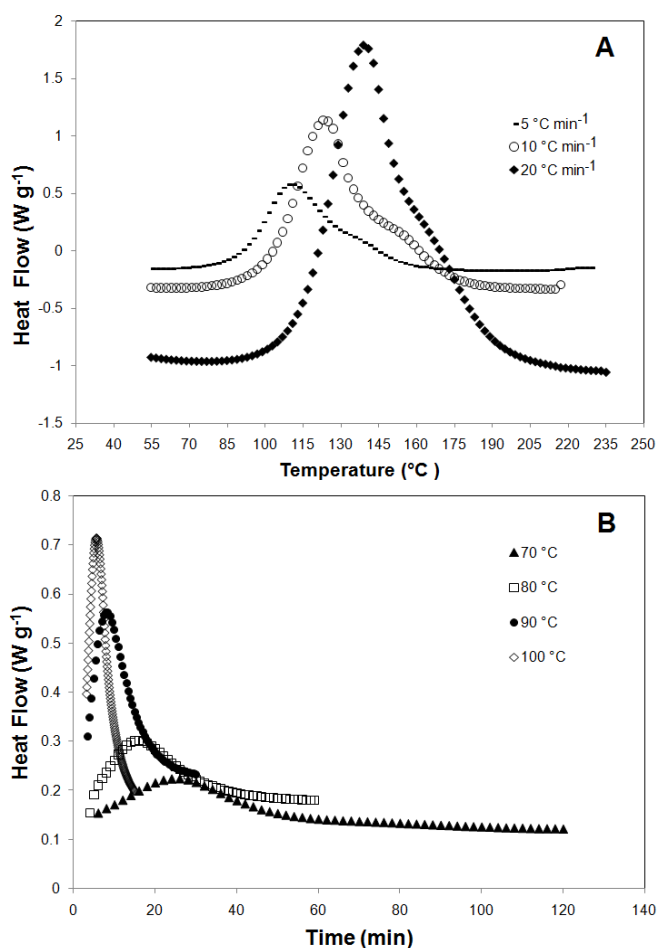


**Figure 4.19** Heat flow profiles in A) non-isothermal and B) isothermal mode for the critical mole ratio of  $\text{OH/NCO}$ .

It is noticed in **Figure 4.19 A** that a second shoulder was also evident in the heat flow profiles with an excess mole ratio of hydroxyl  $\text{OH/NCO}=1.5$ , showing the presence of the secondary hydroxyl reaction. The heat of reaction, peak reaction temperature and conversion at the peak are given in **Table 4-6**.

The heat of reaction and peak reaction temperature tends to increase with an increase in heating rate with a constant conversion achieved at the peak temperature. Furthermore the peak temperature and conversions obtained at the peak are

equivalent (within experimental error) to that obtained for the stoichiometric ratio. The total heat of reaction ( $H_{rxn}$ ) obtained through non-isothermal DSC is higher for the excess hydroxyl mole ratio of OH/NCO=1.5 than the stoichiometric system, suggesting larger conversions are reached.

**Table 4-6** Reaction data for non-isothermal DSC analysis with an excess in hydroxyl groups

Heating Rate °C min <sup>-1</sup>	H <sub>rxn</sub> J g <sup>-1</sup>	T <sub>peak</sub> (°C)	% Conversion @ T <sub>peak</sub>
5	305.83 ± 5.36	110.43 ± 0.39	39.52 ± 1.14
10	312.13 ± 3.28	124.34 ± 0.36	39.51 ± 0.95
20	333.67 ± 2.82	139.15 ± 0.46	39.14 ± 1.28

Ozawa's isoconversional analysis (**Equation (4-9)**) was used to obtain the activation energy at the peak reaction temperature as equal conversions were apparent. The apparent activation energy obtained using Ozawa's expression was 60.31 ± 0.18 kJ mol<sup>-1</sup> which is equivalent to that obtained for the stoichiometric system (58.6 ± 2.6 kJ mol<sup>-1</sup>) and has been reported for polyurethane systems as mentioned previously.

The advanced integral isoconversional method by Vyazovkin <sup>[51]</sup> was also used to determine the activation energy as a comparison to the stoichiometric system, and is shown in **Figure 4.20**.

It is noticed that the activation energy is dependent on conversion; however, it does not vary greatly, giving average activation energy of  $54.2 \pm 1.1 \text{ kJ mol}^{-1}$  compared to  $52.2 \pm 0.5 \text{ kJ mol}^{-1}$  for the stoichiometric ratio. It must be noted that the average activation energy is slightly lower than that obtained using Ozawa's expression. The activation energy profile for excess hydroxyl groups is very similar to that of the stoichiometric system, whereby the activation energy decreases with conversion, although a slower onset of diffusion control is noticed.

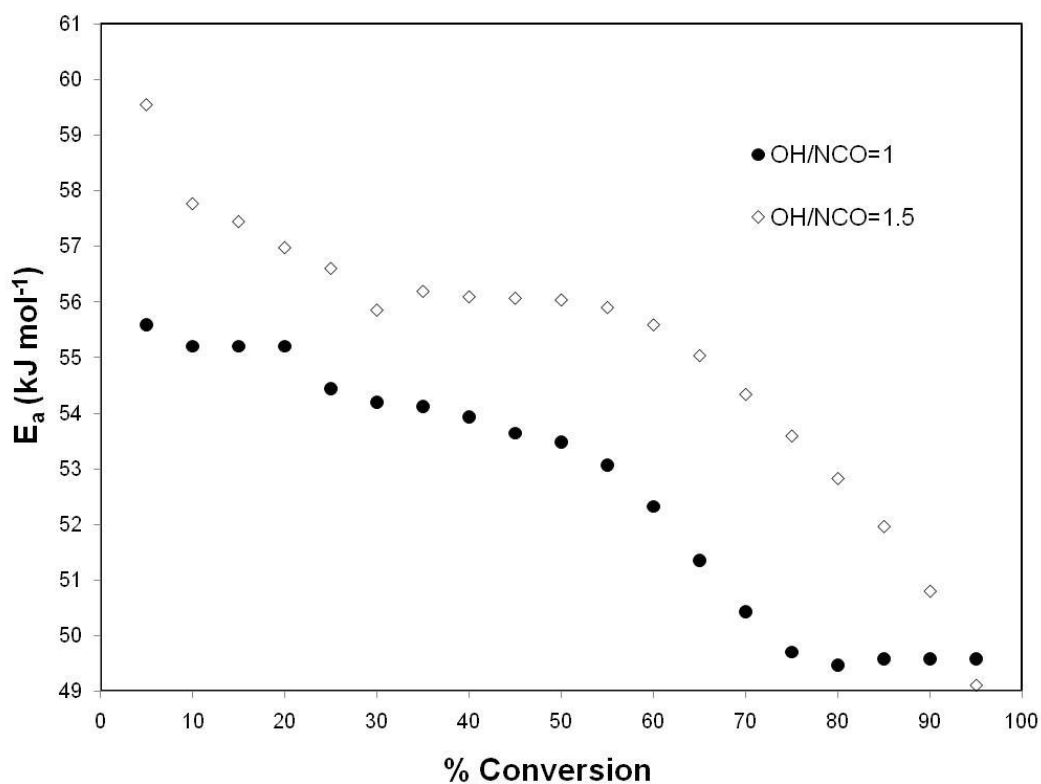


**Figure 4.20** Non-isothermal dependence of activation energy on conversion for differing mole ratios of OH/NCO

Isothermal analysis was also performed for the mole ratio of OH/NCO=1.5. Similar heat profiles were obtained as for the stoichiometric system (**Figure 4.19 B**). An increase in conversion with a reduction in isothermal temperature is evident, which corresponds to the presence of the slower reacting secondary hydroxyl group in glycerol, as mentioned previously.

Investigations of the DSC cured sample for the mole ratio OH/NCO=1.5, through ATR-FTIR analysis (**section 4.3.3, Figure 4.16**), showed that isocyanate groups were practically consumed, with ~93% conversion observed. Thus, isothermal data was treated as for a completely cured sample, by determining conversions achieved using absolute extents of cure (as discussed in the experimental **section 4.2.2.1**). The activation energy dependence on conversion for absolute cure over the entire cure time of 120 min, is given in **Figure 4.21**. As the absolute extent of conversion was used over the entire cure time to determine the activation energy profile, the profile cannot be directly compared to the stoichiometric system, where the cure up to 40 min was used to determine relative extents. However, it is noticed from **Figure 4.21**, that an increase in activation occurs initially, followed by a slight drop towards the end stages of isothermal cure, which suggests the beginnings of a diffusion controlled process. It must be noted however, due to large conversions observed in ATR-FTIR analysis for the completely cured system, the reaction with an excess in hydroxyl groups is largely kinetically controlled. The average activation energy obtained for this system is  $40.5 \pm 2.1 \text{ kJ mol}^{-1}$  which is smaller than the average obtained using non-isothermal data, however, is larger than the average activation energy obtained for the equal stoichiometric system using isothermal analysis which was equal to  $21 \pm 1 \text{ kJ mol}^{-1}$ .

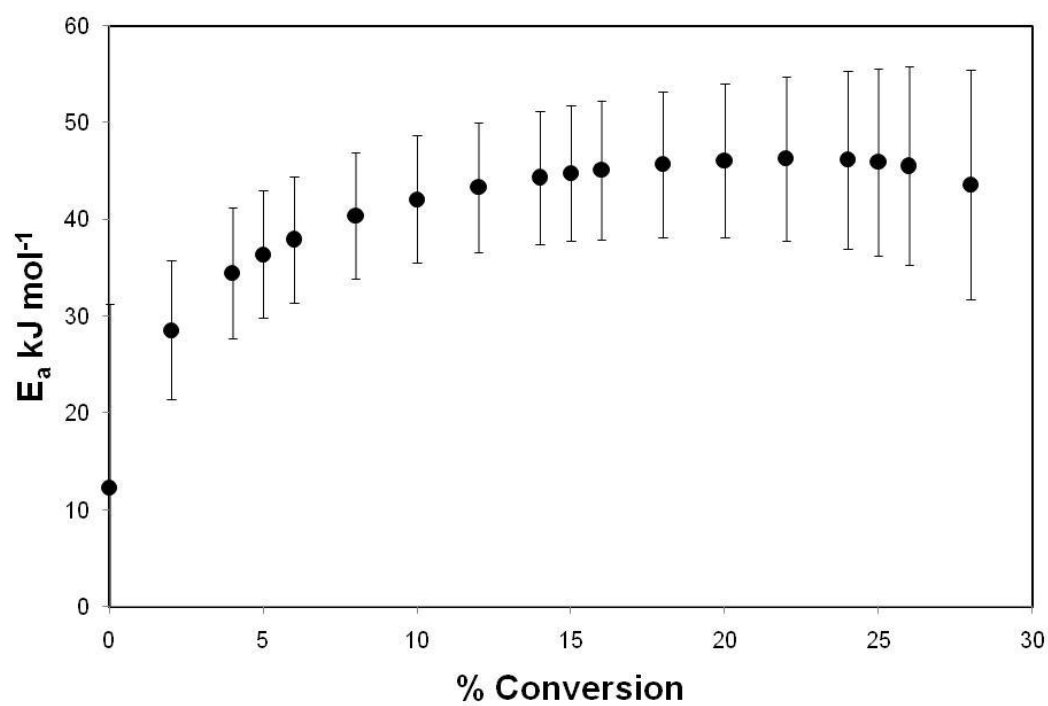


Figure 4.21 Isothermally determined activation energy dependence on conversion for an excess in hydroxyl mole ratio of OH/NCO=1.5 determined using absolute extents of cure.

## 4.4 Conclusions

The polymerisation of oligomeric diisocyanate monomers using tri-hydroxy glycerol, containing two fast reacting primary hydroxyl groups and one slower reacting secondary hydroxyl group, were investigated using thermal and rheological techniques. This work highlighted the complexity of cure for this system. The reactivities of the primary and secondary hydroxyl groups were found to vary with temperature or during extended periods of curing, suggesting that cure did not go to completion at all temperatures, with the ultimate reactivity of both isocyanate and hydroxyl groups being inhibited by the onset of diffusion control towards the end of cure. The primary hydroxyls were found to react three times faster than the secondary hydroxyl groups as corroborated by similar systems investigated in the literature using different characterisation techniques. A comparison between the application of kinetic models and isoconversional methods for DSC data was made, showing that non-isothermal isoconversional analysis was the most reliable in obtaining activation energies for the stoichiometric ratio. It must be noted that only the basic kinetic models were used for the analysis without considering the diffusion rate constant in the modelling approach.

Rheological studies of viscosity increase and  $\tan \delta$  changes revealed a complex cure process, with primary and secondary hydroxyl reactivity being dependant on isothermal cure temperatures, reflecting similar results obtained from isothermal DSC studies. Two separate  $\tan \delta$  peaks were observed, which responded differently to isothermal temperature conditions of cure and were related to the different rate of cure of the primary and secondary hydroxyl groups on the glycerol molecule. The independence of  $\tan \delta$  on frequency was used to determine the point where the polymer formed an infinite network and was no longer able to flow, providing an overall activation energy attained at the gel point of  $77.4 \pm 4.4 \text{ kJ mol}^{-1}$  which was higher than that obtained using isoconversional DSC analysis. The optimum ratio of OH/NCO was determined through non-isothermal DSC and ATR-FTIR, showing that complete cure occurred at a mole ratio of OH/NCO=1.5. An excess of hydroxyl groups could be required to overcome the slower reaction of the secondary hydroxyl group and the diffusion limitations of the reaction as mentioned above.

## 4.5 References

- [1] M. Urban, W. Ludwig, *J. Coat. Technol.* **1996**, 68, 93.
- [2] D. Ihms, J. O. Stoffer, D. Schneider, C. McClain, "The effect of catalysts on kinetics and mechanism of urethane film formation", in *Water-Borne & Higher-Solids Coatings Symposium*, **1983**, 233.
- [3] D. Ihms, J. O. Stoffer, D. F. Schneider, C. McClain, *J. Coat. Technol.* **1985**, 57, 61.
- [4] D. P. Harper, "The evaluation of 4-4' Diphenylmethane Diisocyanate cure in a saturated steam environment", in *Department of Civil and Environmental Engineering*, Washington State University, Washington, **1998**.
- [5] R. B. Prime, "An Introduction to Thermosets", **2005**.
- [6] A. B. Spoelstra, *Polym. Eng. Sci.* **1996**, 36, 2153.
- [7] J. M. Kenny, *J. Appl. Polym. Sci.* **1994**, 51, 761.
- [8] T. J. Hsu, L. J. Lee, *Polym. Eng. Sci.* **1988**, 28, 955.
- [9] S. Du, Z.-S. Guo, B. Zhang, Z. Wu, *Polym. Int.* **2004**, 53, 1343.
- [10] S. Ajithkumar, S. S. Kansara, N. K. Patel, *Eur. Polym. J.* **1998**, 34, 1273.
- [11] F. Dimier, N. Sbirrazzuoli, B. Vergnes, M. Vincent, *Polym. Eng. Sci.* **2004**, 44, 518.
- [12] S. Florez, M. E. Munoz, A. Santamaria, *J. Rheol.* **2005**, 49, 313.
- [13] J. T. Haponiuk, M. Strankowski, T. Lazarewicz, *J. Therm. Anal. Colorim.* **2003**, 74, 609.
- [14] D. S. Kim, J.-T. Kim, W. B. Woo, *J. Appl. Polym. Sci.* **2005**, 96, 1641.
- [15] P. Krol, B. Atamanczuk, J. Pielichowski, *J. Appl. Polym. Sci.* **1992**, 46, 2139.
- [16] A. H. Navarchian, F. Picchioni, L. P. B. M. Janssen, *Polym. Eng. Sci.* **2005**, 45, 279.
- [17] J. M. E. Rodrigues, M. R. Pereira, A. G. de Souza, M. L. Carvalho, A. A. Dantas Neto, T. N. C. Dantas, J. L. C. Fonseca, *Thermochim. Acta* **2005**, 427, 31.
- [18] V. Sekkar, V. N. Krishnamurthy, S. R. Jain, *J. Appl. Polym. Sci.* **1997**, 66, 1795.
- [19] J. Chappel, P. Argust, *Thermochim. Acta* **1996**, 289, 303.
- [20] Z. S. Petrovic, D. Fajnik, *J. Appl. Polym. Sci.* **1984**, 29, 1031.
- [21] Z. S. Petrovic, A. Guo, J. G. Zhang, *J. Polym. Sci.: Part A: Polym. Chem.* **2000**, 38, 4062.
- [22] T. Ando, *Nippon Kagaku Kaishi* **1993**, 10, 1201.

- [23] J. Dodge, "Synthetic Methods in Step-Growth Polymers: Polyurethanes and Polyureas Chapter 4", M.E. Rogers and T.E. Long, Eds., John Wiley & Sons, **2003**, p. 197.
- [24] D. S. Kim, C. W. Macosko, *Korea Polym. J.* **1996**, *4*, 54.
- [25] H. Yeganeh, M. R. Mehdizadeh, *Eur. Polym. J.* **2004**, *40*, 1233.
- [26] H. Yeganeh, M. A. Shamekhi, *Polym. Int.* **2005**, *54*, 754.
- [27] M. L. Costa, L. C. Pardini, M. C. Rezende, *Mater. Res.* **2005**, *8*, 65.
- [28] R. B. Prime, C. Michalski, C. M. Neag, *Thermochim. Acta* **2005**, *429*, 213.
- [29] C. C. Su, E. M. Woo, Y. P. Huang, *Polym. Eng. Sci.* **2004**, *45*, 1.
- [30] S. M. Gasper, D. N. Schissel, L. S. Baker, D. L. Smith, R. E. Youngman, L.-M. Wu, S. M. Sonner, R. R. Hancock, C. L. Hogue, S. R. Givens, *Macromolecules* **2006**, *39*, 2126.
- [31] C. M. Nunez, B.-S. Chiou, A. L. Andrady, S. A. Khan, *Macromolecules* **2000**, *33*, 1720.
- [32] H. Teil, S. A. Page, V. Michaud, J. A. E. Manson, *J. Appl. Polym. Sci.* **2004**, *93*, 1774.
- [33] S. Parnell, K. Min, M. Cakmak, *Polymer* **2003**, *44*, 5137.
- [34] E. C. Steinle, F. E. Critchfield, J. M. Castro, C. W. Macosko, *J. Appl. Polym. Sci.* **1980**, *25*, 2317.
- [35] S. Vyazovkin, N. Sbirrazzuoli, *Macromol. Rapid Commun.* **2000**, *21*, 85.
- [36] R. J. Varley, *Macromol. Mater. Eng.* **2007**, *292*, 46.
- [37] J. Dupuy, E. Leroy, A. Maazouz, *J. Appl. Polym. Sci.* **2000**, *78*, 2262.
- [38] C. E. Miller, B. E. Eichinger, *J. Appl. Polym. Sci.* **1991**, *42*, 2169.
- [39] S. Benali, D. Bertrand, J. Dupuy, G. Lachenal, A. Maazouz, *The Institute of Measurement and Control* **2007**, *29*, 417.
- [40] S. Vyazovkin, N. Sbirrazzuoli, *Macromol. Chem. Phys.* **2000**, *201*, 199.
- [41] M. Sato, *J. Am. Chem. Soc.* **1960**, *82*, 3893.
- [42] C. Texier, M. Taha, A. Maazouz, J. P. Pascault, *Polym. Eng. Sci.* **1997**, *37*, 1238.
- [43] F. Hernandez-Sanchez, H. Vazquez-Torres, *J. Polym. Sci.: Part A: Polym. Chem.* **1990**, *28*, 1579.
- [44] F. Hernandez-Sanchez, R. Vera-Graziano, *J. Appl. Polym. Sci.* **1992**, *46*, 571.
- [45] H. Yeganeh, M. A. Shamekhi, *J. Appl. Polym. Sci.* **2006**, *99*, 1222.

- [46] S. Zeng, K. Ahn, J. C. Seferis, J. M. Kenny, L. Nicolais, *Polym. Compos.* **1992**, *13*, 191.
- [47] J. L. Martin, J. M. Salla, A. Cadenato, X. Ramis, *J. Therm. Anal.* **1992**, *38*, 917.
- [48] U. Khanna, M. Chanda, *J. Appl. Polym. Sci.* **1993**, *49*, 319.
- [49] C. C. M. Ma, C. H. Chen, *J. Appl. Polym. Sci.* **1993**, *50*, 759.
- [50] S. L. Hager, T. B. MacRury, R. M. Gerkin, F. E. Critchfield, *ACS Polymer Preprints* **1980**, 21.
- [51] S. Vyazovkin, *J. Therm. Anal. Calorim.* **2006**, *83*, 45.
- [52] S. Vyazovkin, *J. Therm. Anal.* **1997**, *49*, 1493.
- [53] S. Vyazovkin, *Proceedings of the NATAS Annual Conference on Thermal Analysis and Applications* **2003**, 31st, 026/1.
- [54] F. B. Arlas, L. Rueda, P. M. Stefani, K. Caba, I. Mondragon, A. Eceiza, *Thermochim. Acta* **2007**, *459*, 94.
- [55] S. Vyazovkin, *Int. J. Chem. Kinet.* **1996**, *28*, 95.
- [56] S. L. Hager, T. B. MacRury, R. M. Gerkin, F. E. Critchfield, *ACS Symposium Series* **1981**, *172*, 149.
- [57] A. Y. Malkin, S. G. Kulichikhin, *Adv. Polym. Sci.* **1991**, *101*, 217.
- [58] E. Papadopoulos, M. Ginic-Markovic, S. R. Clarke, *Macromol. Chem. Phys.* **2008**, *209*, 2302.
- [59] R. Mezzenga, A. Luciani, J. A. E. Manson, *Polym. Eng. Sci.* **2002**, *42*, 249.
- [60] C.-Y. M. Tung, P. J. Dynes, *J. Appl. Polym. Sci.* **1982**, *27*, 569.
- [61] H. Yu, S. G. Mhaisalkar, E. H. Wong, *Macromol. Rapid Commun.* **2005**, *26*, 1483.
- [62] J. M. Laza, J. L. Vilas, M. Rodriguez, M. T. Garay, F. Mijangos, L. M. Leon, *J. Appl. Polym. Sci.* **2002**, *83*, 57.
- [63] H. H. Winter, F. Chambon, *J. Rheol.* **1986**, *30*, 367.
- [64] A. M. Kaminski, M. W. Urban, *J. Coat. Technol.* **1997**, *69*, 113.

# **CHAPTER 5**

## **Polyol Emulsion**

## 5 POLYOL EMULSION

### 5.1 Introduction

Current industry trends towards solvent free polyurethane systems due to unsafe volatile organic compound levels, has provided a high demand for water-borne polyurethane coatings.<sup>[1-3]</sup> The first component of the industry coating package is a water dispersed reactant in the form of a polyol emulsion. The polyol emulsion consists of a castor oil-in-water dispersion, emulsified by a nonyl-ethoxylated surfactant, also containing a plasticizer, fragrant oil and silicone oil used to aid in de-aeration. The polyol emulsion stability is detrimental to the shelf-life, and is obtained by the effective dispersion of the castor oil in water using the non-ionic surfactant. The surfactant decreases the interfacial tension between oil and water and stabilises the droplet from coalescing with its neighbouring droplets as shown in **Figure 5.1**.<sup>[4, 5]</sup>

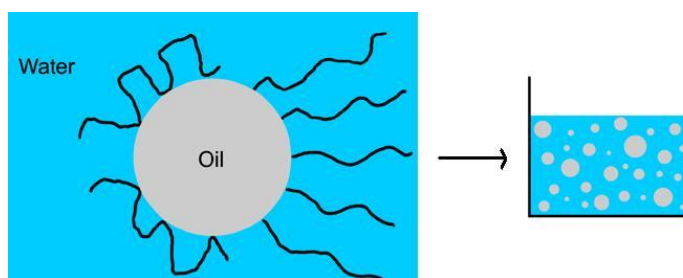


**Figure 5.1** Steric stabilisation of oil-in-water forming an emulsion<sup>[6]</sup>

Determination of the correct surfactant system for emulsions is made by considering its Hydrophilic-Lipophilic Balance (HLB).<sup>[7-9]</sup> The HLB of a surfactant in combination with the oil used, determines whether an oil-in-water or water-in-oil emulsion is formed. The effective dispersion of castor oil in water requires a surfactant HLB of 14.<sup>[9]</sup> The non-ionic surfactant used is uncharged and stabilises the dispersion through steric effects. The hydrophilic nature comes from the poly(ethylene oxide) component of the nonyl-phenol ethoxylate, whose structure is displayed in **Figure 5.2**.<sup>[10-15]</sup>

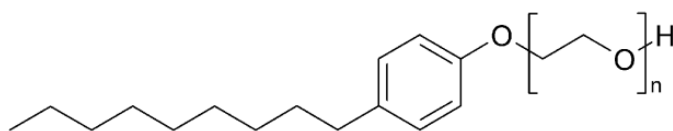


**Figure 5.2 Structure of the nonyl-phenol ethoxylate**

Important parameters in the analysis of emulsions are the volume fraction of the dispersed phase, surfactant type, droplet size and ultimately, the stability over time. The stability of an emulsion is characterised by its resistance to creaming, flocculation, coalescence, phase separation and Ostwald ripening.<sup>[8, 16-19]</sup> In this chapter, measurement of emulsion stability was performed using rheological measurements such as viscosity behaviour and dynamic viscoelastic behaviour as a function of stress, as only a relative comparison of the emulsion properties was required.<sup>[16, 20-22]</sup>

Castor oil and water are two key reactants in the reaction with the PMDI (the second component in the product formulation). The reactions yield a poly (urea-co-urethane) crosslinked system. The reaction between water and isocyanate groups of the PMDI yields carbon dioxide gas, which causes pinholes and in the worst case scenario, blistering and delamination of the coating. Investigations into the rate of foaming which includes gas bubble nucleation and growth are out of the scope of this thesis due to the primary concern being the elimination and reduction of carbon dioxide evolution during cure. However, the importance of carbon dioxide bubble growth and nucleation to the blistering problem is unequivocal due to the properties of the final coating being dependant on the reactive components of materials and small variations of the composition can affect the gas expansion rate, in particular the nature and concentration of the surfactant.<sup>[23, 24]</sup> This is a disadvantage associated with the industry product, as the consistency of the polyol emulsion is in dispute due to the batch wise production process. Inconsistencies between batches can affect the final outcome of the crosslinking reaction and therefore the final coating properties. Determination of how changes in the concentration of surfactant, water and castor oil within the polyol emulsion effect carbon dioxide evolution is therefore of primary importance.

Investigations in Chapters 3 and 4 determined that the glycerol and PMDI reaction occurred at a slower rate than the castor oil- PMDI reaction at the industry ratio. Although castor oil and glycerol both have secondary hydroxyl groups, the secondary hydroxyl group in glycerol is sterically hindered whereas the hydroxyl groups in castor oil are present on long flexible fatty acid chains and are easily accessible for the reaction with isocyanate groups on the PMDI.

As well as the glycerol-PMDI reaction being a delayed reaction, the activation energy and reaction temperature determined by DSC analysis showed the glycerol-PMDI reaction slightly preceded the water-PMDI reaction. Thus, it was postulated that the addition of glycerol to the emulsion may delay the fast crosslinking process to allow for greater diffusion of carbon dioxide from the coating. Increasing the pot-life of the mixture is beneficial in aiding application of the polyurethane screed, which is another main reason for the addition of glycerol. Thus, the addition of more castor oil to reduce carbon dioxide evolution would not be suitable as the pot life would further be reduced. The aim of this chapter is to identify the effect of emulsion compositions on carbon dioxide production and identify suitable improvements to the polyol emulsion for application ease and coating strength. Characterisation of the emulsions was performed using rheological investigations and volumetric testing of carbon dioxide evolution.

## 5.2 Experimental

### 5.2.1 Materials

Materials used in this Chapter have been detailed in previous Chapters 3 and 4 and Appendix A. In addition, silicone oil, 350 cps and dioctyl phthalate were obtained from Sigma Aldrich. Nonyl-phenol ethoxylate was obtained from Huntsman Chemicals, while pine oil (PineChem 530) was obtained from Nuplex resins. All chemicals were used as received. Talc powder was obtained from Omya-Southern PTY. LTD and was used in volumetric testing of carbon dioxide evolution. The product ratio of castor oil to isocyanate  $NCO/OH=1.7$  was maintained in all cases.

#### 5.2.1.1 Emulsion preparation

A number of oil-in-water emulsion series were formed for the varying investigations using a ternary emulsion system of oil, nonionic surfactant and water.

The general procedure for the emulsions is outlined below:

The emulsions were prepared at standard conditions by incorporation of the aqueous phase into the oil phase. The aqueous phase contained the surfactant. Firstly, the surfactant was dissolved in a fraction of the tap water required for the emulsion at standard conditions at a surfactant concentration of 10.7% w/w named the pre-solution (shown to form more stable emulsions). The surfactant pre-solution was left to dissolve for a period of 5-10 minutes with some mechanical agitation using a stainless steel spatula.

The surfactant pre-solution was added to the oil phase during mechanical agitation with a 45° pitched-blade turbine of 50 mm diameter in a cylindrical glass beaker (110 mm diameter). The turbine was positioned just underneath the surface of the oil phase during the surfactant pre-solution addition. It was mixed for 1-2 minutes at 650 rpm before the addition of the remaining water. The emulsion was further mixed for 3 minutes at 650 rpm followed by 1 minute at 850 rpm giving a total mixing time of approximately 5-6 minutes.

Procedural changes from the above in the various emulsion series are outlined in their respective parts below.

### *Simple polyol emulsions*

The emulsions were formed according to the general procedure and the compositions presented in **Table 5-1**. The three variables, oil, water and non-ionic surfactant concentrations were investigated according to conditions A, B and C below, to determine systematically, differences in emulsion properties:

A: Change in surfactant (S) concentration from S1 to S6 by keeping the ratio of castor oil to water constant, equal to the product ratio of 1.88.

B: Change in water (W) concentration from W1 to W5 with the ratio of castor oil to surfactant constant, equal to the product ratio of 68.53.

C: Change in castor oil (CO) concentration from CO1 to CO5 with the ratio of surfactant to castor oil remaining constant, equal to the product ratio of 68.53 to ensure the surface tension was maintained. <sup>[12]</sup>

The product ratios of surfactant, water and castor oil are 0.94 %w/w, 34.3 %w/w and 64.7 %w/w respectively.

**Table 5-1 Emulsion composition for the change in variable concentrations %w/w**

<b>Emulsion</b>	<b>A:S1-S6</b>	<b>B:W1-W6</b>	<b>C:CO1-CO5</b>
	<b>%w/w</b>	<b>%w/w</b>	<b>%w/w</b>
1	0.27	23.2	59.4
2	0.66	28.7	62.2
3	<u>0.94</u>	31.6	<u>64.7</u>
4	1.32	<u>34.3</u>	67.3
5	1.96	37.6	69.2
6	2.60	41.3	

### *Complex polyol emulsions*

The control polyol emulsion is prepared in four stages:

Stage 1: The oil phase consists of the castor oil, dioctyl phthalate (DOP) and the pine oil. The castor oil is initially mixed with DOP for 2 min at 650 rpm, after which pine oil is added and mixed for a further 2 min at 650 rpm.

Stage 2: A 10.7% w/w surfactant in water pre-solution is added to the oil phase and for a further 3 min at 650 rpm.

Stage 3: Silicon oil is added to the emulsion and mixed for 1 min at 850 rpm

Stage 4: Addition of the remaining water and continued mixing for 2 min at 850 rpm  
 All emulsions were made using the above procedure except where one of the components was removed and the mixing step eliminated.

In condition B (below) the glycerol was added as the final step and mixed for a further 2 minutes at 850 rpm.

In condition C (below) the glycerol was added after the stage 3 and mixed for a further 2 minutes at 650 rpm before the addition of the remaining water.

Investigations were performed with the control polyol emulsion to determine the effect of concentration changes of the individual components on the emulsion properties which are detailed below:

A: Systematic change in the control emulsion composition as outlined in **Table 5-2**.

B: Addition of glycerol to the control emulsion as outlined in **Table 5-3**.

C: Substitution of castor oil with glycerol in the control emulsion as outlined in **Table 5-4** with all other components remaining constant.

**Table 5-2 Condition A: Composition of polyol emulsions**

Composition	Control	2	3	4	5	6	7
Castor oil	49.04%	50.81%	49.40%	61.66%	51.19%	62.22%	64.48%
Diocetyl Phthalate (DOP)	20.46%	21.20%	20.61%	0.00%	21.36%	0.00%	0.00%
Pine Oil (PO)	3.48%	0.00%	3.51%	4.38%	0.00%	4.42%	0.00%
Surfactant	0.72%	0.74%	0.72%	0.90%	0.75%	0.91%	0.94%
Silicone Oil (SO)	0.72%	0.74%	0.00%	0.90%	0.00%	0.00%	0.94%
Water	25.56%	26.50%	25.77%	32.16%	26.70%	32.46%	33.64%

Emulsions as formed from **Table 5-2** are outline below:

1. Control polyol emulsion (Simple + SO + PO + DOP)
2. Simple + SO + DOP
3. Simple + PO + DOP
4. Simple + SO + PO
5. Simple + DOP
6. Simple + PO
7. Simple + SO

**Table 5-3 Condition B: Series of polyol emulsions formed by adding glycerol to control polyol emulsion**

<b>Emulsion</b>	<b>Glycerol %w/w</b>
1	0%
2	1%
3	2%
4	4%
5	6%
6	10%

**Table 5-4 Condition C: Increasing glycerol composition in control emulsion by removing castor oil**

<b>Component</b>	<b>4%</b>	<b>8%</b>	<b>16%</b>	<b>25%</b>	<b>32%</b>	<b>40%</b>	<b>49%</b>
Castor Oil	45	41	33	24	16	9	0
Glycerol	4	8	16	25	33	40	49

## 5.2.2 Experimental techniques

### 5.2.2.1 Rheological characterisation

An AR-2000 controlled stress and direct strain control rheometer from TA Instruments, (US) was used with a 6 cm 2° cone and plate geometry. A continuous ramping flow mode was used to measure viscosity under controlled shear stress ranging from 0.01 to 100 Pa. An oscillation procedure at a constant frequency of 1 Hz was used to obtain information on the storage ( $G'$ ) and loss moduli ( $G''$ ).<sup>[16]</sup> Both flow and oscillatory data were collected at 25 °C. All rheological measurements were made on freshly prepared emulsions unless otherwise stated.

To study the isothermal curing reaction between the polyol emulsion and PMDI, a 2 cm 2°, cone and plate configuration was used to achieve a thin gap, allowing a large surface-to volume ratio. Dynamic measurements in oscillatory mode were performed using a frequency of 1 Hz and a strain of 10 % at 65 °C.

### ***5.2.2.2 Conductivity measurements***

Conductivity measurements were performed to establish the presence of an oil-in-water or water-in-oil emulsion structure and to determine variations in the emulsion structure. A WP-84 Conductivity meter was used for the measurements (TPS 122201, K1/ATC/Temp Sensor).

### ***5.2.2.3 Carbon Dioxide measurements***

Volumetric tests to determine differences in carbon dioxide evolution between emulsion compositions were performed according to procedures outlined in Chapter 2.

## 5.3 Results and Discussion

### 5.3.1 Changes in the emulsion structure

Factors which influence emulsion stabilisation and affect the emulsion properties are; the critical micelle ratio depending on the concentration of surfactant in the water phase, the temperature used to incorporate the two immiscible phases and changes in addition of the emulsion components as well as variations in shearing speeds, mixing times and different mixing methods.<sup>[25]</sup>

In the control emulsion, the surfactant is incorporated into the mixture via a pre-solution, using a fraction of the water used in the formulation. HIPEs (high internal phase emulsions) are formed in this way, giving an initial solid-like property of the emulsion with a large volume fraction of the dispersed phase. The fraction of water added at this stage was not always held constant by the industry and there was some confusion as to the use of hot water for the pre-solution of the surfactant. It was thus decided to determine the effect of changes in the surfactant/water ratio and temperature on the emulsion stability. Variations in this percentage were initially investigated through observing the stability of the emulsion over a week. A pre-solution concentration of 10.7% w/w surfactant to water was observed as having the greatest stability due to the length of time the emulsion visibly exhibited one continuous phase.

The volume fraction of the dispersed phase will differ with the pre-solution concentration (where the surfactant is dissolved in the aqueous phase). This in turn can affect the emulsion properties; however, it was not investigated further through rheological techniques as the final emulsion is disturbed by incorporation of the remaining water fraction in the formulation at high shear speeds, changing the volume fraction, particle size distribution and interfacial tension.<sup>[26]</sup> Viscosity versus shear stress profiles were performed for the following conditions as displayed in

**Figure 5.3:**

- No pre-solution of the surfactant in the water phase (all surfactant added to the castor oil)
- 2.75% w/w pre-solution of the surfactant dissolved in 100% w/w of water in the formulation.

- 10.7% w/w pre-solution of the surfactant dissolved in 25.7% w/w of the total water in the formulation.
- 10.7% w/w pre-solution of the surfactant dissolved in 25.7% w/w of the total water in the formulation at 45 °C.
- 10.7% w/w pre-solution of the surfactant dissolved in 25.7% w/w of the total water in the formulation at 45 °C, added at room temperature to the castor oil.

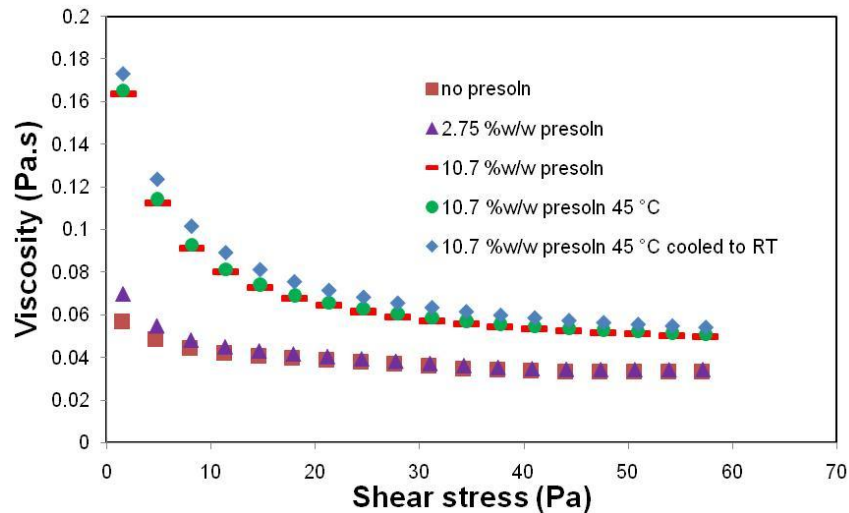


**Figure 5.3 Differences in viscosity behaviour through changes in the emulsion structure**

It is noticed from **Figure 5.3** that increasing the pre-solution concentration of the surfactant measured in % w/w of surfactant in water, gives a higher viscosity than the no pre-solution concentration and 2.75% w/w pre-solution. The viscosity profiles for all emulsions exhibit non-Newtonian shear thinning behaviour. Furthermore, the non-Newtonian behaviour of the emulsions is accentuated at higher surfactant concentrations of the pre-solution. It is also noticed that increasing the temperature of the pre-solution does not have an effect on the viscosity profiles.

Dissolving the surfactant at a higher water temperature and incorporating it at that higher temperature or at room temperature did not show a significant change in the viscosity profiles. Increasing the temperature of hydration for non-ionic poly-oxyethylene surfactants will reduce the hydration ability of the poly-oxyethylene chain increasing its solubility in the oil fraction.<sup>[14, 22]</sup> Thus, greater incorporation of the oil phase may be noticed, causing the emulsion to behave more like a water-in-oil emulsion. This was noticed in the conductivity measurements shown in **Figure 5.4**. The increase in temperature lowered the conductivity of the emulsion, suggesting a

greater incorporation of the oil phase. Furthermore, when the pre-solution was allowed to cool back to room temperature, an increase in the conductivity of the emulsion was noticed, although, it was still lower than when the surfactant was dissolved at room temperature.

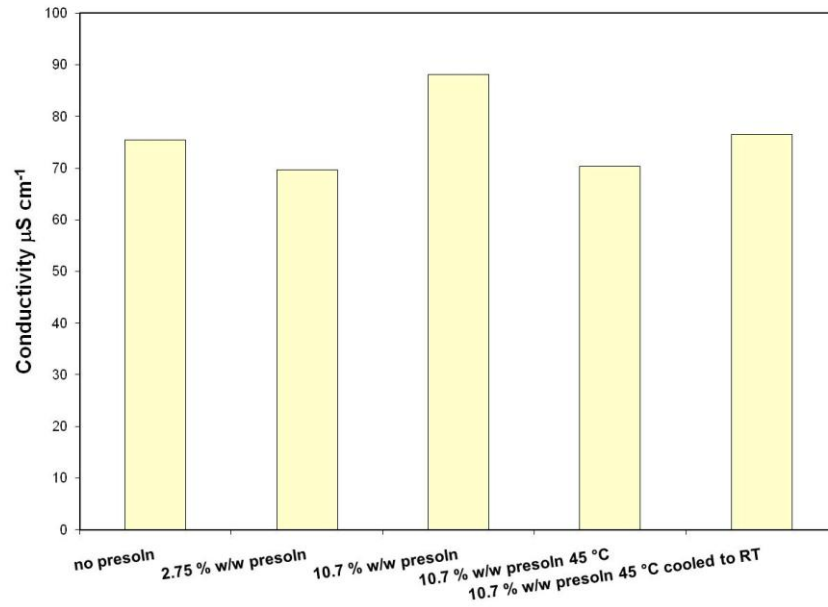


**Figure 5.4** Conductivity measurements for changes in emulsification procedures

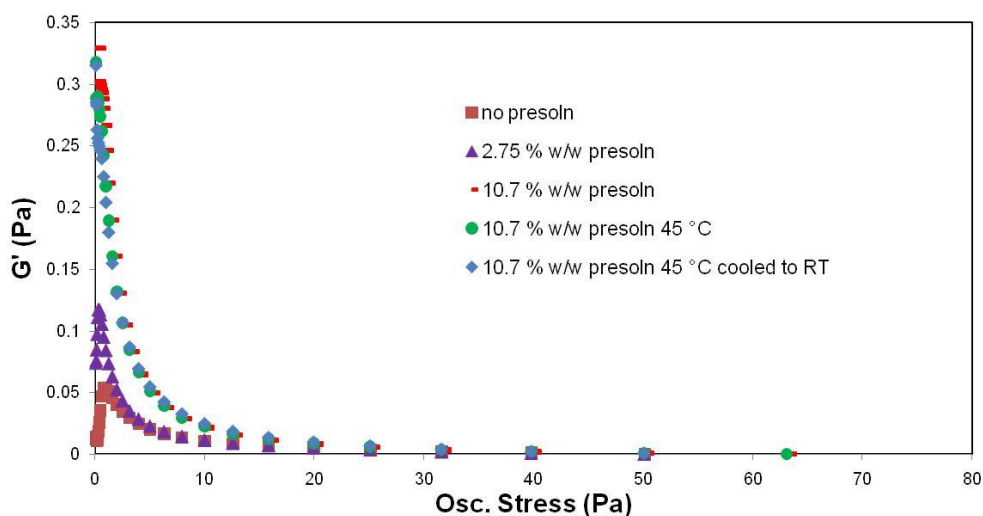


**Figure 5.5** Storage modulus behaviour of variations in the emulsification procedure

Emulsion stability was analysed through changes in the storage modulus of the emulsions under oscillatory stress as shown in **Figure 5.5**. Greater stability was observed with an increase in the pre-solution concentration to 10.7% w/w surfactant, exhibiting a higher storage modulus. Increasing the temperature of the pre-solution to 45 °C had little effect on the storage and loss moduli.

### 5.3.1.1 Effect on carbon dioxide production

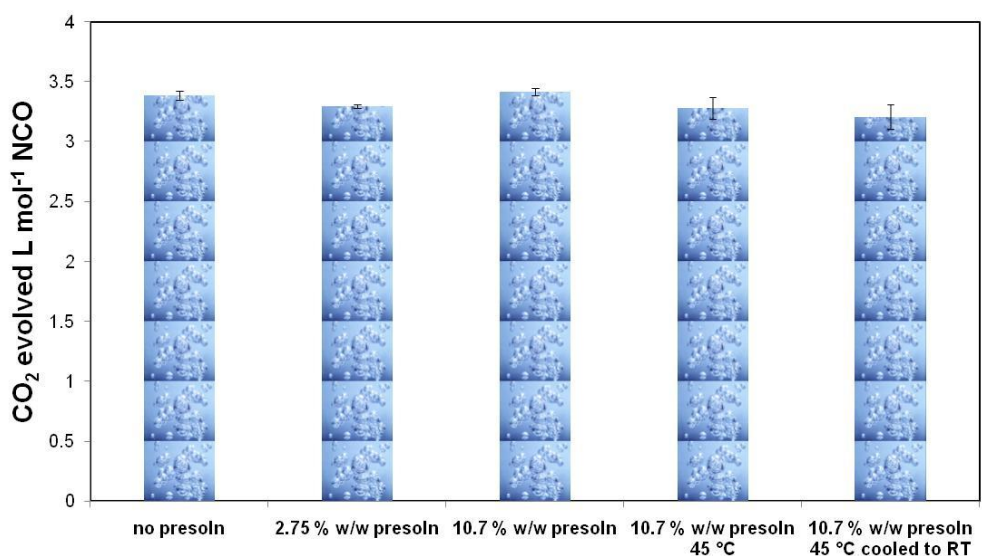


**Figure 5.6** Effect of emulsion structure on carbon dioxide levels

**Figure 5.6** shows the levels of carbon dioxide evolved for the different conditions chosen. No significant change in carbon dioxide values is noticed. Thus, although the structure of the emulsion is obviously compromised by varying the pre-solution concentration of the surfactant as shown through rheological analysis, there is no effect on the levels of carbon dioxide. It is also evident that increases in the pre-solution temperature, allowing for a greater incorporation of the oil-phase, do not have any significant effect on carbon dioxide levels.

Therefore, a surfactant pre solution concentration of 10.7% w/w was chosen for all following emulsion preparations.

### **5.3.2 Variations to the simple emulsion**

The series of experiments performed in this section evaluate how small changes to the emulsion composition affect emulsion stability and the curing reaction between the polyol emulsion and PMDI. Emulsions were formed in series according to **Table 5-1**, by varying either the concentration of surfactant, water or castor oil.

The ratio of surfactant to oil has a bearing on the surface tension of the emulsion, changing this surface tension may affect the emulsion properties, either through destabilising the emulsion or changing the interaction between the oil and water phase. Disturbing the emulsion properties may subsequently have implications on the reaction with PMDI leading to changes in carbon dioxide production in the coating system. Variations in the total amount of water and castor oil either side of the industry ratios could also influence the emulsion properties and thus the reaction of water with isocyanate and the ability to form greater crosslinks through the hydroxyl and isocyanate reaction.

Understanding how small changes of the emulsion composition affect emulsion structure, can provide the industry with information in quality assurance and control, while knowledge of their affect on the carbon dioxide evolution is detrimental in the development of solutions to eliminate blistering upon cure. Rheological investigations and volumetric tests for carbon dioxide evolution were performed to determine how slight variations in the polyol emulsions effect their subsequent reaction with PMDI.

### **5.3.2.1 Emulsion stability**

Viscosity measurements are shown in **Figure 5.7 A, B** and **C** for increasing concentration of surfactant, water and castor oil, respectively.

In general, it is noticed that the polyol emulsions follow shear thinning behaviour, displaying a reduction in viscosity with increasing shear stress. When the shear stress approaches 20- 30 Pa, the emulsion structure is destroyed, therefore, the viscosity decreases to that of the continuous phase of water. **Figure 5.7 A** displays the change in viscosity with surfactant concentration. At 0.66% w/w surfactant, the viscosity is higher, displaying a more Newtonian profile. At such a low surfactant concentration, it is believed that coalescence of the oil droplets occurs within the emulsion, increasing the viscosity. Coalescence of the oil droplets would also explain the more Newtonian profile observed, due to the non-existent emulsion structure, displaying the properties of the continuous phase of water.

It is also visible that the viscosity decreases past a surfactant concentration of 1.32% w/w. The critical concentration of surfactant in the emulsion would thus lie between the product concentration of surfactant and 1.32% w/w surfactant; however this has not been tested. At higher surfactant concentrations, the emulsion structure is destroyed, leading to more Newtonian profiles and lower viscosities.

Increasing the concentration of water in the emulsion showed a reduction in the viscosity at low shear stress (**Figure 5.7 B**), with the behaviour changing from shear thinning to Newtonian flow, which was expected. The effect of increasing castor oil concentration on the viscosity of the emulsions is displayed in **Figure 5.7 C**. As the concentration of castor oil in the emulsion is increased, the viscosity increases in magnitude, as well as exhibiting more of a shear thinning viscosity profile which was also expected due to the higher oil to water ratio.

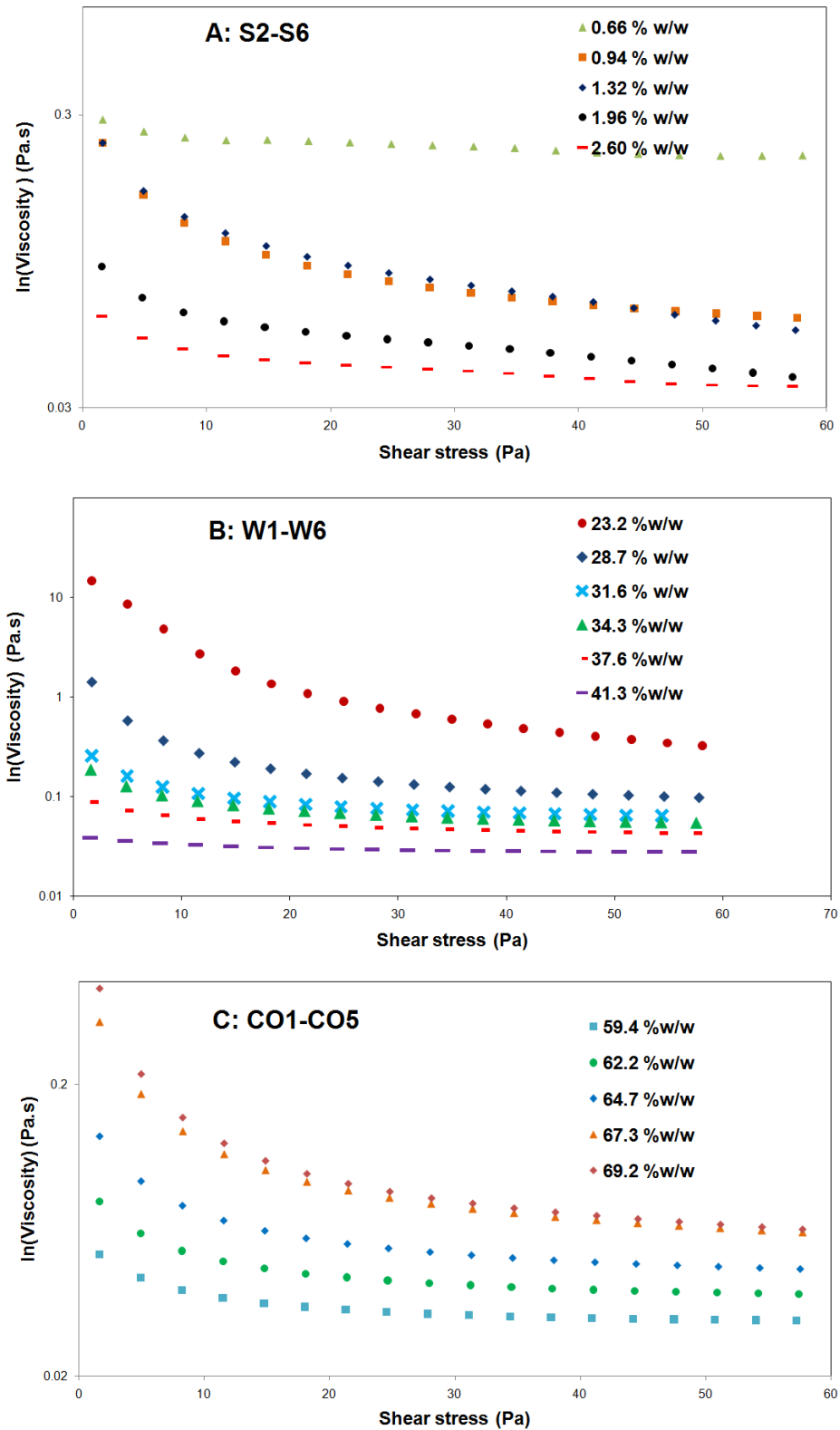


Figure 5.7 Viscosity profiles for emulsion series with increasing levels of A: surfactant, B: water and C: castor oil concentrations.

Oscillatory measurements were carried out to determine the level of emulsion stability. Emulsion stability was measured through changes in the storage modulus ( $G'$ ) as a function of oscillatory stress, which are presented in **Figure 5.8 A, B, C** for emulsion compositions A, B and C respectively (**Table 5-1**). In general observation, the storage modulus,  $G'$  decreases with oscillatory stress. More specifically, **Figure 5.8 A** confirms that 1.32% w/w surfactant is the critical surfactant concentration displaying the greatest stability. The order of increasing stability for the surfactant series, is 1.32% w/w > 0.94% w/w > 0.66% w/w > 1.96 % w/w > 2.6 % w/w.

**Figure 5.8 B** displays that an increase in the water fraction causes a reduction in the storage modulus of the emulsions, suggesting greater stability is achieved at lower water fractions. Increases in castor oil concentration results in an increase of the storage modulus and thus the stability of the emulsions, as displayed in **Figure 5.8 C**.

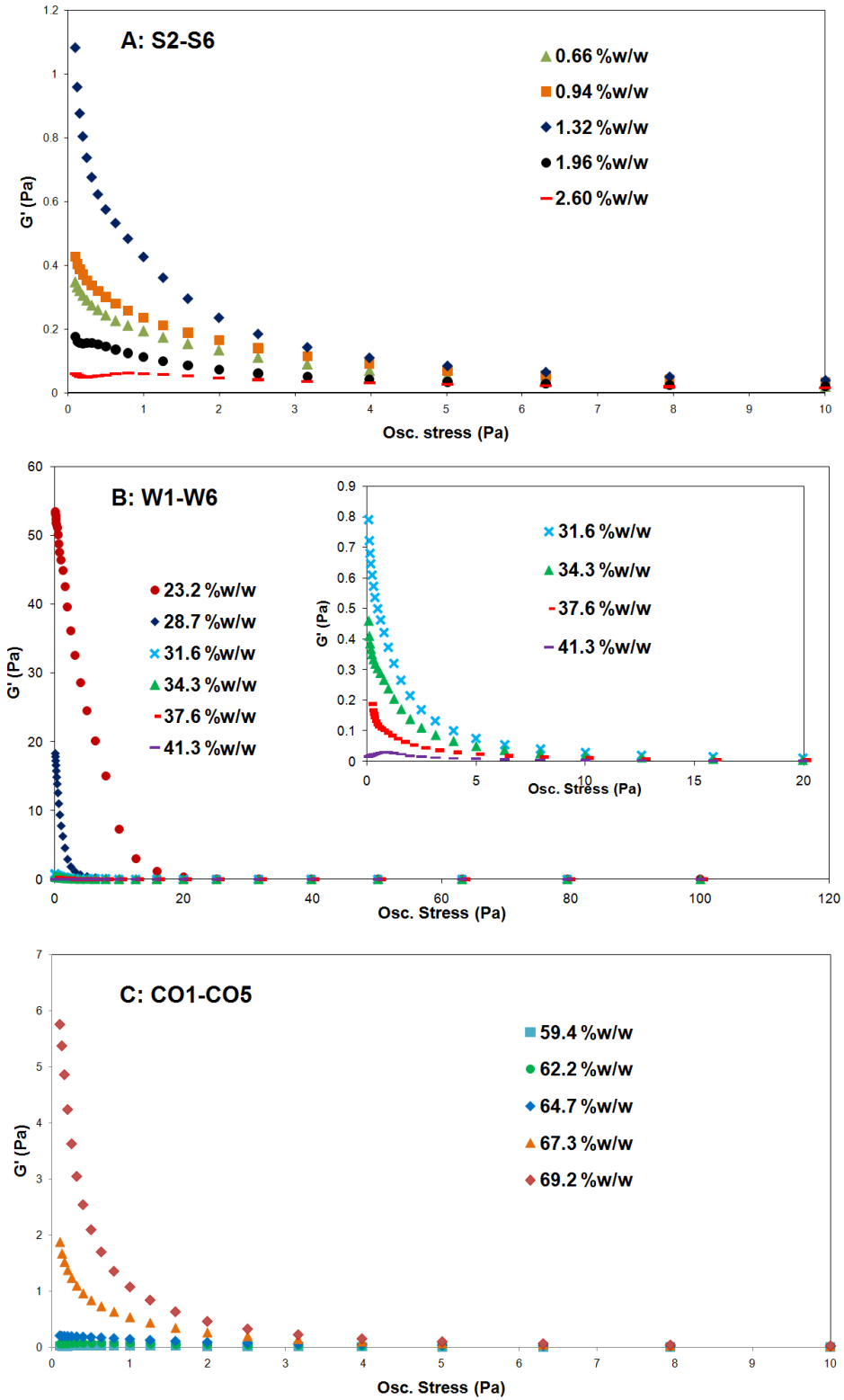


Figure 5.8 Storage modulus profiles for emulsion series with increasing levels of A: surfactant, B: water and C: castor oil concentrations.

**Table 5-5 Conductivity measurements for emulsion series with increasing levels of surfactant, water and castor oil concentrations**

Emulsion	Conductivity ( $\mu\text{S cm}^{-1}$ )		
	S1-S6	W1-W6	CO1-CO5
water	328	328	2314
1	-	47	490
2	115	91	516
3	111	98	549
4	113	111	473
5	103	126	465
6	106	136	

Conductivity measurements (**Table 5-6**) were performed for all emulsions to determine changes in the emulsion structure from the variation in surfactant, water and castor oil concentration.<sup>[27]</sup> An increase in surfactant concentration of the emulsions (S2-S6) resulted in no significant trend, although, a slight decline in conductivity was noticed at the highest concentrations of surfactant used. At higher concentrations of surfactant, a greater percentage of oil is dispersed in the aqueous fraction, due to a narrower drop size distribution, thus, lowering the conductivity of the emulsion.<sup>[25]</sup>

Increasing the water fraction in the emulsion series (W1-W6) showed an increase in conductivity due to the higher volume fraction of the water. Conductivity measurements displayed a decrease in conductivity with increasing castor oil concentration (CO1-CO5) with the exception of the industry ratio which was expected.

### ***5.3.2.2 The effect of varying emulsion composition on carbon dioxide evolution and the crosslinking reaction during the reaction with PMDI***

Carbon dioxide evolution was analysed volumetrically for the reaction between the polyol emulsions and PMDI. The ratio of castor oil to PMDI (NCO/OH=1.7) that is used by the industry was kept constant for each of the surfactant and water emulsion

series tests, while the ratio of water to PMDI was held constant for the castor oil emulsion series. **Figure 5.9** displays the amount of carbon dioxide evolved in litres per mole of isocyanate, with an increase in surfactant, water and castor oil concentration. No significant change in carbon dioxide evolution was observed with an increase in surfactant, water or castor oil concentration giving an average volume of carbon dioxide evolved equal to  $2.76 \pm 0.06 \text{ L mol}^{-1} \text{ NCO}$ .

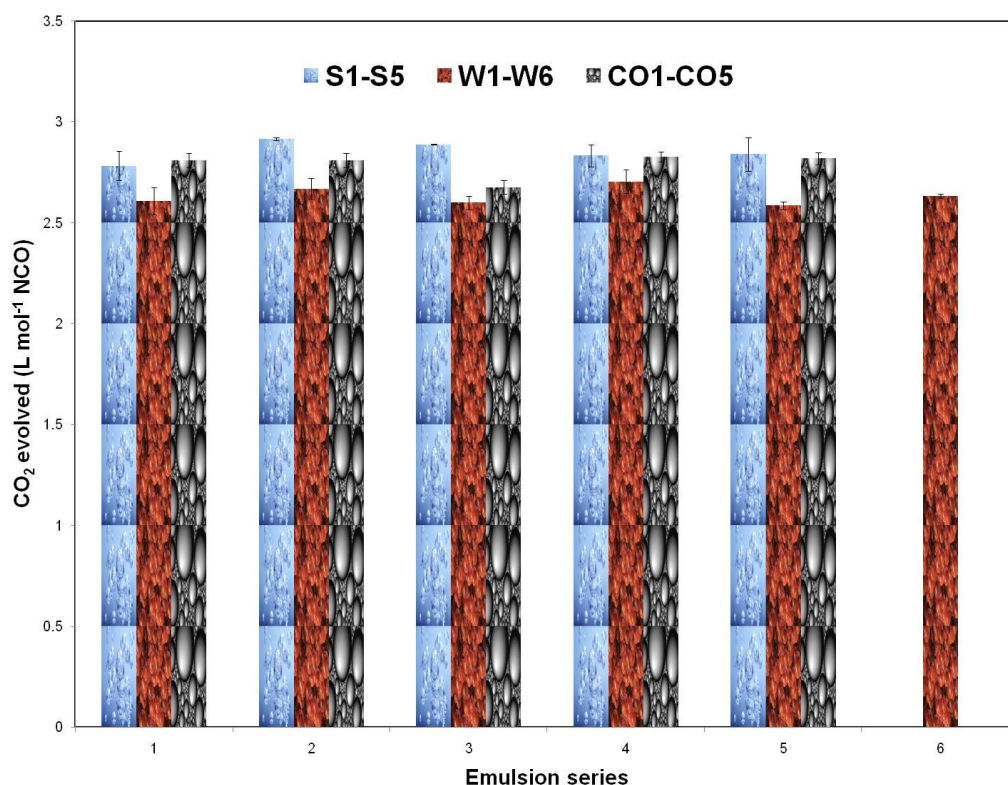


**Figure 5.9 Carbon dioxide evolution for increasing concentrations of surfactant, water and castor oil concentrations in the simple emulsion**

Rheological measurements were also performed to determine the gel time and curing profile, to further elucidate the effect of surfactant, water and castor oil concentration on the reaction. The gel time of the reaction system, determines the pot-life of the coating mixture, thus allowing for better control during coating application. Gel times were measured through the crossover of the storage ( $G'$ ) and loss ( $G''$ ) modulus [28] for the reaction between the polyol emulsion and PMDI, while keeping the industrial product mole ratio of  $\text{NCO}/\text{OH}=1.7$  for the surfactant and water series. The ratio of PMDI to water was kept constant (industry ratio) in the castor oil emulsion series. Gel times obtained for the various emulsion series are given in **Table 5-6**. At

the surfactant ratio of S3=0.94% w/w used by the industry, the gel time was approximately 16 minutes. Lowering the concentration of surfactant further reduced the gel times, while slightly increasing the concentration, greatly increased gel times above 40 minutes. Thus, higher surfactant concentrations provided an increased pot-life, although, the emulsion stability was compromised at these surfactant concentrations (as determined earlier).

The maximum gel time of 40.5 minutes was achieved at the water fraction of W2=28.7% w/w. This was also the point at which the emulsion started behaving more solid-like at very low shear stresses. A gel time of 16 min was obtained for the industry ratio (W4=34.3% w/w), with further increases in the water fraction reducing gel times. Thus, a lower water concentration than the industry ratio improved the pot-life of the mixture.

The castor oil emulsion series displayed the highest gel point at the industry ratio of castor oil (CO3=64.7 % w/w); however, a very large standard error was apparent, suggesting that slight changes in the mass of the reacting components can affect the gel point of the industry ratio. It seems that the critical ratio of components is at the current industry ratio and slight changes in composition around this ratio are detrimental to the pot-life of the mixture.

**Table 5-6 Rheological gel times achieved for increasing surfactant, water and castor oil concentrations**

<b>Emulsion</b>	<b>S1-S6</b>	<b>W1-W6</b>	<b>CO1-CO5</b>
	<b>Gel time</b>	<b>Gel time</b>	<b>Gel time</b>
	<b>(min)</b>	<b>(min)</b>	<b>(min)</b>
1	-	27.3 ± 0.4	12.3 ± 0.1
2	13.4 ± 0.4	40.5 ± 1.8	30.7 ± 1.0
3	16.4 ± 0.3	23.6 ± 1.2	28.4 ± 7.6*
4	43.5 ± 0.5	16.4 ± 0.2	14.0 ± 1.9**
5	44.2 ± 4.0	14.8 ± 0.1	18.5 ± 0.7
6	33.6 ± 0.4	12.6 ± 0.4	

\*%RE<30 \*\*%RE<15

**Table 5-7 Storage modulus obtained at the gel times for increasing surfactant, water and castor oil concentrations**

Emulsion	S1-S6 G' (Pa)	W1-W6 G' (Pa)	CO1-CO5 G' (Pa)
1		$3.0 \times 10^4 \pm 3.8 \times 10^3$ *	$87 \pm 25$ **
2	$142 \pm 32$ *	$274 \pm 42$ *	$4.4 \times 10^4 \pm 1.2 \times 10^4$ **
3	$152 \pm 24$ *	$219 \pm 74$ **	$7.4 \times 10^4 \pm 5.2 \times 10^4$ ♣
4	$419 \pm 128$ **	$152 \pm 24$ *	$261 \pm 3$
5	$396 \pm 65$ *	$91 \pm 24$ **	$457 \pm 13$
6	$533 \pm 90$ *	$71 \pm 14$ *	

\*%RE<20 \*\*%RE<35 ♣%RE>50

**Table 5-7** displays the storage modulus ( $G'$ ) at the gel time (**Table 5-6**) for the varying emulsion series. It is noticed that an increase in the surfactant concentration increased the magnitude in  $G'$ , suggesting that crosslinking is more extensive. The reaction rate is influenced by the particle size distribution of the oil, where lower surfactant concentrations are known to form bigger droplets and broader droplet size distributions, which may inhibit the extent of crosslinking due to the non-homogeneity of the expanding gas bubbles. [29] At higher surfactant concentrations where smaller droplets are formed and narrower drop size distributions exist [25], a greater incorporation of the oil phase was verified by the lower conductivities achieved. Differences in emulsion uniformity and particle size distribution due to variations in surfactant concentration will affect the rate of expansion of carbon dioxide gas formed by the reaction of PMDI and water. [30] Subsequently, the crosslinking reaction is affected. At higher surfactant concentrations the reaction between PMDI and water yields a highly expanded foam with small and homogeneously distributed cells. [24] A more uniform polymerization is thus achieved at higher surfactant concentrations, allowing the reaction to occur over a longer period of time, achieving higher magnitudes in the storage modulus.

Increasing the water concentration of the emulsion, while keeping the castor oil /PMDI ratio constant, decreased the storage modulus at the gel point, with the lowest concentration of water providing an extremely high modulus in comparison. Thus, the crosslinking reaction decreases with increasing water fraction. This can also be explained by the increasing volume fraction of surfactant in these emulsions as the

water fraction was reduced, because the ratio of castor oil to surfactant was kept constant to minimise changes in the surface tension.<sup>[12]</sup>

Increasing the castor oil concentration in the emulsion while keeping the surfactant to castor oil ratio constant and the water to isocyanate ratio constant in the reaction with PMDI, initially increased the storage modulus at the gel point up to a castor oil concentration of CO3=64.7% (equivalent to the industry ratio). This suggests that the industry ratio is the critical ratio in this emulsion series achieving the greatest crosslinking. This is not the case for the surfactant or water series of emulsions tested; however, it is interesting to note that slight changes in the concentrations around the industry ratio (S3, CO3 and to a lesser extent W4) show quite large changes in the gel time. Thus, the industry ratio of water to castor oil to surfactant is critical, with small changes either side of this ratio affecting the pot-life and extent of crosslinking of the mixture, even though no significant effect is observed on carbon dioxide evolution. It is also interesting to note that conductivities of the emulsion series, in particular the water series and castor oil series, correlate extremely well to the storage modulus values obtained at the gel point. The results suggest that a greater incorporation of the oil phase in the emulsions (lower conductivities) increases the extent of crosslinking and the pot-life of the mixture. This was achieved for higher surfactant concentrations, lower water concentrations and slightly lower castor oil concentrations than that currently used by the industry.

### **5.3.3 Effect of various emulsion components on the stability of the control emulsion and its subsequent effect on carbon dioxide evolution**

Analysis of the effect of each non-curing component in the control polyol emulsion on stability of the emulsion and the effect on carbon dioxide production when reacted with PMDI was performed. The emulsions were tested systematically, starting with the simple emulsion containing only castor oil, non-ionic surfactant and water and adding one component at a time until the control polyol emulsion was formed. The composition of the control polyol emulsion developed by the company is displayed as emulsion 1 in **Table 5-2**, which also displays the series of emulsions developed to investigate the effect of non-curing components on emulsion stability. The emulsions were placed under a range of stress at which the viscosity profiles, storage and loss

moduli were obtained. The viscosity profiles and the storage modulus are displayed in **Figure 5.10 A and B** respectively.

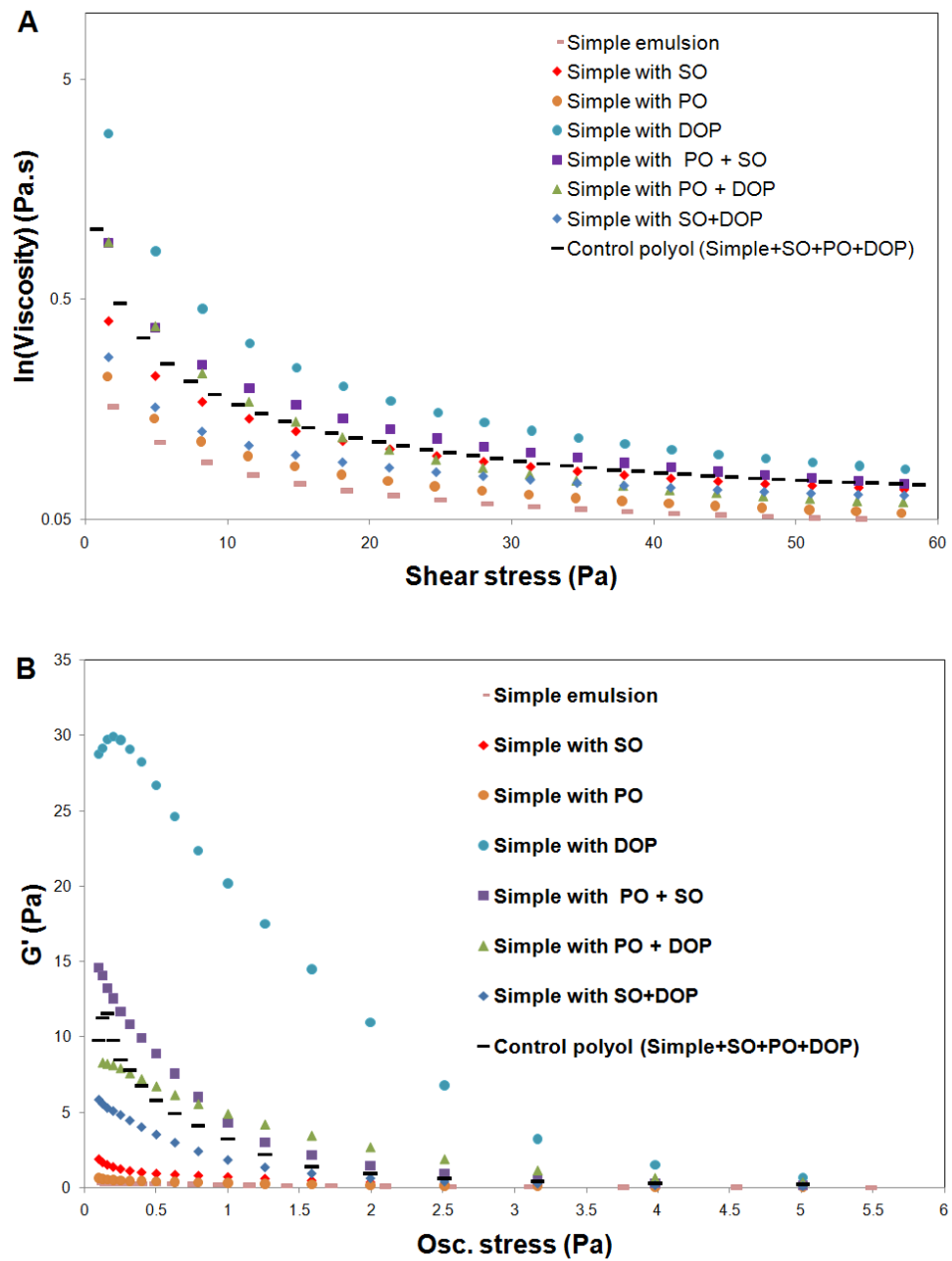


**Figure 5.10 A) Viscosity profiles and B) Storage modulus profiles for variations in the emulsion composition**

The simple emulsion exhibits the lowest viscosity, with a more Newtonian viscosity profile than all other emulsions. It is interesting to note that the addition of dioctyl phthalate (DOP) to the simple emulsion increases the viscosity dramatically and

makes the emulsion behave as a shear thinning liquid rather than a Newtonian profile exhibited by the simple emulsion. The addition of silicone oil (SO) and pine oil (PO) to the simple emulsion does not have a dramatic effect in increasing the viscosity of the simple emulsion, however, the addition of PO and SO independently to the simple emulsion with DOP, dramatically reduces the viscosity, which is more evident for the SO. The addition of SO and DOP independently to the simple emulsion with PO increases the viscosity to the same level. The addition of SO, DOP and PO to the simple emulsion, forms the control polyol emulsion and it is evident the viscosity does not vary greatly from the simple emulsion + PO +SO or the simple emulsion + PO + DOP.

The simple emulsion with DOP also exhibited the largest storage modulus at low shear stress, suggesting greater emulsion stability than all other combinations. DOP is a plasticizer and may improve emulsion stability by reducing oil drop size and polydispersity, as has been observed for other plasticizers used in oil-in-water emulsions.<sup>[31]</sup>

Even though the simple emulsion with PO + DOP shows an initially lower storage modulus than both the simple emulsion with PO + SO and the control polyol emulsion, it has a larger storage modulus over a greater shear stress range indicating its stability is greater with increases in shear stress.

The magnitude of the loss modulus profiles, indicating the viscous behaviour of the emulsions, exhibited a similar order as that obtained for the storage modulus. The storage modulus is greater than the loss modulus at very low shear stress, indicating that the emulsions have a more solid-like property in this stress range with the exception of the simple emulsion with PO.

#### ***5.3.3.1 Effect of the non-curing components on carbon dioxide evolution***

All tests were performed with a constant mole ratio of NCO/OH =1.7 as evident in the industry product. The carbon dioxide evolution in litres per mole of isocyanate present in the reacting mixture is depicted in **Figure 5.11**.

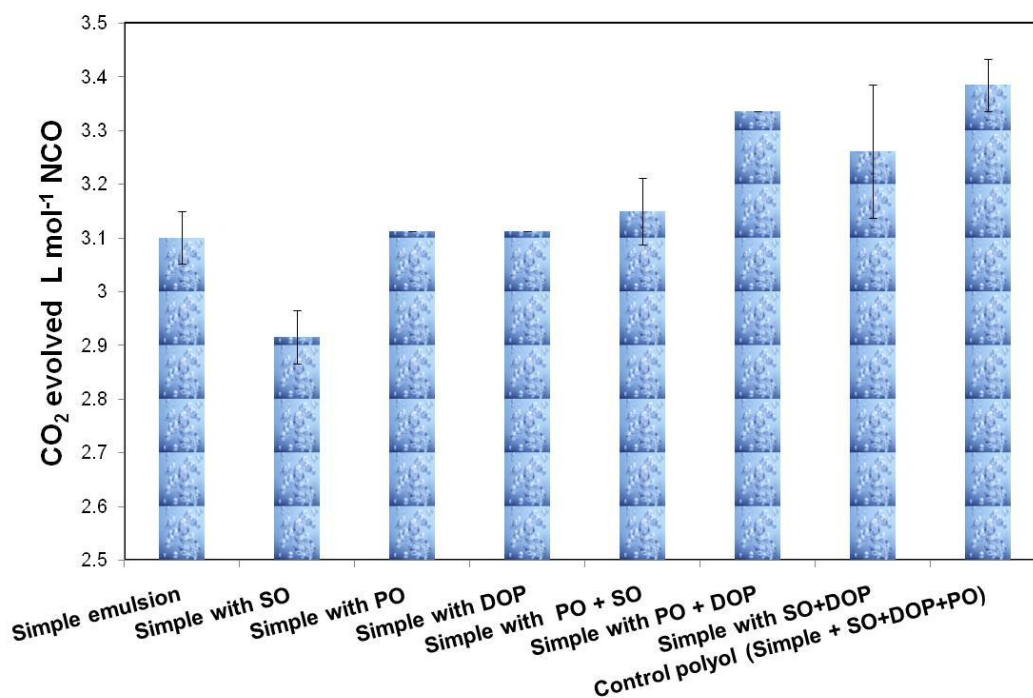


**Figure 5.11** Levels of carbon dioxide evolution while varying the polyol emulsion to determine the effect of formulation components.

It can be seen from **Figure 5.11** that a significant difference exists in the volume of carbon dioxide measured between the simple emulsion and the control emulsion.

It is also interesting to note that SO reduces the carbon dioxide production when added to the simple emulsion, however no significant improvement to the levels are observed when SO is added to emulsions containing PO or DOP. The co-addition of PO with DOP significantly increases the level of carbon dioxide evolved to levels of the control emulsion. These emulsions also exhibit the lowest conductivity values (**Table 5-8**). As mentioned earlier, lower conductivity suggests a greater volume fraction of the dispersed oil phase. Previously, this affected the crosslinking reaction with greater crosslinking achieved at lower conductivities without any affect on carbon dioxide evolution. In this case, there is a distinct affect on carbon dioxide evolution, therefore the emulsion structure has changed to allow for a greater interaction of PMDI and water producing more carbon dioxide or the presence of PO with DOP aids the release of carbon dioxide gas more readily from the reacting mixture.

**Table 5-8 Conductivity measurements for changes in the control polyol emulsion**

<b>Emulsion</b>	<b>Conductivity <math>\mu\text{S cm}^{-1}</math></b>
Simple	92
Simple + SO	78
Simple + PO	72
Simple + DOP	55
Simple + PO+SO	66
Simple + PO + DOP	27
Simple + SO + DOP	30
Control Emulsion (Simple+SO+PO+DOP)	28

#### **5.3.4 Addition of a second polyol**

Lowering the viscosity of the polyol emulsion was considered as a solution to improve the application properties of the industry product during trowelling. Increasing the pot-life of the emulsion was a necessity in order to aid application times. Glycerol was found to react slower than castor oil with the isocyanate (Chapter 4) due to its smaller structure and steric hindrance of the secondary hydroxyl group which allows for the increase in the pot-life of the coating. The addition of glycerol to the polyol emulsion was thus considered for viscosity modification and tests were performed to investigate this. Two methods were employed for the addition of glycerol to the polyol emulsion. Firstly, minimisation of procedural changes during the formation of the polyol emulsions for easy implementation by the industry was investigated. In this procedure, the polyol emulsion is formed in the same manner, with a fraction of glycerol added at the end of the procedure. In the second investigation, the castor oil is progressively replaced with glycerol fractions. Systematic tests were performed by increasing the glycerol concentration in the polyol emulsion using both of the described methods. The effect on viscosity reduction and emulsion stability were determined as well as the effect on carbon dioxide evolution when reacted with PMDI.

### 5.3.4.1 Straight addition of glycerol to emulsion

#### 5.3.4.1.1 Flow properties

The effect of added glycerol at various concentrations on the flow properties of the control sample was investigated through rheological techniques. It is evident from **Figure 5.12** that the control polyol emulsion showed a reduction in viscosity at 4% w/w glycerol addition, after which further increases in the glycerol concentration greatly reduced the viscosity. The same effect was noticed for both the storage and loss moduli. It was also noticed that the viscosity behaviour under shear stress behaved as a shear thinning fluid, with the profile becoming more Newtonian at 6% and 10% w/w glycerol addition.

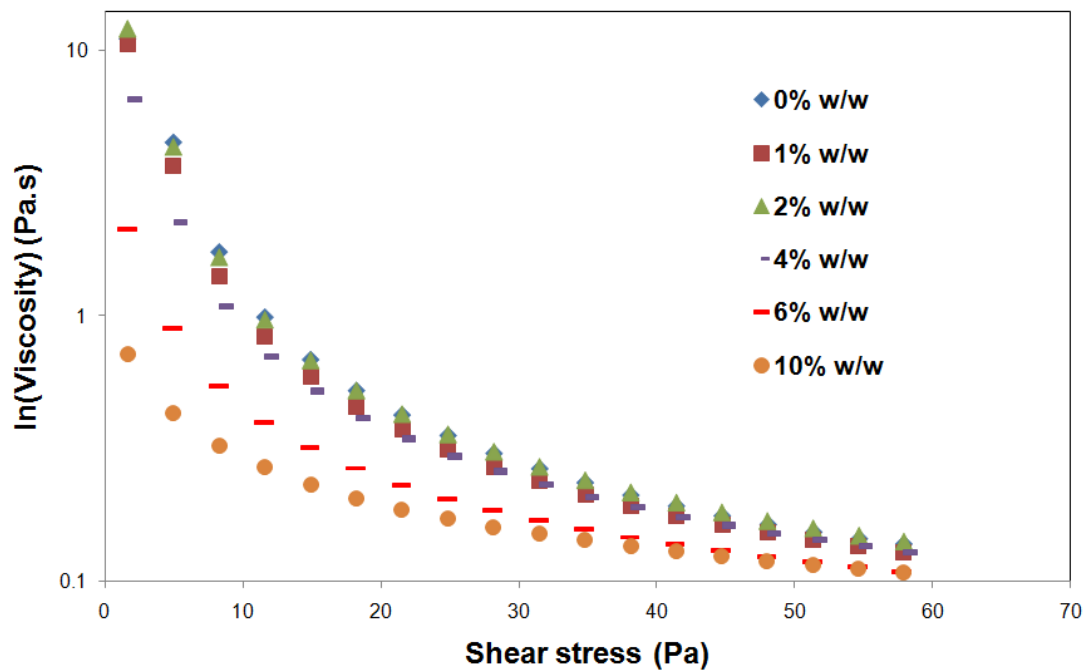
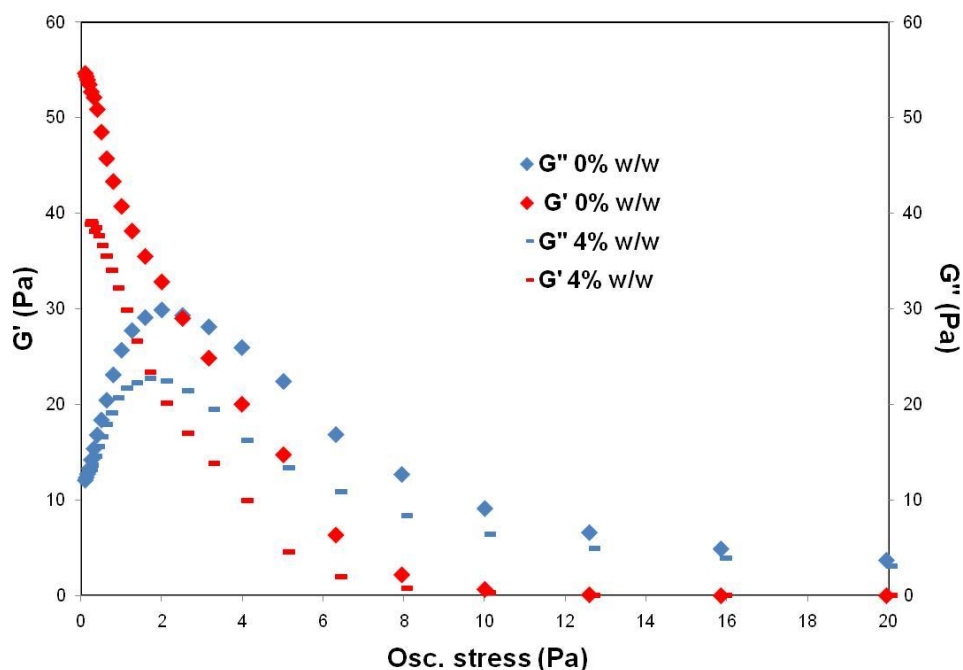


Figure 5.12 Viscosity profiles for increases in glycerol concentration



**Figure 5.13 Storage modulus and loss modulus changes with 4% w/w glycerol addition**

At 4% w/w glycerol addition, there was some compromise in the stability of the emulsion, indicated by a lower magnitude in the storage modulus ( $G'$ ) than the control emulsion (**Figure 5.13**).<sup>[16]</sup> However, the emulsion retained its solid-like behaviour at low stress values, as the storage modulus was still much higher than the loss modulus. At 6% w/w glycerol addition, the stability was further compromised with the magnitude of storage modulus becoming closer to that of the loss modulus, while at 10% w/w glycerol addition the viscous behaviour ( $G''$ ) was greater, thus forming an unstable emulsion.

#### 5.3.4.1.2 Carbon dioxide tests

The series of emulsions with increasing glycerol concentration were used to determine the effect on carbon dioxide evolution when reacted with PMDI. The mole ratio of NCO/OH=1.7 was kept constant with the moles of hydroxyl calculated from the castor oil only. In previous kinetic investigations (Chapter 3 and Chapter 4), it was found that the glycerol and PMDI reaction had a slightly higher activation energy than the castor oil and PMDI reaction and a lower activation energy than the water and isocyanate reaction. Thus, it was hypothesised that with the addition of

glycerol, the water and isocyanate reaction would be delayed with greater crosslinking achieved through reactions between the excess isocyanate groups and the hydroxyl groups on the glycerol.

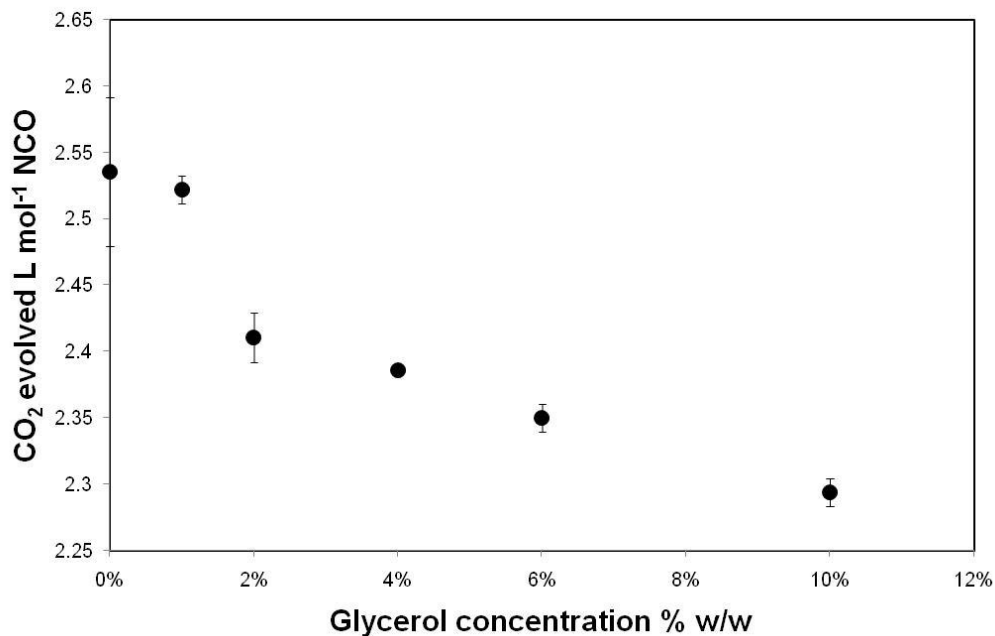


**Figure 5.14 Carbon dioxide evolution for increasing glycerol concentration**

The levels of carbon dioxide obtained for the series of glycerol emulsions are displayed in **Figure 5.14**. Increasing the glycerol concentration reduced carbon dioxide evolution as expected. The levels of carbon dioxide declined rapidly on the addition of 2% w/w glycerol, although no viscosity improvement was achieved at this concentration. 4% w/w glycerol addition is thus a good balance between viscosity modification and reduction of carbon dioxide levels.

The isocyanate to the total hydroxyl ratio (which includes both castor oil and glycerol hydroxyls) with increasing glycerol concentration in % w/w is given in **Table 5-9**. At 4% w/w glycerol addition, there is still an excess of isocyanate groups and a reduction in carbon dioxide evolution of 5.2% was achieved after 24 hours of curing.

**Table 5-9 Isocyanate to total hydroxyl mole ratio in mixture and reduction in carbon dioxide with increasing glycerol concentration**

<b>Glycerol % w/w</b>	<b>NCO/OH addition</b>	<b>%reduction in CO<sub>2</sub></b>
0	1.7	0
1	1.6	0.4
2	1.5	4.4
4	1.3	5.2
6	1.2	6.3
10	1.0	7.8

It is observed in **Table 5-9** that although a stoichiometric ratio of isocyanate to hydroxyl groups is present at 10% w/w glycerol addition, there is only a reduction in carbon dioxide evolution of 7.8%. Thus, there is still preference for the reaction between isocyanate and water, producing carbon dioxide.

In summary, no correlation exists between viscosity reduction or emulsion stability and carbon dioxide evolution. There is a correlation with increasing glycerol content and % carbon dioxide reduction. Reducing the ratio of NCO/OH from 1.7 to 1.5 using only castor oil hydroxyls (**section 5.3.2.2** CO3 *cf.* CO4) did not show any change in carbon dioxide levels, whereas the same increase in hydroxyl groups due to glycerol achieved a reduction of 4.4% carbon dioxide. Thus, it is likely that glycerol aids in reducing carbon dioxide levels not only through the crosslinking reaction, but through changes in the emulsion structure. It is also evident that there is a preference for the reaction between water and isocyanate groups even at the stoichiometric ratio of hydroxyl to isocyanate groups.

#### ***5.3.4.2 Fractionating the control emulsion with glycerol by removing castor oil***

Investigations were performed to determine the level of glycerol that could effectively replace castor oil in the emulsion; improving viscosity and reducing or maintaining levels of carbon dioxide evolution, without compromising emulsion stability.

### 5.3.4.2.1 Flow properties

Viscosity versus shear stress profiles are displayed in **Figure 5.15**. The replacement of castor oil with glycerol from 4% to 49% w/w (all castor oil replaced), greatly affected the viscosity profiles. Even small changes (4% w/w) in the glycerol fraction reduced the viscosity from 10 to 1 Pa.s. A shear thinning profile was still observed up to 25% w/w glycerol, after which the viscosity profiles became more Newtonian.

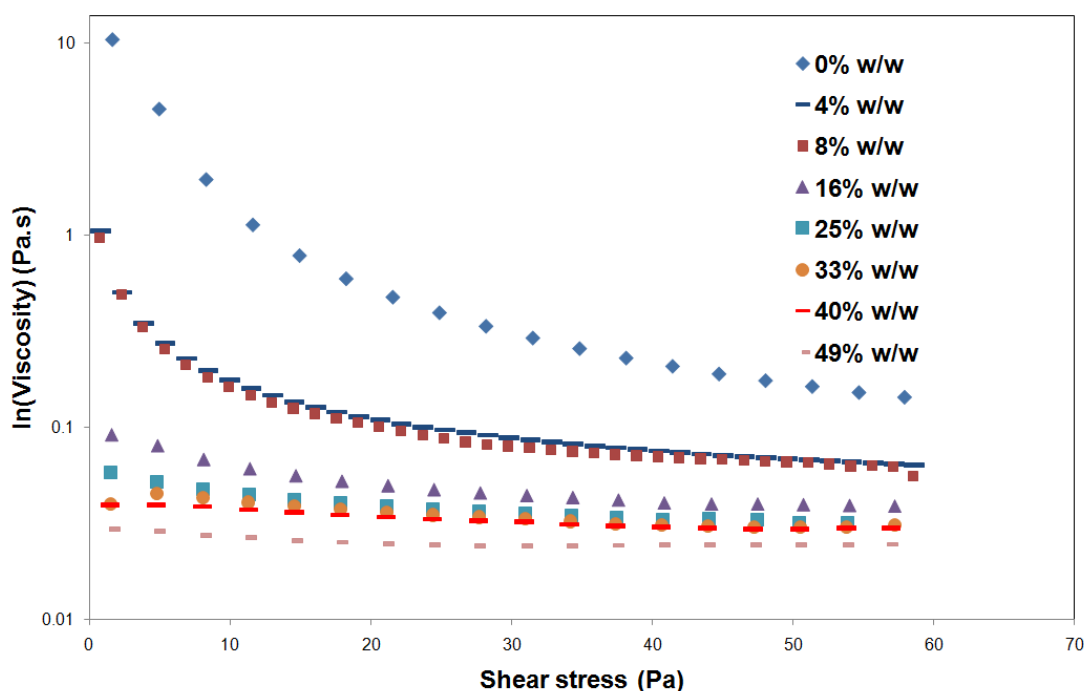


**Figure 5.15** Viscosity profiles for increasing fractions of glycerol in the control emulsion

The emulsion stability as defined by the magnitude of the storage modulus, also decreased greatly with slight increases in the glycerol fraction from  $G' \sim 60$  Pa for the control emulsion to 11 Pa for 4% w/w glycerol fraction. Although 8% w/w glycerol fraction had an initially lower magnitude in the storage modulus than 4% w/w, its storage modulus was higher than at 4% w/w glycerol fraction, suggesting it was more stable over a greater range of stress ( $<10$  Pa) (**Figure 5.16**).

The elastic properties of the emulsions which allow it to behave more solid-like dominated at 4% w/w glycerol fraction, where the storage modulus was greater than the loss modulus. At 8% w/w glycerol fraction the storage and loss modulus were very close in magnitude, after which further increases in the glycerol fraction gave unstable emulsions with predominately viscous behaviour.

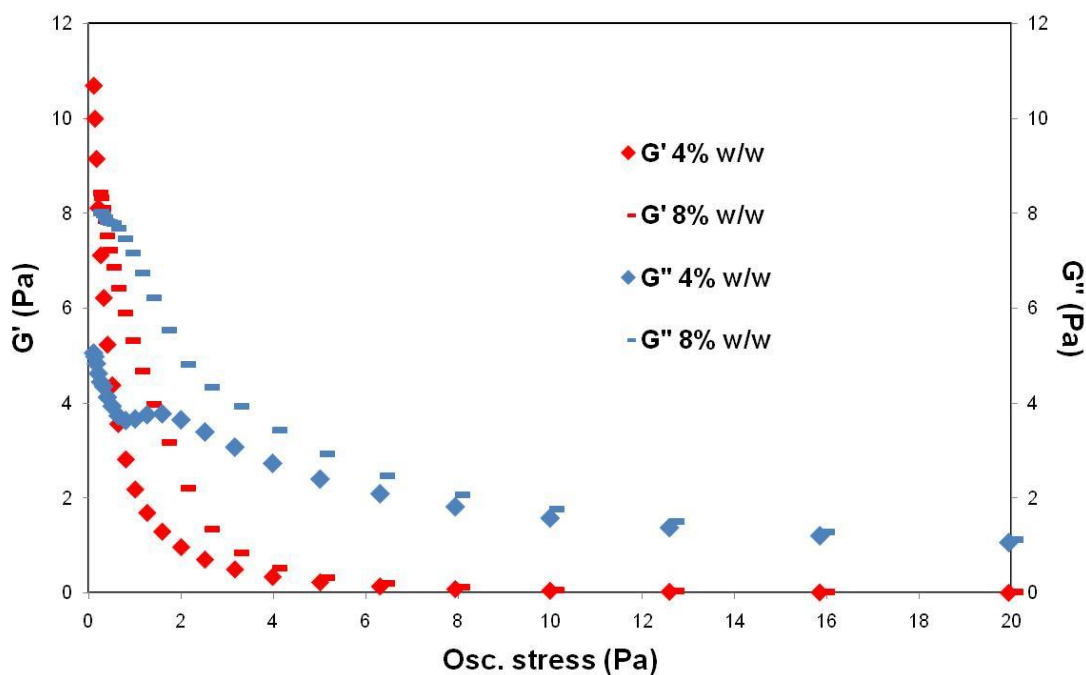


**Figure 5.16 Storage and loss modulus profiles for 4% w/w and 8% w/w fractions of glycerol in the control emulsion**

Thus a 4% w/w glycerol fraction was found to be the critical amount of glycerol that could be used to replace castor oil in the control emulsion. However, a large reduction in the storage modulus from the control emulsion may not be beneficial to the storage properties.

#### 5.3.4.2.2 Carbon dioxide tests

The total weight fraction of the sum of the polyols was kept constant in the reaction with PMDI. Increasing the fraction of glycerol in % w/w, decreased the total carbon dioxide evolved as can be seen in **Figure 5.17**.

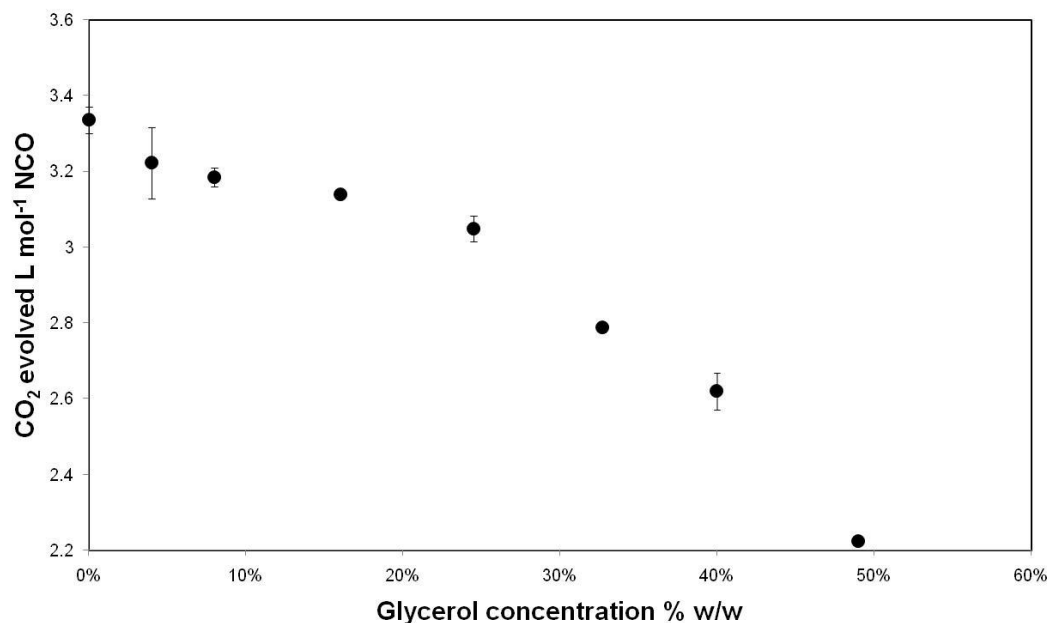


**Figure 5.17 Carbon dioxide evolution for varying weight fractions of glycerol**

**Table 5-10** displays the isocyanate to total hydroxyl mole ratio used in each reaction. It can be seen through the common highlighting in **Table 5-9**, that the addition of smaller amounts of glycerol (4% w/w) at the end of the formulation gave a better reduction in carbon dioxide levels for the same mole ratios (NCO/OH=1.3). Thus, unless glycerol was very much cheaper than castor oil, it would be more beneficial to add 4% w/w glycerol at the end of the formulation to maintain emulsion stability and to aid in reducing carbon dioxide levels. Another benefit to the addition of glycerol at the end of the formulation is the minimal procedural changes for implementation by the industry.

As in the previous glycerol investigations, it is noticed in **Table 5-10** that increasing the glycerol hydroxyl content from NCO/OH =1.7 to 1.4, reduces carbon dioxide evolution by 3.4% whereas no significant change is observed when increasing the hydroxyl content by the same level using castor oil (section 5.3.2.2 CO3 *cf.* CO5).

It was determined in Chapter 4 that the critical ratio needed to increase the extent of reaction between PMDI and glycerol was an excess in hydroxyl groups at a ratio of NCO/OH=0.67 which was shown to be critical in achieving maximum cure.

**Table 5-10 Isocyanate to total hydroxyl mole ratio in mixture and reduction in carbon dioxide with increasing fraction of glycerol showing total replacement of castor oil at 49% w/w**

Glycerol % w/w	NCO/OH fractions	%reduction in CO <sub>2</sub>
0	1.7	0
4	1.4	3.4
8	1.3	4.5
16	1.0	5.9
25	0.8	8.6
32	0.7	16.4
40	0.6	21.4
49	0.5	33.3

#### **5.3.4.3 Addition of glycerol to the control polyol emulsion at 4% w/w**

It is important to note that the addition of glycerol to the control polyol emulsion, at 4% w/w was discovered to be the optimum ratio giving the best combination of viscosity reduction and emulsion stability to aid in application. It also minimises the procedural changes for implementation by the industry partner and provides a small reduction in carbon dioxide evolution.

The competing reaction of glycerol with PMDI is therefore an added complication to the reaction kinetics of the coating. The effect of adding 4% w/w glycerol to the polyol emulsion on the reaction with PMDI was further investigated to compare gel times and the rate of carbon dioxide evolution using the simple emulsion. Rheological and carbon dioxide measurements were thus performed.

##### **5.3.4.3.1 Rheological investigation of the reaction between emulsions and PMDI**

Investigation into the curing profile of the polyol emulsion was performed to elucidate the differences and improvements to the pot-life through the addition of 4% w/w glycerol. The gel time was determined as the crossover of  $G'$  and  $G''$  [28] and is shown in **Table 5-11** for the polyol emulsion and the polyol emulsion with 4% w/w glycerol. The magnitude of  $G'$  (Pa) at the gel point is also displayed and indicates the extent of crosslinking at the gel time.

**Table 5-11 Gel times and magnitude of the storage modulus at the gel point**

<b>Emulsion</b>	<b>Gel time (<math>G' = G''</math>) (min)</b>	<b><math>G'</math> (Pa)</b>
Polyol emulsion	$25.8 \pm 2.9^*$	$6896 \pm 77$
Polyol emulsion + 4% w/w glycerol	$29.7 \pm 1.3$	$13541 \pm 808$

\*%RE&lt;15

An increase in the gel time was observed through the addition of 4% w/w glycerol, however was not significant when accounting for the standard error. More significantly, there was a distinct difference in the extent of crosslinking at the gel time for the different formulations, with the magnitude in  $G'$  (Pa) for the emulsion with glycerol almost double that of polyol emulsion.

A representation of the  $\tan \delta$  profiles of the different emulsions is displayed in **Figure 5.18**. It is evident that the magnitude of  $\tan \delta$  is much greater for the polyol emulsion with glycerol, suggesting that the elasticity of this system is lower than that achieved by the polyol emulsion before the gel point.<sup>[32]</sup> This indicates that the crosslinking reaction is initially delayed, allowing for a greater interaction between isocyanate groups from the PMDI and water (refer to section 5.3.4.3.2 below).

It can also be seen in **Figure 5.18** that  $\tan \delta$  decreases more rapidly for the reaction between PMDI and the polyol emulsion with glycerol and achieves a lower  $\tan \delta$  value indicating a more elastic system and therefore greater crosslinking past the gel point compared to the reaction between PMDI and the polyol emulsion.

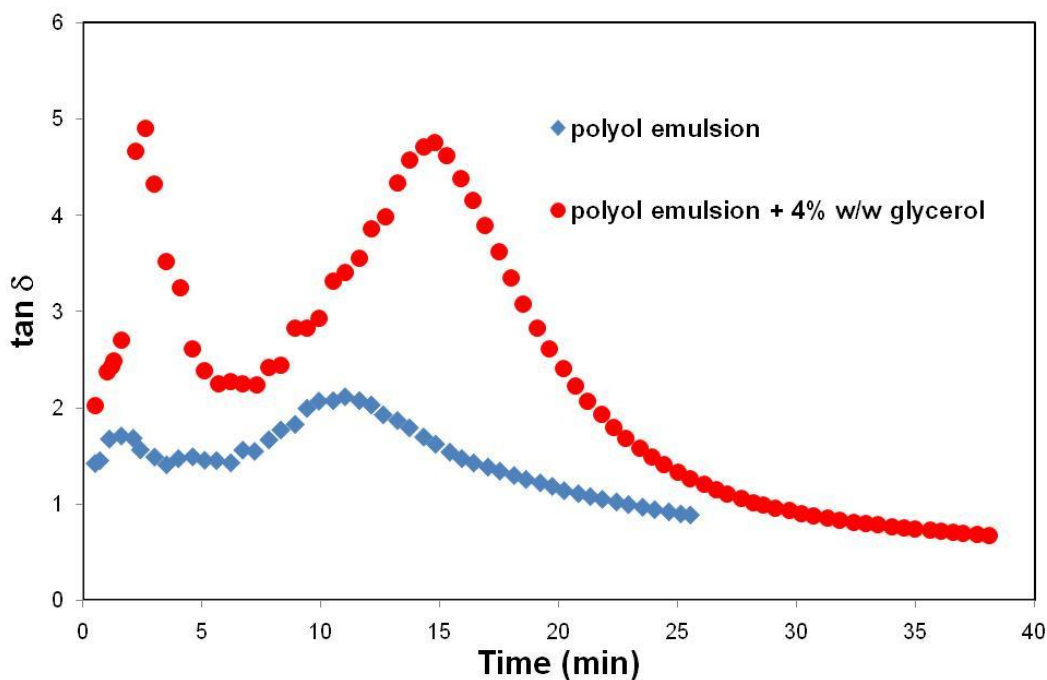


**Figure 5.18 Comparison of the extent of the crosslinking reaction between polyol emulsions and PMDI**

#### 5.3.4.3.2 Carbon dioxide rate analysis

The difference in the rate of carbon dioxide evolution of the two emulsions was also determined through volumetric methods. The reactions were followed over a period of 260 minutes at standard conditions and are displayed in **Figure 5.19**.

The initial rate of carbon dioxide evolution for the polyol emulsion (rate =  $6 \times 10^{-4}$  L mol<sup>-1</sup> NCO min<sup>-1</sup>) was found to be less than that of the polyol emulsion with 4% w/w glycerol (rate =  $7 \times 10^{-4}$  L mol<sup>-1</sup> NCO min<sup>-1</sup>). After approximately 70 minutes of reacting, the rate of evolution of carbon dioxide was equivalent for both emulsions at  $3 \times 10^{-4}$  L mol<sup>-1</sup> NCO min<sup>-1</sup>. This confirms the rheological results, whereby the crosslinking reaction for the polyol emulsion with glycerol and PMDI is initially delayed, with the water and isocyanate reaction predominating. The polyol emulsion with glycerol also has a slightly delayed gel time and this allows for diffusion of carbon dioxide before the crosslinking reaction predominates at the gel time.

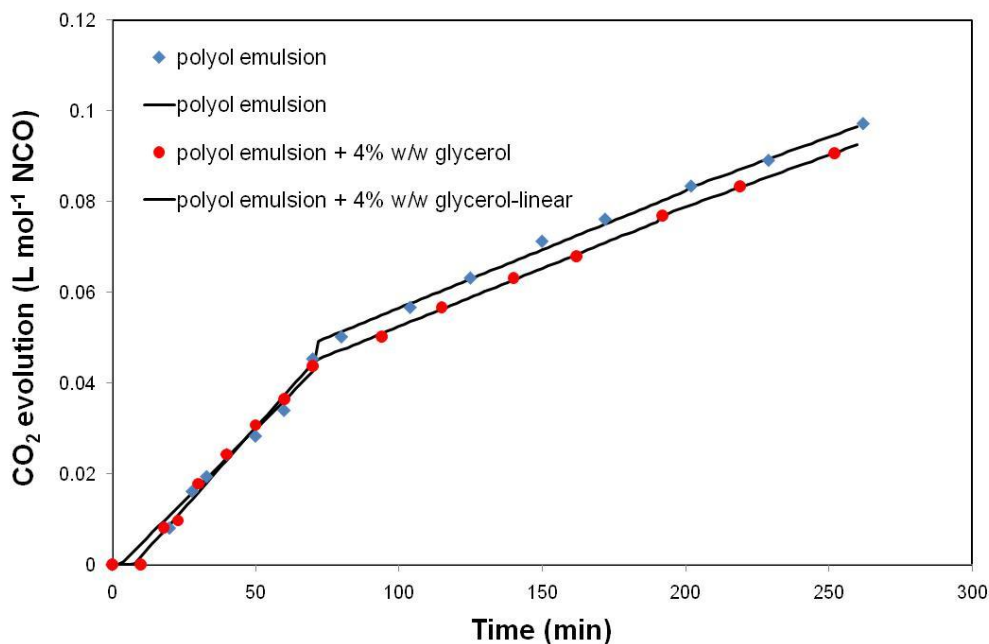


**Figure 5.19 Carbon dioxide evolution with time for the reaction between the polyol emulsion and PMDI and the polyol emulsion with glycerol and PMDI**

## 5.4 Conclusions

Emulsion variables were systematically investigated for their effect on the flow properties of the emulsion through rheological analysis and their subsequent effect on the curing reaction with PMDI through volumetric and rheological tests.

It was determined that the industry ratio of water to castor oil to surfactant is critical, with small changes either side of this ratio affecting the pot-life and extent of crosslinking of the mixture, even though no significant effect is observed on carbon dioxide evolution. A relationship was found to exist between the emulsion conductivities and the storage modulus values obtained at the gel point, in particular for the water and castor oil series of emulsions. A greater incorporation of the oil phase (lower conductivities) improved the extent of crosslinking and the pot-life of the mixture and was achieved for higher surfactant concentrations, lower water concentrations and slightly lower castor oil concentrations than that currently used by the industry.

The non-curing components of the control polyol emulsion were found to increase the level of carbon dioxide evolved through volumetric tests due to the combinatorial

effect of the dioctyl phthalate plasticizer and the pine oil.

The viscosity of the emulsions had no affect on the reaction between water and isocyanate, although lower viscosity emulsions aid in the application properties of the coating.

A 4% w/w addition of glycerol to the polyol emulsion was found to substantially reduce the viscosity of the polyol emulsion while retaining the emulsion stability. It was also determined through rheological characterisation of the curing reaction with PMDI that the crosslinking reaction was delayed at this ratio. The water-isocyanate reaction predominated before the gel time, allowing carbon dioxide to be evolved before extensive crosslinking was achieved at the gel time.

## 5.5 References

- [1] A. Bittner, P. Ziegler, "Water-Borne Two-Pack Polyurethane Coatings for Industrial Applications", in *New Technologies for Coatings and Inks 3rd Congress, Nurnberg, Germany*, **1995**.
- [2] P. B. Jacobs, P. C. Yu, *J. Coat. Technol.* **1993**, 65, 45.
- [3] D. A. Ley, D. E. Fiori, R. Quinn, J., *Prog. Org. Coat.* **1999**, 35, 109.
- [4] Y. Otsubo, R. K. Prud'homme, *Rheol. Acta* **1994**, 33, 29.
- [5] R. Pal, *Colloid Polym. Sci.* **1999**, 277, 583.
- [6] R. Grove, "Notes On Making Cola ", **2005**.
- [7] P. F. Macedo Janus, L. Fernandes Leonardo, R. Formiga Fabio, F. Reis Michael, N. Junior Toshiyuki, A. L. Soares Luiz, E. S. T. Egito, *AAPS Pharm. Sci. Tech.* **2006**, 7, E21.
- [8] T. Tadros, B. Vincent, "Emulsion Stability", in *Encyclopedia of Emulsion Technology: Basic Theory*, P. Becher, Ed., Marcel Dekker INC, **1983**.
- [9] K. Shinoda, K. H., "Phase Properties of Emulsions: PIT and HLB", in *Encyclopedia of Emulsion Technology: Basic Theory*, P. Becher, Ed., Marcel Dekker INC., **1983**.
- [10] T. C. G. Kibbey, K. F. Hayes, *J. Contam. Hydrol.* **2000**, 41, 1.
- [11] D.-B. Ljubica, D. Petar, V. Sovilj, "Structure Building in O/W Emulsions in Shear Induced By Surfactant-nongelling Polymer Interactions", in *3rd International Symposium on Food Rheology and Structure*, **2003**, 529.
- [12] J. Mougel, O. Alvarez, C. Baravian, F. Caton, P. Marchal, M.-J. Stebe, L. Choplin, *Rheol. Acta* **2006**, 45, 555.
- [13] O. Ozer, E. Baloglu, G. Ertan, V. Muguet, Y. Yazan, *Int. J. Cosm. Sci.* **2000**, 22, 459.
- [14] W. Warisnoicharoen, A. B. Lansley, M. J. Lawrence, *Int. J. Pharm.* **2000**, 198, 7.
- [15] W. Warisnoicharoen, A. B. Lansley, M. J. Lawrence, *Pharm. Sci.* [online computer file] **2000**, 2.
- [16] J. Jiao, J. Burgess Diane, *AAPS Pharm. Sci.* **2003**, 5, E7.
- [17] N. A. Mishchuk, A. Sanfeld, A. Steinchen, *Adv. Colloid Interface Sci.* **2004**, 112, 129.

- [18] I. Roland, G. Piel, L. Delattre, B. Evrard, *Int. J. Pharm.* **2003**, 263, 85.
- [19] R. J. Kauten, J. E. Maneval, M. J. McCarthy, *J. Food Sci.* **1991**, 56, 799.
- [20] A. Ponton, P. Clement, J. L. Grossiord, *J. Rheol.* **2001**, 45, 521.
- [21] K. H. Kim, J. M. S. Renkema, T. Van Vliet, *Food Hydrocolloids* **2001**, 15, 295.
- [22] P. Sherman, "Rheological Properties of Emulsions", in *Encyclopedia of Emulsion Technology: Basic Theory*, P. Becher, Ed., Marcel Dekker INC., **1983**.
- [23] S. A. Baser, D. V. Khakhar, *J. Cell. Plast.* **1993**, 29, 197.
- [24] C. Ligoure, M. Cloitrea, C. Le Chatelliera, F. Montia, L. Leibler, *Polymer* **2005**, 46, 6402.
- [25] P. Walstra, "Formation of Emulsions", in *Encyclopedia of Emulsion Technology: Basic Theory*, P. Becher, Ed., Marcel Dekker INC, **1983**.
- [26] H. M. Princen, *J. Colloid Interface Sci.* **1985**, 105, 150.
- [27] B. Latreille, P. Paquin, *J. Food Sci.* **1990**, 55, 1666.
- [28] H. Yu, S. G. Mhaisalkar, E. H. Wong, *Macromol. Rapid Commun.* **2005**, 26, 1483.
- [29] M. Chakraborty, H. J. Bart, *Colloids Surf. A: Physicochem. Eng. Aspects* **2006**, 272, 15.
- [30] G. Biesmans, L. Colman, R. Vandensande, *J. Colloid Interface Sci.* **1998**, 199, 140.
- [31] G. Yilmaz, R. O. J. Jongboom, J. J. G. Van Soest, H. Feil, *Carbohydr. Polym.* **1999**, 38, 33.
- [32] M. Piao, J. Otaigbe, D. Otts, M. Urban, *Polym. Mater. Sci. Eng.* **2004**, 90, 112.

# **CHAPTER 6**

## **Characterisation of the Reactive Aggregate and Combined Solutions**

## 6 REACTIVE AGGREGATE

### 6.1 Introduction

The third component of the coating system under investigation is the mixed reactive and non-reactive aggregate which will be named the fillers in the text below. The fillers consist of reactive Portland cement and lime as well as non-reactive components which include black granite and silica sand.<sup>[1]</sup> The non-reactive components give the coating high abrasion resistance and provide the bulk filler that extends the coating volume.

The complexity of the reaction kinetics increases when one of the components of the polyurethane formulation is water-dispersed. As explained in the introduction (**Scheme 1.12**), the hydration reaction occurs between water in the polyol component with the cement in the filler component and provides the majority of the coating's strength through the formation of calcium silicate hydrates and calcium carbonate.<sup>[2,</sup>

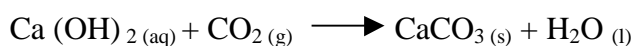
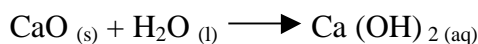
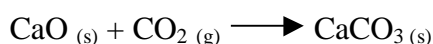
<sup>3]</sup> Calcium carbonate is formed from the subsequent reaction between calcium hydroxide (hydrated lime-  $\text{Ca}(\text{OH})_2$ ) and carbon dioxide which absorbs the carbon dioxide released by the reaction between water and isocyanate groups (see **Scheme 6.1** for details).

When the solution is saturated with calcium hydroxide, hydration of the calcium oxide silicate continues, with further calcium hydroxide formed deposited as crystals. The remaining hydrated calcium oxide silicate is in equilibrium with dissolved calcium hydroxide. Thus, when more water is added, further hydrolysis occurs, raising the concentration of calcium hydroxide in solution where it restabilises in its silicate form.<sup>[4]</sup> The amount of calcium hydroxide released from the hydration reaction depends on the water:solid ratio, temperature and the cement particle size distribution.<sup>[5-8]</sup> Studies have also shown that relative humidity affects the hydration rate during cure.<sup>[9, 10]</sup>

To determine the amount of calcium hydroxide evolved during the hydration process, solvent extraction can be used; however this method yields the total free calcium oxide and hydroxide present in cement. The amount of calcium hydroxide can also be determined by Thermo-Gravimetric Analysis (TGA) by monitoring water loss at two different temperatures, corresponding to the combination of water associated

with silicates and calcium hydroxide, respectively. The quantity of free calcium hydroxide can be determined as the mass loss in the temperature range 460-560 °C and the loss of carbon dioxide from calcium carbonate can be observed in the range 720-920 °C.<sup>[2, 11, 12]</sup>

The lime present in the aggregate helps to control cement hydration largely forming calcium oxide hydrated silicates whose mass loss is noticed at 80-100 °C in TGA analysis. Lime absorbs a fraction of the carbon dioxide evolved from the reaction between isocyanate groups and water according to **Scheme 6.1**.<sup>[1]</sup>



#### **Scheme 6.1 Absorption of carbon dioxide by lime in the fillers**

In this chapter, attempts to characterise the ability of the reactive aggregate to reduce carbon dioxide evolution and methods which improve or inhibit this function are investigated. The reduction of carbon dioxide evolution through addition of calcium oxide and calcium hydroxide was investigated with the subsequent material properties of the optimum compositions tested through DMA. Combinations of the improvements detailed in this chapter and those suggested in chapter 5 have also been investigated with the material properties determined through DMA analysis.

## **6.2 Materials and Methods**

### **6.2.1 Materials and sample preparation**

The main materials used in this Chapter are described in Chapters 3 and 4 and Appendix A. Desmodur VL R10 with a functionality of 2.7 and viscosity of 100-150 mPa.s was used as received from Bayer Chemicals.

Portland cement obtained from Blue Circle, as received, for testing purposes, however samples of cement used in tests were taken from the centre of the bag to

ensure material used had been minimally affected by environmental factors such as hydration and/or carbon dioxide ingress.

Calcium hydroxide was obtained from May & Baker LTD, while calcium oxide was obtained from the British Drug Houses LTD, both were dried before use. High purity carbon dioxide gas was obtained from BOC gasses and used for cement ageing tests. A standard control polyol emulsion (P1) was used for investigations in this chapter. Variations to the standard control emulsion (P1) were also used and compositions are detailed in **Table 6-1**.

**Table 6-1 Polyol emulsion compositions for coating variations**

Components	P1	P2	P3	P4
	% w/w	% w/w	% w/w	% w/w
Castor Oil	49.00	49.00	41.00	49.00
Diocetyl Benzyl Phthalate	20.44	20.44	20.44	20.44
Pine oil	3.48	3.48	3.48	3.48
Surfactant	0.72	0.72	0.72	0.72
Silicone	0.72	0.72	0.72	0.72
Water	25.56	25.56	25.56	30.56
glycerol	0	4.00	8.00	0

Variations in the filler composition of the coating were prepared according to **Table 6-2**.

**Table 6-2 Filler compositions for coating variations**

Components	F1	F2	F3	F4	F5
	% w/w				
16/30 silica	0	0	12	12	65.3
30 silica	0	0	16.4	12.6	12.6
granite	0	0	53.3	53.3	0
Portland cement	100	75	16.6	16.6	16.6
Calcium hydroxide	0	25	1.7	5.5	5.5

The product ratio of NCO/OH= 1.7 has been used; however, in all cases, the hydroxyl component was calculated from the castor oil only. The materials were mixed at standard conditions (25 °C at atmospheric pressure) using an overhead drill mixer with a 5 cm diameter fan blade, unless the coating was tested at the industry site where a power drill was used with unknown revolutions per minute, using a typical paint stirrer.

## **6.2.2 Methods**

### **6.2.2.1 TGA**

A TGA 2950 Thermogravimetric Analyzer (TA Instruments) was used to measure the hydration levels of cement and to determine the effects of ageing on cement composition. The samples were placed in a platinum crucible and decomposition studied under a nitrogen environment at 50 ml min<sup>-1</sup>. Samples of 10-40 mg were run from room temperature to 900 °C at a heating rate of 10 °C min<sup>-1</sup>. Temperature calibrations were performed using aluminium and nickel.

### **6.2.2.2 Carbon dioxide Measurement**

Volumetric tests to measure carbon dioxide evolution were performed as detailed in Chapter 2.

### **6.2.2.3 DMA**

DMA measurements were performed using a TA Instruments DMAQ800 in single cantilever bending deformation mode. The samples were cured at room conditions for a period of at least 48 hours before DMA runs. DMA tests were carried out at a frequency of 1 Hz, amplitude of 20 µm, in the temperature range of -100 °C to 180 °C with a heating ramp of 2 °C min<sup>-1</sup>.

The glass transition temperature  $T_g$ , was taken as the temperature at which the loss factor  $\tan \delta$  reached a maximum. Liquid nitrogen was used to achieve the sub-ambient temperatures.

#### **6.2.2.4 Ageing tests**

Cement ageing was performed by exposing the cement to a high carbon dioxide atmosphere and to a high relative humidity environment (see ageing procedures used, as specified below). Volumetric tests to evaluate carbon dioxide evolution when reacted with the polyol emulsion and PMDI were performed, as well as TGA analysis of the aged cement on its own.

##### *Carbon dioxide environment:*

Fresh Portland cement (30g/jar) was placed in glass jars before introducing carbon dioxide to the jar and sealing it with a screw cap lid. Cement from the top layer of the sample was removed for TGA and carbon dioxide tests at varying times over a 46 hour period. Times chosen for the study included 4.5, 20, 30 and 46 hours.

##### *Relative humidity environment:*

A 5 litre air tight plastic container was used for the high relative humidity environment. The relative humidity was increased in the container to approximately 75% RH using a saturated sodium chloride solution in a 10 cm diameter open jar, which was left to equilibrate over night. A layer of fresh Portland cement 1 cm thick was spread along the base of the container at 65% RH. Samples were taken from the surface of the cement at intervals of 0, 40, 60, 100 and 172 hours from different areas of the cement's surface. The relative humidity was checked at each time interval resulting in 65% RH for all samples.

## 6.3 Results and Discussion

### 6.3.1 Characterisation of the current industry ratio and improvements

The effect of cement and calcium hydroxide in the reactive aggregate on carbon dioxide evolution from the reaction between water in the polyol emulsion and isocyanate groups was investigated. Calcium hydroxide is added to the industry product within the filler component to aid in the absorption of carbon dioxide, forming calcium carbonate as depicted in **Scheme 6.1**. The effect of cement and calcium hydroxide at the product ratio on carbon dioxide evolution is observed in **Figure 6.1**. The polyol emulsion reaction with PMDI using talc powder as the inert filler was employed as the control.

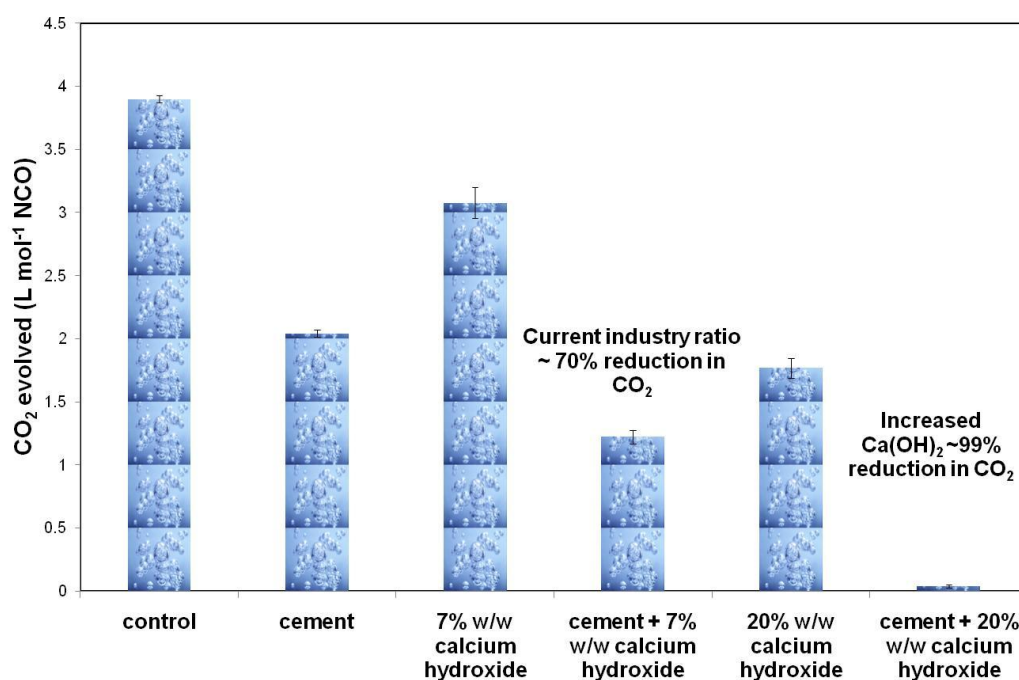


**Figure 6.1** Comparison of current industry fillers with an increased level of calcium hydroxide

As expected, the cement and calcium hydroxide in the product filler composition reduce carbon dioxide evolution through the reactions shown in **Scheme 6.1**. The combined effect of the cement and calcium hydroxide reduce the carbon dioxide evolved by approximately 70%. It would therefore appear that it is this residual carbon dioxide released from the coating which is the primary cause of blistering during curing. Increasing the level of hydrated lime ( $\text{Ca}(\text{OH})_2$ ) or quick lime ( $\text{CaO}$ )

in the filler component, was therefore considered as suitable and practical option to further reduce the amount of carbon dioxide evolved.

The reduction in carbon dioxide with increasing calcium hydroxide (%w/w of mixture) is displayed in **Figure 6.2**. Complete absorption of carbon dioxide evolved by the reaction between water and PMDI occurs at 27.5% w/w  $\text{Ca}(\text{OH})_2$ .

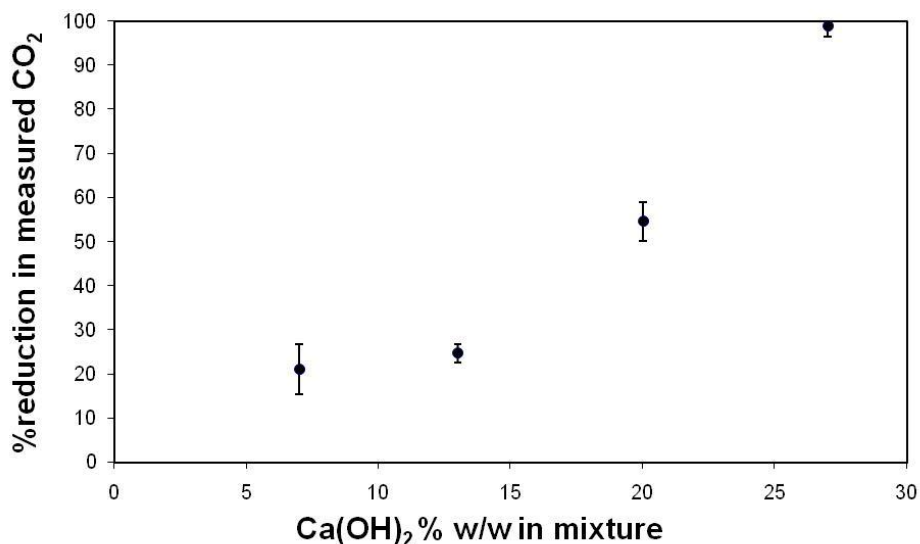


**Figure 6.2** Reduction in carbon dioxide evolution through the addition of calcium hydroxide

It was postulated that dried calcium oxide would offer a greater reduction in carbon dioxide levels per mole of material, due to its ability to react with both carbon dioxide and water forming calcium hydroxide. Dried calcium oxide at varying levels was thus employed to evaluate the effect on carbon dioxide evolution. The results displaying the per cent reduction in carbon dioxide evolution with an increase in calcium oxide concentration in %w/w of mixture are shown in **Figure 6.3**. Although complete absorption of carbon dioxide occurs at 32% w/w level of calcium oxide, this point is most likely an outlier, suggesting that the limit has been reached and any further calcium oxide added has no significant effect. At 27.4% w/w calcium oxide, a reduction in carbon dioxide of  $97 \pm 4\%$  was achieved, suggesting this is the limiting level of calcium oxide. Thus, there is no significant difference in the use of calcium hydroxide or calcium oxide in the filler component. Therefore, increasing the calcium hydroxide component in the fillers was employed to reduce carbon dioxide evolution.

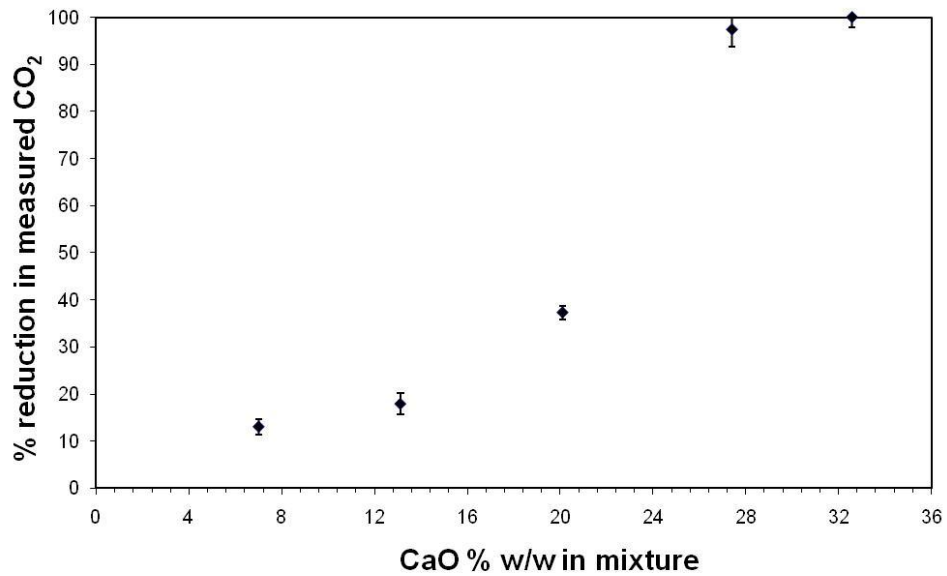


**Figure 6.3 Reduction in carbon dioxide evolution through the addition of calcium oxide**

Using the 20% w/w level of calcium hydroxide in conjunction with the current ratio of cement in the fillers, significantly reduces the carbon dioxide evolved by approximately 99% as shown in **Figure 6.1**. This is translatable to an increase in the level of calcium hydroxide in the fillers from 1.7% w/w to 5.5% w/w. To compensate for an increased in filler mass, an equal weight percentage of 30 silica was removed (F4 in **Table 6-2**).

### 6.3.2 Ageing of cement

Another important consideration is the efficacy of aged cement in reducing carbon dioxide levels in the coating, formed from the reaction of PMDI with the polyol emulsion at the ratio of NCO/OH=1.7. Ageing of Portland cement was simulated through two methods. The first was exposing Portland cement to a saturated carbon dioxide gas environment and the second method was to expose Portland cement to a high humidity environment. Thermo-Gravimetric Analysis (TGA) was employed to follow the degree of calcium carbonate formation through the mass loss observed in the range 720-920 °C using TGA, while the degree of hydration was determined by the combination of water associated with silicates and calcium hydroxide, measured as the mass loss in the temperature range of 100-120 °C and 460-560 °C, respectively.<sup>[2, 11, 12]</sup>

### 6.3.2.1 Carbon dioxide environment

Portland cement was exposed to a carbon dioxide saturated atmosphere for varying lengths of time. **Figure 6.4** displays the levels of moisture, calcium oxide silicate hydrates, and calcium hydroxide and calcium carbonate levels over time. It is evident that calcium carbonate levels increase with time, as expected, while the hydrated silicates decrease with time. In the reaction between carbon dioxide and calcium hydroxide, water is formed. This water may further hydrate the calcium oxide silicates releasing a greater amount of calcium hydroxide as is evident in **Figure 6.4** at longer exposure times.

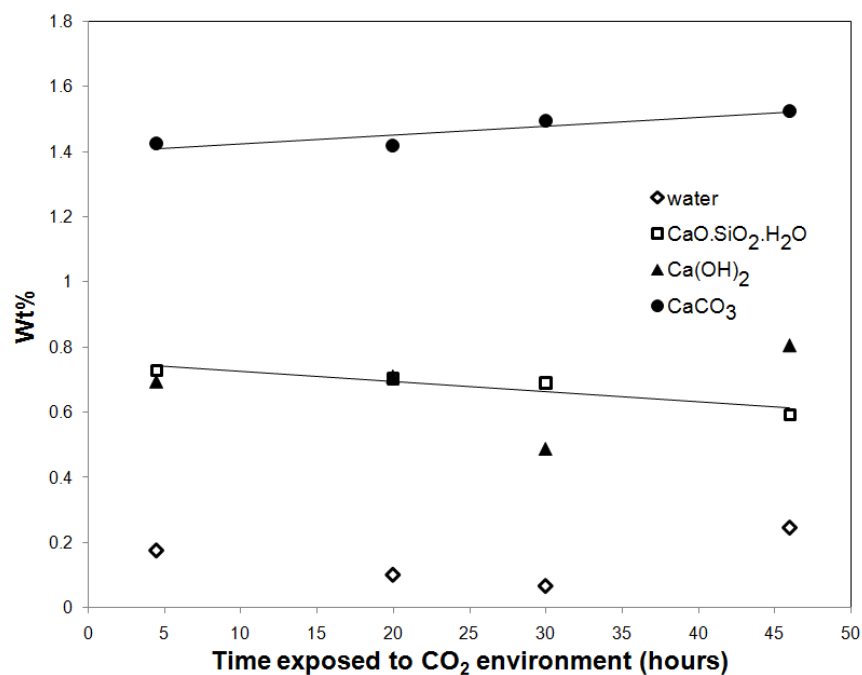


**Figure 6.4** TGA results for carbon dioxide exposed Portland cement

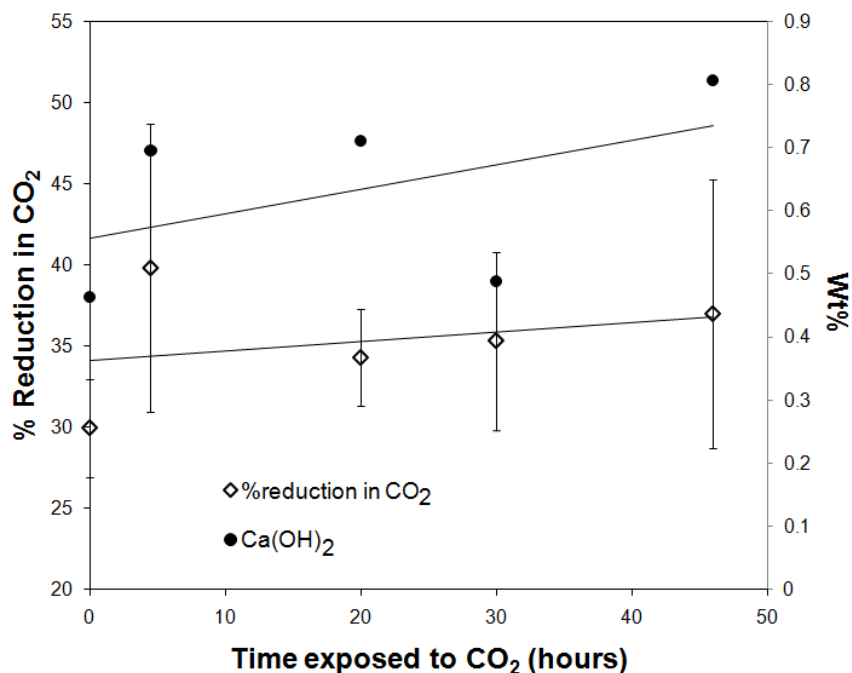


**Figure 6.5** Reduction in carbon dioxide levels in the reaction of PMDI with polyol emulsion using carbon dioxide exposed cement at varying time intervals.

The efficacy of carbon dioxide aged Portland cement in the reduction of carbon dioxide levels released by the reaction of isocyanate groups from PMDI and water in the polyol emulsion was examined and is displayed in **Figure 6.5**.

Perhaps somewhat unexpectedly, greater reduction in carbon dioxide levels can be achieved with an increased exposure time of the Portland cement to carbon dioxide, even though the calcium carbonate levels increase (**Figure 6.4**). This can be explained from data obtained in **Figure 6.5**, which shows the levels of calcium hydroxide also increases on exposure to carbon dioxide.

Therefore, it can be concluded, that for Portland cement exposed to carbon dioxide, the free calcium hydroxide reacts with carbon dioxide to form calcium carbonate and water which further reacts with the calcium oxide silicates in the cement to produce more calcium hydroxide products (**Scheme 6.1**).<sup>[1, 4]</sup> Carbon dioxide produced from the isocyanate and water reaction can therefore react with this additional calcium hydroxide, reducing evolved carbon dioxide levels.

### 6.3.2.2 Relative humidity environment

Portland cement was exposed to a high relative humidity environment ~ 65% RH over a period of 172 hours. Samples were taken at varying intervals and tested for the level of hydration using TGA. The efficacy of Portland cement in the reduction of carbon dioxide levels formed by the reaction between PMDI and the polyol emulsion was also tested. **Figure 6.6** displays the reduction in carbon dioxide levels achieved with increasing exposure time to the high relative humidity environment due to the formation of calcium hydroxide.

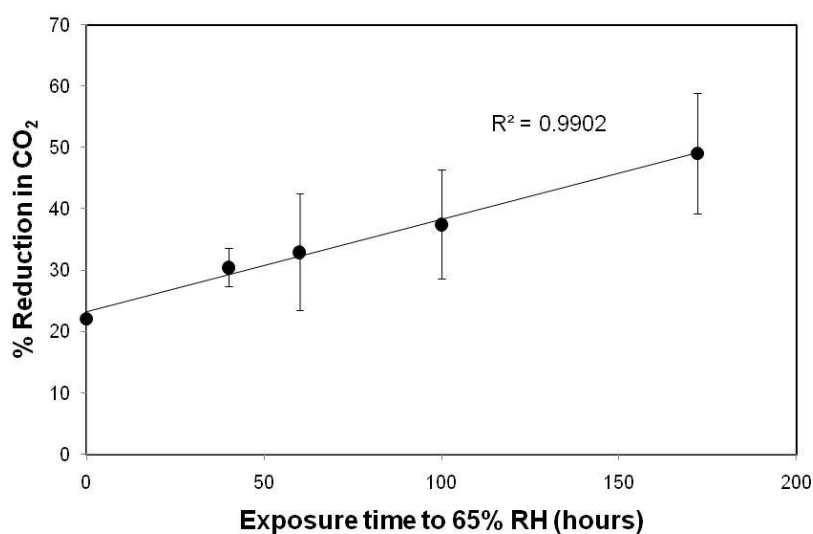


**Figure 6.6** Efficacy of Portland cement exposed to a high relative humidity environment over 172 hours

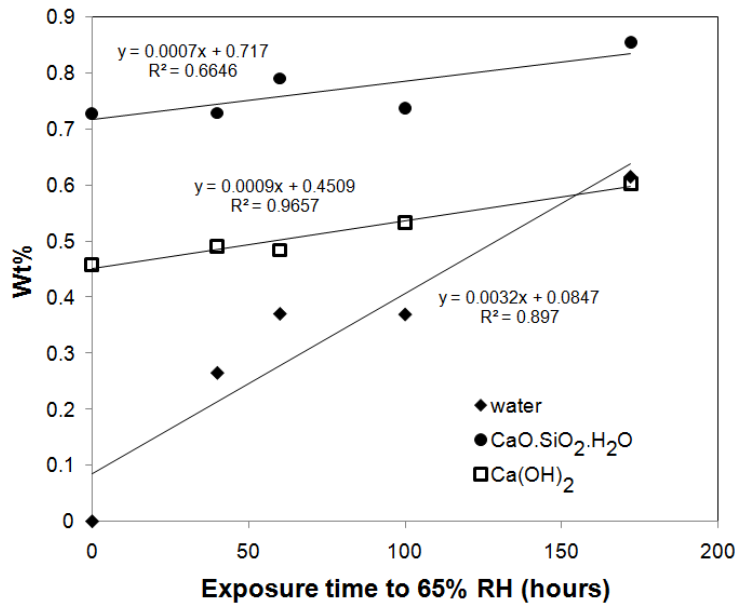


**Figure 6.7** TGA analysis of the hydration reaction over time for Portland cement exposed to a high humidity environment

TGA analysis, as seen in **Figure 6.7**, shows an increase in the water content, hydrated calcium oxide silicate content and calcium hydroxide content with increased exposure time. The free calcium hydroxide with time was correlated to the per cent reduction of carbon dioxide levels and was found to have a proportional relationship as seen in **Figure 6.8**. Thus, exposure of Portland cement to carbon dioxide and high relative humidity environments increase the calcium hydroxide content, which aids in reducing the carbon dioxide evolved by the water-isocyanate reaction. Therefore, ageing of the cement will not impede its ability to reduce carbon dioxide evolution in the product formulation.

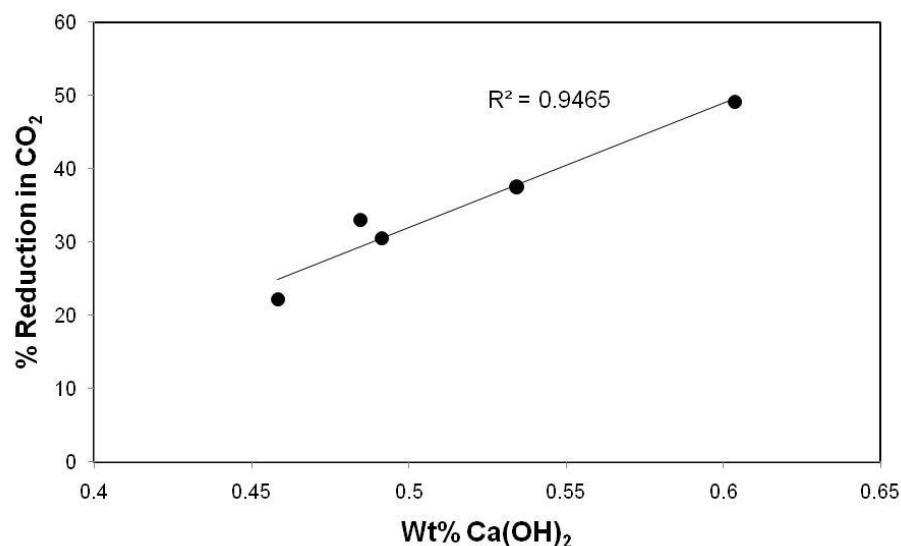


**Figure 6.8 Correlation of the calcium hydroxide levels present in Portland cement at varying exposure times to a high humidity environment with its ability to reduce carbon dioxide evolution in the coating formulation**

In conclusion, the results for aged Portland cement were somewhat surprising. Intuitively, it may have been expected that aged Portland cement, through carbon dioxide and moisture absorption might have adversely affected the ability of the Portland cement filler to absorb carbon dioxide, produced from the water-isocyanate reaction. However, in fact, the reverse was found. These environmental contaminants (humidity and carbon dioxide) actually increase the Ca(OH)<sub>2</sub> levels in the portland cement which assist in reducing carbon dioxide, produced from the water-isocyanate reaction.

### **6.3.3 Characterisation of the cured material using DMA for comparison of various proposed solutions**

Mechanical analysis was performed using DMA by measuring the glass transition temperature ( $T_g$ ) and the storage modulus ( $G'$ ) to monitor the differences in the coating composition. Combinations of polyol emulsions with varying filler compositions were trialed for solutions to the blistering problem as determined in previous investigations. The effect of glycerol addition in the polyol emulsion and the increase in concentration of calcium hydroxide in the fillers were the major two improvements investigated. A lower viscosity, commercially available isocyanate

(DVLR10) was also obtained for comparison, due to its improved application properties. The  $T_g$  and storage modulus ( $G'$  MPa) at 24 °C representing comparative strength at standard conditions for the variations in coating composition are presented in **Table 6-3**. Compositions of the polyol emulsions (P1-P4) and fillers (F1-F5) are given in **Table 6-1** and **Table 6-2**.

**Table 6-3 Comparison of  $T_g$  and storage modulus for various coating compositions**

Sample reaction with PMDI	$T_g$ °C	$G'$ MPa @ 24 °C	Description
P1/ F1	119.9 ± 0.5	695 ± 19 <b>(676-714)</b>	Control polyol with cement
P1/ F2	147.1 ± 0.9	1814 ± 151 <b>(1663-1965)</b>	Control polyol with cement and 20% w/w Ca(OH) <sub>2</sub> filler
P2/ F2	144 ± 1	1976 ± 131 <b>(1845-2107)</b>	Polyol - 4% w/w glycerol added with cement and 20% w/w Ca(OH) <sub>2</sub> filler
P3/ F2	151.0 ± 0.3	2052 ± 22 <b>(2030-2074)</b>	Polyol - 8% w/w glycerol substitution with cement and 20% w/w Ca(OH) <sub>2</sub> filler
P4/ F2	149	1756 ± 191 <b>(1565-1947)</b>	Polyol - 5% w/w water addition with cement and 20% w/w Ca(OH) <sub>2</sub> filler
P1/ F3	138.1 ± 0.4	1925.5 ± 45.5 <b>(1880-1971)</b>	Control polyol with control fillers at current industry ratios
P1/ F5	143.1 ± 9.9	2578.5 ± 297.5* <b>(2281-2876)</b>	Control polyol with 5.5% w/w Ca(OH) <sub>2</sub> , no granite (extra silica)
P2/ F4	133.8 ± 0.1	2131 ± 355* <b>(1776-2486)</b>	Polyol - 4% w/w glycerol added with 5.5% w/w Ca(OH) <sub>2</sub> in fillers
P3/ F4	143.5 ± 4.9	2790.5 ± 356.5* <b>(2434-3147)</b>	Polyol - 8% w/w glycerol substitution with 5.5% w/w Ca(OH) <sub>2</sub> in fillers
P2/ F5	150.1 ± 0.6	2069 ± 541* <b>(1528-2610)</b>	Polyol - 4% w/w glycerol added with 5.5% w/w Ca(OH) <sub>2</sub> , no granite (extra silica) in fillers
P3/ F5	129.7 ± 7.6	1812.5 ± 1.5 <b>(1811-1812.5)</b>	Polyol - 8% w/w glycerol substitution with 5.5% w/w Ca(OH) <sub>2</sub> , no granite (extra silica) in fillers
Sample reaction with DVLR10			
P1/ F3	137.7 ± 6.9	1341 ± 2 <b>(1339-1343)</b>	Control polyol with control fillers at current industry ratios
P3/ F4	145.3 ± 2.2	2060 ± 125 <b>(1935-2185)</b>	Polyol - 8% w/w glycerol substitution with 5.5% w/w Ca(OH) <sub>2</sub> in fillers
P3/F5	151.2 ± 1.0	1932 ± 55 <b>(1877-1987)</b>	Polyol - 8% w/w glycerol substitution with 5.5% w/w Ca(OH) <sub>2</sub> , no granite (extra silica) in fillers

\*%RE<20 ▲%RE<30

Addition of calcium hydroxide content in the filler component (P1/F1 compared to P1/F2), showed a dramatic increase in the storage modulus and  $T_g$  of the coating. An

increase in strength is expected from the addition of calcium hydroxide due to its reaction with carbon dioxide evolved by the water-isocyanate reaction yielding calcium carbonate.<sup>[2, 3]</sup>

Increasing the hydroxyl content through the addition of 4% w/w glycerol (P2/F2) displayed a slightly higher storage modulus than the control polyol emulsion (P1/F2), however was not significantly different. Replacement of 8% w/w castor oil with glycerol in the polyol emulsion (P3/F2) also showed a higher storage modulus than the control emulsion and was significantly improved. There was no significant difference between the glycerol emulsions investigated (P2/F2 and P3/F2, P2/F4 and P3/F4, P2/F5 and P3/F5). This suggests that glycerol does increase the storage modulus of the control coating with a mole ratio of NCO/OH=1.3 (*cf.* NCO/OH=1.7), which is more significant when the castor oil is substituted for glycerol. These results also confirm earlier investigations in Chapter 5 (**Table 5-11**), where the crosslinking was more extensive at the gel time for the reaction between PMDI and the polyol emulsion with 4% w/w glycerol determined by the higher value of the storage modulus compared to the control emulsion. The post-cure time of the coating samples before DMA analysis could be the reason for the difference in storage modulus observed (although insignificant) between glycerol emulsions (P2 and P3). Glycerol contains a slower reacting secondary hydroxyl, as well as two fast primary hydroxyl groups and therefore delays in DMA analysis could allow the secondary hydroxyl group on glycerol to form a greater number of crosslinks increasing the storage modulus.<sup>[13]</sup> Thus, due to the greater number of secondary hydroxyls in P3 (8% glycerol substitution) relative to P2 (4% glycerol addition) a greater degree of post-curing reactions could be possible. This would result in a greater storage modulus for P3/F combinations over P2/F combinations, which is the case for two out of three filler combinations tested.

Ease of application of the coating system has been of concern to the coating applicators (trowel-hands). One solution to aid the application of the coating is to lower the viscosity of the coating components. Reducing the viscosity of the polyol emulsion can be achieved through the addition of glycerol as determined previously (investigated in chapter 5). Another solution proposed, was to increase the water content in the polyol emulsion and thus lower the viscosity, as no significant affect on carbon dioxide evolution was found at slightly higher water concentrations

(Chapter 5). It was postulated that increasing the concentration of water in the polyol emulsion by 3.5% w/w (P4/F2) would aid in viscosity reduction. However, the strength of the coating might be compromised, as an increase in the water fraction was found to reduce gel times and the storage modulus, thus reducing the crosslinking reaction (Chapter 5). A 3.5% w/w excess of water in the polyol emulsion was tested in the coating composition using cement and calcium hydroxide as the reactive aggregate (P4/F2) and compared to the control polyol emulsion (P1/F2). No significant difference in the storage modulus or  $T_g$  was observed.

A commercially available, lower viscosity isocyanate (DVL10) with the same functionality as PMDI was also tested for its comparative strength (P1/F3, P3/F4 and P3/F5 DVL10). Although having better application properties, the storage modulus decreased significantly for P1/F3 and P3/F4. This effect was not observed when using fillers (F5) which consisted of a smaller average particulate size (discussed further below).

Reducing the bulk volume of the coating by decreasing the average particle size of the fillers was trialled to aid in the coating application. The removal of black granite and replacement with equal parts of silica gave the coating a smoother texture, while still retaining some abrasion resistance. Comparison of coating strength showed that no significant difference was observed between fillers with granite (F4) and silica replacement (F5), except when the aggregate was reacted with P3 and PMDI. The storage modulus decreased significantly from (P3/F4)  $2790.5 \pm 356.5$  MPa to (P3/F5)  $1812.5 \pm 1.5$  MPa whereas no significant difference was observed in the reaction with P3 and the lower viscosity isocyanate (DVL10).

The combined viscosity reduction of P3 and DVL10 compared to P3 and PMDI (viscosities shown in **Table 6-4**), might aid in dispersing the smaller particulates of the 16/30 silica used in the replacement of granite in the fillers. This provides a more uniform distribution of the reacting components thereby increasing the crosslinking reaction and strength of the coating. In granite compositions, the larger particulates might aid in dispersing the mixture more uniformly during mixing of higher viscosity liquids. Dispersion of liquids in solids is affected by the level and type of agitation, vessel geometry, as well as the physical properties of the liquid and solid components. Liquid viscosity, density and solid particle size distribution, wetting characteristics and density could all play a significant role in the mixing efficiency of

this system.<sup>[14]</sup> The theory of mixing solids consisting of varying particulate sizes into the liquid component of the coating is out of the scope of this thesis due to its added complexity, although needs to be optimised for material consistency.

**Table 6-4 Viscosity variations of polyol emulsions and oligomeric isocyanates investigated**

Sample	Viscosity (mPa.s)
P1	10500
P2	6500
P3	970
PMDI	220
DVLR10	130

## 6.4 Conclusions

The current level of cement and calcium hydroxide in the fillers reduced carbon dioxide evolution by 70%, which was not sufficient in preventing random blister formation during curing. It was found that cement ageing with time does not impede Portland cement's ability to reduce carbon dioxide evolution formed in the reaction between the polyol emulsion and PMDI during curing. In contrast, it was shown to have a positive effect in the reduction of carbon dioxide.

The improvements suggested for the coating according to the above investigations and those of previous chapters are to increase calcium hydroxide in the fillers to 5.5% w/w while using a lower viscosity polyol emulsion that included glycerol. It was found that 4% w/w glycerol addition to the current polyol emulsion extends the liquid volume, which aids mixing and provides the least change for implementation by the industry partner. An increase in water content of 3.5% w/w is also a possible solution to aid in reducing the viscosity of the polyol emulsion without significantly affecting the coating's material properties. These combined solutions will reduce carbon dioxide evolution while providing a coating that is easily mixed and applied. Future work will require investigation into the mixing/blending of the liquid components with the aggregate mixture to establish correct particulate size in order to form a self-levelling version of the coating, which was out of the scope of this thesis.

## 6.5 References

- [1] G. A. Howarth, *Surf. Coat. Int. Part B: Coat. Transact.* **2003**, 86, 111.
- [2] D. Hermawan, T. Hata, S. Kawai, W. Nagadomi, Y. Kuroki, *J. Wood Sci.* **2002**, 48, 179.
- [3] J. Zelic, D. Rusic, R. Krstulovic, *J. Therm. Anal. Calorim.* **2002**, 67, 613.
- [4] F. M. Lea, "The Chemistry of Cement and Concrete", Third edition, Edward Arnold Ltd, **1970**.
- [5] D. P. Bentz, E. J. Garboczi, C.-J. Haecker, O. M. Jensen, *Cem. Concr. Res.* **1999**, 29, 1663.
- [6] D. P. Bentz, O. M. Jensen, K. K. Hansen, J. F. Olesen, H. Stang, C.-J. Haecker, *J. Am. Ceram. Soc.* **2001**, 84, 129.
- [7] J. J. Thomas, H. M. Jennings, *J. Am. Ceram. Soc.* **2002**, 85, 2293.
- [8] D. P. Bentz, *Cem. Concr. Res.* **2006**, 36, 238.
- [9] R. G. Patel, D. C. Killoh, L. J. Parrott, W. A. Gutteridge, *Mater. Struct.* **1988**, 21, 192.
- [10] K. A. Snyder, D. P. Bentz, *Cem. Concr. Res.* **2004**, 34, 2045.
- [11] J. Zelic, R. Krstulovic, E. Tkalcec, P. Krolo, *Cem. Concr. Res.* **2000**, 30, 145.
- [12] I. Pane, W. Hansen, *Cem. Concr. Res.* **2005**, 35, 1155.
- [13] J. Chappel, P. Argust, *Thermochim. Acta* **1996**, 289, 303.
- [14] V. A. Atiemo-Obeng, W. R. Penney, P. Armenante, "Solid-Liquid Mixing", in *Handbook of Industrial Mixing: Science and Practice*, V.A.A.-O. Edward L. Paul, Suzanne M. Kresta, Ed., Wiley-Interscience, **2004**.

# **CHAPTER 7**

## **Conclusions & Recommendations**

## 7 CONCLUSIONS & RECOMMENDATIONS

The research conducted in this thesis highlighted that carbon dioxide evolved during cure, from the reaction of water contained in the polyol emulsion with isocyanate in the oligomer polymer component of the coating, was the cause of random blister formation within the material. The research also quantified the carbon dioxide evolution and developed a process for successfully eliminating the carbon dioxide released and subsequent blister formation. In addition to this, a solid fundamental understanding about the cure chemistry of this polyurethane/polyurea system was established.

The rate of carbon dioxide diffusion from the coating, the gelation time and the influence of the surface-air interface are all key aspects in the formation of random blisters. The primary concern of this thesis was the elimination and reduction of carbon dioxide evolution during cure; thus, the diffusion kinetics of the carbon dioxide evolved and the curing effects at the surface-air interface were out of the scope of this research. However, understanding the gel time of the coating and the reaction kinetics of the highly crosslinked poly (urea-*co*-urethane) cement composite coating aided the development of solutions to random blister formation. The properties of the final coating are dependent on the reactive components of materials and small variations of the composition can affect the gas expansion rate, in particular the nature and concentration of the surfactant.<sup>[1, 2]</sup> Investigations into the rate of foaming which includes gas bubble nucleation and growth are important areas of investigation in understanding blister formation and should be considered as future work.

Due to the complexity of the coating formulation, individual reactions which provide the crosslinking and subsequent network structure were investigated individually and modelled. These included the reaction kinetics between the hydroxyl functional groups of the polyol (castor oil) and isocyanate groups (PMDI) and the reaction kinetics between water and isocyanate functional groups. Characterisation of the reactions was performed using Differential Scanning Calorimetry (DSC), Pressure DSC (PDSC), rheology and FTIR. The kinetics of cure for the polyurethane reaction between castor oil and oligomeric isocyanate as monitored using different techniques showed that activation energies were in good agreement with each other. DSC results

were analysed through isoconversional methods, which showed that a competitive reaction scheme existed for a stoichiometric system, suggesting the presence of isocyanate groups with differing reactivity in the PMDI oligomers. An increase in the rate of reaction during isothermal FTIR also confirmed this. Greater conversions were achieved at temperatures below 50 °C for the stoichiometric system using rheological measurements. This was attributed to curing below the glass transition temperature, leading to vitrification. The viscosity growth for the stoichiometric system was described by an exponential equation before the point of gelation and the rate of viscosity increase was described by a viscometric rate constant  $k_{\eta}$  for the initial stages of cure. A low viscosity build up was evident in the excess isocyanate system, which is currently employed in the industry formulation. The complete consumption of the hydroxyl groups was verified through analytical tests. A polyurethane adduct was formed exhibiting a reduction in viscosity with increasing temperature, once all hydroxyls were consumed. FTIR results showed the reaction was kinetically controlled and that higher than expected conversions were achieved for the excess isocyanate system due to the reaction of isocyanate groups with moisture in the air.

Pressure differential scanning calorimetry (PDSC) was employed to determine the reaction kinetics of the polyurea reaction where the heat of reaction was found to be higher than that achieved for the polyurethane reaction (38 kJ mol<sup>-1</sup> equiv. NCO *cf.* 25 kJ mol<sup>-1</sup> equiv. NCO). Higher peak temperatures and activation energies (70 kJ mol<sup>-1</sup> *cf.* 38-45 kJ mol<sup>-1</sup>) were also achieved, suggesting the polyurea reaction required a greater amount of energy to activate the reaction, although, once activated, the polyurea reaction was more exothermic than the polyurethane reaction. The evolution of carbon dioxide was detected using PDSC through the pressure increase during cure, which was a novel application. It is unsure whether there was a gradual release in carbon dioxide, or if the amount of carbon dioxide formed was released at one specific moment, causing a large pressure increase after 60% conversion due to the acceleration of the water and isocyanate reaction. Increasing the mole ratio of water to isocyanate showed an increase in pressure; however, this was mainly due to the heat evolved from the reaction. Volumetric analysis, demonstrated that no significant change in carbon dioxide evolution was evident with increasing water to isocyanate mole ratios. The rate of the water and isocyanate reaction was 1<sup>st</sup> order

with respect to water consumption using volumetric carbon dioxide analysis; 2<sup>nd</sup> order with respect to isocyanate consumption using FTIR analysis and 2<sup>nd</sup> order with respect to carbon dioxide evolution using volumetric carbon dioxide analysis. Thus the overall rate of the water-isocyanate reaction was found to be proportional to  $[\text{H}_2\text{O}][\text{NCO}]^2$ .

This work highlighted for the polyurethane reaction in the current industry formulation that the ratio of castor oil to PMDI (a molar excess of PMDI) does not contribute to the crosslinking reaction; however, this may work synergistically with the water-PMDI reaction to increase crosslinking density in the coating. The investigation into the reaction kinetics of the proposed synergism is suggested as future work; although, difficulty may exist in finding a suitable quantitative method due to the release of carbon dioxide gas. PDSC, although suitable for the water-isocyanate reaction, does not give clear exotherms for the different reactions present. FTIR methods have their limitations due to sampling temperatures and/or sample preparation; in addition there is a difficulty in differentiating overlapping peaks. Rheological analysis gives information on the combinatorial effects of the crosslinking reactions; however, difficulty exists in the differentiation of the reactions, which is required to determine the kinetic parameters.

The work performed for the initial reactions provided the basis for modification and improvement of the current industry product. Increasing the pot-life of the coating mixture by increasing gel times was found to occur through the addition of a slower reacting polyol. Glycerol was chosen for this application due to its slow secondary hydroxyl group as well as its ability to mix well with PMDI due to the delayed reaction. As well as being a slower reaction, the activation energy and reaction temperature determined by DSC analysis showed that the glycerol-PMDI reaction slightly preceded the water-PMDI reaction, thus, the glycerol-PMDI reaction was postulated to be a preferred reaction in the presence of water. It was therefore hypothesized that the addition of glycerol to the emulsion would delay the fast crosslinking process to allow for greater diffusion of carbon dioxide from the coating before gelation. Experimental work carried out in this thesis verified this hypothesis. Another benefit for the use of glycerol was its ability to reduce the viscosity of the polyol emulsion, allowing for improved application properties of the coating mixture. The polymerisation kinetics of PMDI with glycerol was thus investigated

using thermal and rheological techniques due to the lack of literature describing the reaction kinetics of multifunctional reactants with functional groups of varying reactivity. This work highlighted the complexity of cure for this system. The reactivity of the primary and secondary hydroxyl groups were found to vary at higher temperatures or during extended periods of curing. The primary hydroxyls were found to react three times faster than the secondary hydroxyl groups as corroborated by similar systems investigated in the literature, using alternative characterisation techniques. A comparison between application of kinetic models and isoconversional methods for DSC data was made. Isothermal DSC showed that an autocatalytic kinetic model fitted the experimental data well, although, analysis of non-isothermal DSC data using a second order model gave approximately the same reaction order, without fitting the data as well. Diffusion rate constants were omitted from the reaction models, as more commonly accepted kinetic models for polyurethane systems in the literature were used in this body of research, for comparison to isoconversional methods. Isoconversional methods, specifically, Vyazovkin's<sup>[3]</sup> integral isoconversional method, was applied to both isothermal and non-isothermal data for the stoichiometric ratio and for the analysis of the critical mole ratio of OH/NCO=1.5, which was determined through non-isothermal DSC. Isoconversional analysis of DSC data resulted in the activation energy varying with conversion for both stoichiometric and excess hydroxyl ratios. Incomplete cure was evident in both isothermal and non-isothermal modes, becoming diffusion controlled in the final stages of cure for both mole ratios investigated. Isothermal DSC analysis clearly demonstrated that cure did not go to completion at all temperatures, with the ultimate reactivity of both isocyanate and hydroxyl groups being inhibited by the onset of diffusion control towards the end of cure, which was less evident for the excess hydroxyl ratio due to a larger extent of conversion being achieved. Rheological studies of viscosity increase and  $\tan \delta$  changes revealed a complex cure process, with primary and secondary hydroxyl reactivity being dependant on isothermal cure temperatures, reflecting similar results obtained from isothermal DSC studies. Two separate  $\tan \delta$  peaks were observed, which responded differently to isothermal temperature conditions of cure, which were related to the different rate of cure of the primary and secondary hydroxyl groups on the glycerol molecule. Future work, investigating the difference in reactivity of the primary and secondary hydroxyls

through FTIR analysis is proposed. The independence of  $\tan \delta$  on frequency (Winter-Chambon<sup>[4]</sup> theory) was used to determine the point where the polymer formed an infinite network and was no longer able to flow. Gel times determined for the glycerol-PMDI system were much higher than those achieved for the castor oil-PMDI system at the stoichiometric ratio.

The polyol emulsion variables were systematically investigated for their effect on the flow properties of the emulsion through rheological analysis and for their subsequent effect on the curing reaction with PMDI, through volumetric carbon dioxide tests and rheological tests. It was determined that the industry ratio of water to castor oil to surfactant was critical, with small changes either side of this ratio affecting the pot-life and extent of crosslinking of the mixture, even though no significant effect was observed on carbon dioxide evolution. A relationship was found to exist between the emulsion conductivities and the storage modulus values obtained at the gel point, in particular for the water and castor oil series of emulsions. A greater incorporation of the oil phase (lower conductivities) improved the extent of crosslinking and increased the pot-life of the mixture. This was achieved for higher surfactant concentrations, lower water concentrations and slightly lower castor oil concentrations than that currently used by the industry. The non-curing components used in the current industry polyol emulsion, were found to increase the level of carbon dioxide evolved, due to the combinatorial effect of the dioctyl phthalate plasticizer and the pine oil, shown in volumetric carbon dioxide tests. The viscosity of the emulsions had no effect on the reaction between water and isocyanate, although, lower viscosity emulsions aided in the application properties of the coating. A 4% w/w addition of glycerol to the polyol emulsion was found to substantially reduce the viscosity of the polyol emulsion, while retaining the emulsion stability. It was also determined through rheological characterisation of the curing reaction with PMDI, that the crosslinking reaction was delayed at this ratio; thus, a greater pot-life was achieved. The water-isocyanate reaction was found to predominate before the gel time, allowing carbon dioxide to be evolved before extensive crosslinking was achieved at the gel time. Addition of the glycerol to the polyol emulsion also allowed for minimal procedural changes during the formation of the polyol emulsion which can be easily implemented by industry. In this procedure, the polyol emulsion was formed in the same manner, with a fraction of glycerol added at the end of the

procedure. Emulsion technology is an extensive area for investigation and in this research project was only able to be analysed in its most simplistic form. Despite this, an effective comparison of the emulsion variables was obtained, which aided in the understanding and improvement of the curing reactions occurring in the coating formulation. Future work would require a more thorough investigation on emulsion structure, the effects of shearing and the effects of varying surfactants.

The current level of cement and calcium hydroxide in the fillers reduced carbon dioxide evolution by 70%, which was not sufficient in preventing random blister formation during curing. It was found that cement ageing with time did not impede Portland cement's ability to reduce carbon dioxide evolution formed in the reaction between the polyol emulsion and PMDI during curing. In contrast, it was shown to have a positive effect in the reduction of carbon dioxide. The suggested improvements to the coating could best be obtained by increasing the calcium hydroxide in the fillers to 5.5% w/w while using a lower viscosity polyol emulsion that includes the addition of glycerol. A 4% w/w glycerol addition to the current polyol emulsion was found to extend the liquid volume which also aided mixing and provided a practical and simple solution that could be implemented by the industry partner. An increase in water content of 3.5% w/w was also a possible solution to aid in reducing the viscosity of the polyol emulsion without significantly affecting the coating's material properties, which were determined through Dynamic Mechanical Analysis (DMA). These combined solutions reduced carbon dioxide evolution, and provided a coating that was easily mixed and applied. Future work would require investigations into the mixing/blending of the liquid components with the aggregate mixture to establish correct particulate size in order to form a self-levelling version of the coating. Effects of shearing on the application properties of the coating mixture are therefore an important consideration which was out of the scope of the thesis and should be considered for future investigations.

## References

- [1] S. A. Baser, D. V. Khakhar, *J. Cell. Plast.* **1993**, 29, 197.
- [2] C. Ligoure, M. Cloitrea, C. Le Chateliera, F. Montia, L. Leibler, *Polymer* **2005**, 46, 6402.
- [3] S. Vyazovkin, *J. Therm. Anal. Calorim.* **2006**, 83, 45.
- [4] H. H. Winter, F. Chambon, *J. Rheol.* **1986**, 30, 367.

# **Appendix A**

## **Material Characterisation**

# 1 PMDI

Oligomeric diphenylmethane diisocyanate (PMDI) was used throughout the course of the project, consisting of a functionality of 2.7 and viscosity of 200-250 mPa.s. It was used as received from Dow Plastics (PAPI 20), with the typical composition of PMDI given in **Figure 1.A**.

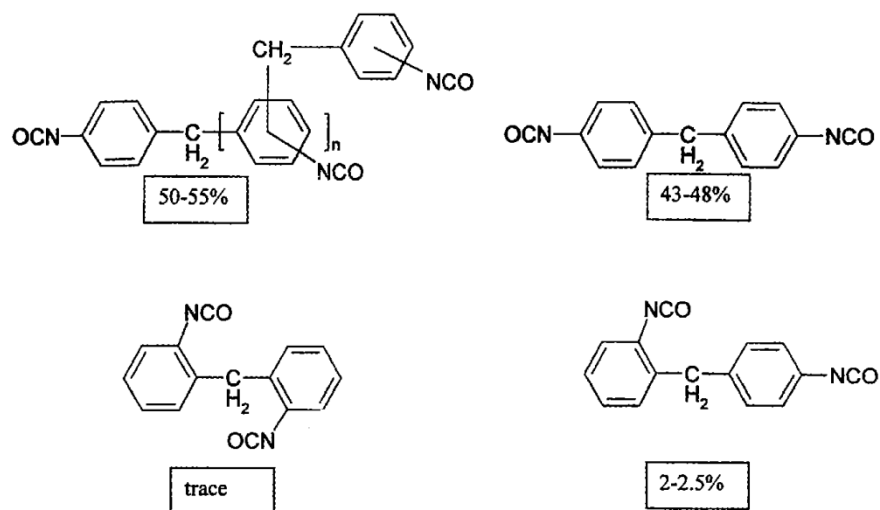


**Figure 1.A** Typical composition of PMDI<sup>[1]</sup>

Care was taken to minimise contact to humid environments by storing the PMDI under a blanket of nitrogen. The characterisation of the PMDI was performed over the course of a year (8-9 samples) to determine the effects of ageing due to polymerisation and moisture. This was performed using <sup>1</sup>H Nuclear Magnetic Resonance (NMR), Attenuated Total Reflectance Fourier Transform InfraRed (ATR-FTIR) and rheological analysis.

The NMR spectra were carried out on a Varian Gemini FT-NMR liquid nitrogen cooled 300 MHz spectrometer using VNMR 6.1 analysis software with a Sun Unix system workstation. Sample preparation required approximately 10 mg of the PMDI to be dissolved in deuterated chloroform. Chloroform-*d* (99.9%) supplied by Sigma-Aldrich Chemical Company Pty Ltd was stored under nitrogen and used as supplied without further purification.

The typical spectrum obtained is shown in **Figure 1.B**.

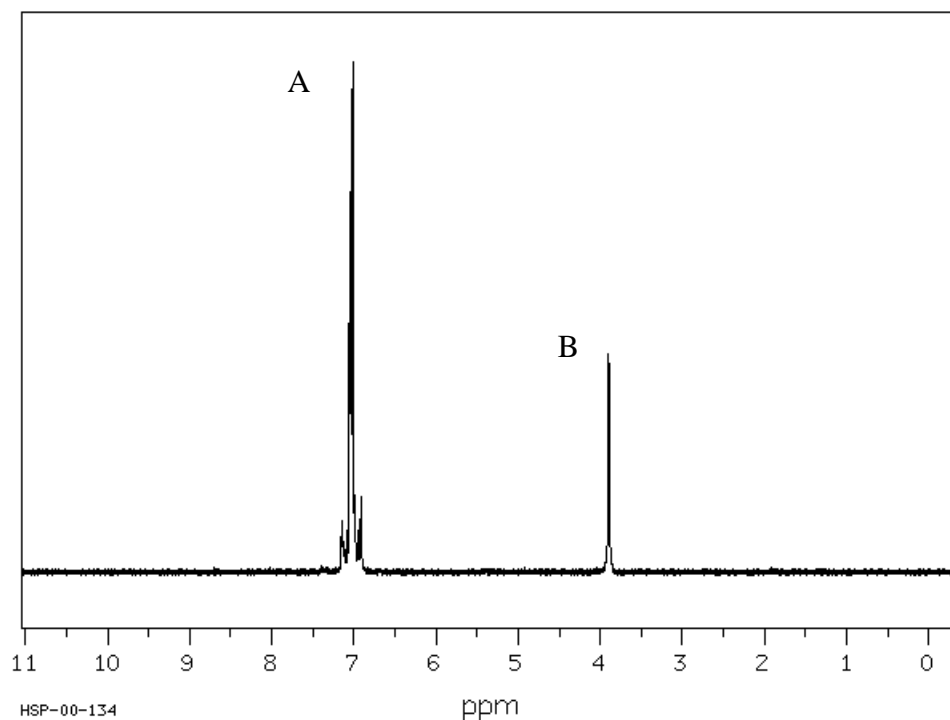


**Figure 1.B** Typical  $^1\text{H}$ -NMR spectrum with peaks representing for A) aromatic and B) alkyl protons<sup>[2]</sup>

The NMR shift at 7 ppm refers to the protons attached to the aromatic rings in PMDI, while the shift at 3.9 ppm refers to the protons attached to alkyl carbons.<sup>[3]</sup>

The ageing process was followed by determining the change in the repeating unit,  $n$  over time. This was performed by considering the ratio of the aromatic protons to the alkyl protons in PMDI, with the repeating unit as shown below in **Figure 1.C**.

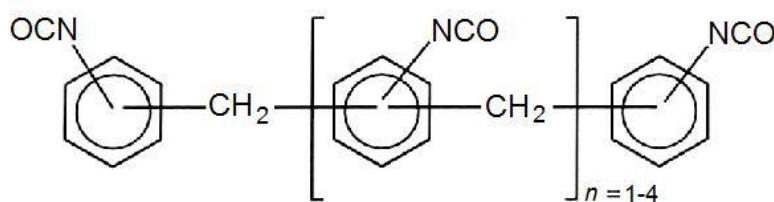


**Figure 1.C** General structure of PMDI<sup>[4]</sup>

If it is considered that the number of aromatic protons is equal to  $8+3n$  where  $n$  is the number of repeating units in the PMDI oligomer and the number of alkyl protons is equal to  $2+2n$ , then the ratio of the aromatic protons to the alkyl group protons can be used to deduce  $n$ , as follows.

$$R = \frac{8+3n}{2+2n} = \frac{\textit{Aromatic shift}}{\textit{Alkyl shift}} \quad (1-A)$$

Rearranging **Equation (1-A)** for  $n$ , gives **Equation (1-B)**

$$n = \frac{8-2R}{2R-3} \quad (1-B)$$

It was found that  $n$  varied from sample to sample, however, this was insignificant, with an average value of  $n$  equal to  $1.18 \pm 0.08$ , which is less than 10% relative error. ATR-FTIR was also performed by monitoring the isocyanate peak at  $2270 \text{ cm}^{-1}$ .<sup>[5]</sup> The area of this peak was determined for the samples used in the above NMR analysis and was also found to vary for each sample; however, this was also insignificant with an average area equal to  $241 \pm 3$  units, which is less than 5% relative error. Rheological analysis performed on the same samples gave an average value of viscosity equal to  $245 \pm 4$  mPa.s, which was less than 5% relative error and within specification.

Therefore, no significant difference was observed in the bulk PMDI over time.

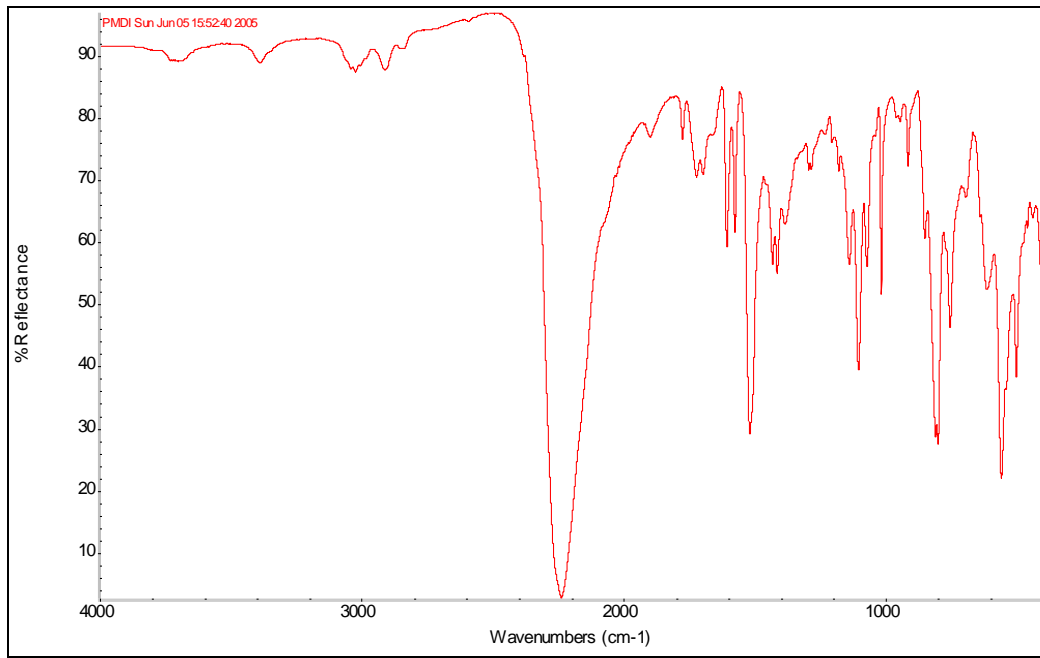
## 2 ANALYSIS OF RAW MATERIALS

Thermogravimetric analysis (TGA) was performed for the main materials used throughout the project and are presented in **Table 2-A**. Onset temperatures of decomposition and the total mass loss are presented. The TGA technique is presented in Chapter 2, with samples heated up to 600 °C.

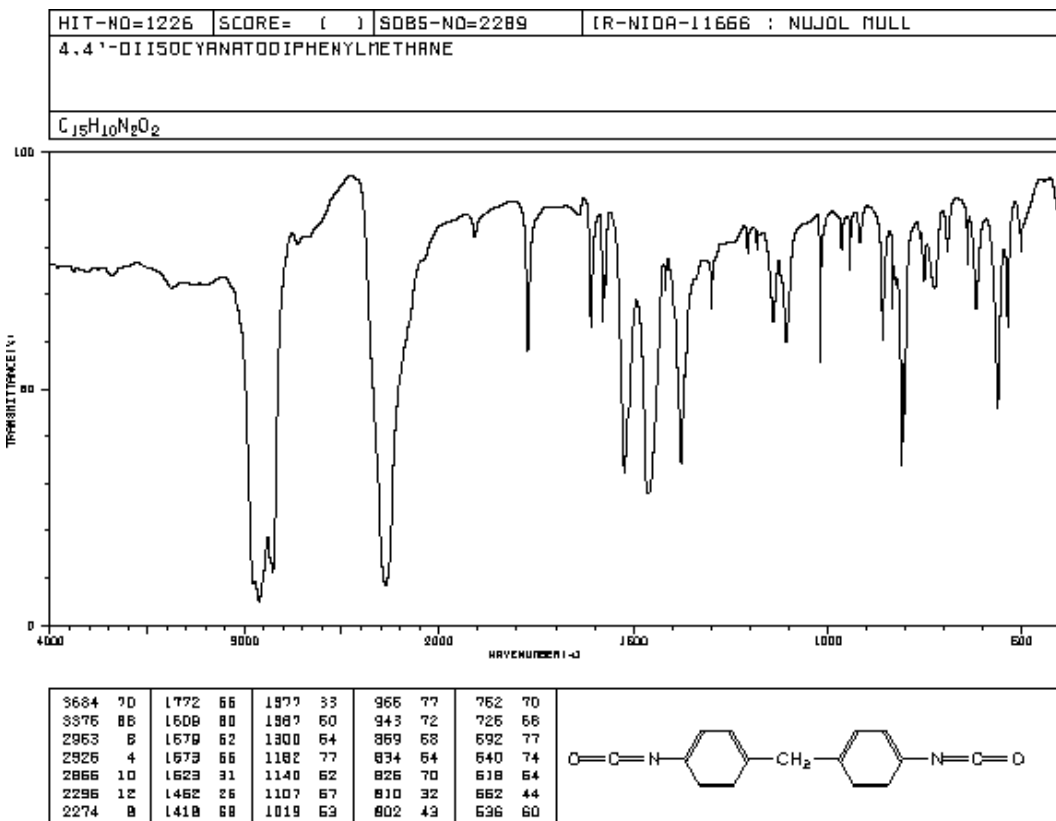
**Table 2-A Summary of TGA parameters for raw materials**

<b>Sample</b>	<b>% Weight Loss</b>	<b>T<sub>onset</sub> °C</b>
PMDI	71.03%	185.6
Castor oil	99.46%	350
Glycerol	99.96%	186
Diocetyl phthalate	99.97%	252
Pine oil	99.73%	102
Silicone Oil	90.70%	405
nonionic surfactant	97.55%	316
Desmodur VL R10	60.59%	226

ATR-FTIR spectra were collected for the main materials used throughout this thesis and are compared to spectra obtained using the online spectral database SDBS, which are shown below.<sup>[2]</sup> Very good agreement is observed with spectra obtained using ATR-FTIR analysis when compared to the online database.

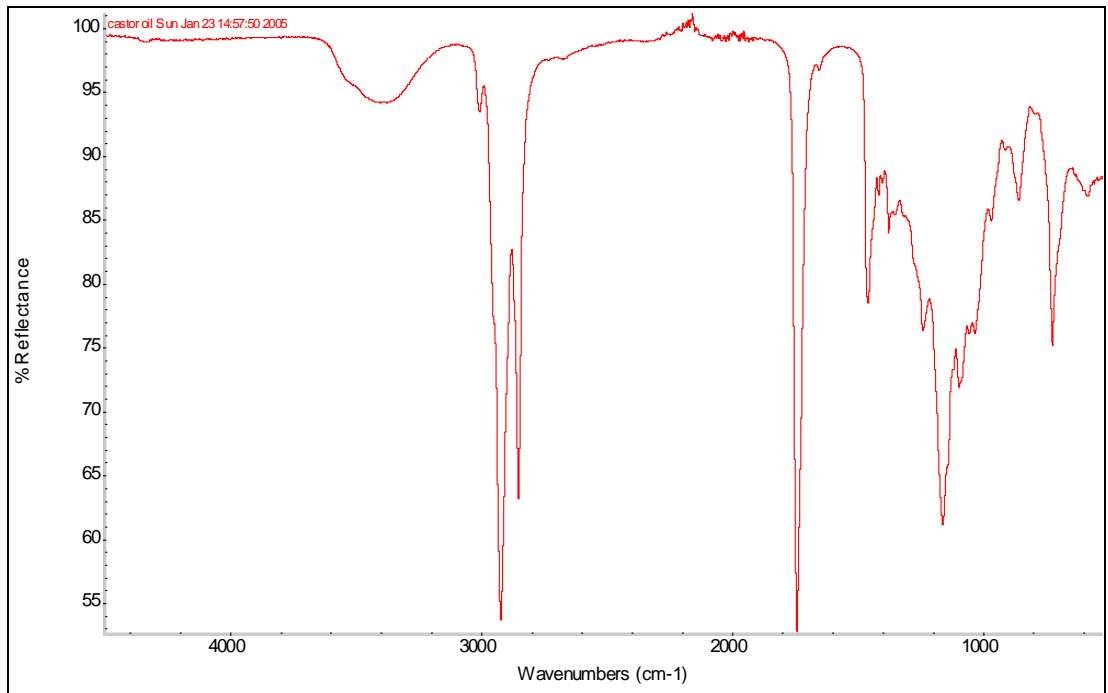


A)



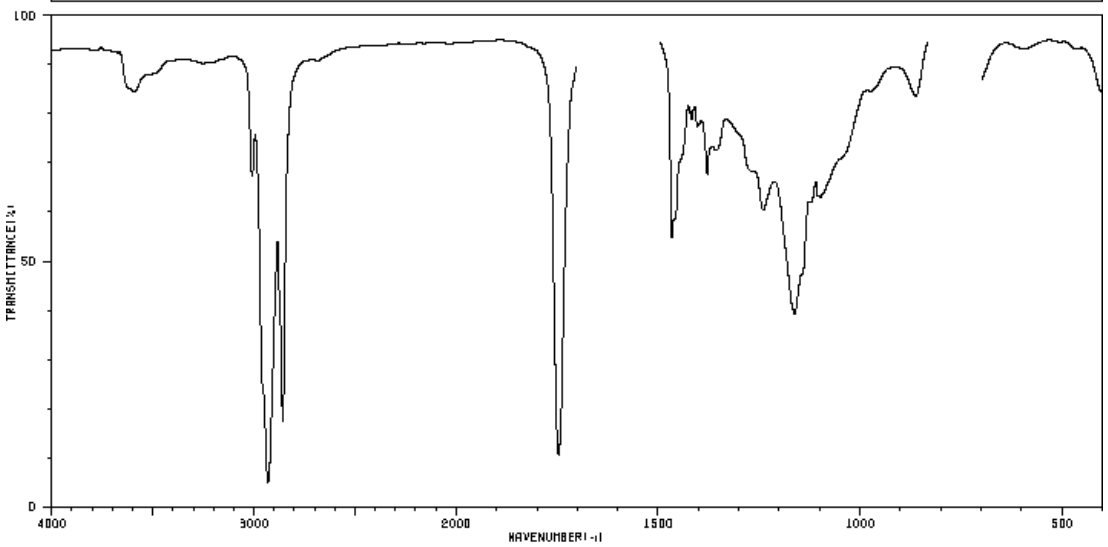
B)

Figure 2.A IR spectra for A) PMDI obtained by ATR-FTIR compared to B) MDI spectra obtained from SDBS<sup>[2]</sup>



A)

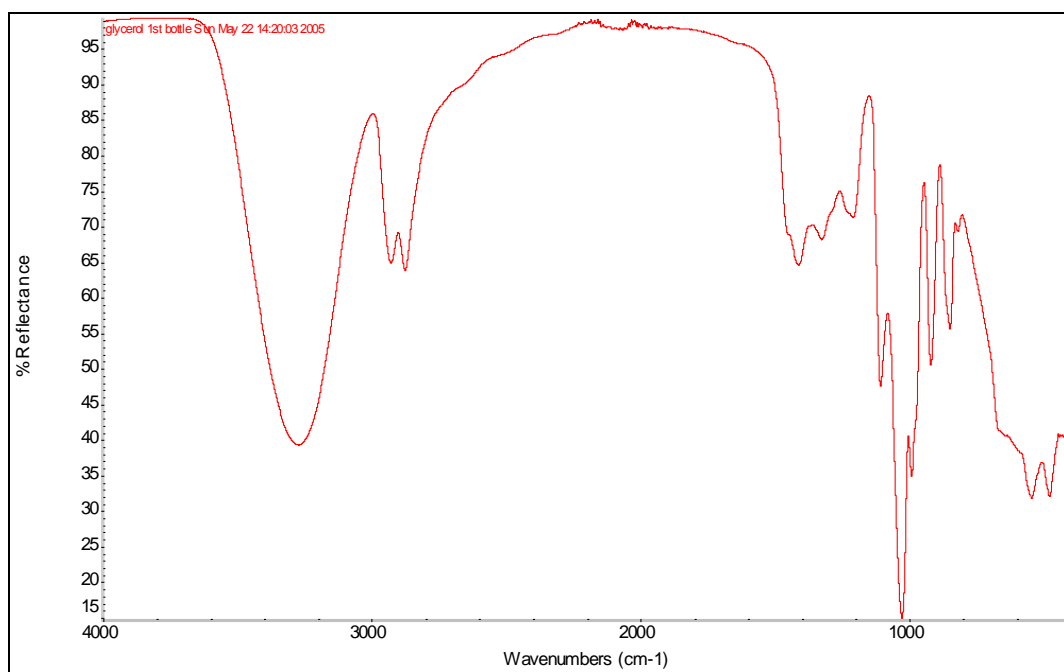
HIT-NO=1427	SCORE= ( )	SDBS-NO=1936	IR-NIDA-08670 : CCL4 SOLUTION
CASTOR OIL			



3610	81	1746	10	1360	70
3590	81	1467	52	1240	58
3008	84	1458	57	1163	37
2964	22	1417	77	1097	60
2930	4	1403	74	1092	60
2872	38	1379	64	863	81
2857	16	1366	70		

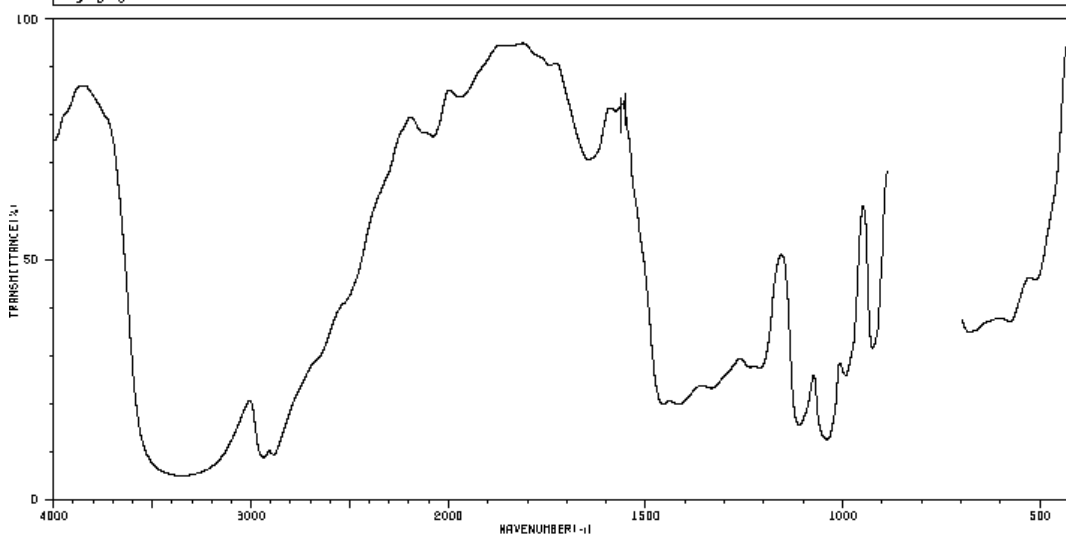
B)

Figure 2.B IR spectra for A) castor oil obtained by ATR-FTIR compared to B) castor oil spectra obtained from SDBS<sup>[2]</sup>

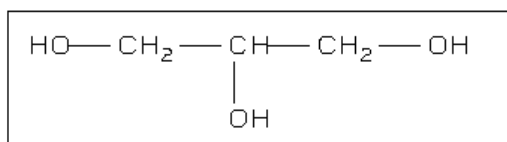


A)

HIT-NO=1274	SCORE= ( )	SDBS-NO=2517	IR-NIDA-08714 : CCL4 SOLUTION
GLYCEROL			
$C_3H_8O_3$			

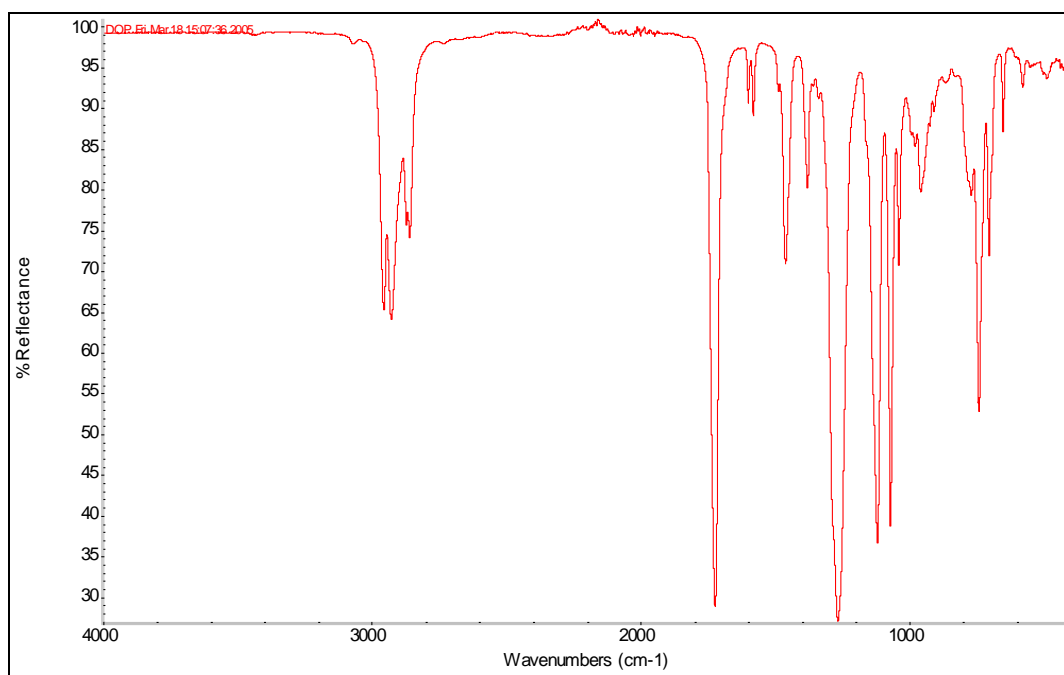


2936	4	1040	7
2103	68	998	18
1970	77	953	18
1643	62	924	23
1564	68	673	26
1551	70	668	26
1111	9		



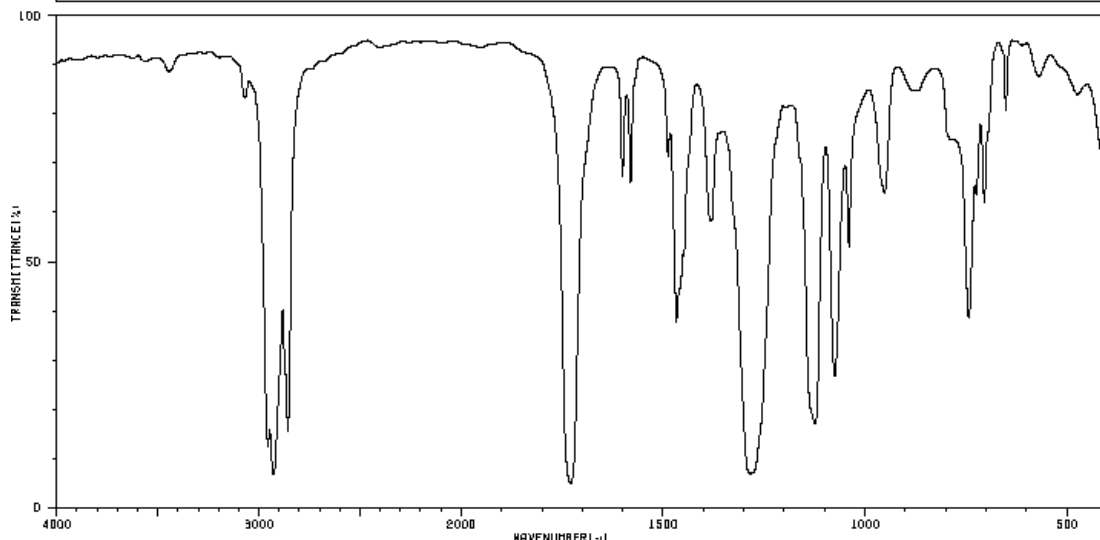
B)

Figure 2.C IR spectra for A) glycerol obtained by ATR-FTIR compared to B) glycerol spectra obtained from SDBS<sup>[2]</sup>

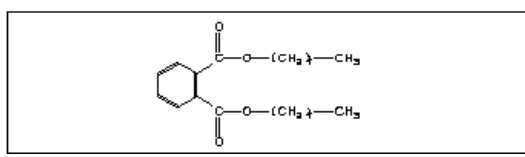


A)

HIT-NO=3894	SCORE= ( )	SDBS-NO=8360	IR-NIDA-45724 : LIQUID FILM
DIOCTYL PHTHALATE			
C <sub>24</sub> H <sub>38</sub> O <sub>4</sub>			



3444	84	1601	64	1124	16	744	37
3070	79	1580	64	1075	25	724	60
2956	12	1488	68	1040	50	705	60
2927	6	1467	36	952	62	662	77
2871	26	1449	49	881	81	570	84
2857	14	1384	55	875	81	474	61
1729	4	1285	6	870	81		



B)

Figure 2.D IR spectra for A) diethyl phthalate obtained by ATR-FTIR compared to B) diethylphthalate spectra obtained from SDBS<sup>[2]</sup>

## References

- [1] R. G. Dillingham, C. Moriarty, *J. Adhes.* **2003**, *79*, 269.
- [2] T.Saito, K.Hayamizu, M.Yanagisawa, S.Kinugasa, K.Tanabe, T.Tamura, O.Yamamoto, "Spectral Data Base System for Organic Compounds", *National Institute of Advanced Industrial Science and Technology (AIST)*, online database, accessed **2008**.
- [3] J. Hanson, "Overview of Chemical Shifts in H-NMR", accessed online **2008**.
- [4] I. P. o. C. S. (IPCS), "Concise International Chemical Assessment Document No. 27, Diphenylmethane diisocyanate (MDI)", **2001**.
- [5] A. M. Kaminski, M. W. Urban, *J. Coat. Technol.* **1997**, *69*, 113.